



Optimizing cortical feedback strategies for a closed-loop brain machine interface

Henri Lassagne

► To cite this version:

Henri Lassagne. Optimizing cortical feedback strategies for a closed-loop brain machine interface. Neurobiology. Sorbonne Université, 2023. English. NNT : 2023SORUS042 . tel-04076095

HAL Id: tel-04076095

<https://theses.hal.science/tel-04076095>

Submitted on 20 Apr 2023

HAL is a multi-disciplinary open access archive for the deposit and dissemination of scientific research documents, whether they are published or not. The documents may come from teaching and research institutions in France or abroad, or from public or private research centers.

L'archive ouverte pluridisciplinaire **HAL**, est destinée au dépôt et à la diffusion de documents scientifiques de niveau recherche, publiés ou non, émanant des établissements d'enseignement et de recherche français ou étrangers, des laboratoires publics ou privés.

Sorbonne Université

École doctorale Cerveau Cognition Comportement

NeuroPSI, ICN

Équipe « Traitement Sensori-moteur et Plasticité »

Dir. Daniel Shulz

Optimizing cortical feedback strategies in a brain-machine interface context

Présentée par : **Henri Lassagne**

Thèse de doctorat de Neurosciences

Dirigée par : **Valérie Ego-Stengel**

Co-supervision : **Luc Estebanez et Daniel Shulz**

Présentée et soutenue publiquement le 21/03/2023

Devant un jury composé de :

Sylvain Crochet (*EPFL, Lausanne*) : Rapporteur

Thomas Brochier (*Institut de Neurosciences de la Timone, Marseille*) : Rapporteur

Gisella Vetere (*ESPCI, Paris*) : Examinatrice

Brice Bathellier (*Institut de l'Audition, Paris*) : Examinateur

Sami El-Boustani (*University of Geneva, Genève*) : Examinateur, président du jury

Valérie Ego-Stengel (*NeuroPSI, Saclay*) : Directrice de thèse

Summary

Pioneering studies aim to improve the everyday life of motor-impaired patients by providing motor rehabilitation devices controlled directly by brain activity. In order to use these neuroprostheses efficiently, patients need online sensory feedback to guide and correct ongoing movements. It is known that precise somatosensory information from the body parts, and not only visual information, is vital for dexterous control. Thus, brain-machine interfaces (BMIs) should both read neural activity from the brain and feed back sensory information about the prostheses current state. Recent efforts in closed-loop BMI systems are addressing this challenge promisingly. However, an understanding of the neuronal mechanisms of sensorimotor integration will be necessary to optimize sensory feedback delivery. In this thesis, we are using a low-latency, closed loop brain-machine interface for head-fixed mice, which combines electrophysiological recordings in M1 and optogenetic stimulation in the primary somatosensory cortex (S1). We aim to reveal general rules about how the brain uses spatio-temporal patterns of cortical activity in order to generate feedback-corrected motor commands, and further understand the mechanisms behind the computational rules for sensory-guided behavior. Firstly we showed that taking into account the topographical organization of the whisker barrel cortex, which highly reflects the organization of the whisker pad, favors the learning of a sensory guided task. Secondly, we implemented an ultra-fast incremental control algorithm to study the impact of latency in BMI learning. We expect that mimicking the physiological intrinsic latency of the sensorimotor system should promote learning.

Remerciements

Si j'admets que je me serais bien volontiers épargné l'exercice ardue qu'est l'écriture des remerciements de thèse, il m'est forcé d'admettre que l'ampleur de l'aide, du soutien et de la qualité scientifique et humaine dont j'ai pu bénéficier tout au long de ces 4 années est bien trop importante pour que je puisse m'esquiver.

Je tiens à commencer par remercier la protagoniste principale, Valérie. Vraiment, je ne pense pas qu'un étudiant en thèse puisse rêver d'un meilleur encadrement que celui dont j'ai pu bénéficier. Merci pour ton aide, bien sûr sur le plan scientifique, mais surtout pour ton soutien indéfectible, ta présence et ta capacité à toujours voir le bon côté des choses, tout en supportant mes élucubrations et en me motivant avec du chocolat noir d'exception... Je n'oublierais jamais cette période de ma vie rythmée de réunions thé et chocolat, et si ma thèse s'est aussi bien passée, c'est surtout grâce à toi.

Luc, le premier jour de mon stage de M2, tu m'as mis devant un code dans un langage mystérieux en m'expliquant qu'il fonctionnait à moitié et qu'il fallait régler ça... Finalement, ton optimisme presque irrationnel face à mes compétences m'a poussé à aller vers l'inconnu. Merci aussi pour ta touche d'humour en toute circonstances.

Dan, merci de m'avoir accueilli dans cette équipe si chaleureuse, je dois dire que tu diriges vraiment cette équipe d'une main experte, que ce soit sur le plan scientifique et humain. Je tiens tout de même à confesser que je préfère le vin rouge du sud-ouest au vin argentin.

Isabelle, j'ai beaucoup apprécié discuter avec toi, les diners d'équipe (et ce malgré les discours), et la voix raisonnée que tu as pu apporter devant la folie des grandeurs de Luc.

Je tiens tout particulièrement à remercier Aurélie pour plus de raisons que je ne puisse écrire, en pensant tout particulièrement à ta bonne humeur et le séjour que j'ai pu passer un été à Massy.

Merci tout particulièrement à Guillaume pour ton soutien, qu'il s'agisse d'histologie, de trajets à la cantine de Gif avec Christophe ou pour démonter joyeusement des meubles. Merci aussi à Aline pour m'avoir aidé en étant toujours compréhensive devant mon incompétence administrative évidente.

Je tiens également à remercier Aamir et Dorian pour m'avoir formé avec autant d'enthousiasme et d'attention, je pense particulièrement à mes premières chirurgies qui terminaient à 21h. Ce fut un réel plaisir de travailler avec vous et de commencer ma thèse dans d'aussi bonnes conditions. Merci aussi à Anton pour avoir su faire preuve d'autant de discrétion que de gentillesse.

Merci à Yannick pour avoir été le phare qui éclaire les ténèbres de notre vie (je vais finalement léguer ton handspinner aux générations futures), et à Sophie et Timothé pour nos longues discussions politico-culinaires, sans oublier Evan. Merci à Zineb pour ta bonne humeur et d'avoir supporté mes jérémiades à longueur de journée. Enfin je tiens à remercier Fan pour ton sourire radieux et ton rire jamais bien loin, Max pour ne m'avoir jamais écrasé aux échecs, et Édouard et Clément pour votre soutien dans le complot pour renverser la dictature de L.E. Merci aussi à Esther et à Mathieu pour l'aide et l'intérêt que vous avez porté à mon projet, vous avez été super.

Alexandre, je suis réellement impressionné par ta rapidité et ton efficacité à comprendre le fratras que je te laisse... Ce fut vraiment génial de travailler et bavarder avec toi malgré mes problèmes de santé. Je te souhaite le meilleur pour la suite et j'ai hâte qu'on se retrouve autour d'un bon dîner.

Merci infiniment à tout le personnel de l'animalerie sans qui aucun de mes travaux n'aurait abouti, je pense tout particulièrement à Valérie et ses bons points que je garde toujours dans mon portefeuille, Christophe pour la salle et les accouplements, Sandra pour le génotypage, Patricia et Jocelyne pour l'autoclave, mais je suis sûr que la liste ne s'arrête pas là...

Merci aux rapporteurs et examinateurs d'avoir porté de l'intérêt à cette étude accepté de l'évaluer, je réalise très bien que c'est une charge de travail en plus pas toujours facile ou agréable à s'imposer.

Merci à mes amis et ma famille qui ont su me rappeler que c'est important de bien respirer, en pardonnant mes étourderies un peu trop fréquentes.

Enfin, merci à Clémentine, ma jolie dresseuse de crocodiles.

Contents

Summary	2
List of Figures	7
I INTRODUCTION	9
1 A spatio-temporal sensorimotor integration	10
1.1 A natural closed loop system	10
1.1.1 From the exterior world to the cortex	10
1.1.2 The primary motor cortex and its role in motor commands	11
1.1.3 Sensory-motor cortices connectivity	14
1.1.4 Delays in the control system	16
1.2 The whisker system in rodents	19
1.2.1 In the follicles	19
1.2.2 From the periphery to the cortex	19
1.2.3 A topographical sensorimotor integration in the whisker motor cortex	21
1.2.4 Multi-whisker integration	22
1.3 Topographical organization for different primary and secondary areas	23
1.3.1 Retinotopy, a topography in the visual system	23
1.3.2 Tonotopy and higher visual areas	25
2 Plasticity in the brain and its limits	27
2.1 Plasticity at the neuronal level	27
2.1.1 What is plasticity ?	28
2.1.2 Neuronal operant conditioning	28
2.1.3 Tools to promote plasticity	31
2.1.4 Limits	32
2.2 Functional reorganization in the brain	32
2.2.1 Topographical reorganization	34
2.2.2 Overlapping functionality	36
2.2.3 Plasticity in the whisker cortices	36
3 Brain-Machine Interfaces, tools to connect the brain to the exterior world	38
3.1 What is a BMI ?	38

3.1.1	In the medical field	39
3.1.2	Bi-directional BMIs, a tool to study the brain mechanisms	40
3.2	Optimizing control and cortical feedback on a cortical sensori- motor neuroprostheses	40
3.2.1	The ideal brain-machine interface	41
3.2.2	Decoding neuronal activity	42
3.2.3	Biomimicry versus adaptation, stimulating the cortical maps	44
3.2.4	Embodiment	46
II METHODS AND RESULTS		48
4	A Closed-loop brain-machine interface to study sensorimotor integration	49
4.1	Continuity within somatosensory cortical map facilitates learning	49
4.1.1	Summary	49
4.1.2	Participation statement	49
4.2	Cortical closed-loop brain-machine interface requires biomimetic feedback	68
4.2.1	Summary	68
4.2.2	Participation statement	68
4.3	Preliminary results: Matching natural closed loop latencies pro- motes sensorimotor learning	96
4.3.1	Summary	96
4.3.2	Participation statement	96
4.3.3	Material and methods	97
4.3.4	Preliminary Results	101
4.3.5	Perspectives	102
III DISCUSSION		103
IV APPENDIX		113
Supplementary Article 1: Control of a robotic prosthesis simula- tion by a closed loop brain-machine interface		114
Supplementary Article 2: Mechanical coupling through the skin affects whisker movements and tactile information encoding		128
Bibliography		145

List of Figures

1.1	Sensory pathway and cortical mapping in the primary somatosensory cortex.	12
1.2	Action Zones in the Motor Cortex of the Monkey	14
1.3	Sensory-motor connectivity in mice	15
1.4	Taxonomy of Bottom-Up Sensory Feedback Processing To Guide and Select Motor Actions.	18
1.5	The rodent whiskerpad	20
1.6	Topographical organization of tactile sensory pathways	22
1.7	Cortical maps in the primary visual cortex	25
1.8	Primary auditory cortex and higher visual areas	26
2.1	Cortical neurons operant conditioning	30
2.2	Prominent spontaneous activity patterns are more easily conditioned.	33
2.3	Cortical maps plasticity	35
3.1	Spatio-temporal resolution of the different techniques for human brain readout	39
3.2	Idealized bidirectional brain-machine interface for prosthetic control.	41
3.3	A point-process approach for motor command in a BMI task.	43
4.1	A closed-loop BMI with incremental control and optogenetic feedback.	98
4.2	BMI learning example with physiological latency and incremental control.	100
4.3	Neuronal strategy of solving the BMI task for one mouse.	102
4.4	Cortical activity generated by rotation of an object in the whisker array.	108
4.5	Switching to 200 ms latency for a trained animal	110

Foreword

This thesis aims to optimize the delivery of cortical feedback in a closed-loop sensorimotor brain-machine interface. Of course, this theme in itself is extremely vast, as in this kind of device, there are a lot of variables that one can play with. This thesis concentrates mainly on two aspects of this optimization: First, the impact of the spatial distribution of the cortical stimulation. Second, the importance of the closed-loop latency of the system, meaning the time-lapse between the brain message generating the movement and the delivery of the corresponding feedback cortical stimulation.

To help the reader understand the context of the studies presented in the methods and results section, I start by introducing the sensory motor system in Part I, focusing on the cortex. In the first chapter of the introduction I spend some time detailing the model used in the following studies, namely the whisker system in rodents, and describe the interesting cortical topographical organizations in primary cortical areas. The second chapter describes the plasticity mechanisms that could be at play during brain-machine interface learning and their limits. As in the first chapter, I emphasize on plasticity occurring at the cortical map level, and more specifically what happens for the somatosensory cortex. In the last chapter of the introduction, I explain how all of this is exploited with brain-machine interfaces, describe the recent breakthroughs that were made in this field with a few examples, as well as the main difficulties and challenges that the BMI community faces.

In Part II, the main results yielded by this PhD are presented, in the form of a series of articles, each of them with a short presentation. The last study aims to directly compare learning with different latencies, is still at its early stage, and will be completed to achieve reproducible and well controlled results. Finally in the Discussion, we place our work in the general framework and literature on the BMI field, and discuss the perspectives of this work. Two additional articles to which I contributed but not directly related to my PhD project are added in the Appendix.

Part I

INTRODUCTION

Chapter 1

A spatio-temporal sensorimotor integration

1.1 A natural closed loop system

Movement is continuously shaped by sensory information. To explore an environment, find food and perform most actions, animals need sensory feedback (Scott, 2016; Ahissar and Assa, 2016; Sauerbrei et al., 2020). In humans, proprioception is crucial for limb positioning, while touch is critical for object manipulation. In fact, loss of proprioception and touch can be disastrous, as observed in somatosensory-impaired patients who do not "feel" their body (Sacks, 1985; Chesler et al., 2016; Cole, 2016). Sensorimotor closed-loop control is needed for maintaining posture and moving in space, but also for fine dexterity to manipulate objects precisely (Johansson and Flanagan, 2009). The human's body thus permanently integrates in close-to-real time feedback from the outside to correct motor commands. These adjusted motor commands in the brain generate efferent copies who are then re-injected in the loop and compared with sensory inputs to correct movement. To perform this loop correctly, brain messages are not only timed very precisely, but are also spatially constrained through topographical structures. In this first section, the anatomy and functionality of this natural sensorimotor system will be described non-exhaustively, with some examples of research conducted with humans, monkeys and rodents.

1.1.1 From the exterior world to the cortex

Our body is filled with sensors which provide us information about the world which surrounds us. Specifically, tactile information is encoded by somatosensory neurons. The peripheral branches of these neurons innervate the skin and transduce mechanical stimulus into action potentials. Very quickly, the mes-

sage is transmitted by a chain of three neurons, going through the brainstem, the thalamus and terminating in the parietal lobe, in the primary somatosensory cortex (Figure 1.1 (A)). In the somatosensory cortex, a mapping of the entire body emerges. This mapping was first observed with electrical microstimulations (Penfield and Boldrey, 1937). The "homunculus" described is a deformed, continuous representation of the entire body (limbs, hands, face) as if printed on the cortex (Figure 1.1 (B)). The representation of each part of the body is roughly proportional in size to the complexity and diversity of the sensory information that this body part is supposed to convey. For example, the representation of the hand and fingers is highly disproportional compared to its size in the exterior world. Apart from this anatomical description, the exact use of the sensory cortex and the internal computations that it makes remain unclear. While the standard view sees the somatosensory cortex only as a sensory map, there is evidence that its function is not as simple (Brecht, 2017): First, lesions of the cortex in rats and humans have shown that the cortex is not necessary to feel objects, at least for crude sensations. Second, with some reorganization of intracortical connectivity, the cortex is capable of generating "phantom limbs" even in the absence of peripheral nerves, going beyond the role of a one to one sensory map.

As for the proprioceptive messages, which provide information about self movement and body position, they rely on the activation of proprioceptors : muscle spindles, Golgi tendon organs, and joint receptors. The message also ends up in the somatosensory cortex. In particular, Brodmann area 3a of the human somatosensory cortex responds mainly to the stimulation of these proprioceptors. For the mouse, this is less obvious and it is thought that proprioceptive inputs are handled in a more diffuse manner.

1.1.2 The primary motor cortex and its role in motor commands

On the motor side, it is known that proper sensory and motor function involve many cerebral areas as the cerebellum, the basal ganglia, the thalamus, and several cortical areas... In particular, generating optimal sequences of movement relies on higher order motor centers, including the primary motor cortex (M1). Just like with the somatosensory cortex, Penfield mapped a "motor homunculus" through direct microstimulations of the cortex.

Even though the function of M1 is still hotly debated (Omrani et al., 2017), there is ample evidence that motor cortex controls the initiation of voluntary

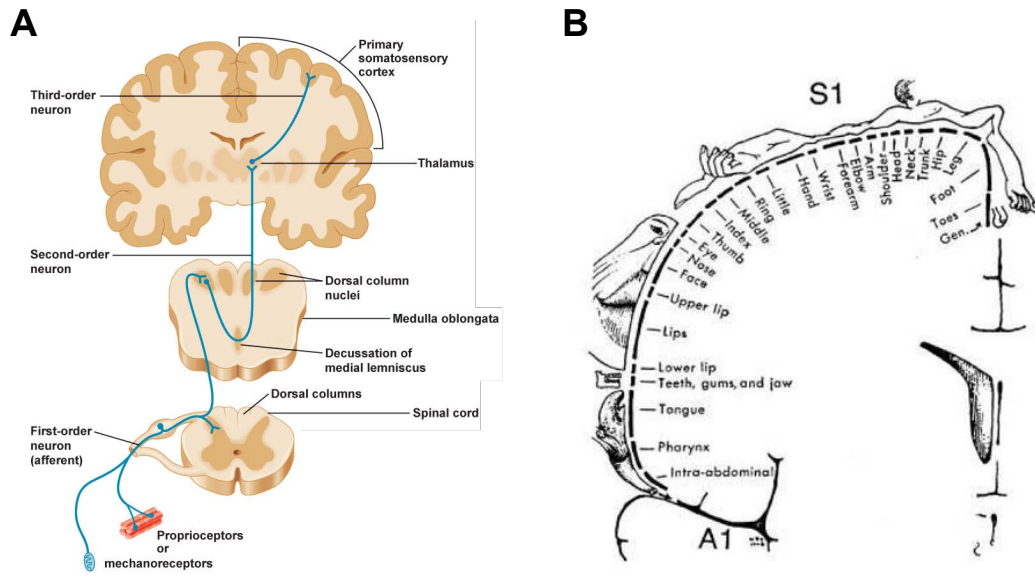


Figure 1.1: Sensory pathway and cortical mapping in the primary somatosensory cortex.

(A) Touch and proprioceptive sensory pathway adapted from 2011 Pearson education.

(B) Homunculus described by Penfield in 1937.

movement. For example, microstimulations of M1 elicit movement of body parts in humans (Penfield and Boldrey, 1937), monkeys (Graziano and Aflalo, 2007) and rodents (Petersen, 2014), while inactivation of M1 blocks voluntary movements (Guo et al., 2015). Analysis of the spiking activity of M1 neurons shows that neurons are individually tuned to movement parameters, and that distinct output patterns of subpopulations of M1 neurons take place during distinct motor actions (Georgopoulos et al., 1986). These output patterns lead to muscle activations via several direct and indirect pathways. As far as to what exactly the M1 neurons are tuned best, although most agree that the primary motor cortex is useful for complex motor commands (Lawrence and Kuypers, 1968), there are still several approaches:

First, some researchers tend to correlate directly the activity of the primary motor cortex with the subsequent contractions in the different muscles. In 2003, Sergio and Kalaska (Sergio and Kalaska, 2003) trained monkeys to exert force, in a static fashion, with their arm in 8 different directions and from eight different positions, while recording single neurons in the caudal part of M1. Their main hypothesis was that if motor activity could depend on arm posture, it could be implicated in the transformation of internal models of motor commands into patterns of muscle activation. They showed that, while the recorded neurons were broadly tuned to force in specific directions, this

was also the case for muscle activity as these two are intrinsically correlated already. More importantly, just as muscle activity, they showed that neuronal activity was strongly dependent on the arm position, in term of firing rates and in term of direction tuning, supporting their theory. In fact, firing rates in M1 were often shown to be correlated with movement parameters, such as distance, speed or even curvature.

Second, other models put the primary motor cortex in control of higher level movements, representing specific behaviors. Specifically, it has been show that electrical stimulation of M1 with relevant, long time scales was accompanied with complex, reproducible behavioral repertoires with similar final postures (Figure 1.2). The postures surprisingly did not depend on the direction of the movement (Graziano et al., 2002). One striking example of behavior induced by stimulation was a combination of approaching a gripped hand to the mouth while opening the latter at the same time. For each of these behaviors, the monkey froze at the final position until the stimulation was over. Notably, it was shown later that these movement could adapt to perturbations, materialized by added weight on the arm. (Graziano et al., 2005).

Third, it has been suggested that measuring the activity of individual M1 neurons was not enough to decode motor intent. Indeed, single neuron variability is often difficult to interpret, so more complex mathematical methods analysing the activity of large amount of neurons are needed. Following this logic, by looking at principal component projections of the neuronal activity to extract the most orthogonal informations out of the multidimensional data, it was shown that the neural state of monkeys follows a rhythmic, rotational and highly reproducible structure when doing a simple reaching task. Interestingly, this rotational structure could not be seen when applying this analysis on standard models, for which neural activity would encode direction, speed, or other kinematic variables (Churchland et al., 2012). Going further, it was shown later with a novel decision task, during which a monkey needed to spend some "preparatory time" visualizing the movement that had to be done, that M1 activity before movement could be decoded to predict the latter. Analysing this activity with a linear classifier, even hesitation by the monkey during the preparatory time could be detected (Kaufman et al., 2015).

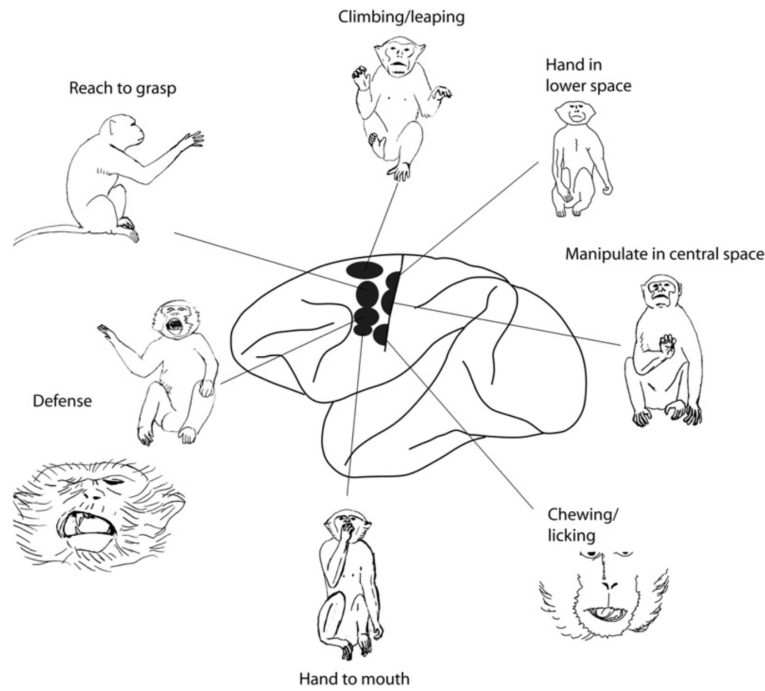


Figure 1.2: Action Zones in the Motor Cortex of the Monkey (Graziano and Aflalo, 2007).

These categories of movement were evoked by electrical stimulation of the cortex on the behaviorally relevant timescale of 0.5 s. Images traced from video frames. Each image represents the final posture obtained at the end of the stimulation-evoked movement. Within each action zone in the motor cortex, movements of similar behavioral category were evoked. Action zones in the motor cortex of the monkey described in (Graziano et al., 2002, 2005)

Beyond movement generation, the role of M1 is especially prominent for learning a new motor skill (Kawai et al., 2015). Our brain can indeed learn to generate complex motor commands while integrating seamlessly sensory cues enabling us to reach an exquisite level of precision of our body movements. Recent studies suggest that these procedural memory engrams first form in the sensorimotor cortex, and later transfer to other parts of the brain as movement become highly stereotyped.

1.1.3 Sensory-motor cortices connectivity

In most mammals, S1 and M1 are distinct but adjacent to each other. Their topography is arranged in a mirror image and they are heavily and reciprocally interconnected. In humans, the primary somatosensory cortex and the primary motor cortex are connected through anatomical connections, short U-shaped fibers beneath the central sulcus (Catani et al., 2012). These anatomical connections are organized according to the topographical structure of these two cortices. Beyond the anatomical descriptions, these connections clearly have a

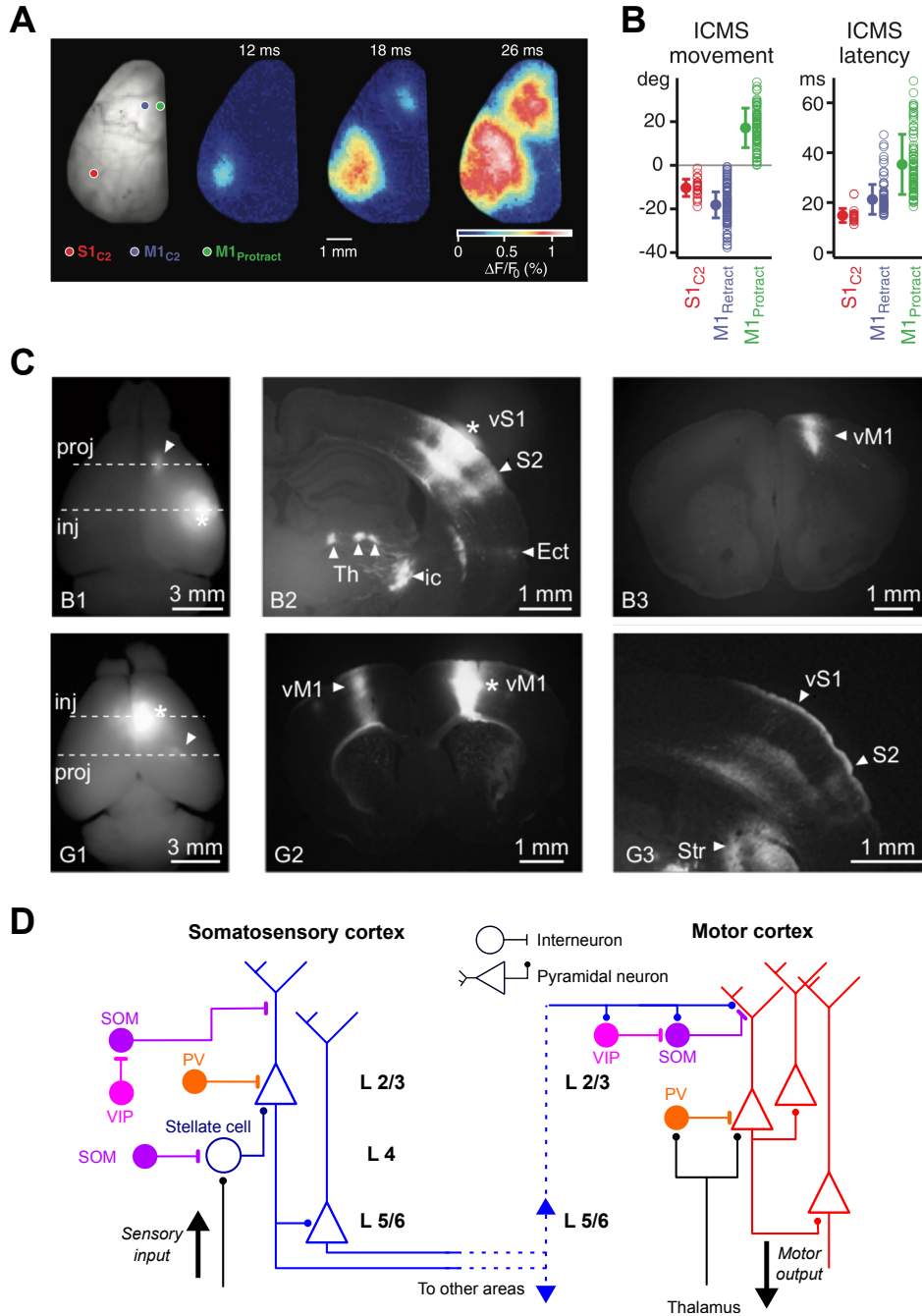


Figure 1.3: Sensory-motor connectivity in mice

(A) VSD imaging after a single whisker deflection, adapted from (Matyas et al., 2010) and similar to (Ferezou et al., 2007).

(B) Movement amplitude and latency evoked by ICMS of S1-C2, M1-protract and M1-Retract (Matyas et al., 2010).

(C) Up : Injections in vS1 and projections to vM1. Image B1: AAV-tdTomato injected into vS1 (asterisks) and projection to vM1 (arrowhead). Dashed lines correspond to the sections containing the injection site in vS1 (inj) and the projection site in vM1 (proj). Image B2: Coronal section through the vS1 injection site (asterisk). Image B3: Coronal section through vM1. Down: injections in vM1 and projections to vS1. Image G1: AAV-eGFP injected into vM1 (asterisks) and projection to vS1 (arrowhead). Dashed lines correspond to the sections containing the injection site in vM1 (inj) and the projection site in vS1 (proj). Image G2: Coronal section through the injection site (asterisk) and projection to contralateral vM1. Image G3: Coronal section showing vS1. Adapted from (Mao et al., 2011)

(D) Non-exhaustive schematic of neuronal connections from the primary somatosensory to the primary motor cortex in rodents. Descriptions coming from (Petersen and Crochet, 2013; Papale and Hooks, 2018; Chen et al., 2015b).

functional role: A study with Autism Spectrum Disorder patients, (Thompson et al., 2017) suggests that this direct connection between S1 and M1 is necessary to interact finely with the environment.

In rodents, this connectivity has already been exhaustively described (Ferezou et al., 2007; Mao et al., 2011). There are direct axonal projections connecting functionally the whiskers with S1 and then M1, while stimulating electrically the primary somatosensory cortex (whiskers) generates whisker retraction with low latencies (Matyas et al., 2010) (Figure 1.3 A, B, C)), suggesting that the primary somatosensory cortex would send direct whisker retraction commands to the muscles.

Interestingly, the anatomical connections between S1 and M1 are segregated. From S1 to M1, most connections come from layer 2/3 and 5a in S1, from extragranular cells vertically aligned with the layer 4 septa (Alloway et al., 2004), and project mostly to layer 2/3 and 5a neurons in M1. From M1 to S1, monosynaptic connections mainly originating from layer 2/3 and 5a neurons project to deep layers neurons in S1 (5a and 5b) (Petreanu et al., 2009).

In the meanwhile, interneurons VIP (and other ionotropic serotonin receptor expressing neuron), SOM and PV interact to play a role in shaping sensory inputs and motor output (Example connection in Figure 1.3 D). Although their exact role remain unclear, several hypotheses have been suggested, beyond the role of providing simple neuronal stability, such as influencing the timing of signals through feed-forward inhibition.

On the behavioral level, these excitation/inhibition processes and sensory messages in the motor cortex are supposedly guiding motor behavior to initiate movements (Zagha et al., 2015). Specifically, these connections are also reshaped by the learning of a sensorimotor task (Chen et al., 2015a). These plasticity processes will be further explored in chapter 2.

1.1.4 Delays in the control system

Just like in any other system, sensorimotor communication between the muscle and the central nervous system (CNS) takes time. While the somatosensory system computes information, on average, faster than the visual system (around 30 ms faster), sensorimotor information processing and sending corrections to the CNS still takes a significant amount of time. On the motor

side, the creation of an internal feedback model through efferent copies (supposedly in the cerebellum (Wolpert et al., 1998)) may be useful to make the computations faster, by comparing this efferent copy with sensory mismatches. Nevertheless, the propagation of the information from the CNS to the muscle still takes dozens of milliseconds. Of course, at least in lower mammals, most casual sensorimotor tasks don't require much use of the cortex and can rely on computations made directly by the spinal cord and brainstem, just like locomotion and most reflexes (DiGiovanna et al., 2016).

Sensorimotor tasks each run with its specific latency range, which depend on the complexities of the computations needed to generate and correct the appropriate movement (Scott, 2016). In this review, the author describes the different computations and timings needed by the motor system to integrate sensory feedback (Figure 1.4). In the muscles, three differentiable electromyogram (EMG) signals can be recorded after inducing an external perturbation, R1 signal being the first to arrive in around 25 ms, R2 in 50 and R3 in around 75 ms. On the other hand, after a cue to trigger a movement, the subject needs to switch from a controlled postural static position to the initiation of movement. In that case, it takes relatively longer to trigger EMG signals in the muscles, starting from 120 ms for a simple reaction time. As such, a fast stretch response will trigger after 25 ms (R1), while a motor response involving a choice will take longer, around 170 ms.

On the behavioral side, the results are less clear, but also seem to strongly depend on the task. With a reciprocal tapping task, it has been shown that a delay in haptic feedback can be disruptive if it is above 200 ms, while delays in the visual feedback are far more problematic starting from around 70ms (Jay and Hubbard, 2005). However in a tracking task, it seems to be the opposite with haptic feedback delays having an impact on performance as early as a 25 ms delay (Jay et al., 2007).

All in all, although these different timings and delays seem to be a mere consequence of physiological constraints that are imposed on our central nervous system to transfer and compute information, they could have a critical role in the operation of the sensorimotor loop. As such, they should not be set aside when studying sensorimotor mechanisms. This will be very important for the last study of this thesis, in which we aim to evaluate the impact of latency in a closed-loop sensorimotor brain-machine interface.

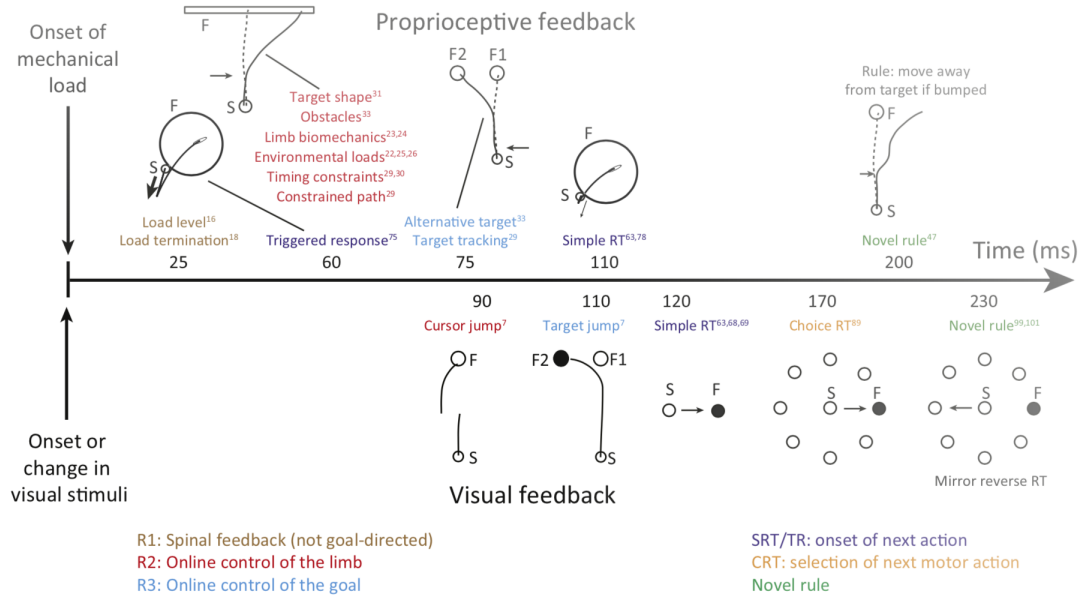


Figure 1.4: Taxonomy of Bottom-Up Sensory Feedback Processing To Guide and Select Motor Actions (Scott, 2016).

Timeline denotes the time from a sensory stimulus (mechanical or visual) to motor response [electromyogram (EMG) signal onset] of arm muscles related to each factor. Somatosensory and visual information support similar functional classes, although slightly delayed for the latter because of retinal processing. Each color denotes a functional class of feedback processing. Inset diagrams illustrate specific examples on the use of bottom-up sensory feedback processing. Arrows for proprioceptive feedback reflect the load (and its size) applied to the limb. Broken lines denote an unperturbed movement and an unbroken line denotes a movement when a load was applied. Filled circles denote that a visual target was shifted during movement (target jump) or when it was illuminated to initiate a movement [reaction time (RT) tasks]. Arrows for visual feedback examples denote direction of hand movement. S and F denote the start and final spatial goals, respectively. For online control of the goal, F1 is the initial target that is jumped to F2 during movement. Superscripts denote references related to each class or type of corrective response.

1.2 The whisker system in rodents

Although non-exhaustively, we described in the previous section some main aspects of the sensorimotor system in mammals, as well as some questions that remain unanswered. We shall now focus on the specific sensorimotor system that will be at the core of our study, the mouse whisker sensorimotor system, and describe more specifically its anatomical and functional aspects. Mice have the reputation to have a poor visual system, and unlike humans, do not have a fovea. To compensate for this poor vision, mice use their whiskers to probe their environment. They use them to investigate new objects, for navigation, as well as for social interactions (Sofroniew and Svoboda, 2015).

1.2.1 In the follicles

In rodents, whiskers are organized in rows (A, B, C, D and E) and columns (1, 2, 3, 4...). The most posterior column of whiskers is composed of the straddlers (alpha, beta, gamma and delta), which are the biggest whiskers in the pad (Figure 1.5 A). Each whisker emerges out of a follicle. By applying a force on the whisker shaft, the whisker inside the follicle will bend in a S-shaped fashion (Ego-Stengel et al., 2019; Luo et al., 2021), activating several sensory mechanoreceptors.

Similar to the human, the sense of touch by mice whiskers starts with transduction by mechanoreceptors. Throughout the follicle, several types of mechanoreceptors can be found (Rice et al., 1993; Ebara et al., 2002, 2017): Merkel endings mostly in the upper and middle parts of the follicle, Reticular endings in the lower parts, club endings within the ringwulst of the follicle, and several others (Figure 1.5 B). Some of these mechanoreceptors are useful for touch, while others are designed for sensing stretch, pressure vibrations, or even orientation (Tonomura et al., 2015). These follicles are innervated with two different types of nerves, non-myelinated superficial ones and deep, mainly myelinated ones. These nerves transfer the information from the mechanoreceptors to the next step, the trigeminal ganglions (TG).

1.2.2 From the periphery to the cortex

After action potentials in TG neurons are triggered by these mechanoreceptors, the information travels through 3 different pathways: the lemniscal pathway, which is the major pathway, the extra-lemniscal pathway, and finally the par-lemniscal pathway. Briefly, throughout the lemniscal pathway, information

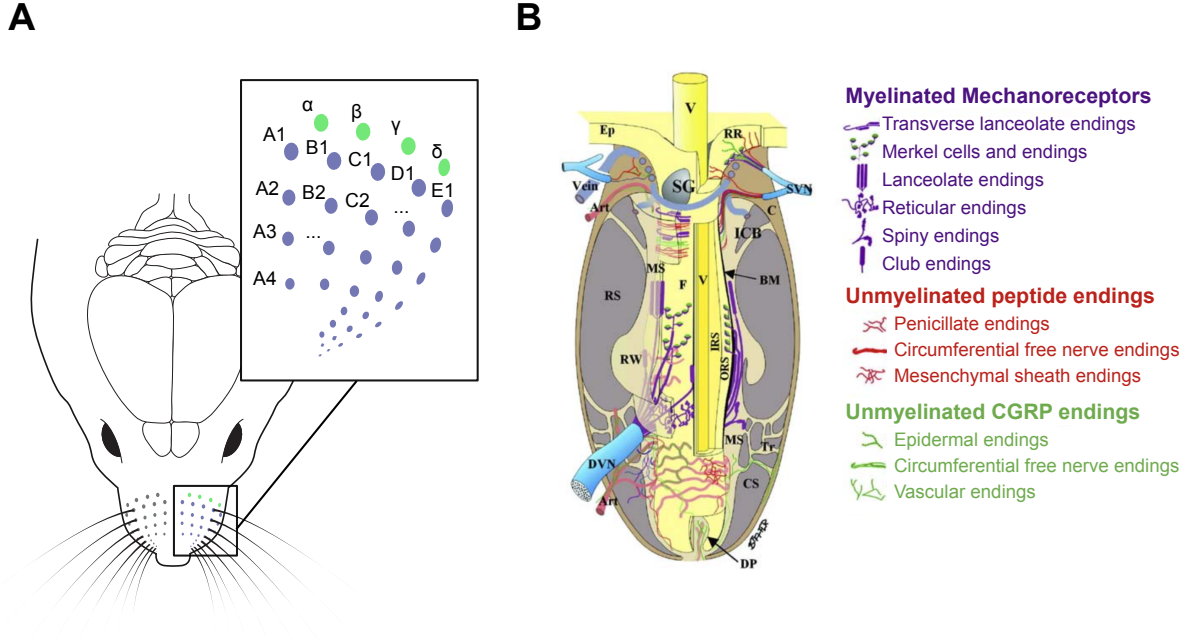


Figure 1.5: The rodent whiskerpad

(A) Organization of the whiskerpad.

(B) Schematic of the internal structure of the follicle with the different mechanoreceptors and nerves, adapted from (Staiger and Petersen, 2021).

travels through the PrV nucleus in the brainstem, then the core part of the ventro-postero-medial nucleus of the thalamus (VPMdm), and finally projects mostly to the layer IV of the whisker primary somatosensory cortex, the barrel cortex (vS1) (Figure 1.6 A). The extra-lemniscal pathway passes through another nucleus of the brainstem, the SpV, and similarly also by the VPM but this time in its "tail" part (VPMvl), before ending in vS1 and S2. Lastly, the paralemniscal pathway travels through the SpV, then the postero-medial nucleus in the thalamus (PoM), and at last vS1 and S2 (Figure 1.6 A). These 3 different pathways are thought to have complementary roles in shaping sensorimotor processes (Yu et al., 2006).

One striking feature of these different pathways is how the topographical organization of the whiskers in the snout is conserved while the sensory message travels, and can be seen anatomically, in the form of "barrelettes" in the brainstem, "barreloids" in the thalamus and finally the well known "barrels" in vS1 (Figure 1.6 B, C). They can be revealed easily through cytochrome oxydase staining of brain slices. These anatomical structures each respond preferentially to a specific whisker, e.g. its principal whisker, and are arranged in the same fashion as the whiskers on the snout, following the same nomenclature.

While the lemniscal pathway mainly project onto the barrels themselves, the other two pathways mainly project onto the space in between these structures, the septa.

Specifically, the cortical region containing the barrels in layer IV is remarkable. Although the first thorough description of barrels was done fifty years ago (Woolsey and Van der Loos, 1970), it quickly became one of the most studied cortical region in the mouse model to study the cortical processes behind tactile information. Following the work of Hubel and Wiesel for sensory coding in the primary visual cortex (Hubel and Wiesel, 1959), similar work was done in the barrel cortex, showing that neurons in the barrel cortex could respond selectively to low level features, such as orientation, velocity, amplitude, vibration frequency... (Estebanez et al., 2018). However, most simple computations done by the whisker system do not require the use of the cortex, In fact, most behavioral studies of barrel cortex suggest that it is necessary for placing and recognizing tactile objects in a complex environment, or following a specific timing. All in all, it suggest that the cortex computes a spatio-temporal integration of sensory inputs to guide complex behaviors, notably by integrating multi-whisker information.

1.2.3 A topographical sensorimotor integration in the whisker motor cortex

Be it in humans or in mice, active movements often lead to tactile inputs. These sensory inputs are then processed in order to adjust future trajectories of movements. To support this sensorimotor integration, there is a need for strong connectivity between the sensory and motor cortices (as already mentioned in (Figure 1.3). Interestingly, in the mouse whisker cortices, these sensorimotor anatomical connections are also arranged topographically (Ferezou et al., 2007). In this context, single deflections of whiskers were performed while recording the activity of the primary motor cortex (M1) with voltage sensitive dye. And indeed, a topographical map of whisker emerged, although smaller than the whisker barrel cortex in S1. For whiskers, the primary motor cortex is mostly characterized by two distinct areas (Matyas et al., 2010; Ferezou et al., 2007; Haiss and Schwarz, 2005), which differ by the behavior induced by their respective electrical microstimulations : One of them corresponds to a retraction of the whisker pad, while the other corresponds to its protraction. Interestingly, the "sensory" topographical map in M1 is located in between these two representations.

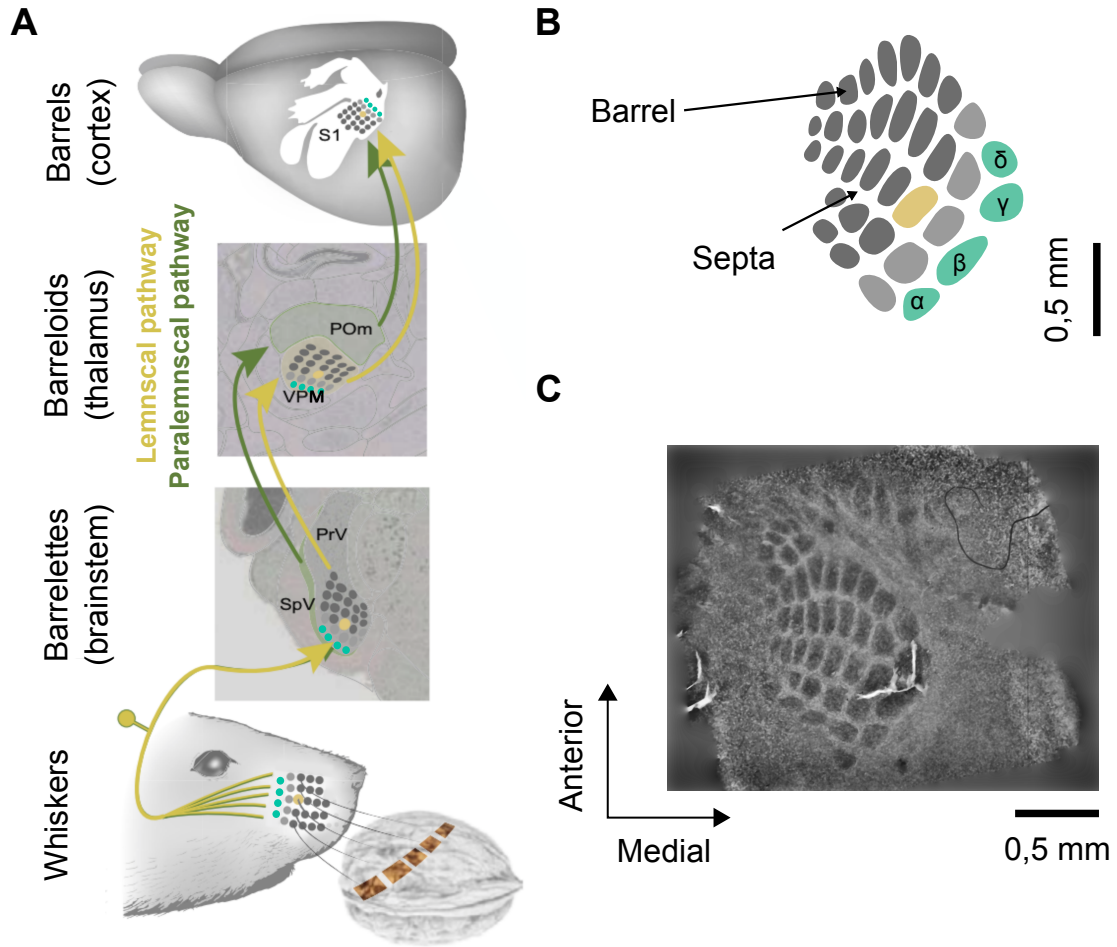


Figure 1.6: Topographical organization of tactile sensory pathways

(A) Sensory pathways for whisker tactile inputs, adapted from (Staiger and Petersen, 2021).
 (B) Schematic of the organization of the whisker barrel cortex.
 (C) Histology reconstruction of the whisker barrel cortex, with cytochrome-oxidase marking of brain slices, using a homemade software from the lab of Daniel Shulz (Perronnet et al., 2016).

1.2.4 Multi-whisker integration

The receptive fields of individual barrel cortex neurons often turn out to encompass several whiskers, depending on the stimulation context (Jacob et al., 2008; Le Cam et al., 2011). This is far from the one-to-one relation that would most likely emerge from a dominant role of the topography (Estebanez et al., 2018). In fact, even at the level of the whisker pad, the mechanical coupling between different whiskers through the skin suggests that further computations need to be done to extract relevant information from peripheral stimuli (see Supplementary Article 2, Ego-Stengel et al. (2019)). Beyond the encoding of whisker identity, barrel cortex neurons tuning to other features such as

stimulus phase and multi-whisker coherence (Estebanez et al., 2012) do not follow a one-to-one relationship, and are organized either in a barrel-centered fashion (Andermann and Moore, 2006; Kremer et al., 2011; Estebanez et al., 2016), or in a salt and pepper fashion (Kerr et al., 2007). Increasingly, the functional properties identified in the rodent barrel cortex can be compared to the ability of the primary visual cortex of cats and monkeys to capture spatial features in a complex visual scene. Not only do barrel cortex neurons carry low-level feature selectivities including whisker direction and phase sensitivity, but also higher order multi-whisker selectivities including center-surround and edge detection. Although these findings deconstruct the notion that the topographical organization of the barrel cortex could underpin most of the barrel cortex neuronal selectivities, evidence stemming from work done in V1 suggest that mechanisms based on the lateral propagation of cortical activity through a topographically structured cortex can provide a prediction of upcoming stimulus displacements within the visual field (Muller et al., 2018).

All in all, although the barrel cortex function seems to do so much more than to respond to single whisker stimulation, it still segregates its activity into clusters of neurons in layer IV, shortly after a peripheral stimulation. Each cluster relates to one whisker, and is organized in an orderly fashion closely resembling the organization of the whiskerpad. Why ? Is it a mere consequence of early development or is there a functional reason to it ?

1.3 Topographical organization for different primary and secondary areas

In this part, we will describe the similarities and differences between primary cortices of different modalities, touch, vision and audition, and see that in fact, topography is not specific to tactile and motor modalities. Unfortunately, even if these "cortical maps" were described, their function and the reason for their emergence is still debated (Kaas, 1997).

1.3.1 Retinotopy, a topography in the visual system

Ever since the early 20th century and WW1, both the British neurologist Gordon Holmes and the Japanese doctor Tatsui Inouye were the first to study war head wounds of the occiput to provide insights on the mapping between the retina and the primary visual cortex (V1) (Fishman, 1997). Even if there were some mistakes in the first characterization of the "cortical retina", such as the lack of magnification of the central vision on the cortex (15 degrees

of field occupy about 70 percents of the striate cortex), the remarkable mapping of the visual cortex that is retinotopy was unveiled: It became clear that the visual space is represented topographically and continuously on the cortical surface. This map was further refined with the pioneering studies by Hubel and Wiesel on receptive fields of individual neurons (Hubel and Wiesel, 1959, 1962). Using light stimulation of the retina with simple light spots of different shapes, they managed to demonstrate several keystone properties of individual neurons receptive fields, including orientation selectivity and ocular dominance. In fact, although its mapping is continuous and not discrete, the topographical arrangement of V1 resembles the barrel cortex due to its visual space/cortical space correspondance. Interestingly, the primary visual cortex also features other just as important overlapping mesoscopic maps, such as the orientation map, the ocular dominance map, direction selectivity, spatial frequency... (Figure 1.7).

Another striking common characteristic of both the whisker barrel cortex and the primary visual cortex lies in their similar columnar architecture with thalamocortical afferents, which synapse mainly in layer IV, then project onto layer II/III, and finally spread to the rest of the cortical layers. These cortical columns, corresponding barrels in the somatosensory cortex, were believed to form single cylindric cortical units that efficiently treat a specific information (Mountcastle, 1957). However, it has been shown that even within a single cortical column, receptive fields of different neurons can differ in size and selectivity depending on the layer they belong to (Gilbert, 1977; Gilbert and Wiesel, 1979).

Mouse vision is thought to be very different to that of humans, notably because of the lack of of proper fovea, meaning a region of the retina for which the resolution is much better than for the rest of the visual space. Because of this, mice and rats are thought to scan their surroundings in a grossly fashion, without concentrating on small details. Interestingly, their primary visual cortex is organized in a very similar fashion as humans in terms of topography (Figure 1.7 A, B). However, a zone in the mouse visual cortex for which population receptive fields are much smaller was recently discovered, the "fovea", similar to the fovea in humans, showing that the mouse model for studying vision may not be as bad as claimed previously (van Beest et al., 2021).

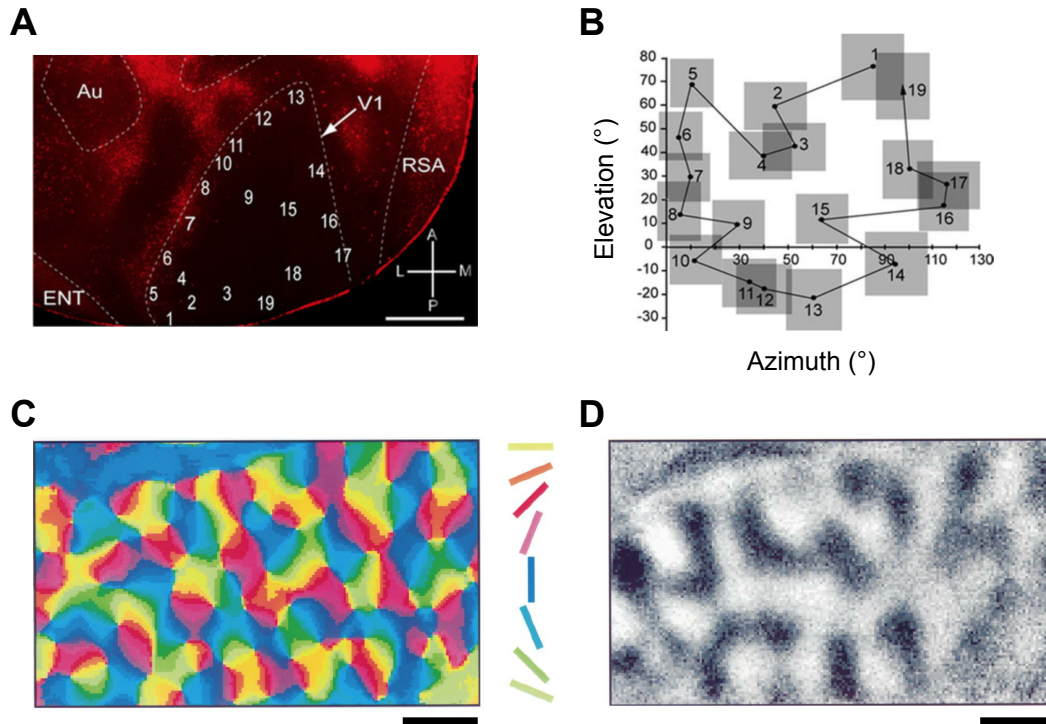


Figure 1.7: Cortical maps in the primary visual cortex

(A) Flattened left mouse occipital cortex showing callosal connections labeled by axonal tracing with fluororuby (red). Numerals indicate recording sites in V1, whose receptive fields are shown in B (Wang and Burkhalter, 2007).

(B) Plots of receptive fields recorded in left V1 after stimulation of right visual hemifield. Numerals correspond to recording sites shown in A.

(C) Orientation preference map in cat visual cortex. The angle of the preferred orientation is color-coded according to the key shown on the right. Orientation domains are organized in a pinwheel-like manner. Scale bar 1 mm (Hubener et al., 1998). Note that the center of this pinwheel are, in a sense, topographical discontinuities of this map.

(D) Ocular dominance map in cat visual cortex. Black codes for contralateral and white for ipsilateral eye preference. Scale bar 1 mm, same patch of cortex as in C (Hubener et al., 1998).

1.3.2 Tonotopy and higher visual areas

In the auditory cortices, in opposition to touch and vision, sound frequency alone does not give information about the layout space of the exterior world. Still, the auditory cortex is organized topographically. Although a debate still remains on the exact definition of each different zone in the auditory cortex (Tsukano et al., 2015), see also (Ceballo et al., 2019), it remains clear that the auditory cortex is split into different areas, each of them topographically organized through a tonotopic gradient, from low to high frequency (Figure 1.8 A). As for higher visual areas, it has been shown in mice that the primary visual cortex actually projects directly onto 9 other different topographic maps (Figure 1.8 A). Although they seem to contain a complete representation of

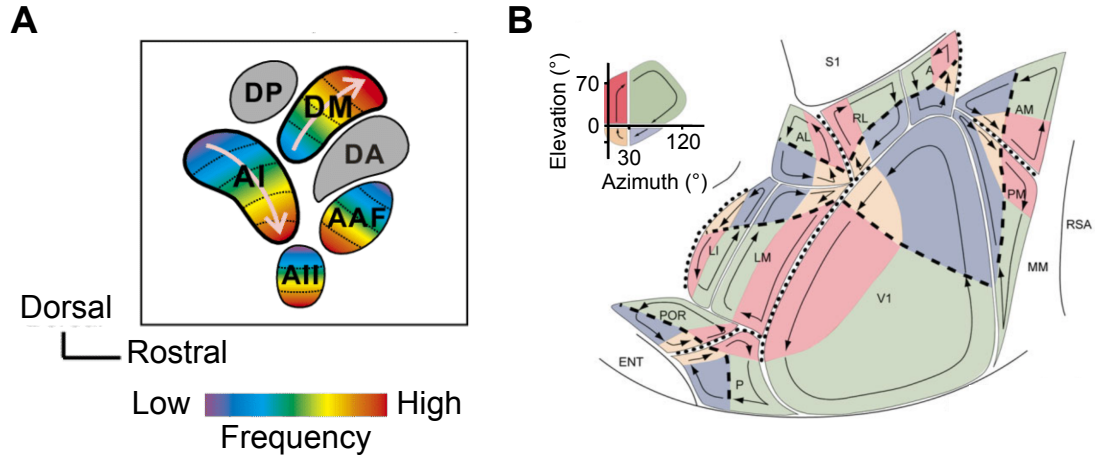


Figure 1.8: Primary auditory cortex and higher visual areas

(A) Schematic maps of the mouse auditory cortex in (Tsukano et al., 2015).

(B) Visuotopic maps of striate and extrastriate areas in mouse visual cortex. The maps were constructed by tracing the intracortical connections of known visuotopic locations of V1. The different quadrants of the visual hemifield are color coded (inset). Arrows indicate the orientation of the maps as shown in the inset. Each area contains a complete and orderly visuotopic map, which is topologically equivalent to the contralateral visual hemifield. Note that the visuotopic maps are registered across areal borders to minimize map discontinuities. Adapted from (Wang and Burkhalter, 2007).

what happens at the level of the retina, their receptive fields seem much bigger than those in V1 (Wang and Burkhalter, 2007) (as V1 occupy much more space) , and their map is more likely to be a deformed, poor representation of spatio-visual information compared to V1.

In this first chapter, we have described rapidly the main characteristics of sensorimotor integration, and more specifically highlighted that both timings and topographical aspects of sensory and motor cortices seem crucial for brain computations. Following these principles, different cortical maps emerge for different modalities, as each cortex seems to minimize spatial discontinuities across variables to optimize its computations. In the next part, we will focus on a very specific phenomenon at the very core of our study which can change these maps to fit the environment, or even give a new purpose to whole parts of the brain: Plasticity. In our study, plasticity is critical for both sensory and motor aspects, as we aim to study integration and learning of novel stimulations, while observing neuronal changes in the primary motor cortex during a sensorimotor task.

Chapter 2

Plasticity in the brain and its limits

Whenever we walk, whenever we play the piano or taste good cheese, our brain changes to fit the environment. Among other mechanisms, synapses all over our nervous system are constantly reinforced or weakened as we learn and experience life. Plasticity is a core feature of the nervous system as it makes sensorimotor learning possible, is considered a primary mechanism for memory consolidation, and is responsible for rewiring the brain in case of traumatic injury. For the record, it could even permit a man, Phineas P. Gage to live for years after an iron rod was literally driven through its frontal lobe, although with a strong personality change (Van Horn et al., 2012). Beyond this specific old case for which the role of plasticity is not very clear, harnessing plasticity for medical purpose is one of the main challenge of the twenty-first century, be it for trying to restore lost functions after a spinal cord injury or to limit the effect of neurodegenerative diseases. Indeed, it has been shown that plasticity is lower in the dorsolateral prefrontal cortex for early Alzheimer disease cases (Kumar et al., 2017), but is also somehow altered in patients with migraine, dystonia, schizophrenia, Parkinson’s disease... In our study, the limits of plasticity in the sensorimotor cortices is tested, to see the brain’s adaptation to artificial feedback delivery, as well as the neuron’s ability to change its firing patterns to drive an actuator.

2.1 Plasticity at the neuronal level

Plasticity can be evaluated at different scales. ”Small” neuronal changes in connections and function can have an impact at a much broader scale. In this first subpart, we will focus on what can happen at the level of a single or very limited number of neurons.

2.1.1 What is plasticity ?

This phenomenon was first put into light in 1949 with the Hebbian theory: "Let us assume that the persistence or repetition of a reverberatory activity (or "trace") tends to induce lasting cellular changes that add to its stability. ... When an axon of cell A is near enough to excite a cell B and repeatedly or persistently takes part in firing it, some growth process or metabolic change takes place in one or both cells such that A's efficiency, as one of the cells firing B, is increased." (Hebb, 1949). Although a bit outdated and not covering all cases of plasticity, it remains clear that long term potentiation (LTP) appears when some neurons fire sequentially and repeatedly. It was then first demonstrated experimentally in 1973 by Bliss and Lomo. We will not go deep into the details of the different mechanisms of plasticity here, but there are several, including the increase of the number of ion channels in the synaptic cleft following repeated stimulation, the sprouting of an axon to reconfigure its connections to the other neurons, or the reorganization of dendritic spines (Xu et al., 2009; Hayashi-Takagi et al., 2015; Chen et al., 2015b; Fu and Zuo, 2011). In these last pioneering studies on mice motor cortex, the researchers managed to very locally identify dendritic spines appearing and disappearing when learning a motor task, and even play with them with optogenetics to disturb the related behavioral task, providing to the scientific community for the first time a causal proof that these plasticity mechanisms are at the origin of motor memory.

Some studies also try causal approaches to test the Hebbian theory by inducing associative plasticity with repeated and timed stimulation of different sets of neurons (Fregnac et al., 1988; Shulz and Fregnac, 1992), and see how it impact the firing rates of these neurons and consequences on behavior (Vetere et al., 2019).

2.1.2 Neuronal operant conditioning

In this part, we will adress a very specific and remarkable type of induced plasticity: Neuronal operant conditioning. It has been long shown that neuronal activity can be modulated/changed if rewarded synchronously with chosen activity patterns. It was first shown with motor units conditioning in the tibialis anterior with Harrison and Mortensen's work (Harrison and Mortensen, 1962) and in the right abductor pollicis brevis (Basmajian, 1963). In 1969, Fetz was the first to show evidence of a possible conditioning of cortical neurons (Fetz, 1969), He recorded units in the precentral motor cortex of monkeys and

rewarded high rates of activity by delivering food pellets. During training, monkeys received some feedback about the current firing rates of the conditioned units, in the form of visual or auditory cues, but feedback alone did not lead to high firing rates, and this conditioning only happened when the feedback was repeatedly correlated with food delivery, and not in naïve animals (Figure 2.1 A). In Fetz's steps, several similar studies (Schmidt et al., 1978; Wyler and Burchiel, 1978) with different kinds of feedback and similar results.

This new paradigm brought new possibilities to neurosciences. Fetz's original purpose was to provide a way to control the cortical activity to correlate it with muscles activity and movement. It now goes way beyond that, as it has been shown that motor cortex neurons similarly fire with imagined movements (Jeannerod, 1995) or movement preparation (Wise, 1985), and that motor neuron conditioning is often dissociated with movement (Carmena et al., 2003). Similarly, it was shown much later that this plasticity was not at all limited to motor cortex neurons, but could also be conditioned in other areas, including the medial temporal lobe (Cerf et al., 2010) or even the primary visual cortex (Neely et al., 2018). In this last study on mice, two groups of neurons of the primary visual cortex, changed each day, drove bilaterally a sound cursor (Figure 2.1 B). Over a few days, the animals learn to get rewards by adjusting the activity of these two groups of neurons and shift the cursor to the rewarded position (Figure 2.1 C, D). Beyond the growing interest of the scientific community towards the mechanism of plasticity reflected in operant conditioning, this approach is also very promising in the field of brain-machine interfaces, tackled in chapter 3. Specifically, our team has long started working in this direction by connecting the motor cortex of rats to the linear position of a water bottle. The water-deprived rat had to adjust the activity of one neuron to bring the bottle close to its mouth to get water (Arduin et al., 2013, 2014). Much more recently, it was shown on epileptic patients implanted with electrodes that neuronal operant conditioning was possible even in memory related structures (hippocampus, amygdala), as 10 out of 17 patients managed to drive a visual cursor with individual neuron activity. Very interestingly, learning was associated with a decorrelation between the conditioned neuron and the other recorded neurons, as well as a local increase of the coherence of the conditioned neuron with the local power in the beta band (Patel et al., 2021). To conclude this part, these studies confirm that operant conditioning of single unit activity is feasible in humans, independently of their original functional properties.

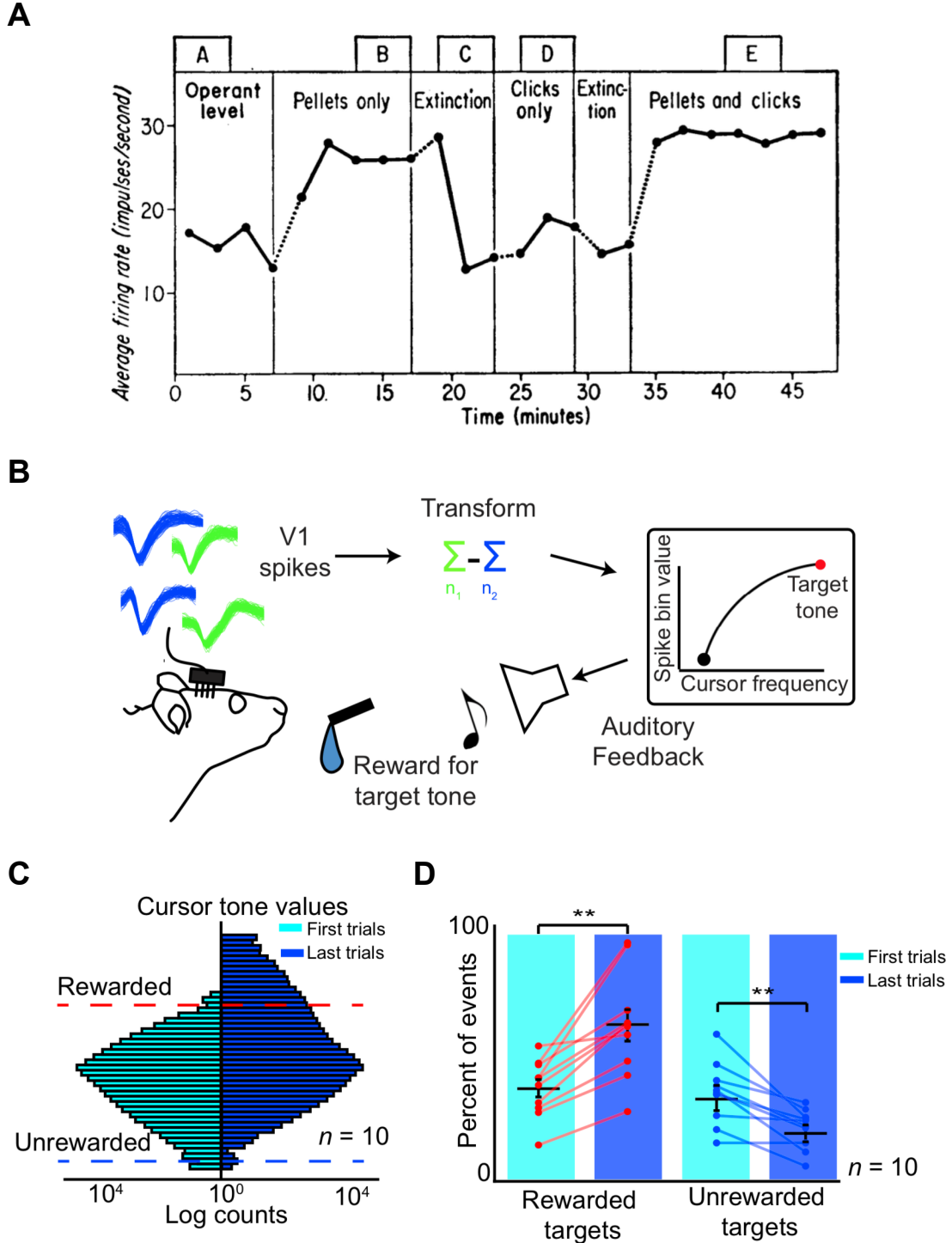


Figure 2.1: Cortical neurons operant conditioning

(A) Firing rate of precentral cortex cell as a function of reinforcement schedule (Fetz, 1969).
 (B) Schematic of a V1-BMI paradigm (Neely et al., 2018). Activity of well-isolated V1 units (top left) were used to generate auditory tones using a differential transform (top right). Animals were rewarded for producing a target tone (red). A second tone (black) at the opposite end of the frequency range terminated the trial but was not rewarded.

(C) Mean distribution of cursor values for all animals for the first trials (first 10 min) compared to the last trials (last 10 min) of sessions during the late period (last 3 sessions). Cyan bars show the initial distribution, based on baseline activity, used to set the task parameters, while blue bars show the distribution at the end of the training session for the last trials. Dashed lines show the thresholds corresponding to the rewarded and unrewarded targets (Neely et al., 2018).

(D) Quantification of rewarded and unrewarded target hits for the first trials the last trials (same as C) for the late period (mean of the last 3 sessions) (Neely et al., 2018).

2.1.3 Tools to promote plasticity

As mentioned above, plasticity has become one of the hot topics in neurosciences, as neuroscientist try to take advantage of it to cure patients and/or understand better. Overall, strategies to induce or to enhance plasticity mostly include neuronal stimulation and/or the use of chemicals. The recent articles of Gregoire Courtine’s lab on spinal cord injuries illustrate successfully and promisingly the potential of harnessing plasticity for the medical field. Precisely, they showed on rats with severe spinal cord injury that electrochemical stimulation of lumbar circuits could not only restore locomotor performance, but reorganize the local circuit to induce a long term cortical dependent recovery of motor functions (Asboth et al., 2018). They soon translated this research on humans, showing that repeated electrical stimulation timed with movement intent promoted locomotion recovery, and that the effect continued even after stopping the neuromodulation protocol (Wagner et al., 2018).

Another method is to provide medication. As many neurological diseases are thought to have a link with a local change in plasticity, researchers have been trying to play with neurons and synapses so that they would be more (or less) subjected to plasticity. So far, many mechanisms which could be targeted to enhance or suppress plasticity have been identified (Nitsche et al., 2012), including modulating the dopaminergic system, the GABAergic system, the voltage-gated ion channels, and many other pathways that could influence the calcium influx. This has led teams to use pharmacological constructs targeting neuroplasticity and study the impact on behavior. For example, tianeptine, an antidepressant modifying spontaneous activity and serotonin recapture in the hippocampus, has been shown to restore hippocampal LTP and memory in mouse model for Huntington’s disease (Zhang et al., 2018). Other studies focus on the consolidation and reconsolidation of memory. Interestingly, LTP is often thought to at least partially depend on the synthesis of proteins (Frey et al., 1988), so some studies manage to impact the recollection of traumatic experience with the use of a protein synthesis inhibitor (anisomycin), in the lateral basal nucleus of the amygdala. This strategy seems to work only if anisomycin was injected right after the reactivation of the memory (Nadel and Land, 2000). Of course, protein synthesis is not the only target of this field of research, as LTP induction strongly relies on the neurotransmitters (Ca^{2+} ...), and other endogenous neuromodulators (including endocannabinoids).

2.1.4 Limits

Although seemingly all encompassing, brain plasticity may not be a tool as powerful as we want it to be. If it were, any person would probably become a pro tennis player in a matter of hours. In fact, papers showing large-scale reorganization of networks are probably just as numerous as papers showing that the neuronal network is more hardwired than it is plastic, and that phenomena like learning or brain recovery only occur within certain limits in the adult.

Beyond the object of this thesis, which explores the limits of the mesoscale integration of artificial patterns of activity and their links to cortical maps, similar studies have been done exploring the limits of neuronal operant conditioning (Sadtlir et al., 2014). In this very interesting brain-machine interface paradigm, the researchers have trained rhesus macaques to control the activity of a few neurons to drive a virtual cursor from a central position to a surrounding rewarded one (Centre-out BCI task, Figure 2.2 A). The novelty here lies in the way the neurons are decoded to drive the actuator: the researchers established prior to each training session the multidimensional subspace representing the characteristic activity patterns of the neural space (Figure 2.2 B). They found that monkeys could learn a new control mapping lying within this multidimensional space relatively easily, while learning to drive the cursor with activity patterns outside of this manifold remained challenging (Figure 2.2 C). Although the training time was short, as the manifold was recalculated each session, the authors conclude that learning and plasticity are limited by the original wiring of the network.

Another obvious limit is that we are far from being able to specifically play with the plasticity of targeted cells and see the impact on behavior, but often use tools or molecules that could have other impacts. It is often hard to say if the plasticity change, supposedly induced, has a causal link to the apparent change in behavior.

2.2 Functional reorganization in the brain

Neuronal operant conditioning in general, or the study of dendritic spines for motor memory mentioned above relates to the micro-scale study of plasticity. Even though its mesoscale organization, including cortical maps, is mostly

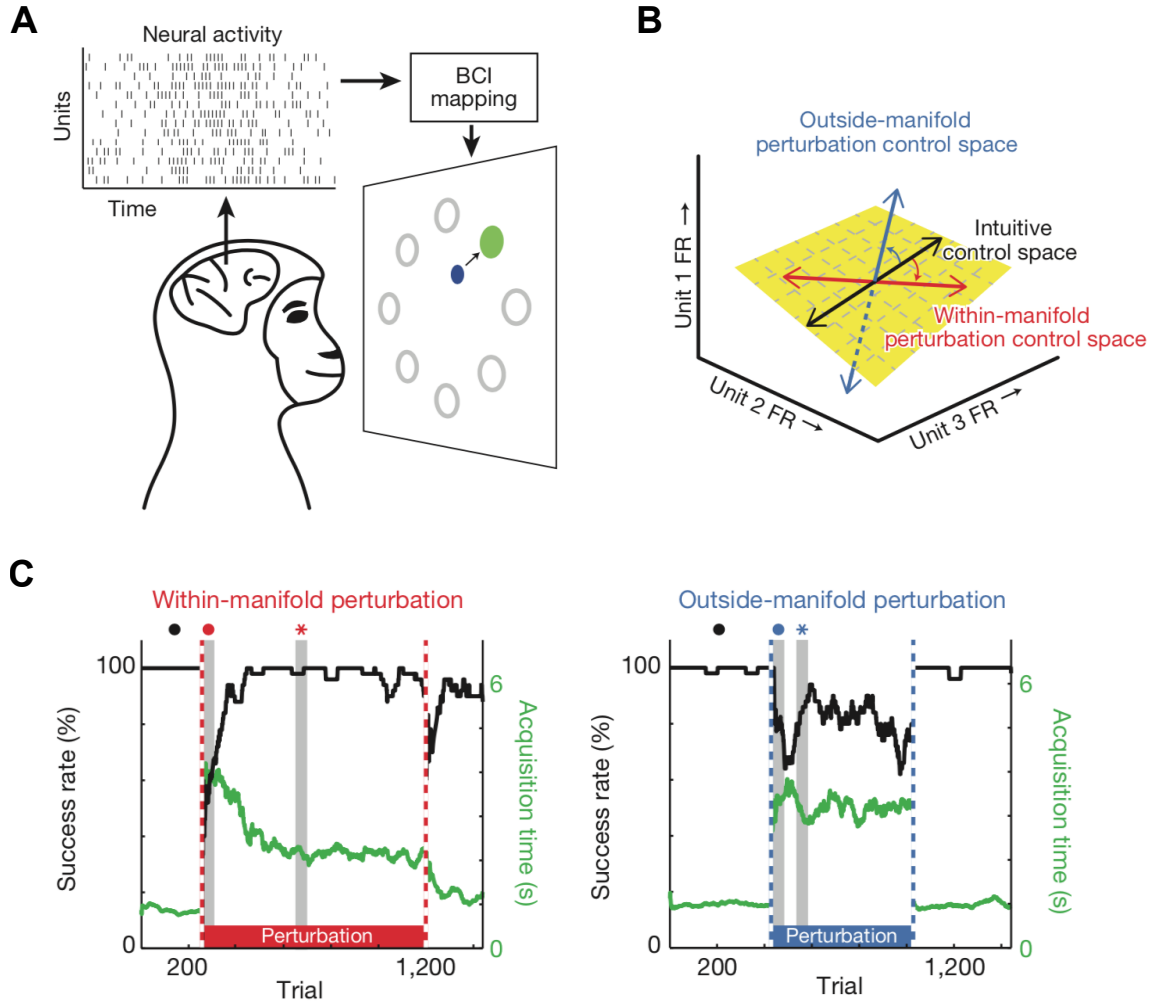


Figure 2.2: Prominent spontaneous activity patterns are more easily conditioned (Sadtler et al., 2014).

(A) Monkeys moved the BCI cursor (blue circle) to acquire targets (green circle) by modulating their neural activity. The BCI mapping consisted of first mapping the population neural activity to the intrinsic manifold using factor analysis, then from the intrinsic manifold to cursor kinematics using a Kalman filter.

(B) A simplified, conceptual illustration using three units. The intrinsic manifold (yellow plane) characterizes the prominent patterns of co-modulation. Neural activity maps onto the control space (black line) to specify cursor velocity.

(C) Task performance during one representative within-manifold perturbation session and one representative outside-manifold perturbation session. Black trace, success rate; green trace, target acquisition time. Dashed vertical lines indicate when the BCI mapping changed. Grey vertical bands represent 50-trial bins used to determine initial (red and blue dots) and best (red and blue asterisks) performance with the perturbed mapping.

hard coded, the functional reorganization of large networks in the brain can also happen. In this section, we will discuss how and to what extent these mesoscale plasticity phenomena occur.

2.2.1 Topographical reorganization

Reorganization of the cortex through plasticity mechanisms can take different forms. Particularly, anatomical reorganization after lesions seems to occur mostly during the development stage (Van der Loos and Woolsey, 1973; Staudt, 2010), even if some anatomical changes in the somatosensory cortex can be observed in adults rats after incomplete spinal cord injuries (Ghosh et al., 2009). In the context of this thesis and the brain-machine interface field in general, plasticity and network reorganization during development, although very interesting, will not be discussed any further. Remarkably, in the adult brain, even if functional somatotopic maps for motor and sensory cortices are mostly preserved (Andersen and Aflalo, 2022), the functional reorganization of the brain can still be present after an alteration in the periphery. In fact, fundamental functional changes in cortical maps can happen after a lesion, through training or even after a noticeable environmental change.

It has been shown that some human amputees experiencing a phantom limb remarkably had a phantom sensation of their hand when touching areas on the face or on the amputation stump, creating at these locations a topographically organized map of their fingers (Figure 2.3 A) (Ramachandran, 1998). Interestingly, this could be expected as the hand area is close to the face and upper arm areas in the Penfield homunculus (Figure 1.1 B). Meanwhile, in the digit representation in S1 of monkeys, there has been interesting works putting into light topographical reorganization of the network: - The representation of an amputated digit can be "invaded" by neighboring digit as it shrinks (Merzenich et al., 1984); - This representation can fuse if the fingers are just stuck together for a time (Allard et al., 1991). - The digit representation size itself was shown to be malleable as it could expand through repeated stimulation of the tips of the digits with a wheel (Jenkins et al., 1990) (Figure 2.3 B).

These changes are not restricted to limbs or fingers, but strongly depend on how much the network is solicited. A study on rats showed that after a skin rotation surgery preserving most of the innervation, the receptive fields (RF) of the skin slowly evolve to recover continuity: "Double RFs" were created after the skin flap as receptive fields could respond to the stimulation of distal parts on the skin due to the 180 degrees rotation. These "Double RFs" slowly transformed into "Crossing RFs", recovering continuity across the scar. This plasticity was accelerated when the skin was stimulated with a paintbrush (Rosselet et al. (2008), Figure 2.3 C).

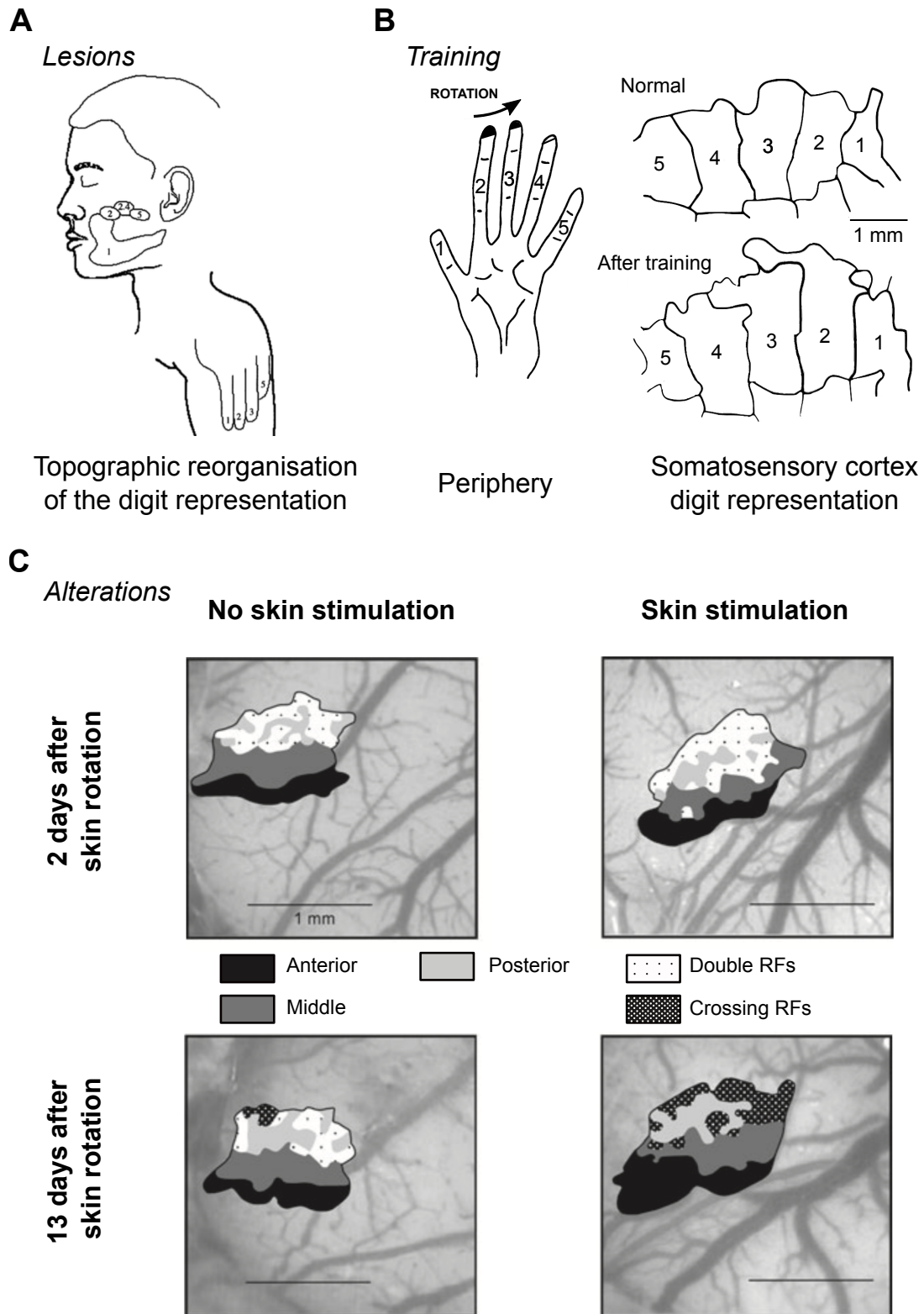


Figure 2.3: Cortical maps plasticity

(A) Distribution of reference fields in a patient with an amputated arm (Ramachandran, 1998).

(B) Reconstructions of the hand representation in a single monkey before and after differential stimulation, for which the monkey had to maintain contact with a rotating disk to receive pellet reward. Note the growth of the representation for digit 2 and 3 after training (Jenkins et al., 1990).

(C) Spontaneous and nursing-induced remodeling of the ventrum skin representational area, after pedicle flap rotation (Rosset et al., 2008).

2.2.2 Overlapping functionality

With all these possibilities of rearrangement of functional connectivity in topographical cortices, we can wonder if the newly created functional map replaces the previous arrangement, or if the two of them overlap and/or are interchangeable within a short time scale. This question is actually very important to the BMI field, as the targeted cortical areas for artificial stimulation feedback always have an original physiological function that we often do not want to disturb. Overall the literature seems to agree that a new functional arrangement induced by plasticity does not remove/impede the previous connectivity. In the paper cited above with the ventral skin rotation, the authors showed that the induced receptive fields could reverse to their previous locations in a matter of minutes (Rosselet et al., 2008).

If we look at the scale of single neurons, it is also important to note that after neuronal conditioning (similar to Figure 2.1 and Figure 2.2), the conditioned neurons seem to keep their original physiological function: A recent study showed that even after conditioning individual V1 neurons to a BMI task, stability of neural tuning to visual stimuli presented outside of the task context was not perturbed, nor was the response amplitude of individual neurons, while the estimated amount of information carried in V1 was unchanged (Jeon et al., 2022). A similar study was performed in the motor cortex of macaques, for which simultaneous retention of two maps was observed with no interference, one for the BMI task and one for the original tuning of conditioned neurons (Ganguly and Carmena, 2009).

2.2.3 Plasticity in the whisker cortices

Through this thesis, we will use the whisker sensorimotor system as a model for S1. It is interesting to note that the plasticity of this model has already been studied quite a bit, notably by the host lab, reaching the same conclusions as work done on monkeys and on humans (Shulz and Ego-Stengel, 2012). Similar to the work performed by Jenkins on the finger representation, depriving sensory inputs from all whiskers but one led to an expansion of the representation of the spared whisker and increased responses there (Glazewski and Fox, 1996), while other studies also show similar results with different techniques (Diamond et al., 1993; Bender, 2006; de Celis Alonso et al., 2008). Exposing adult rats to a naturalistic environment for four to six weeks also led to functional and anatomical changes of the barrel map: Specifically, functional changes were observed in layer II/III with sharpened receptive fields, while

small anatomical changes occurred in layer IV (Polley et al., 2004). Overall, just like plasticity in other cortices and other models, it is more effective early in life: cortical depression of deprived whisker input mostly happen before adulthood (Glazewski and Fox, 1996).

We have described how the primary cortices, although well topographically organized and with strong spatio-temporal restrictions, can be molded through repeated novel peripheral stimulations. We have also seen how the brain can modulate its activity to fit a change in the environment and lead to rewards. We will now explore a specific application of these mechanisms that we already mentioned, brain-machine interfaces.

Chapter 3

Brain-Machine Interfaces, tools to connect the brain to the exterior world

3.1 What is a BMI ?

Brain-machine interfaces, or BMIs, as their name imply, are tools connecting the brain to a device. They can take many forms, invasive or not invasive, and can have very diverse applications... BMIs focusing on sensory rehabilitation tend to stimulate the brain while motor BMIs and BMIs for communication decode the brain activity and transform into computer commands. Each of them can target different areas of the nervous system, and can have different methods of recording or stimulating the brain. Each of them also has its own advantages and drawbacks. On humans, BMIs tend to rely more on non-invasive recording methods, such as electroencephalography (EEG), functional magnetic resonance imaging (fMRI) or functional transcranial doppler (fTCD/FUS), but also on slightly more invasive methods including electrocorticography (ECoG) and rarely intracranial electrodes. In fact, intracranial electrodes are only used when they are already in place for medical reasons (Patel et al., 2021; Caldwell et al., 2019). Overall, the chosen recording method will strongly depend on what the BMI will be used for, and more specifically the spatio-temporal constraints on the neural activity that we want to record, the signal to noise ratio as well as the recording stability. These parameters can strongly affect the information transfer rate, critical to the BMI performances. (Figure 3.1). Further developments led to bi-directional BMIs, which combine the recording of brain activity and closed-loop stimulation of the brain. This advancement yet again brought several stimulation methods into light and many challenges of several fields of expertise: engineering, signal processing, neuroscience... (Lebedev and Nicolelis, 2017).

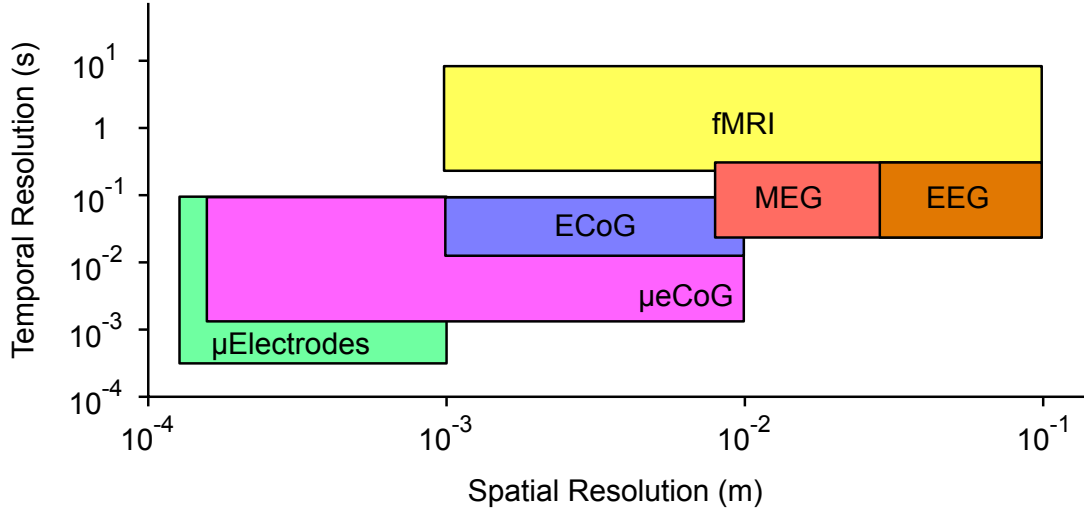


Figure 3.1: Spatio-temporal resolution of the different techniques for human brain readout

Adapted from (Thukral et al., 2018).

3.1.1 In the medical field

The applications of BMIs in the medical field are countless. Some of them allow locked-in syndrome (LIS) patients to communicate or to voluntarily move a robotic arm (Birbaumer, 2006; Hochberg et al., 2012), others provide deep brain stimulation to stop a starting epilepsy crisis (Fountas and Smith, 2007), while many of them just passively record the brain activity to provide feedback to the user, for example telling him whether or not he had a good night sleep. The first applications are in fact quite promising, but still not up to the challenge: Current P300-based BMI communication device allow LIS patients to type one word every few minutes (Akram et al., 2014), while the dexterity attained by current neuroprostheses is clearly not at the level of refined arm movement (Bensmaia and Miller, 2014).

Meanwhile, for the BMI that stimulate the brain to convey a message, the new cochlear implants show some astonishing results with subjects recovering up to the point of using a telephone (Lenarz, 2018). These implants are safe, easy to implant and durable so that patients can use them everyday, making it a huge success. However, the different retinal implants such as Argus 2 developed by the company Second Sight Medical Products are not performing well enough yet, restoring vision but with a poor identification of complex shapes, and few pixels (Stronks and Dagnelie, 2014). Unfortunately, this remains true for current cortical implants in the primary visual cortex (Chen et al., 2020; Fernández et al., 2021).

All in all, future BMIs may provide a way to restore sight to the blind, movement and sensory inputs to spinal cord injured patients, while detecting strokes and other diseases in real time. However, there is so much left to design and understanding the brain mechanisms remains critical if we want to better interact with it.

3.1.2 Bi-directional BMIs, a tool to study the brain mechanisms

While the BMI community is in strong need of more knowledge on how the brain works, it is also important to note that closed-loop brain-machine interfaces is also a way to interrogate the network and draw conclusions on the brain functions. Compared to standard observational methods, studying a phenomenon with a BMI has the advantage of having knowledge of both the inputs and the outputs of the system. For instance, In a BMI task for which a certain brain activity pattern is reinforced with stimulations, correlations between learning and changes in activity appear, while causality can be achieved by interfering with either side of the BMI. And in fact, besides the direct translational BMI research on monkeys and then human that has been going on in several labs, part of the BMI field focuses on understanding how the brain works, including mechanisms of sensorimotor integration, neural constraints on learning, or plasticity mechanisms through the brain (Neely et al., 2018; Athalye et al., 2018; Golub et al., 2018).

3.2 Optimizing control and cortical feedback on a cortical sensorimotor neuroprostheses

In this last section, we will discuss specifically the subpart of the BMI field, concerned with cortical sensorimotor prostheses. Targeting the cortex rather than more peripheral nerves has both its advantages and its drawbacks. Its first advantage is its resilience: some diseases or lesions make the recording or stimulation impossible to do in the periphery (i.e spinal cord injury...). Second is its complexity, the mass of information that can be accessed in the cortex within a narrow space is tremendous. In terms of plasticity, as we described in the last chapter, we could expect that the network would adapt and be reconfigured to the BMI task, even for an intracortical BMI. However, even though the cortex is one of the easiest brain structure to record from, to achieve a good signal to noise ratio, it remains more invasive and more dangerous to target it rather than the periphery. Another obvious flaw in targeting the cortex is actually the lack of knowledge about it. Up until now, researchers working on

sensorimotor systems have managed to characterize the peripheral inputs and outputs quite thoroughly, be it for motor control and muscle recruitment, or for touch, audition and vision. However the complexity of sensory and motor cortices has not been cracked yet.

In short, intracortical BMI probably have more potential than peripheral ones in terms of information and possibilities, but they are more difficult to implement due to the natural protection of the skull and the shallow understanding that we have of the cortex. However, our understanding of the cortex is evolving fast, and closed-loop BMI may be exactly the test we need to understand it even more.

3.2.1 The ideal brain-machine interface

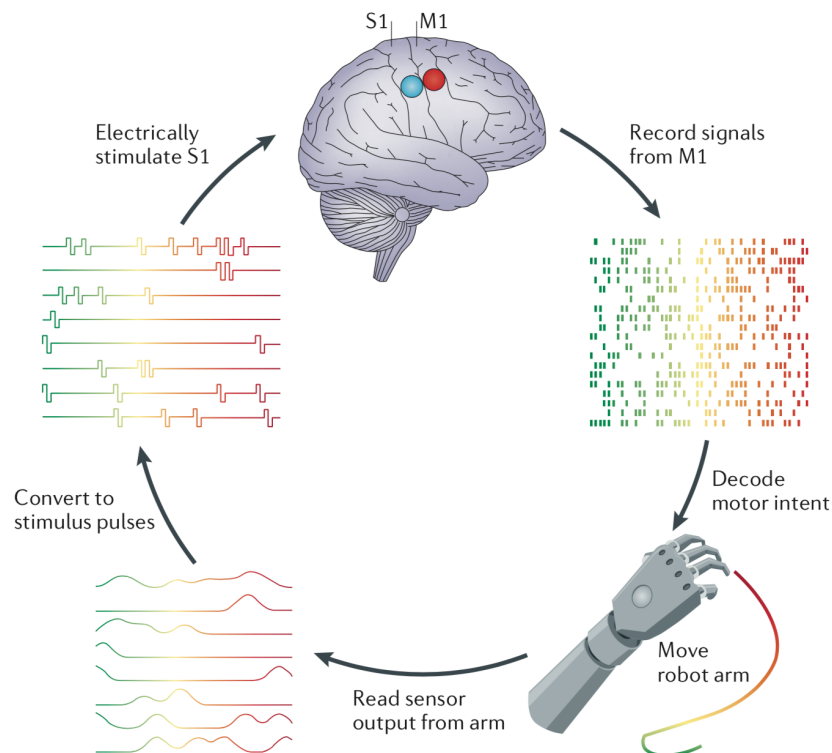


Figure 3.2: Idealized bidirectional brain–machine interface for prosthetic control (Bensmaia and Miller, 2014).

Neural signals from motor-related areas of the brain—for example, the primary motor cortex (M1)—that encode the intended movement (motor intent) are decoded and used to control the movement of the prosthetic limb. Sensors on the prosthetic limb convey information about movements of the limb and any objects with which it comes into contact. The output of these sensors is converted into patterns of electrical stimulation (stimulus pulses), which are delivered to sensory areas of the brain—for example, the primary somatosensory cortex (S1)—via chronically implanted arrays of electrodes.

It is now well known that tactile and proprioceptive feedback from our limbs and fingers are very important to perform a sensory motor task. In fact, visual feedback alone is not sufficient for motor control (Chesler et al., 2016), and a simple task like lighting a match can become very difficult after anesthetizing the sensory nerves (Johansson and Flanagan, 2009; Johansson and Westling, 1984; Monzée et al., 2003). Similarly, inactivating the somatosensory cortex also deteriorates motor control (Brochier et al., 1999; Mathis et al., 2017). However, most current neuroprostheses only record brain activity to transform it into movement, and do not provide any sensory or proprioceptive feedback to the user. And although some research teams try to adress this challenge promisingly (O’Doherty et al., 2011; Armenta Salas et al., 2018; Prsa et al., 2017), there is still a huge margin for progress. This is the reason why future BMIs for tetraplegic patients should both record signals from the brain, the primary motor cortex being an excellent candidate, in order to move the robotic arm, and with the help of some sensors, send back some proprioceptive and tactile information to the brain. The remaining question is how? On the control part, what is a good decoder ? On the sensory side, what can we do to provide relevant and interpretable information to the brain that can somehow contain the complexity of a prosthesis movement ?

3.2.2 Decoding neuronal activity

When building a sensorimotor BMI, the first hurdle concerns the motor command. Once again in the scientific community, researchers debate on how to do it. One main hurdle is that most of the time, as a limited number of motor cortex neurons are recorded, the recorded information is incomplete. To make up for it, the BMI field converged on the use of Kalman filters (Hochberg et al., 2012; Orsborn et al., 2014; Sadtler et al., 2014). Basically, for each time step, the Kalman filter predicts the following state of the system. As soon as the next time step arrives, the new measured state is compared to the predicted one and corrected. The objective of such filtering is to be able provide a continuous estimation of the state of a system even if the real-time measures are noisy or incomplete.

More recently, other methods seem to have achieved better performances than Kalman filters. Using dimensionality reduction and single trial modeling of the neural space dynamics (similar to Churchland et al. (2012)), A recent paper shows that the time constants of a Kalman filter may smooth the brain

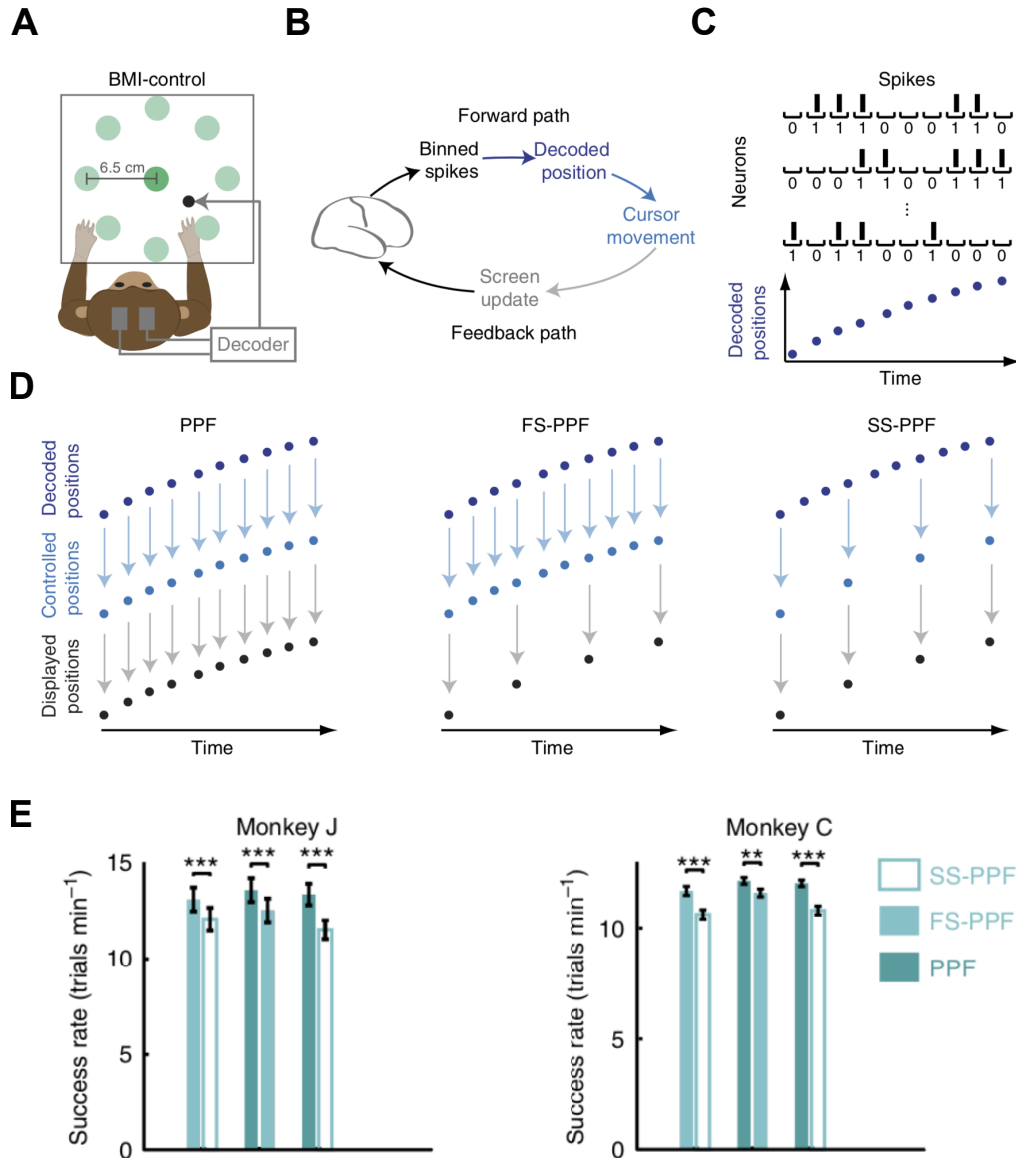


Figure 3.3: A point-process approach for motor command in a BMI task. Adapted from (Shanechi et al., 2017).

(A) Monkey performing the self-paced delayed centre-out movement task in brain control. The BMI paradigm introduces a novel bidirectional pathway between the brain and the prosthetic.

(B) BMI control and feedback loop.

(C) Each row corresponds to the spikes for a different hypothetical neuron. Spikes are binned in small intervals such that each interval contains at most one spike. This creates a discrete-time point process. Example decoded positions in one dimension versus time are shown in dark blue and are updated with every 0 and 1. Hence any control and feedback rate below this high bin rate can be obtained.

(D) The process of generating the controlled and feedback positions for the 3 different conditions are shown for the same hypothetical spike train. Control rate is manipulated by adjusting how often the decoded position is sent to the prosthetic and used to control the task (controlled positions in light blue). Task success is assessed based on these controlled positions. Feedback rate is adjusted by changing the rate at which feedback of the controlled positions is provided to the subject (displayed positions in black). PPF consists of both a fast control and a fast feedback rate, FS-PPF consists of a fast control and a slow feedback rate, and SS-PPF consists of a slow control and a slow feedback rate. Please note that success is assessed by analysing with the controlled positions rather than the displayed one.

(E) Performance comparison between each condition for two monkeys.

activity too much, losing rapid brain dynamics for which the neural activity is informative (Kao et al., 2015). In the meanwhile, Carmena’s lab (Shanechi et al., 2017) showed that the control rate and feedback rate of a brain-machine interface need to be very fast in order to increase BMI performance, as they also achieved performance beyond Kalman filters by processing spikes in 5ms bins (Figure 3.3 A, B, C). The idea here was not necessarily to have a very fast loop but rather to evaluate the impact of control and feedback rate in BMI performance (Figure 3.3 D). The monkeys actually performed better with the fastest rates (Figure 3.3 E), meaning that the rapid dynamics of the brain need to be taken into account when designing a BMI.

Overall it seems that all the temporal aspects of the brain activity, fast and slow, are useful for a BMI decoder. It is also important to note that for a closed loop BMI relying on visual or artificial feedback, the speed of the loop may also have a huge impact on BMI performance, as it directly reflects the physiological timings of the sensorimotor loop (Scott, 2016). However, there is a strong limitation in term of technicality here, as it is not trivial to read neural activity, decode it and move appropriately a robotic arm, or even control the position of a cursor on a screen, with speeds of a few tens of milliseconds as it naturally happens for our limbs.

3.2.3 Biomimicry versus adaptation, stimulating the cortical maps

Now that we’ve seen different ways of dealing with noise and incomplete datasets, with real-time approaches and filters, the most important question remains: Is it better to stick to the physiology and try to be biomimetic? In that case, on the recording and control side, we would use neurons that are already tuned or correlated to arm movements to control a prosthesis, while on the stimulation side, we would try to recreate natural patterns of activity that normally happen while touching an object with the fingers or moving the arm. The induced activity would have to mimic sufficiently natural brain activity to take into account the position of the contact, the pressure applied, the proprioceptive inputs... On the opposite, some researchers tend to think that the brain has a high capability to adapt and fit any BMI task, so that biomimetism should not be necessary for fine dexterity.

Basically, taking biomimetism into account requires much more technical effort and understanding of sensorimotor modalities, so if it does not improve performance, what is the point?

On the motor side, while the effect of biomimetism itself is not so clear yet, it seems that following the physiological rules remains useful: While we have seen in chapter 2 that single neuron conditioning can take place even in V1 (Neely et al., 2018), there seems to be a limit in the sense that it is easier to condition neurons to follow activity patterns within their dynamical range (Sadtlir et al., 2014). Overall the results of the debate remain unclear: In fact researchers disagree on the very static or dynamical nature of neuronal tuning in the motor cortex (Chestek et al., 2007; Rokni et al., 2007), even though a more recent study is more optimistic on its stability (Jensen et al., 2022). On the positive side, it has been shown that BMI training induce the formation of a cortical map for prosthetic function which is stable across time that can be recalled, similar to our recalling of motor skills (Ganguly and Carmena, 2009). Several very successful human and non-human primate BMI training first determined the preferred orientation of neurons through real movement or observations of movement (Velliste et al., 2008; Collinger et al., 2013). In these studies, the direction of the robotic arm movement is decided by summing neuronal "vectors" consisting of their firing rates and preferred orientation, which is actually an attempt at using neurons for what they usually do. Overall, it seems that biomimicry becomes important when a large number of neurons are conditioned at the same time. This would be logical in a sense, as a network of neuron may be more rigid, with more "locked" degrees of freedom than a single neuron.

On the sensory side, whether to do a biomimetic feedback or relying entirely on adaptation is a prominent question in the BMI field (Tabot et al., 2015). Most studies arbitrarily choose one or another, but there has not been any clear demonstration of the advantages and drawbacks of both methods. Part of it is due to the actual methods of stimulation. Be it with intracortical microstimulations (ICMS) or with optogenetic methods, our understanding of the brain, as well as our technological advancements, are not sufficient to perfectly replicate natural patterns of activity. In fact, most studies operate with different understandings of biomimetism, relying either more on temporal patterns of natural activity or spatial aspects, making them difficult to compare. Also, it is possible to mimic natural patterns of activity, but on another modality that has no relationship to the BMI task: For example, stimulating the lip representation instead of the arm's to represent the movement of a prosthesis. As such, biomimetism has quite a broad definition, and to test its real impact

on learning, researchers can only extract one of its properties to test it in a well controlled paradigm. Still, the first results are quite promising, as discrimination of artificial stimulation works quite well (Romo et al., 1998). Going further, by stimulating with optogenetics or ICMS the right whisker barrel in S1 in a go/no-go task, it has been shown that animals can generalize instantly from natural to artificial stimulation (Sachidhanandam et al., 2013; O’Connor et al., 2013; Leal-Campanario et al., 2006). This was also done at the level of the single neuron, with an impressive study driving spatial behaviour by stimulating hippocampal cells (Robinson et al., 2020). Generalization remains true for other modalities, such as taste (Peng et al., 2015), vision (Chen et al., 2020), or somatosensation in other areas (Tabot et al., 2013). In other studies, animals have managed to distinguish artificial patterns of activity with different stimulation frequencies in dynamical tasks (O’Doherty et al., 2011; Thomson et al., 2013). Interestingly, spatial patterns of stimulation onto the barrel cortex could be used by a mouse for a localization task, demonstrating the interchangeability of modalities for feedback delivery (Hartmann et al., 2016). However, if we are indeed able to generate tactile sensations on humans (Caldwell et al., 2019), we are currently unable to do the same for proprioceptive inputs.

To conclude this part, it seems intuitive that the more biomimetic a stimulation is, the easier it is integrated by the network. Indeed, the plasticity phenomena that we have described in Chapter 2 are not without limits, so that adaptation to a new stimulation can not be perfect. However, this should be hard to demonstrate, all the more because a novel stimulation can be seen as more salient even if less informative, which may impact strongly the learning curves.

3.2.4 Embodiment

While every closed-loop sensorimotor BMI designer yearns to achieve and demonstrate fine dexterity, there is a complex phenomenon that could be crucial for this aim: embodiment. Embodiment refers to the fact that if the central nervous system is the driver of the body, the body also influences the CNS. For this the CNS has to be wired in a way so that the limb, or prosthesis in our case, is a part of the body. Embodiment is well illustrated with the well known rubber hand illusion (Botvinick and Cohen, 1998). In this illusion, subjects are placed in front of a table with their arm hidden from sight, while a visible fake hand is placed next to it. Both the real and fake hands are

stimulated synchronously with a brush, but when the real hand stopped being stimulated, participants still felt the brush touch as if the fake hand belonged to them. This phenomenon is not restricted to humans, as it was also shown with mice with the "rubber tail illusion" (Wada et al., 2016). Supposedly, tactile and proprioceptive feedback could help subjects with the embodiment of their prostheses, while it is not exactly sure if the feedback biomimeticism could improve this aspect. However, embodiment of a prosthesis could be induced to amputees by stimulating the brain or the remaining stump (Collins et al., 2017; Marasco et al., 2011). Although poorly understood, the lack of embodiment is one of the main reasons why amputees abandon their prosthesis, so further BMI research should aim to reproduce it.

Part II

METHODS AND RESULTS

Chapter 4

A Closed-loop brain-machine interface to study sensorimotor integration

4.1 Continuity within somatosensory cortical map facilitates learning

4.1.1 Summary

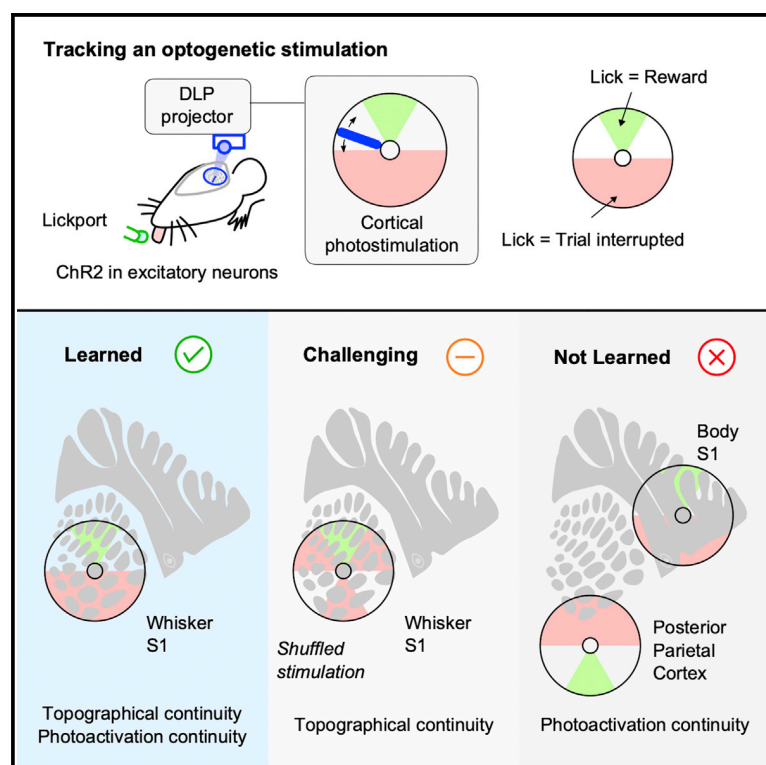
This article constitutes the output of the main results of the first two years of this PhD. It focuses on how sensory information should be delivered on the cortex using optogenetics, in order to be efficiently used by the animal. Many studies on artificial sensory feedback disagree on the way sensory feedback should be delivered to the different cortical areas, and specifically on the question of biomimetism that we addressed in the third chapter of the introduction. Here our working hypothesis was that strict biomimicry of the stimulation is not necessary to drive behavior. However, following the organization of the existing cortical maps on the cortex, regardless of the modality, is critical. To this aim, we designed a continuous protocol of stimulation sweeping through the cortex of mice, and the animals had to behave differently according to the position of the stimulation. Mice were only able to learn the task when there was a perfect match between the structure of the stimulation and the structure of the targeted cortical area.

4.1.2 Participation statement

In this work, I contributed to the conception of the project, the experimental design and the building of the setup. I wrote the code for the hardware and for the analysis, performed almost all the experiments, generated all the figures and wrote the article with inputs from all authors.

Continuity within the somatosensory cortical map facilitates learning

Graphical abstract



Authors

Henri Lassagne, Dorian Goueytes, Daniel E. Shulz, Luc Estebanez, Valerie Ego-Stengel

Correspondence

valerie.ego-stengel@cns.fr

In brief

Lassagne et al. design a mesoscale optogenetic discrimination task in mice targeting several cortical areas. Mice become experts at tracking the rotating photostimulation bar but only when both the photostimulation trajectory and the cortical map topography are continuous.

Highlights

- Mice accurately track an optogenetic stimulation bar over the cortical surface
- Continuity of the cortical area's topography is critical for learning
- Spatiotemporal continuity of the photoactivation trajectory supports learning
- This study demonstrates the functional role of continuity in cortical maps



Lassagne et al., 2022, Cell Reports 39, 110617
 April 5, 2022 © 2022 The Authors.
<https://doi.org/10.1016/j.celrep.2022.110617>

Report

Continuity within the somatosensory cortical map facilitates learning

Henri Lassagne,¹ Dorian Goueytes,¹ Daniel E. Shulz,¹ Luc Estebanez,^{1,2} and Valerie Ego-Stengel^{1,2,3,*}

¹Université Paris-Saclay, CNRS, Institut des Neurosciences Paris-Saclay, 91400 Saclay, France

²These authors contributed equally

³Lead contact

*Correspondence: valerie.ego-stengel@cnrs.fr

<https://doi.org/10.1016/j.celrep.2022.110617>

SUMMARY

The topographic organization is a prominent feature of sensory cortices, but its functional role remains controversial. Particularly, it is not well determined how integration of activity within a cortical area depends on its topography during sensory-guided behavior. Here, we train mice expressing channelrhodopsin in excitatory neurons to track a photostimulation bar that rotated smoothly over the topographic whisker representation of the primary somatosensory cortex. Mice learn to discriminate angular positions of the light bar to obtain a reward. They fail not only when the spatiotemporal continuity of the photostimulation is disrupted in this area but also when cortical areas displaying map discontinuities, such as the trunk and legs, or areas without topographic map, such as the posterior parietal cortex, are photostimulated. In contrast, when cortical topographic continuity enables to predict future sensory activation, mice demonstrate anticipation of reward availability. These findings could be helpful for optimizing feedback while designing cortical neuroprostheses.

INTRODUCTION

Primary sensory areas of the neocortex are involved in sensory perception of several modalities. For example, microstimulations of specific areas of the cortex in humans produce vivid visual, tactile, or auditory percepts (Dobelle et al., 1974; Penfield and Boldrey, 1937; Penfield and Rasmussen, 1950; Schmidt et al., 1996).

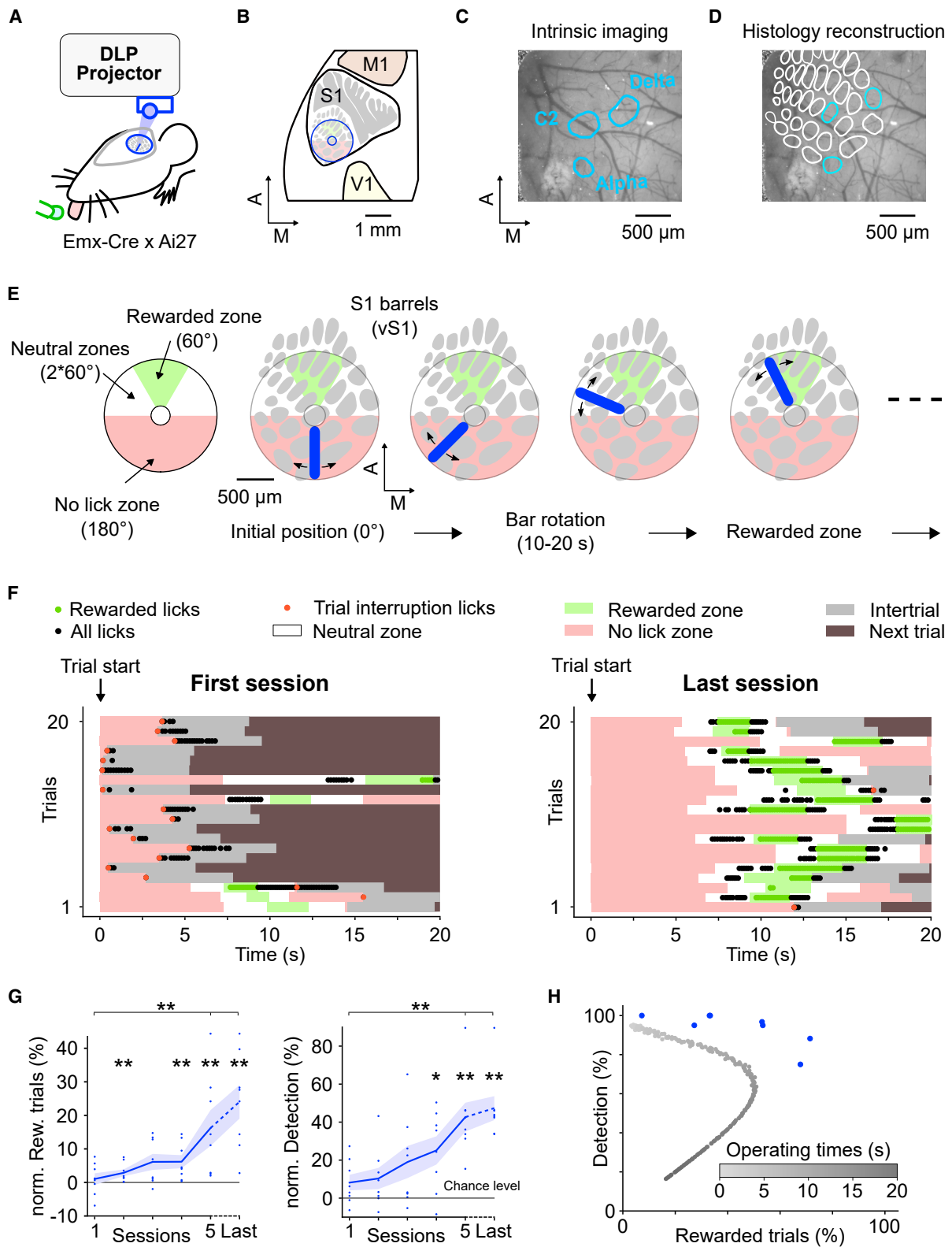
These sensory areas are organized topographically with respect to the periphery (Daniel and Whitteridge, 1961; Merzenich et al., 1975; Penfield and Boldrey, 1937). In the primary somatosensory cortex (S1), Penfield and collaborators have shown that neighboring cortical zones encode information from neighboring patches of skin on the body (Penfield and Boldrey, 1937). Such cortical representation of the body surface in S1 is a common feature of mammals. In rodents, the whiskers' follicles on the snout are connected to distinct clusters of cells within S1, called barrels (Woolsey and Van der Loos, 1970), that retain the spatial organization of the follicles.

One question concerns to what extent activation of neuronal ensembles in the cortical maps is necessary and sufficient for eliciting percepts that can drive behavior (Ceballos et al., 2019a; Chen et al., 2020; Dalgleish et al., 2020). Animals can be trained to report direct cortical stimulation of primary sensory areas for all modalities (Ceballos et al., 2019a; Chen et al., 2020; Choi et al., 2011; Houweling and Brecht, 2008; Huber et al., 2008; Peng et al., 2015). Interestingly, several studies have shown that animals trained in a localized sensory perception task could rapidly generalize when the peripheral stimuli were replaced by

cortical microstimulations (Chen et al., 2020; Leal-Campanario et al., 2006; O'Connor et al., 2013; Peng et al., 2015; Romo et al., 1998; Sachidhanandam et al., 2013; Tabot et al., 2013; Venkatraman and Carmena, 2011). This seemingly immediate interchangeability of natural and artificial stimuli strongly supports a prominent role of cortical activity in sensory perception. Stimulation of distinct cortical zones in a topographic sensory map elicited localized percepts matching the expected peripheral locations on the sensory organ (Bosking et al., 2017; Ceballos et al., 2019a; Chen et al., 2020; Flesher et al., 2016; Winawer and Parvizi, 2016). This result has been interpreted as additional evidence that the topographical organization of sensory areas serves a fundamental function for sensory processing (Harding-Forrester and Feldman, 2018; Kaas, 1997). However, there is no direct evidence that cortical topography is important for brain function. On the contrary, it has been suggested that topography could be a mere consequence of the way cortical areas form early in development. In this alternative view, the spatial arrangement of cortical zones as an orderly mosaic may have no functional impact on the computations performed by the cortex (Lashley, 1939). To solve this controversy, it becomes necessary to directly manipulate cortical activity at the scale of the topographic organization of the cortex, and test its causal impact on behavior.

Almost all studies linking cortical activity and perception have focused on single-stimulus detection, or discrimination between a few stimuli each presented individually. However, more complex stimuli in which information is spatially and temporally distributed are more likely to engage the computational capacity





(legend on next page)

of the cortical network. Indeed, at the microcircuit level, functional topography is known to be intrinsically associated with precise intracortical connectivity diagrams (Jiang et al., 2015; Narayanan et al., 2015; Rockland et al., 1982). These highly non-random connections result in differential sensory processing, depending on the spatiotemporal sequences of neurons being activated. Notably, the cortex seems particularly useful to differentially integrate multiple sensory inputs over time, via nonlinear transformations (Estebanez et al., 2018; Nogueira et al., 2021).

To test the role of topography in cortical function, two different types of mesoscopic patterns should thus be contrasted: on the one hand, topographic patterns that match the cortical activation patterns known to occur following peripheral stimulation, and on the other hand, non-topographic patterns that do not match expected cortical activation, for example because they correspond to synchronous stimulation of distant peripheral zones that do not normally occur. Our underlying hypothesis in contrasting such patterns is that they should result in different cortical processing because of the detailed structure of the cortical network.

We carried these tests by causally manipulating the activity of cortical neurons in transgenic mice, using dynamical patterns of optogenetic activation. By design, the behavior of the mouse could only be due to perception of cortical activity. We applied a continuously moving stimulus projected onto different cortical areas: the primary somatosensory cortex (vS1), known for its orderly two-dimensional topography; the trunk and legs area primary somatosensory area (bS1), which contains discontinuities in its topography; and the posterior parietal cortex (PPC), which lacks a clear topography. Our results point to differential sensory processing in topographic and non-topographic areas.

RESULTS

Mice learn the angular position of a rotating optogenetic stimulus projected onto the barrel cortex

In this study, we tested whether head-fixed, water-restricted mice expressing channelrhodopsin in excitatory cortical neurons could actively track the position of a photostimulation applied on vS1 (Figures 1A and 1B). We first determined the location of at least three barrels, including the C2 barrel, by intrinsic imaging (Figure 1C). The locations were confirmed postmortem by histological barrel map reconstruction (Figures 1D (Perronnet et al., 2016)). We then projected a rotating bar of light inside a disk

centered on the C2 barrel (Figure 1E). The light bar turned smoothly and differently for each trial, activating sequentially contiguous zones of the barrel cortex (Figure S1). Mice could obtain reward by licking when the photostimulation bar was within a specific rewarded zone (Figure 1E). Licking when the bar was in the no-lick zone immediately ended the trial and started a 5-s intertrial interval without stimulation.

In Figure 1F, the first 20 consecutive trials are shown for the first and 10th session for one mouse. During the first session, the mouse licked randomly, which often cancelled the trial. During the 10th session, the mouse successfully refrained from licking in the no-lick zone, until approaching the rewarded zone. All eight trained mice learned the task in 5 days (Figure 1G). Rewarded trials increased on average by over 15% (Figure 1G left, Wilcoxon test, $p = 0.0078$), while the detection level, calculated only on trials with available reward, increased up to 40% above chance level (Figure 1G right, Wilcoxon test, $p = 0.0078$). This corresponded to over 90% of detection calculated on all trials (Figure S2). Taken together, these learning curves suggest that all mice learned both to locate which sector of the stimulated cortical area leads to reward availability and to refrain from licking in the no-lick zone in order to increase the total number of rewarded trials. Three mice out of eight were trained for more than 5 days, and population analysis on the last sessions pooled across all mice showed that performance continued to increase (Figure 1G, “last”).

We were concerned that the mice might learn the average timing from the onset of the trial to the entrance in the rewarded zone, without relying on the angular position of the photostimulation. Thus, we designed an algorithm that solves the task using only time cues. The results from this algorithm are shown in Figure 1H for all possible times of onsets of licks (operating times). As expected, at short operating times (light gray points), most licks fell in the no-lick zone, which in turn resulted in very low numbers of rewarded trials. The longest operating times (dark gray points) led to late lick onsets, which missed the rewarded zones. All mice demonstrated higher performance than any version of the temporal algorithm (Wilcoxon, $p = 0.0078$). Thus, mice did indeed use the spatial location of the stimulation to guide licking, and not only temporal cues.

To further investigate spatial learning, we analyzed the radial distribution of the photostimulation angle for all lick times before and after learning (Figure 2A top, same sessions as in Figure 1F; see also Figure S3). The proportion of licks for the rewarded zone increased with training from 19% to 61%, while the proportion of

Figure 1. Mice were trained to lick for rewards when a moving photostimulation bar entered a defined vS1 zone

- (A) Sensory-guided licking task. A digital projector sends frames through an optical window. A water tube detects licks and delivers rewards when appropriate.
(B) Location of the stimulation disk over vS1 (cortical map adapted from Knutsen et al., 2016, and Vanni et al., 2017).
(C) Contours of the intrinsic imaging responses for individual deflection of whiskers Alpha, C2, and Delta overlaid on surface blood vessels.
(D) Histological reconstruction of the barrel map for the experiment in (C).
(E) When the bar was in the green zone, licks were rewarded. In the red zone, a lick ended the trial. In the white zones, licks were ignored. Right: snapshots from one trial.
(F) Raster plots of licks (dots) during 20 consecutive trials in the first and 10th session for one mouse.
(G) Average learning curves (\pm SEM, $n = 8$ mice) quantified by the detection level and the percentage of rewarded trials, normalized by subtracting the chance level (see STAR Methods). Data are presented for the first five sessions and the last session of training for each mouse, regardless of the number of trained sessions. Wilcoxon tests, * $p < 0.05$, ** $p < 0.01$.
(H) Performance curve of an algorithm solving the task with a pure temporal strategy (see STAR Methods). Each gray dot is the performance of the algorithm triggering licks at a specific time, the operating time (grayscale), across all 252 possible trials. Blue dots are the mice performance on their last session.

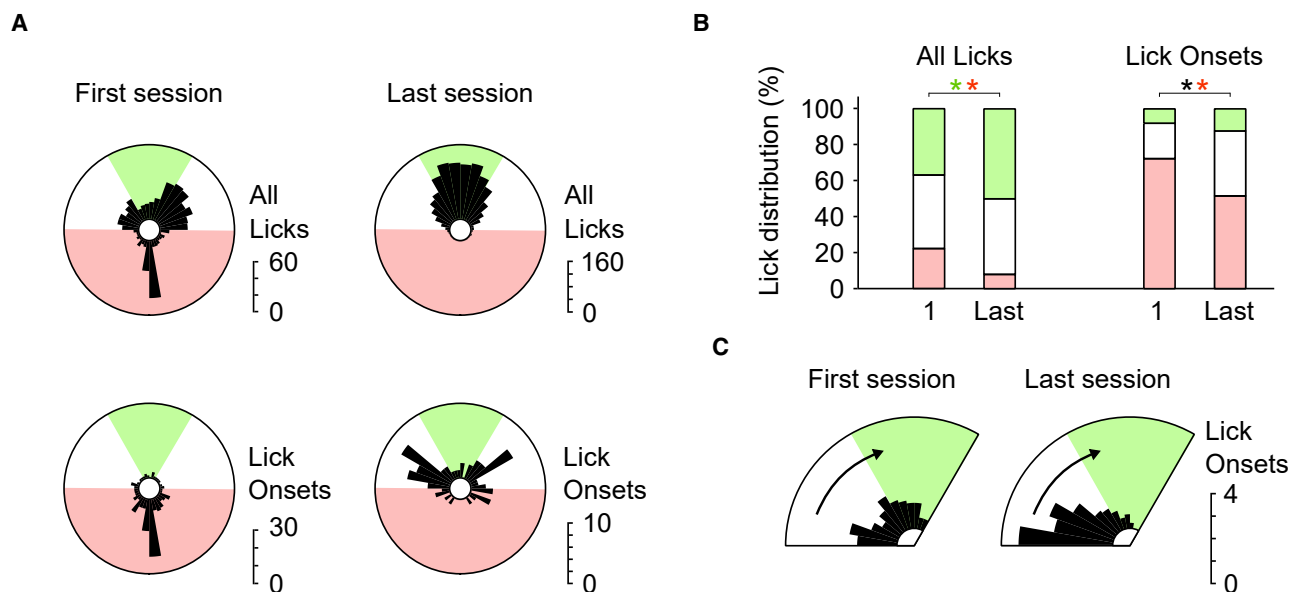


Figure 2. Redistribution of the angular positions of the optogenetic bar at lick times shows spatial anticipation of the reward

(A) Spatial distribution of the optogenetic stimulus angle for all licks (top) and lick onsets (bottom), for the sessions from Figure 1F.

(B) Average distribution of all licks and lick onsets for which the optogenetic bar was in the rewarded, no-lick, and neutral zones for the first and last session ($n = 8$). One-sided Wilcoxon tests, $^*p < 0.05$, colors match the zones (black = neutral zone).

(C) Average spatial distribution of the stimulus angle for lick onsets in the neutral and rewarded zones. Trials entering from the right were symmetrized before averaging. Only the first 20 rewarded trials of a given session were used for this analysis, ensuring that the mice were highly motivated.

licks for the no-lick zone decreased from 26% to 1%. Interestingly, after learning, lick onsets occurred mainly for the zones flanking the rewarded zone (Figure 2A, bottom). This suggests that the mouse started licking after the bar left the no-lick zone, even before entering the rewarded zone. Population analysis confirmed this redistribution of licks and lick onsets across cortical photostimulation zones (Figure 2B, $n = 8$ mice, Wilcoxon tests, $^*p < 0.05$) and specifically right after entry in the neutral zone (Figure 2C).

After learning the task, three mice were trained for a further 5 days with a more challenging, extended no-lick zone (Figure S4). The high performance and increased alignment of lick onsets to the no-lick/neutral zones border further demonstrates the fine readout resolution attained (Figures 2C and S4G).

Mice use the spatial continuity of the stimulation space to solve the task

To check if the anticipatory licking shown in Figure 2C is based on spatial rather than temporal cues, we trained three naive mice in a shuffled condition (Figure 3A; see STAR Methods). Across the 10 sessions of training, the percentage of rewarded trials did not increase significantly, remaining far below values reached in the standard condition (Figure 3B, Mann-Whitney [MW] test; $p = 0.018$). Nonetheless, two out of three mice reached a 100% detection level after 10 days. These results suggest that the spatial discontinuities reduced the proportion of successful trials, but that mice could still learn the rewarded zone location as much as in the standard condition. Interestingly, when we looked at the time course of successful trials, we found that mice strategy

differed from that in the standard task: they started licking only when the optogenetic bar reached the rewarded zone, instead of anticipating its entry (example in Figures 3C versus 2F). We quantified this observation by measuring the delay between lick onset and entry in the rewarded zone. In the standard condition, mice anticipated the rewarded zone entry by a median of ~ 1 s, in contrast to the ~ 300 -ms delay in the shuffled condition (Figure 3D), and the absence of licks in the neutral zone just preceding the rewarded zone (Figure 3E). Anticipation of the rewarded zone eventually emerged after an additional 3 days of training (Figure 3D).

We wondered whether mice that had already learned the task in the standard condition could easily adapt to the shuffled condition. Three expert mice in the standard condition were tested in the shuffled condition. Despite a drop in performance, these mice remained experts at detecting the rewarded zone (100% detection level) but stopped anticipatory licking (Figure 3F, $p < 0.0001$), demonstrating again a direct effect of the spatial continuity of trajectories on behavior.

To summarize, these results suggest that, in order to track the cortical optogenetic bar and predict its trajectory, mice exploit the spatial continuity of cortical stimulation.

Learning is disrupted by discontinuities in the cortical map

To further test this finding, we asked if discontinuities in the targeted cortical map itself might also affect learning. We trained naive mice to learn the same task while centering the photostimulation outside of the barrel cortex. First, we selected a cortical

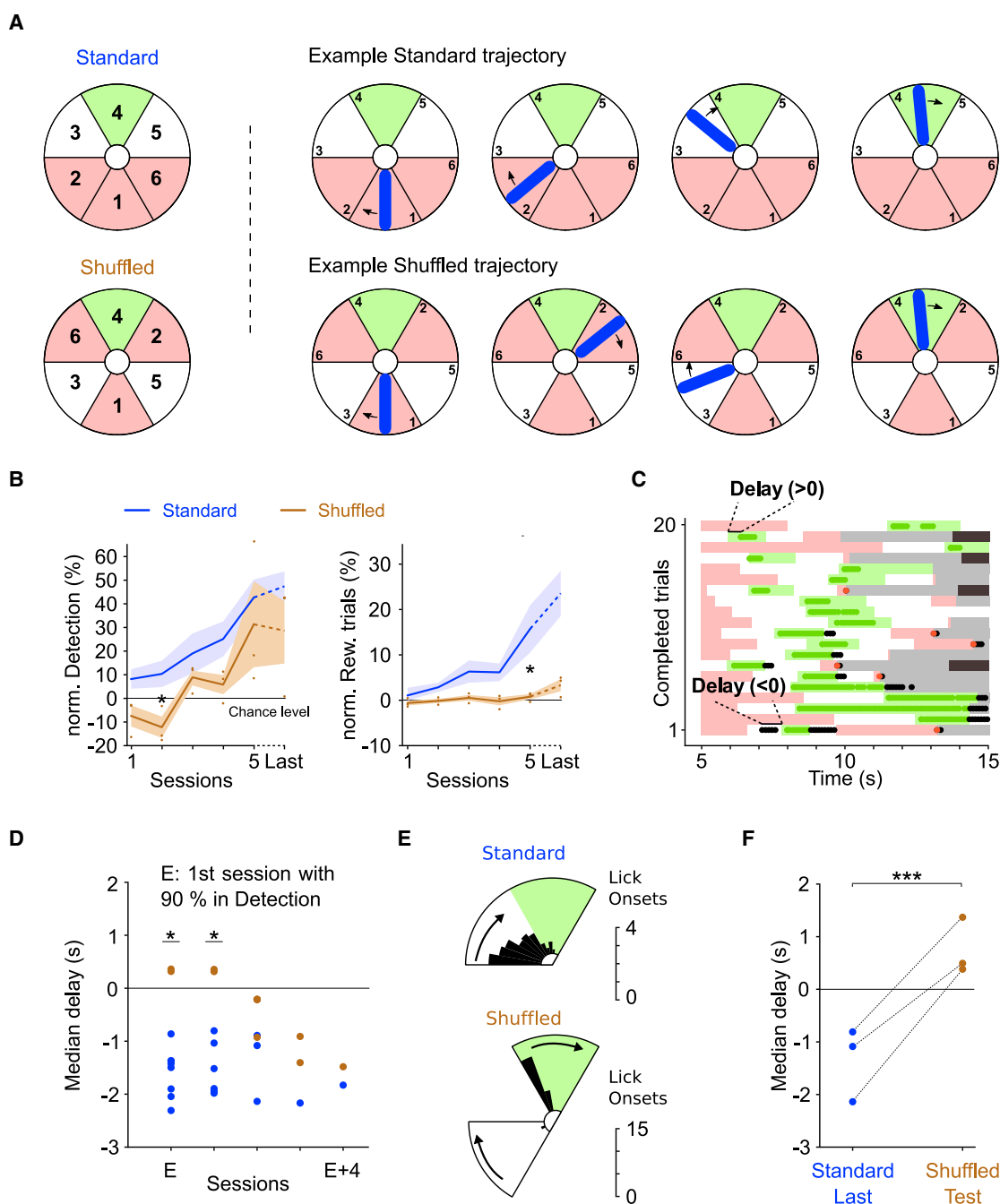


Figure 3. Mice rely on the spatial continuity of the stimulated area to learn the task

(A) Left, reorganization of angular sectors of the stimulation disk from the standard condition (top) to the shuffled condition (bottom). Sectors 1 and 4 are unchanged; other sectors are permuted. Right, example snapshots of the same trajectory in both conditions. As several sectors are swapped, the stimulation bar jumps from one sector to another, but stays in the no-lick, neutral, and rewarded zones following exactly the same timeline as in the standard condition.

(B) Average learning curves (\pm SEM) for the standard (blue, $n = 8$) and shuffled (brown, $n = 3$) conditions. Two-sided MW test, $*p < 0.05$.

(C) Raster plot of 20 consecutive completed trials for a mouse trained in the shuffled condition, for the first session with a high (>90%) detection level (session 6). Delay is the time from entry in the rewarded zone to first reward.

(D) Median delay for the standard (blue) and shuffled (brown) conditions. For each mouse, session E is the first session with a detection level above 90%. Only consecutive sessions with a detection rate of 90% or more are shown. One-sided MW test, $*p < 0.05$.

(E) Average spatial distributions of stimulus angle for lick onsets for rewarded trials (as in Figure 2C), for standard and shuffled conditions in session E + 1.

(F) Median delay for the last session in the standard condition, and for a test session in the shuffled condition 1 day later ($n = 3$ mice). One-sided MW calculated for each mouse, $***p < 0.001$.

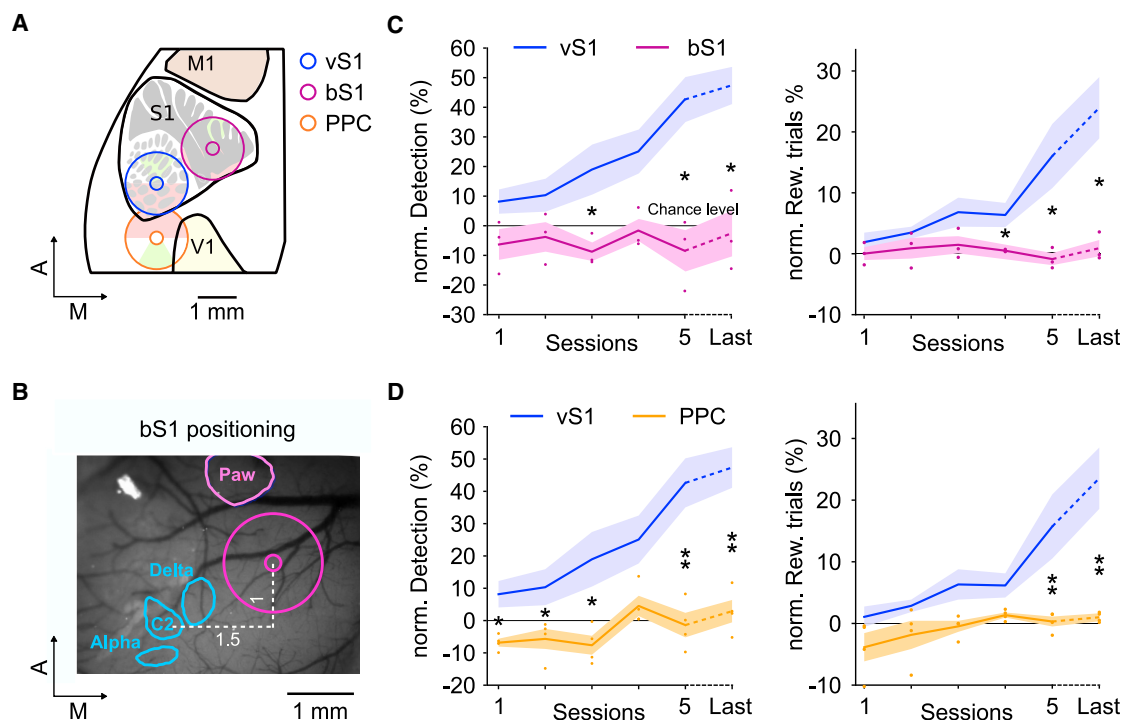


Figure 4. Learning is only possible in a cortical area that contains a continuous topographic representation

(A) Stimulation disks including rewarded/no-lick zones on vS1 (blue), bS1 (magenta), and PPC (orange).

(B) Contours of the intrinsic imaging responses for individual deflection of whiskers Alpha, C2, and Delta (blue), and for mechanical vibration on the paw (pink), overlaid on surface blood vessels. Magenta, stimulation disk on bS1.

(C) Average learning curves (\pm SEM) for stimulation of vS1 (blue, $n = 8$) and bS1 (magenta, $n = 3$).

(D) Same as C for PPC (orange, $n = 4$). In two mice, PPC training followed vS1 training. This might explain the significant differences in detection observed in the first session. (C, D) Two-sided MW, * $p < 0.05$, ** $p < 0.01$.

area (bS1) where the adjacent trunk, limb, and snout representations resulted in discontinuities in the cortical map (Figures 4A and 4B). None of the mice reached performance comparable with mice trained with photostimulation on vS1 (Figure 4C; MW test on the last sessions; rewarded trials, $p = 0.032$; detection, $p = 0.019$). Second, we centered the stimulation on PPC in four mice already trained on vS1. The rationale was to select a non-primary sensory area, for which topography is not a strong organizing principle. Similar to mice trained on bS1, these mice did not learn the task (Figure 4D; rewarded trials, $p = 0.008$; detection, $p = 0.008$ compared with vS1 mice). This difference in performance could not be due to a lack of induced activity: we recorded electrophysiological activity while projecting patterns of light on the cranial window and found reliable activity induced by photostimulation, regardless of the electrode position (Figure S1). Together, these results suggest that the continuous topography present in vS1 is necessary for learning the optogenetically mediated task.

DISCUSSION

We have shown that mice can learn to use patterned cortical stimulations as dynamical cues to guide their behavior. Learning only occurred when the stimulus was continuous across space and time, and when the target area included a continuous

topographic map of the sensory periphery. Our findings thus fit with the general idea that the topography of a cortical area shapes input integration in neuronal networks.

Mesoscopic cortical patterns causally drive behavior

In order to activate the cortical surface with high-resolution dynamical patterns, we chose to use optogenetic stimulation, which activates predominantly upper layers (Yizhar et al., 2011). The dense horizontal intracortical connectivity in these layers supports continuous propagating waves of depolarization at a mesoscopic scale (Muller et al., 2018; Vilarchao et al., 2018). The fact that mice were able to lick in response to supragranular mesoscopic patterns is direct evidence that patterns at that scale can indeed acquire functional relevance for perception and behavior.

Mice learn the optogenetic task similarly to a sensory go/no-go task

During learning, mice first improved their task performance by licking when the optogenetic bar entered the rewarded zone. In parallel, many trials were still aborted because of licks in the no-lick zone. This asymmetric learning for rewarded and non-rewarded trials is similar to the dynamics described in a classic go/no-go sensory discrimination task (Bathellier et al., 2013). Interestingly, the delay between optogenetic stimulation and lick

response was comparable with reaction times following peripheral stimulation, ~300 ms (Figure 3) (Abbasi et al., 2018; Ceballo et al., 2019b; El-Boustani et al., 2020; Huber et al., 2008; Sachidanandam et al., 2013). Thus, mice integrate cortical stimuli similarly to peripheral stimuli into perception and behavior.

Breaking spatiotemporal continuity disrupts learning

We tested two different ways of disrupting the continuity of optogenetic perception. First, we manipulated the spatiotemporal parameters of the cortical stimulus by shuffling spatial zones of the stimulated area. Second, we applied stimulation on an area in which topography is discontinuous, such as bS1. In both cases, learning was severely impaired (Figures 3 and 4). In bS1, this could be due to the fact that the optogenetic bar crosses cortical zones that correspond to non-contiguous peripheral skin zones. Thus, the stimulation could be perceived as a stimulus jumping between many different locations; for example, jumping from limbs to trunk. If, as proposed, S1 serves as a body model to simulate and predict ongoing behavior (Brecht, 2017), the induced S1 activity could indeed be difficult to read out. Continuity of activity in a topographic area would then be critical for sensorimotor anticipation and learning.

Biomimetism facilitates neuroprosthetic learning

Beyond a better understanding of sensory perception, our findings could be key to the efficient delivery of sensory information in the context of sensorimotor neuroprostheses (Chen et al., 2020; Dadarlat et al., 2015; Hartmann et al., 2016; O'Doherty et al., 2011). Recent active neuroprostheses tend to match as closely as possible the spatial and temporal aspects of physiological cortical responses to tactile and proprioceptive inputs (Flesher et al., 2021; Tabot et al., 2015), as well as to visual inputs (Dobelle, 2000; Fernández et al., 2021). However, most studies relied on discrete patterns of stimulation in space and time, whereas everyday prosthesis use is likely to generate complex, continuous sensory feedback. Here, we have designed a class of spatially and temporally continuous feedback at the cortical surface. Although this remains a partial biomimetic activation, it shares some features of known cortical activity patterns, notably the propagation of cortical waves of activation (Muller et al., 2018). In our study, such stimulation of a topographically organized sensory cortex could be integrated with a high degree of spatial precision into behavior, including anticipatory processes that could promote dexterous movements of a closed-loop neuroprosthesis.

Longer-timescale reorganization of the cortex during learning

With additional training, learning the disrupted conditions may eventually occur. For example, the activity patterns evoked in S1 in the shuffled condition share features with those following the surgical rotation of a skin flap while keeping nerve fibers intact (Rosselet et al., 2008). In those experiments, cortical topography was remodeled over the course of 2 weeks, so that a new somatosensory map emerged, matching perfectly the new contiguity of peripheral skin zones. Both maps then co-existed, suggesting that several readout schemes can be implemented simultaneously in a cortical area. In our experiments,

a reorganization of spatial readout mechanisms by downstream areas could still be at play. The extent of such reorganization during neuroprosthesis use has been debated (Makin and Ben-smaia, 2017). Recent studies on participants using a sensorimotor bionic arm suggest that long-term perceptual alignment of the prosthesis and the missing limb requires that sensor location and the connected nerve sensation should roughly match (Cuberovic et al., 2019; Ortiz-Catalan et al., 2020; Schofield et al., 2020). Thus, remapping in adults may occur, but only to a certain degree (Tabot et al., 2015).

Limitations of the study

In this study, we targeted several cortical areas to explore how mice can efficiently read out patterns of neural activation. While their different topographical arrangement can explain our results, these cortical areas may differ in additional ways, including the level of expression of the ChR2 transgene. However, transgene expression appears similar across the neocortex of our mouse line, as detailed histological sections generated for the Allen Brain Atlas show (Madisen et al., 2012). We further checked that, in our experimental conditions, optogenetic stimulation evoked reliable spiking activity (Figures S1D and S1E). Similar activation has been reported in primary auditory cortex using the same mouse line (Ceballo et al., 2019b). We are therefore confident that the photostimulation pattern activated the cortex adequately in all our experimental conditions. Another concern is that these areas project to different brain regions, which might affect the behavioral output during the task. Further experiments will be necessary to explore this hypothesis.

STAR★METHODS

Detailed methods are provided in the online version of this paper and include the following:

- KEY RESOURCES TABLE
- RESOURCE AVAILABILITY
 - Lead contact
 - Materials availability
 - Data and code availability
- EXPERIMENTAL MODEL AND SUBJECT DETAILS
- METHOD DETAILS
 - Mouse preparation
 - Optogenetic photostimulation
 - Behavioral training
 - Histology
- QUANTIFICATION AND STATISTICAL ANALYSIS

SUPPLEMENTAL INFORMATION

Supplemental information can be found online at <https://doi.org/10.1016/j.celrep.2022.110617>.

ACKNOWLEDGMENTS

We thank Guillaume Hucher, Esther Fournel, and Aurélie Daret for experimental help and support. We thank Isabelle Ferezou and Evan Harrell for advice. We thank ANR (Neurowhisk 14-CE24-0019, Mesobrain 20-CE37-0013, MotorSense 21-CE37-0012, iCODE, and NeuroSaclay 11-IDEX-0003-02),

FRM DEQ20170336761, CNRS|80Prime, FRC AAP2018, and the 3DS foundation.

AUTHOR CONTRIBUTIONS

D.E.S., L.E., and V.E.-S. initiated and supervised the project. H.L., D.G., D.E.S., L.E., and V.E.-S. designed the experiments. H.L. performed the experiments with help from D.G. H.L. analyzed the data with support from V.E.-S. and L.E. H.L. wrote the paper with inputs from all authors.

DECLARATION OF INTERESTS

The authors declare no competing interests.

Received: September 21, 2021

Revised: December 21, 2021

Accepted: March 14, 2022

Published: April 5, 2022

REFERENCES

- Abbasi, A., Goueytes, D., Shulz, D.E., Ego-Stengel, V., and Estebanez, L. (2018). A fast intracortical brain-machine interface with patterned optogenetic feedback. *J. Neural Eng.* **15**, 046011.
- Bathellier, B., Tee, S.P., Hrovat, C., and Rumpel, S. (2013). A multiplicative reinforcement learning model capturing learning dynamics and interindividual variability in mice. *Proc. Natl. Acad. Sci. U S A* **110**, 19950–19955.
- Bosking, W.H., Sun, P., Ozker, M., Pei, X., Foster, B.L., Beauchamp, M.S., and Yoshor, D. (2017). Saturation in phosphene size with increasing current levels delivered to human visual cortex. *J. Neurosci.* **37**, 7188–7197.
- Brecht, M. (2017). The body model theory of somatosensory cortex. *Neuron* **94**, 985–992.
- Ceballos, S., Bourg, J., Kempf, A., Piwkowska, Z., Daret, A., Pinson, P., Deneux, T., Rumpel, S., and Bathellier, B. (2019a). Cortical recruitment determines learning dynamics and strategy. *Nat. Commun.* **10**, 1479.
- Ceballos, S., Piwkowska, Z., Bourg, J., Daret, A., and Bathellier, B. (2019b). Targeted cortical manipulation of auditory perception. *Neuron* **104**, 1168–1179.e5.
- Chen, X., Wang, F., Fernandez, E., and Roelfsema, P.R. (2020). Shape perception via a high-channel-count neuroprosthesis in monkey visual cortex. *Science* **370**, 1191–1196.
- Choi, G.B., Stettler, D.D., Kallman, B.R., Bhaskar, S.T., Fleischmann, A., and Axel, R. (2011). Driving opposing behaviors with ensembles of piriform neurons. *Cell* **146**, 1004–1015.
- Cuberovic, I., Gill, A., Resnik, L.J., Tyler, D.J., and Graczyk, E.L. (2019). Learning of artificial sensation through long-term home use of a sensory-enabled prosthesis. *Front. Neurosci.* **13**, 853.
- Dadarlat, M.C., O'Doherty, J.E., and Sabes, P.N. (2015). A learning-based approach to artificial sensory feedback leads to optimal integration. *Nat. Neurosci.* **18**, 138–144.
- Dalgleish, H.W., Russell, L.E., Packer, A.M., Roth, A., Gauld, O.M., Greenstreet, F., Thompson, E.J., and Häusser, M. (2020). How many neurons are sufficient for perception of cortical activity? *ELife* **9**, e58889.
- Daniel, P.M., and Whitteridge, D. (1961). The representation of the visual field on the cerebral cortex in monkeys. *J. Physiol.* **159**, 203–221.
- Dobelle, W.H. (2000). Artificial vision for the blind by connecting a television camera to the visual cortex. *ASAIO J.* **46**, 3–9.
- Dobelle, W.H., Mladejovsky, M.G., and Girvin, J.P. (1974). Artificial vision for the blind: electrical stimulation of visual cortex offers hope for a functional prosthesis. *Science* **183**, 440–444.
- El-Boustani, S., Sermet, B.S., Foustoukos, G., Oram, T.B., Yizhar, O., and Petersen, C.C.H. (2020). Anatomically and functionally distinct thalamocortical inputs to primary and secondary mouse whisker somatosensory cortices. *Nat. Commun.* **11**, 3342.
- Estebanez, L., Férézou, I., Ego-Stengel, V., and Shulz, D.E. (2018). Representation of tactile scenes in the rodent barrel cortex. *Neuroscience* **368**, 81–94.
- Fernández, E., Alfaro, A., Soto-Sánchez, C., Gonzalez-Lopez, P., Lozano, A.M., Peña, S., Grima, M.D., Rodil, A., Gómez, B., Chen, X., et al. (2021). Visual percepts evoked with an intracortical 96-channel microelectrode array inserted in human occipital cortex. *J. Clin. Invest.* **131**, e151331.
- Flesher, S.N., Collinger, J.L., Foldes, S.T., Weiss, J.M., Downey, J.E., Tyler-Kabara, E.C., Bensmaia, S.J., Schwartz, A.B., Boninger, M.L., and Gaunt, R.A. (2016). Intracortical microstimulation of human somatosensory cortex. *Sci. Transl. Med.* **8**, 141–361.
- Flesher, S.N., Downey, J.E., Weiss, J.M., Hughes, C.L., Herrera, A.J., Tyler-Kabara, E.C., Boninger, M.L., Collinger, J.L., and Gaunt, R.A. (2021). A brain-computer interface that evokes tactile sensations improves robotic arm control. *Science* **372**, 831–836.
- Goueytes, D., Abbasi, A., Lassagne, H., Shulz, D.E., Estebanez, L., and Ego-Stengel, V. (2019). Control of a robotic prosthesis simulation by a closed-loop intracortical brain-machine interface. In 2019 9th International IEEE/EMBS Conference on Neural Engineering (NER) (IEEE), pp. 183–186.
- Harding-Forrester, S., and Feldman, D.E. (2018). Somatosensory maps. *Handb. Clin. Neurol.* **151**, 73–102.
- Hartmann, K., Thomson, E.E., Zea, I., Yun, R., Mullen, P., Canarick, J., Huh, A., and Nicolelis, M.A.L. (2016). Embedding a panoramic representation of infrared light in the adult rat somatosensory cortex through a sensory neuroprosthesis. *J. Neurosci.* **36**, 2406–2424.
- Houweling, A.R., and Brecht, M. (2008). Behavioural report of single neuron stimulation in somatosensory cortex. *Nature* **451**, 65–68.
- Huber, D., Petreanu, L., Ghitani, N., Ranade, S., Hromádka, T., Mainen, Z., and Svoboda, K. (2008). Sparse optical microstimulation in barrel cortex drives learned behaviour in freely moving mice. *Nature* **451**, 61–64.
- Jiang, X., Shen, S., Cadwell, C.R., Berens, P., Sinz, F., Ecker, A.S., Patel, S., and Tlilas, A.S. (2015). Principles of connectivity among morphologically defined cell types in adult neocortex. *Science* **350**, aac9462.
- Kaas, J.H. (1997). Topographic maps are fundamental to sensory processing. *Brain Res. Bull.* **44**, 107–112.
- Knutsen, P.M., Mateo, C., and Kleinfeld, D. (2016). Precision mapping of the vibrissa representation within murine primary somatosensory cortex. *Philos. Trans. R. Soc. B Biol. Sci.* **371**, 20150351.
- Lashley, K.S. (1939). The mechanism of vision. XVI. The functioning of small remnants of the visual cortex. *J. Comp. Neurol.* **70**, 45–67.
- Leal-Campanario, R., Delgado-García, J.M., and Gruart, A. (2006). Microstimulation of the somatosensory cortex can substitute for vibrissa stimulation during Pavlovian conditioning. *Proc. Natl. Acad. Sci. U S A* **103**, 10052–10057.
- Madisen, L., Mao, T., Koch, H., Zhuo, J., Berenyi, A., Fujisawa, S., Hsu, Y.-W.A., Garcia, A.J., Gu, X., Zanella, S., et al. (2012). A toolbox of Cre-dependent optogenetic transgenic mice for light-induced activation and silencing. *Nat. Neurosci.* **15**, 793–802.
- Makin, T.R., and Bensmaia, S.J. (2017). Stability of sensory topographies in adult cortex. *Trends Cogn. Sci.* **21**, 195–204.
- Merzenich, M.M., Knight, P.L., and Roth, G.L. (1975). Representation of cochlea within primary auditory cortex in the cat. *J. Neurophysiol.* **38**, 231–249.
- Muller, L., Chavane, F., Reynolds, J., and Sejnowski, T.J. (2018). Cortical travelling waves: mechanisms and computational principles. *Nat. Rev. Neurosci.* **19**, 255–268.
- Narayanan, R.T., Egger, R., Johnson, A.S., Mansvelder, H.D., Sakmann, B., de Kock, C.P.J., and Oberlaender, M. (2015). Beyond columnar organization: cell type- and target layer-specific principles of horizontal axon projection patterns in rat vibrissa cortex. *Cereb. Cortex* **25**, 4450–4468.
- Nogueira, R., Rodgers, C.C., Bruno, R., and Fusi, S. (2021). The non-linear mixed representations in somatosensory cortex support simple and complex tasks. Preprint at bioRxiv. <https://doi.org/10.1101/2021.02.11.430704>.

- O'Connor, D.H., Hires, S.A., Guo, Z.V., Li, N., Yu, J., Sun, Q.-Q., Huber, D., and Svoboda, K. (2013). Neural coding during active somatosensation revealed using illusory touch. *Nat. Neurosci.* **16**, 958–965.
- O'Doherty, J.E., Lebedev, M.A., Ifft, P.J., Zhuang, K.Z., Shokur, S., Bleuler, H., and Nicolelis, M.A.L. (2011). Active tactile exploration using a brain-machine-brain interface. *Nature* **479**, 228–231.
- Ortiz-Catalan, M., Mastinu, E., Greenspon, C.M., and Bensmaia, S.J. (2020). Chronic use of a sensitized bionic hand does not remap the sense of touch. *Cell Rep.* **33**, 108539.
- Penfield, W., and Boldrey, E. (1937). Somatic motor and sensory representation in the cerebral cortex of man as studied by electrical stimulation. *Brain* **60**, 389–443.
- Penfield, W., and Rasmussen, T. (1950). *The Cerebral Cortex of Man; a Clinical Study of Localization of Function* (Macmillan).
- Peng, Y., Gillis-Smith, S., Jin, H., Tränkner, D., Ryba, N.J.P., and Zuker, C.S. (2015). Sweet and bitter taste in the brain of awake behaving animals. *Nature* **527**, 512–515.
- Perronnet, L., Vilarchao, M.E., Hucher, G., Shulz, D.E., Peyré, G., and Ferezou, I. (2016). An automated workflow for the anatomo-functional mapping of the barrel cortex. *J. Neurosci. Methods* **263**, 145–154.
- Rockland, K.S., Lund, J.S., and Humphrey, A.L. (1982). Anatomical banding of intrinsic connections in striate cortex of tree shrews (*Tupaia glis*). *J. Comp. Neurol.* **209**, 41–58.
- Romo, R., Hernández, A., Zainos, A., and Salinas, E. (1998). Somatosensory discrimination based on cortical microstimulation. *Nature* **392**, 387–390.
- Rosselet, C., Zennou-Azogui, Y., Escoffier, G., Kirmaci, F., and Xerri, C. (2008). Experience-dependent changes in spatiotemporal properties of cutaneous inputs remodel somatosensory cortical maps following skin flap rotation. *Eur. J. Neurosci.* **27**, 1245–1260.
- Sachidhanandam, S., Sreenivasan, V., Kyriakatos, A., Kremer, Y., and Petersen, C.C.H. (2013). Membrane potential correlates of sensory perception in mouse barrel cortex. *Nat. Neurosci.* **16**, 1671–1677.
- Schmidt, E.M., Bak, M.J., Hambrecht, F.T., Kufta, C.V., O'Rourke, D.K., and Vallabhanath, P. (1996). Feasibility of a visual prosthesis for the blind based on intracortical microstimulation of the visual cortex. *Brain J. Neurol.* **119**, 507–522.
- Schofield, J.S., Shell, C.E., Beckler, D.T., Thumser, Z.C., and Marasco, P.D. (2020). Long-term home-use of sensory-motor-integrated bidirectional bionic prosthetic arms promotes functional, perceptual, and cognitive changes. *Front. Neurosci.* **14**, 120.
- Tabot, G.A., Dammann, J.F., Berg, J.A., Tenore, F.V., Boback, J.L., Vogelstein, R.J., and Bensmaia, S.J. (2013). Restoring the sense of touch with a prosthetic hand through a brain interface. *Proc. Natl. Acad. Sci. U S A* **110**, 18279–18284.
- Tabot, G.A., Kim, S.S., Winberry, J.E., and Bensmaia, S.J. (2015). Restoring tactile and proprioceptive sensation through a brain interface. *Neurobiol. Dis.* **83**, 191–198.
- Vanni, M.P., Chan, A.W., Balbi, M., Silasi, G., and Murphy, T.H. (2017). Meso-scale mapping of mouse cortex reveals frequency-dependent cycling between distinct macroscale functional modules. *J. Neurosci.* **37**, 7513–7533.
- Venkatraman, S., and Carmena, J.M. (2011). Active sensing of target location encoded by cortical microstimulation. *IEEE Trans. Neural Syst. Rehabil. Eng.* **19**, 317–324.
- Vilarchao, M.E., Estebanez, L., Shulz, D.E., and Férézou, I. (2018). Supra-barrel distribution of directional tuning for global motion in the mouse somatosensory cortex. *Cell Rep.* **22**, 3534–3547.
- Winawer, J., and Parvizi, J. (2016). Linking electrical stimulation of human primary visual cortex, size of affected cortical area, neuronal responses, and subjective experience. *Neuron* **92**, 1213–1219.
- Woolsey, T.A., and Van der Loos, H. (1970). The structural organization of layer IV in the somatosensory region (S I) of mouse cerebral cortex: the description of a cortical field composed of discrete cytoarchitectonic units. *Brain Res.* **17**, 205–242.
- Yizhar, O., Fenno, L.E., Davidson, T.J., Mogri, M., and Deisseroth, K. (2011). Optogenetics in neural systems. *Neuron* **71**, 9–34.

STAR★METHODS

KEY RESOURCES TABLE

REAGENT or RESOURCE	SOURCE	IDENTIFIER
Experimental models: organisms/strains		
Emx-cre X Ai27 transgenic mice	Madisen et al., 2012	Crossing RRID: IMSR_JAX:005628; RRID: IMSR_JAX:012567
Software and algorithms		
C++ Software Handling the behaviour	This paper	https://doi.org/10.5281/zenodo.6337587
Code used to analyze the data	This paper	https://doi.org/10.5281/zenodo.6337587
Intrinsic Imaging Software	This paper	https://doi.org/10.5281/zenodo.6337587
Other		
DLP, Vialux V-7001, 462 nm blue LED	Vialux	N/A
CCD camera (Basler acA640120 um)	Basler	N/A

RESOURCE AVAILABILITY

Lead contact

Further information and requests for resources should be directed to and will be fulfilled by the lead contact, Valérie Ego-Stengel (valerie.ego-stengel@cns.fr).

Materials availability

This study did not generate new material.

Data and code availability

- Data reported in this paper will be shared by the [lead contact](#) upon request.
- All original code has been deposited on GitHub and is publicly available as of the date of publication. The DOI is listed in the [key resources table](#).
- Any additional information required to reanalyze the data reported in this paper is available from the [lead contact](#) upon request.

EXPERIMENTAL MODEL AND SUBJECT DETAILS

We used 6-week-old Ai-27 x EMX-Cre mice, expressing channelrhodopsin in excitatory neurons across the cortex ([Madisen et al., 2012](#)). Experimental procedures have been approved by the French Ministry of Research and Ethics Committee #59 as part of project #858-2015060516116339. A total of 14 mice (6 female, 8 male) were successfully implanted, water restricted, and then trained in the task. During the training period, mice only had access to water during the sessions as reward, and right after the session for supplementation whenever necessary.

METHOD DETAILS

Mouse preparation

Surgeries were performed on anesthetized mice (1%–4% isoflurane anesthesia in 100% air) placed on a regulated heating pad. The state of the anesthesia was assessed by breathing rate and response to tail pinch. The scalp was resected after lidocaine-induced local anesthesia (200 mg/L, 0.1 mL) and conjunctive tissues were removed. A head-post was glued (cyanoacrylate glue) to the skull, then strengthened with dental cement. A 5 to 6 mm diameter craniotomy was then performed while preserving the dura, centered either on the stereotaxic coordinates of the C2 barrel in the primary somatosensory cortex (P1.5–L3.3 mm), or on a more medial location in between the paw representation and the barrel cortex (P0.5–L2.3 mm). A glass optical window of diameter 5 or 6 mm was glued to the borders of the craniotomy. The remaining exposed skull was covered with dental cement. At the end of the surgery, we administered subcutaneously an analgesic (2 mg/mL Metacam, 0.1 mL) and an antibiotic (2.4% Borgal, 0.2 mL). Intrinsic imaging sessions through the window were performed 5 to 10 days after the surgery. During an imaging session, either a single whisker or the right forepaw was stimulated with a piezoelectric bender (Physics Instruments) 100 Hz, 5 ms square wave deflection) while red light (625 nm) was projected on the window right below light saturation. A CCD camera acquired 659*494 px images at a rate of

60 fps. The images were analyzed for space-time fluctuations in luminescence (Optimage, Thomas Deneux, NeuroPSI). These intrinsic imaging sessions were used to locate the C2, Alpha and Delta barrel locations, as well as the forepaw location (Figures 1C and 4B). More details can be found in Abbasi et al., (2018).

Optogenetic photostimulation

During training, optogenetic stimulation was performed through the optical window (Figure 1A) using a Digital Light Processing module (DLP, Vialux V-7001, 462 nm blue LED). Stimulation patterns consisted of light bars 700 microns long and 150 microns wide, rotating on a disk of diameter 1.5 mm. This pattern was chosen as part of our interest in encoding the angle of a joint (Goueytes et al., 2019). The disk was centered on the C2 barrel location (vS1, Figure 1B, $n = 11$ mice). In three additional mice, the stimulation was centered on a point 1.5 mm medial and 1 mm rostral to the C2 barrel, thus on the trunk and legs representation (“body” S1, bS1, Figures 4A and 4B). Among the 14 mice, four were subsequently trained with the stimulation centered on the posterior parietal cortex (PPC), 1.5 mm caudal to the C2 barrel (Figure 4A; three mice after vS1 training, one after bS1 training). To avoid overstimulation of cortical areas, the center of the stimulated disk was never illuminated (white spot in Figure 1D). Photostimulation was done at high power (measured, 10–15 mW per mm^2). Using a photodetector, we ensured that the edge of the photostimulation was sharp; intensity decreased to 5% at 20 microns from the edge. Spiking activity resulting from similar photostimulation was demonstrated previously (Abbasi et al., 2018; Ceballo et al., 2019b; Madisen et al., 2012). In pilot experiments, we checked that the particular light bar designed for this study also evoked spiking across the optical window. We conducted electrophysiological recordings with 1-shank electrodes (Neuronexus, 64-channel multisite extracellular electrode, A1x64-Poly2-6mm-23S-160) inserted obliquely through a small opening in the cranial window, while projecting patterns of light on S1 (Figure S1D). We typically performed several penetrations at different entry points along the anterior-posterior axis, thus exploring different parts of S1 and surroundings. Analysis of individual single-unit spike trains (Blackrock acquisition system, Spyking Circus) demonstrated strong neural activation by the optogenetic bar moving above the location of the recording site (Figure S1E). These results confirmed that optogenetic stimulation of neocortex in Emx-Cre x Ai27 mice induces neural activation (Ceballo et al., 2019b; Madisen et al., 2012).

Behavioral training

After surgery and intrinsic imaging, mice were water restricted. Training started two days later. During the first session, the mouse was habituated to head-fixation and learned to lick water from a small tube. During this session, licks always triggered water rewards, and nothing happened if the mouse did not lick. Each subsequent session lasted 30 min, during which a randomized set of trials was presented to the mouse. Trials were separated by 5 s.

In the standard condition, each trial consisted in the presentation of one trajectory of the photostimulation bar, starting from the most caudal position, and then rotating towards a rostral rewarded zone with different dynamics. The bar angular position was updated every 10 ms. Each trajectory was taken from a database of 252 pre-loaded trajectories. These were obtained from a closed-loop BMI study performed with different mice (Goueytes et al., 2019). In that study, the activity of motor cortex neurons was used to drive the rotating bar. From the initial full dataset, we kept only the 126 trajectories lasting between 10 and 20 s, entering at least once the rewarded zone (green zone, Figure 1E). To remove a possible right/left bias, for each trajectory, its symmetric trajectory with respect to the rostro-caudal axis was added to the database, yielding the full set of 252 smooth trajectories with evolving dynamics (Figures S1A–S1C).

A lick had different consequences depending on the angular location of the photostimulation bar at that time. A lick when the light bar was in the rewarded zone (green area, Figure 1E) led to an immediate 10 μL water reward. A lick in the no-lick zone (red area) immediately ended the trial and was followed by the 5 s intertrial interval, during which the cortex was not photostimulated. A new trial started immediately after the 5 s period. A lick in the neutral zones (white areas) had no consequence. If the mouse drank more than 3 mL of water during one session, only one lick out of two was rewarded with water during the following sessions, starting with the first lick inside the rewarded zone. The rewarded zone spanned 60°, except for three mice for which it spanned 50°.

Mice were trained for 5 to 10 daily sessions of 30 min each. Three mice initially trained for 5 days in the standard condition on vS1 were then trained for 5 days in a difficult condition, in which the size of the no-lick zone was increased so that the task became more challenging (Figure S4, these were the three mice trained with a 50° rewarded zone). Three other mice were also initially trained in the standard condition and were then tested for one session in a shuffled condition (Figures 2A–2F), in which the contiguity of the cortical sectors crossed during the trajectories was modified. Specifically, the stimulation disk was divided in six 60° sectors, and these sectors were swapped so that the trajectory jumped from one sector to another at the boundaries. The starting position and rewarded zone were unchanged. Another group of three naive mice were directly trained in the shuffled condition on vS1 (Figures 2B–2E).

Mice were usually trained every day for 10 days once enrolled in a protocol. However, in the first experiments, training was often stopped after 5 days of vS1 stimulation in the standard condition because the performance of the mice was already very high. When training duration varied across mice, the last session of each mouse was labelled Last for group analysis.

Histology

After training, mice were deeply anesthetized with isoflurane (4%–5%), euthanized by cervical dislocation, and perfused with para-formaldehyde (PFA). The brains were stored in PBS for two days or more, and then S1 tangential slices (100 microns thick) were cut and stained with cytochrome C oxidase. The alignment of the stained barrels and the blood vessels were computed using a

homemade software (Perronnet et al., 2016). Briefly, this software uses the position of the transversal vessels to realign each slice with respect to each other. At the end of the process, the slice showing the blood vessels on the surface of the cortex and the slices showing the stained barrels could be superimposed accurately (Figure 1D).

QUANTIFICATION AND STATISTICAL ANALYSIS

We quantified performance by assessing the percentage of trials that were rewarded in each session. We also computed a detection value (Figure 1G), corresponding to the percentage of entries into the rewarded zone for which the mouse obtained at least one reward. Therefore, the detection value was not affected by trials that were interrupted before reaching the rewarded area. Overall, a high detection value indicates that the mouse learned to lick when the light bar was in the rewarded zone, while a high percentage of rewarded trials requires that in addition, the mouse learned to refrain from licking in the no-lick zone. These two measures of performance were normalized session by session by estimating a chance level obtained by bootstrapping. For each session, one hundred shuffled sessions were generated by loading random sequences of trajectories from the database while keeping the temporal sequence of licks from the real session. The simulated protocol followed all the task rules: if during a simulated trajectory, a lick happened while photostimulation was in the no-lick zone, a 5 s intertrial interval was enforced and a new trial was loaded thereafter. The average performance of these simulations was then subtracted from the performance of the real session to obtain the normalized performance (Figures 1G, 2B, 3C, and 3D).

To demonstrate that mice were using spatial information from the cortical stimulus and not only a temporal strategy, we designed an algorithm that solves the task exclusively by using time elapsed from the start of the trial. In the simplest version, this algorithm waits a fixed amount of time, called its operating time, then licks continuously until the end of the trial. In the version we used, instead of a fixed value, we picked waiting times randomly from a Gaussian distribution centered on the operating time, and with a standard deviation equal to the smallest standard deviation of response times observed in a trained mouse. We generated one such algorithm for each operating time from 0 to 20 s (with 0.01 s steps). For each operating time, we quantified the performance of the algorithm by the detection value and percentage of rewarded trials for a full session comprised of the 252 different trials.

To quantify the behavioral licking response of the mice as a function of cortical location, we analyzed the distribution of angular positions of the optogenetic bar at lick times (Figures 2A–2C). However, as a lick in the rewarded zone leads to a reward and thus to more licks, these plots often showed large numbers of licks not necessarily linked to the simultaneous photostimulation location. To disambiguate first licks from others, we defined an onset lick as a lick that was not preceded by another lick in the last 3 s.

Each statistical test used is described in the text and/or in the figure legends. *: $p < 0.05$. **: $p < 0.01$. ***: $p < 0.001$.

Cell Reports, Volume 39

Supplemental information

**Continuity within the somatosensory cortical
map facilitates learning**

Henri Lassagne, Dorian Goueytes, Daniel E. Shulz, Luc Estebanez, and Valerie Ego-Stengel

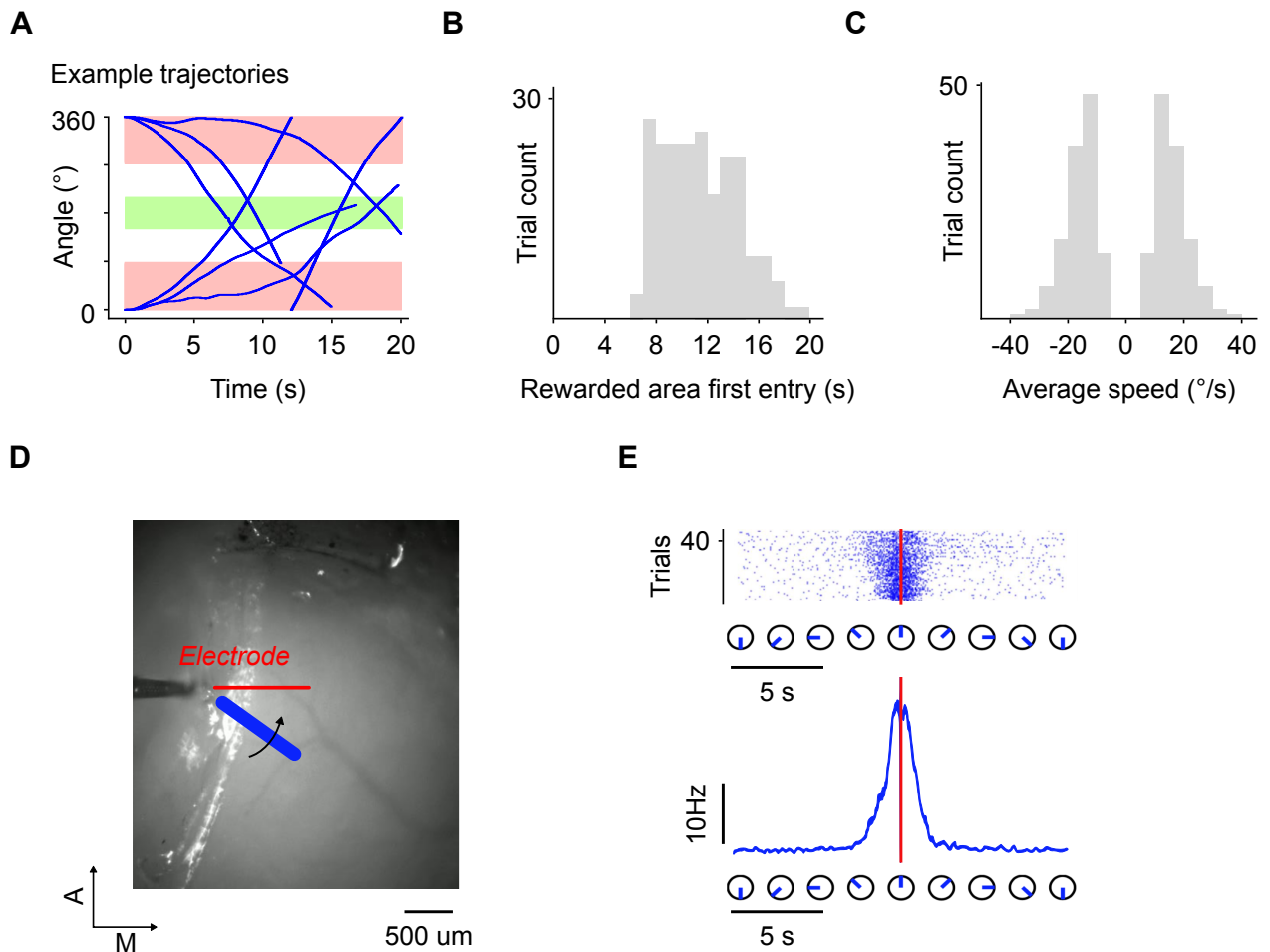


Figure S1. Optogenetic task dynamics and neural activation. Related to Figure 1.

(A) Six example trajectories of the optogenetic stimulation. The reference angle 0° corresponds to the angle for the lowest point on Figure 1E, most posterior on the cortical surface. The photostimulation bar could rotate several times around the center, and could reverse directions.

(B) Distribution of the times of first entry of the optogenetic stimulation in the Rewarded zone, for the 252 trajectories in the database.

(C) Distribution of the average angular speed of the optogenetic stimulation, for the 252 trajectories in the database. The bar can move either clockwise or counterclockwise.

(D) Recordings in S1 with a silicon longitudinal multi-site electrode (Neuronexus, 64-channel multisite extracellular electrode, A1x64-Poly2-6mm-23S-160), while stimulating the cortex with a moving optogenetic bar. Here the bar is of same width but longer than for the behavioral task, so that we could ensure that it passes over most electrode sites. The red line indicates the electrode shank in the brain.

(E) Top: Example raster plot of spikes from a single unit as the optogenetic bar rotates, demonstrating strong activation.

Bottom: Peri-Stimulus Time Histogram of the same spiking activity.

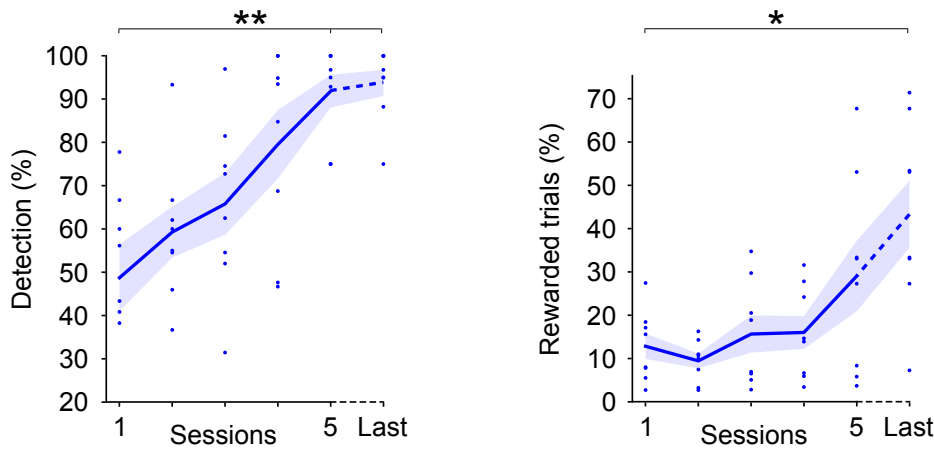
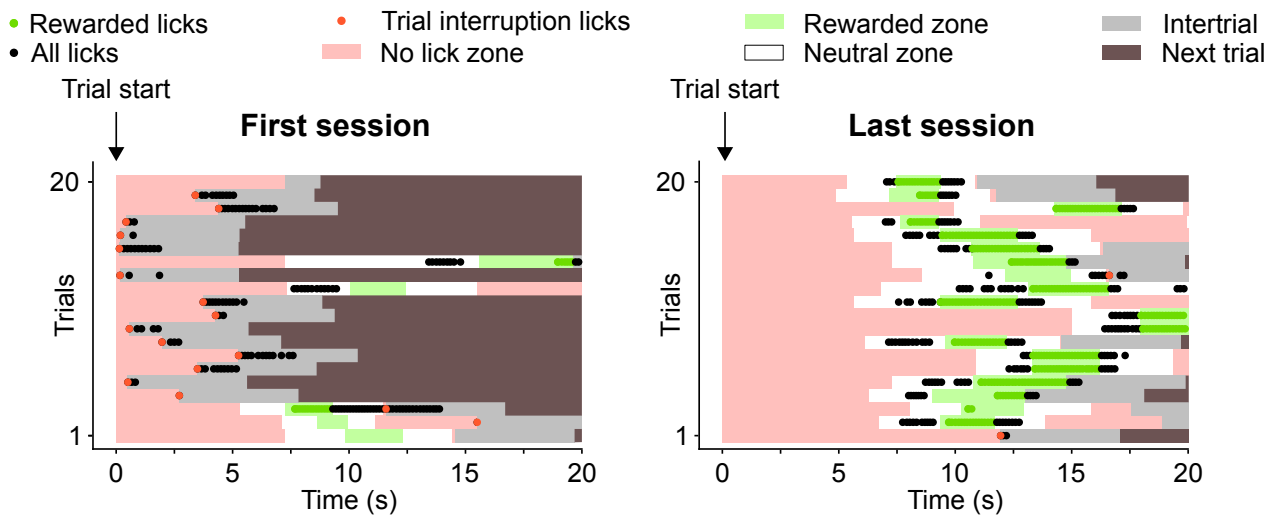


Figure S2. Raw Learning curves. Related to Figure 1.

Learning curves as in Figure 1G, but before subtracting the chance level calculated by bootstrapping the trials for each individual session (see Methods)

A



B

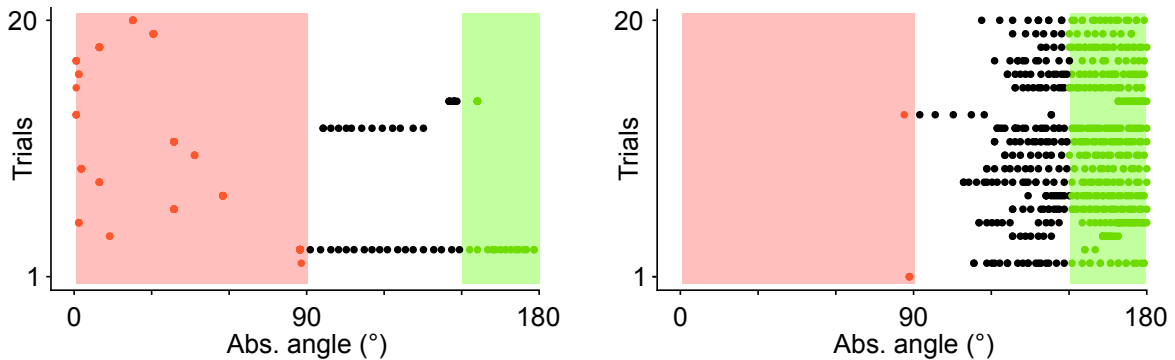


Figure S3. Mice learn to lock their licking behavior to the stimulation angle in cortical space. Related to Figure 1.

(A) Raster plots of licks (dots) as a function of time after trial onset, during 20 consecutive trials in the first and tenth session for one mouse. Same graphs as Figure 1F.

(B) Raster plots similar to Panel A, but as a function of the absolute angle of the photostimulation bar on the cortical surface. The reference angle 0° corresponds to the lowest point of Figure 1E, most posterior on the cortical surface. Angles were mapped to $[-180^\circ, 180^\circ]$ before taking the absolute value. Note that because the horizontal axis represents angles, licks on the right do not necessarily happen before licks on the left.

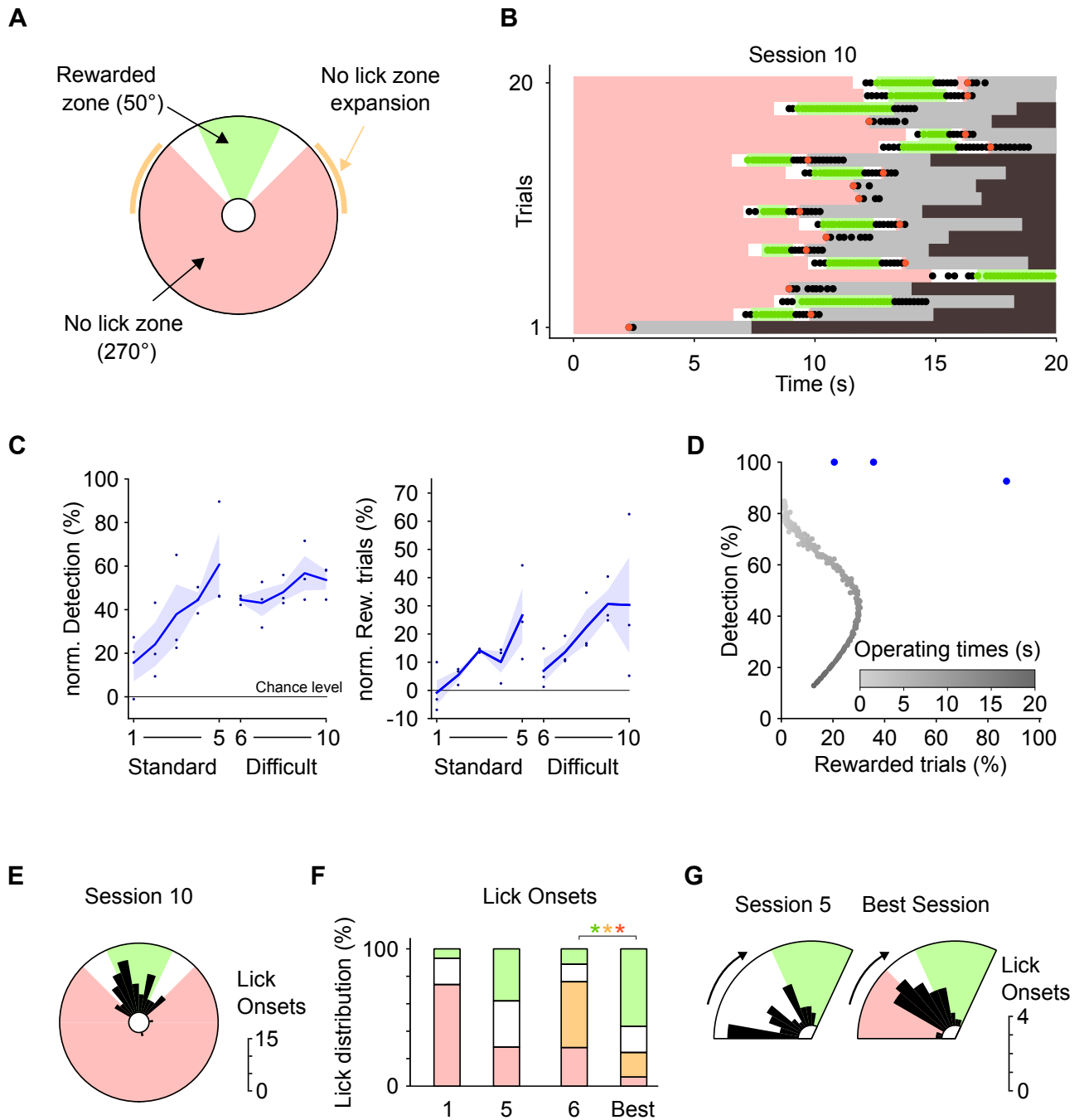


Figure S4. Mice finely discriminate spatial zones of stimulation. Related to Figure 2.

(A) In the difficult condition, the no-lick zone was expanded from 180° to 270° while the neutral zones were each reduced from 60° to 20°. Orange lines: expanded area of the no-lick zone.

(B) Raster plot of licks (dots) during the first 20 trials of the last session of a mouse trained on the difficult task for 5 days, after having been trained on the standard task for 5 days. Conventions are the same as for Figure 1F. Lick onsets largely occur in the neutral and rewarded zones.

(C) Average learning curves (\pm SEM, $n = 3$ mice), quantified by the normalized detection level (Left), and the normalized percentage of rewarded trials (Right).

(D) Performance curve of an algorithm solving the difficult condition task with a pure temporal strategy (see Methods and Figure 1H). The blue dots indicate the mice performance during their last session.

(E) Spatial distribution of the optogenetic stimulus angle for lick onsets for the session shown in panel B.

(F) Average distribution of lick onsets for which the optogenetic bar was in the rewarded, no-lick and neutral zones, for the first and last (or best) session of the two training conditions. Orange corresponds to licks in the no-lick expansion zone. Best session corresponds to each mouse's highest performance among session 9 and session 10. This adaptation of the quantification was necessary because the task was very challenging, so performance was highly variable.

(G) Average spatial distribution of the stimulus angle for lick onsets for the neutral and rewarded zones. Trials entering from the right were symmetrized before averaging as for Figure 2C. Only the first 20 rewarded trials of a given session were used for this analysis, ensuring that the mice were highly motivated.

4.2 Cortical closed-loop brain-machine interface requires biomimetic feedback

4.2.1 Summary

This second study asks how spatio-temporal patterns of artificial activity in the cortex are integrated by the network, when they provide the only information about an ongoing motor task. In this work, the stimulation consists of several "spots" of lights targeting individually the different barrels of the somatosensory cortex. One crucial aspect of this study is that compared to the first article, the animals are now driving a closed-loop BMI. Primary motor cortex neurons are recorded by single unit electrophysiology and, through a command algorithm, drive the position of the photostimulation. This allowed us to study more specifically mechanisms of sensorimotor integration and BMI learning in a closed-loop context. Similar to study 4.1, mice reached better performance when the feedback was closest spatio-temporally to the structure of the targeted cortex.

4.2.2 Participation statement

This study relies on a setup already described in 2018 (Abbasi et al., 2018) to which I did not contribute. After the first batches of experiments and analysis were performed by Aamir Abbasi, a lot of questions remained, making the interpretation of the results difficult. I adapted the setup for new photostimulation patterns, prepared and trained six mice, participated in the analysis and provided figures and inputs for the review and the new version of the article. (under third review, Nat Commun.)

Brain-machine interface learning is facilitated by specific patterning of distributed cortical feedback

A. Abbasi^{1†}, H. Lassagne^{1†}, L. Estebanez^{1†}, D. Goueytes¹, D. E. Shulz^{1‡} and V. Ego-Stengel^{1‡*}

Affiliations

¹Université Paris-Saclay, CNRS, Institut des Neurosciences Paris-Saclay (NeuroPSI), 91190, Gif-sur-Yvette, France.

*Correspondence: valerie.ego-stengel@cnrs.fr

[†]Equal contribution.

[‡]Equal contribution.

Summary

Neuroprosthetics offer great hope for motor-impaired patients. One obstacle is that fine motor control requires near-instantaneous, rich somatosensory feedback. Such distributed feedback may be recreated in a brain-machine interface using distributed artificial stimulation across the cortical surface. Here, we hypothesized that neuronal stimulation must be contiguous in its spatiotemporal dynamics in order to be efficiently integrated by sensorimotor circuits. Using a closed-loop brain-machine interface, we trained head-fixed mice to control a virtual cursor by modulating the activity of motor cortex neurons. We provided artificial feedback in real time with distributed optogenetic stimulation patterns in the primary somatosensory cortex. Mice developed a specific motor strategy and succeeded to learn the task only when the optogenetic feedback pattern was spatially and temporally contiguous while it moved across the topography of the somatosensory cortex. These results reveal new properties of sensorimotor cortical integration and set new constraints on the design of neuroprosthetics.

Keywords

Brain-machine interface, cortical map, topography, motor, somatosensory, barrel cortex, chronic electrophysiological recordings, behavior, optogenetics, closed-loop neuroscience.

INTRODUCTION

Accurate limb control requires somatosensory feedback. For instance, local peripheral anesthesia blocking afferent tactile sensation in humans reduces dexterity and impairs fine motor control of the hand (Johansson and Westling, 1984; Monzée et al., 2003). Similarly, cortical inactivation of somatosensory cortex in animals has profound effects on motor control (Brochier et al., 1999; Mathis et al., 2017). The critical role of somatosensory feedback has also been described in studies of patients that suffer from severe tactile or proprioceptive deficits. These patients learn to rely extensively on visual feedback, but remain unable to manage normal motor control (Chesler et al., 2016; Miall et al., 2018; Sainburg et al., 1995).

In the context of neuroprosthetics, proprioceptive and touch-like feedback originating from the prosthesis improves control (Flesher et al., 2019), and enables texture-like percepts that cannot be obtained through visual feedback alone (O'Doherty et al., 2019). Such artificial touch-like information has been provided through direct activation of the cerebral cortex via electrical stimulation (Armenta Salas et al., 2018; Flesher et al., 2021; O'Connor et al., 2013;

O'Doherty et al., 2011; Romo et al., 1998; Tabot et al., 2013) or optogenetics (Abbasi et al., 2018; Prsa et al., 2017). Beyond the choice of the neuronal stimulation technology, an important challenge is the design of the geometry and dynamics of the feedback patterns used to provide relevant sensory feedback information.

The design of artificial sensory feedback is particularly critical for replicating the functionality of a spatially distributed sense such as touch (Badde and Heed, 2016). Temporal modulation of one single stimulation channel, such as realized by optogenetic stimulation of S1 in the BMI experiments of Prsa and collaborators (2017), cannot suffice in this case. Rather, many independent channels of stimulation will be necessary to convey tactile information arising from different peripheral locations. Indeed, recent approaches have implemented simultaneous artificial stimulations at multiple locations in the somatosensory cortex (Flesher et al., 2016; Hartmann et al., 2016). However, it remains unclear if any arbitrary feedback pattern can be applied, or if the somatosensory-motor cortical areas can only integrate efficiently inputs with a specific type of spatio-temporal structure matched to the classical somatosensory topography (Penfield and Boldrey, 1937).

Here, we take advantage of the well-known whisker system of the mouse to explore this question (Diamond and Arabzadeh, 2013; Petersen, 2019). Anatomically, the primary somatosensory cortex (S1) of the mouse snout is organized into distinct columns, called barrels, that each receive dominant inputs from one corresponding whisker. These inputs combine with dense subcortical and intracortical lateral connectivity (Deschenes, 2009; Feldmeyer, 2012) and give rise to rich encoding of complex multiwhisker features, which can be found at the level of individual neurons as well as in the cortical map (summarized in Estebanez et al., 2018). Specifically, given the strong tuning of S1 neurons to the direction of bar-like multiwhisker deflections on the snout (Jacob et al., 2008; Vilarchao et al., 2018), and their tuning to progressive movement of objects across the whiskerpad (Laboy-Juárez et al., 2019), we hypothesized that stimulations that generate spiking activity in spatio-temporally contiguous barrel cortex locations may be more efficiently integrated into motor control, compared to spatio-temporally scattered patterns of cortical activation. This hypothesis is further supported by the fact that mice generate sequences of consecutive whisker deflections in the rostro-caudal direction during the exploration of their environment (Hobbs et al., 2016), suggesting that such stimuli are behaviorally relevant.

We tested this hypothesis by training mice to control a virtual cursor using the modulation of the activity of a few neurons, called Master neurons, recorded in the whisker area of the primary motor cortex (M1) (Arduin et al., 2013). Mice received online one of 5 different spatiotemporal patterns of cortical feedback generating spiking activity in S1. These patterns ranged from a sweeping, bar-like feedback where the barrels that were simultaneously or sequentially activated were all contiguous, up to a spatiotemporally fully randomized pattern, also including a condition without feedback. The inputs were delivered on the surface of the cortex by photostimulation of subsets of always 5 barrels among the 22 most caudal barrels. Importantly, we focused on the impact of changes in the structure of patterned stimulation, while the total surface area, intensity and temporal frequency of stimulation remained always fixed. We found that learning was largely dependent on the structure of the feedback and was highest in the bar-like feedback condition, where the photostimulated barrels are spatially and temporally contiguous. Learning in this specific condition revealed active motor control, as the neuronal activity that drove the virtual cursor reorganized and became dominated by one of the Master neurons.

RESULTS

Patterned optogenetic feedback on S1 enables learning in a closed-loop brain-machine interface

We implanted a total of 16 mice with a chronic, closed-loop brain-machine interface consisting of a head fixation bar, chronic silicon tetrodes in layer 5 of whisker M1 (Fig. 1a,b, Supplementary Fig. 1, 2) and a chronic optical window over S1 (see Methods).

After initial sessions where we habituated the mice to remain head-fixed and lick for water, we trained the mice to solve a 1D cursor control task via the brain-machine interface. To this aim, we sorted 3 “Master” neurons from the raw M1 neuronal activity (7 Master neurons in two mice, see Methods). The activity of these neurons controlled the movements of a virtual cursor during the sessions. Their summed firing rate was measured every 10 ms and was smoothed with a 100 ms kernel. It was then normalized by the firing rate distribution measured during a 3-minute baseline that preceded each session. Finally, we discretized the normalized values into 8 positions of a virtual cursor (see Methods, Fig. 1c and Supplementary Fig. 3).

Whenever the virtual cursor was in the rewardable position (Fig. 1c,e, only in position 5, except in our first experiments — see Methods), the mice could obtain a water droplet by licking a port located next to their tongue. Water rewards could be triggered only by licking on the spout. Therefore, in the absence of licking during the presence of the virtual cursor in the rewardable position, no water was made available to the mouse.

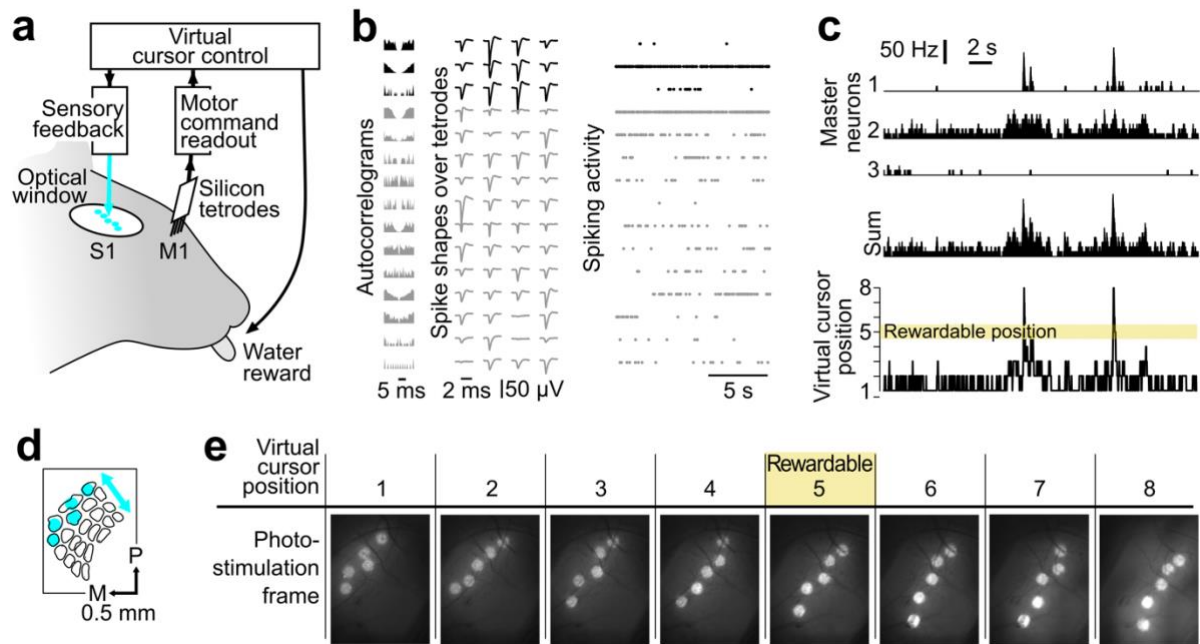


Fig. 1 Mice controlled a virtual cursor using whisker M1 neuronal activity while online optogenetic feedback was delivered to whisker S1. **a** General view of the closed-loop interface. The mice were head-fixed. A chronic silicon probe in M1 read out spiking activity and a chronic optical window over S1 allowed delivery of a photostimulation feedback. **b** Action potentials from 15 single units obtained during baseline activity in M1. The autocorrelograms (left), the spike shapes on the tetrodes (middle) and the spiking activity in time (right) are shown for each single unit. Black: Master neurons that are selected to control the virtual cursor. Gray: Neighboring neurons recorded simultaneously. **c** Example Master neurons activity and corresponding virtual cursor position. Top: Time histograms of the 3 Master neurons activity. Middle: Sum of their activity. Bottom: Position of the virtual cursor computed from the summed activity of the Master neurons. The virtual cursor must be in position 5 for the mouse to obtain a reward by licking. Bin size 10 ms. **d** Schematic of the first photostimulation frame of the bar-like photoactivation on the map of S1 barrels. P: posterior, M: medial. **e** Snapshots of the cortical surface

illustrating bar-like photostimulation frames for each virtual cursor position. Only when the virtual cursor was in position 5, licks were rewarded.

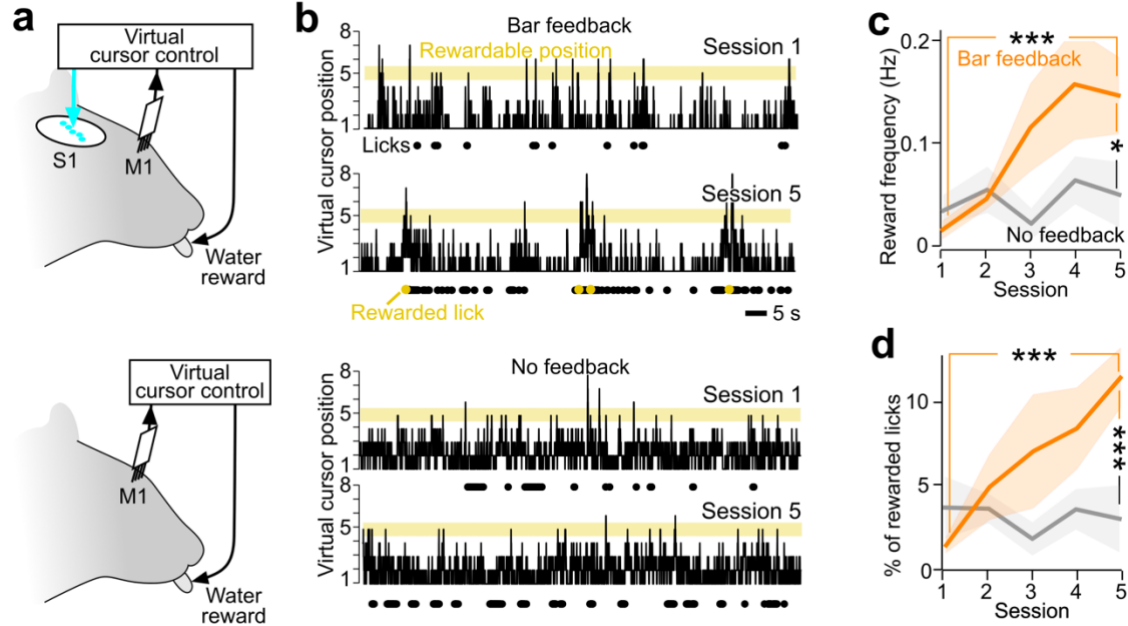


Fig. 2 Sensory feedback to the whisker part of S1 enhances task performance. **a** Schematic of the Bar feedback and No feedback conditions. **b** Position of the virtual cursor computed from the merged activity of the Master neurons, in the first versus the fifth training session of one mouse, in the Bar feedback condition (top) and in the No feedback condition (bottom) (100 s displayed). Yellow background: rewardable position. Black dots: lick times. Yellow dots: rewarded lick times. **c** Performance quantified by the average frequency of rewards per session across training, comparing the Bar feedback condition (orange, 10 mice) and the No feedback condition (grey, 8 mice). Shaded backgrounds: \pm standard error of the mean (SEM). *: $p < 0.05$. **: $p < 0.01$. ***: $p < 0.001$, non-parametric Mann-Whitney tests. **d** Same as c for the specificity of licking, quantified by the percentage of rewarded licks across behavioral sessions (number of rewarded licks divided by total number of licks and multiplied by 100).

During the task, the current position of the virtual cursor was provided online to the mice through patterned optogenetic stimulation of S1 that triggered local, low-latency spiking activity (see Methods). The mice expressed constitutively channelrhodopsin in pyramidal neurons (Emx-Cre;Ai27 strain, Madisen et al., 2012). The photostimulations were dynamically updated, with an intrinsic hardware latency of 12 ± 5 ms from the firing of the Master neurons to the corresponding photostimulation update (Abbasi et al., 2018).

At each time point, the pattern of cortical illumination consisted of focused spots that targeted five of the S1 barrels. We arranged these spots to form a bar-like arrangement of barrel activations, sweeping on barrels corresponding to caudal whiskers for position 1 of the virtual cursor, up to rostral whiskers for position 8 (Bar feedback, Fig. 1d-e).

A 30 min training session per day was delivered during five days. To obtain more rewards, mice had to increase the amount of time during which the virtual cursor was in the rewardable position, and/or improve their ability to lick in those time windows.

When Bar feedback was provided (Fig. 2a, top), the mice were able to increase significantly their performance within the 5 consecutive training sessions (example in Fig. 2b, top). On the first session the mice licked, but the virtual cursor was almost never in the rewardable position at the same time, and the mice obtained almost no water. On the fifth day training session, the same mice performed licking bouts at times when the virtual cursor entered the rewardable position, and thus obtained rewards more frequently. Overall, over the course of five training sessions, the performance measured as the frequency of rewards significantly increased more

than ten times (from 0.014 to 0.19 rewards/s; orange curve of Fig. 2c, Mann-Whitney $U = 5$, $p < 0.001$, $n = 10$ mice). In contrast, in the absence of optogenetic feedback (Fig. 2a,b, bottom), the mice failed to reliably increase the frequency of rewards despite the same amount of training (0.025 vs 0.022 rewards/s; gray curve in Fig. 2c, Mann-Whitney $U = 31$, $p = 0.48$, $n = 8$ mice among the 10 tested in the Bar feedback condition).

Importantly, the increased reward frequency in the Bar feedback condition was accompanied by an increase in the specificity of licking, measured by the percentage of licks that were rewarded among all licks (Fig. 2d, Mann-Whitney $U = 1$, $p < 0.001$). This indicated that the mice did not simply increase their licking frequency irrespective of the virtual cursor position in order to solve the task. We conclude from these data that the optogenetic feedback to the barrel cortex was required for learning to control this brain-machine interface within five training sessions.

Shuffling the spatiotemporal structure of the feedback disrupts learning

We hypothesized that in these initial experiments, the specific spatio-temporal structure of the Bar feedback helped the mice to control the virtual cursor, whereas other types of feedback might not result in similar fast task learning. To explore this question, we selected a subset of 3 additional feedback conditions that degraded the spatio-temporal structure of the original Bar feedback in controlled ways (Fig. 3a).

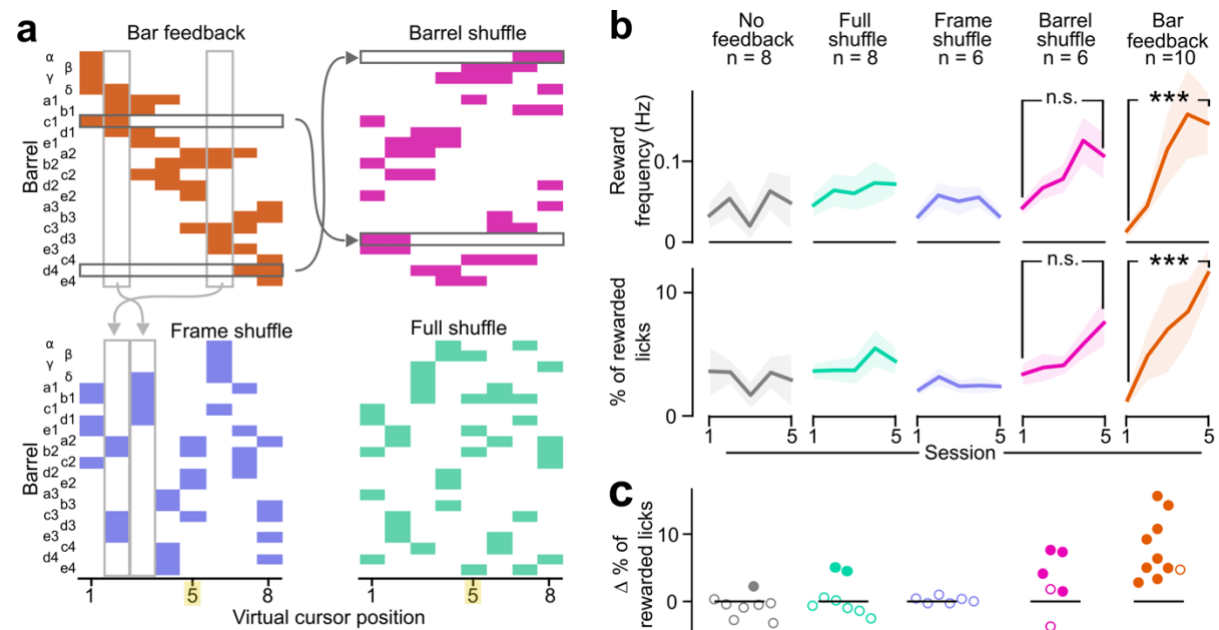


Fig. 3 Disrupting the spatiotemporal structure of the bar feedback impairs learning. **a** Spatial and temporal structure of the feedback across frames in the four tested conditions. Horizontal arrows: barrel identity permutation to generate the Barrel shuffle from the Bar feedback. Vertical arrows: frame identity permutation to generate the Frame shuffle from the Bar feedback. Yellow highlight: rewardable virtual cursor position. **b** Reward frequency (top) and percentage of rewarded licks (bottom) of the mice over 5 training sessions. ***: $p < 0.001$, non-parametric Mann-Whitney tests. Shaded backgrounds: \pm standard error of the mean (SEM). Bar feedback and No feedback data is the same as in Fig. 2. **c** Difference between the proportion of rewarded licks of the mice between the first versus fifth training session. Each point represents a mouse. Filled point: bootstrap significance test, $p < 0.05$.

In the *Barrel shuffle* condition, we degraded the spatial arrangement of the Bar feedback by randomly shuffling the identity of the photostimulated barrels, therefore removing the contiguity and spatial alignment between simultaneously activated barrels, but preserving temporal overlap of 2-3 barrels from one frame to the next (6 mice; see all photostimulation frames in Supplementary Fig. 4). In the *Frame shuffle* condition, we preserved the spatial organization of the photoactivated barrels within one frame, while in contrast, the correspondence of the frames with the virtual cursor position was shuffled. This rearrangement disrupted the overlap and contiguity of the displayed frames during evolutions of the virtual cursor (6 mice). Finally, in the *Full shuffle*, both the spatial position of the barrels and the frame-to-cursor correspondence were randomized (8 mice).

We trained mice to control the virtual cursor by M1 neuronal activity while receiving these different feedback patterns. Apart from the spatial content of the optogenetic frames themselves, training was identical to that implemented for the Bar feedback or No feedback conditions. In these experiments, the mice remained actively engaged. They licked and obtained rewards throughout all training sessions (Supplementary Fig. 5a). However, in contrast to the Bar feedback condition, we found no significant increase in mice performance across sessions (Fig. 3b). In the Barrel shuffle condition, we noticed a trend towards an increase in the reward frequency and in the percentage of rewarded licks, but it did not reach significance (Fig. 3b, reward frequency: Mann-Whitney $p = 0.064$; % rewarded licks $p = 0.132$) although 4 mice out of 6 did show a significant increase in the percentage of rewarded licks (Fig. 3c).

Through these experiments, we consecutively trained mice to learn the task with multiple different feedback structures. Therefore, the order of the training sequence might have had an impact on the learning performance. We explored this potential effect with two groups of three mice which followed consecutively training in the No feedback, Full shuffle and Bar feedback conditions, in two different orders (Supplementary Fig. 5b). Irrespective of the protocol training order, significant learning was observed only in the Bar feedback condition (Mann-Whitney $U = 0$, $p = 0.04$). We conclude that the order of the different training protocols did not impact the learning process. Overall, we found that the spatiotemporal structure of the feedback impacted heavily the behavioral performance of the mice, and that the Bar feedback enabled fastest learning.

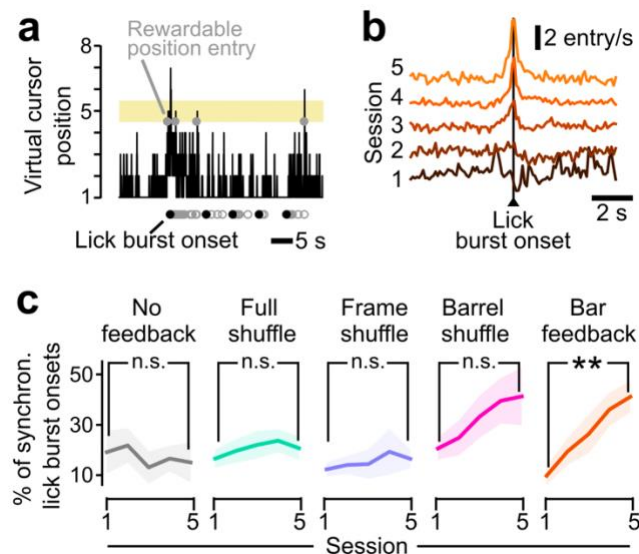


Fig. 4 Mice learned to synchronize licking with the entries of the virtual cursor in the rewardable position. **a** Example of the virtual cursor position as a function of time. Gray open circles: licks. Black dots: onsets of lick bursts. Gray dots on virtual cursor position 5 indicate entries of the virtual cursor in the rewardable position. To avoid confusion, rewarded licks are not highlighted. **b** Population average time histograms

of the number of entries of the virtual cursor in the rewardable position around all lick burst onsets, for the Bar feedback condition, across the five training sessions. Baseline levels were shifted upward for clarity. **c** Percentage of lick bursts that are synchronous (within ± 100 ms) with entry of the virtual cursor in the rewardable position. **: Mann-Whitney, $p < 0.01$. Shaded backgrounds: \pm SEM.

5 Mice learn to lick during time windows of reward availability

Next, we asked which mechanisms could underlie the ability of mice to improve their performance over 5 sessions. One hypothesis is that the mice improved their licking behavior by timing their licks more accurately relative to entries of the virtual cursor in the rewardable position. Given the tendency of mice to lick in long rhythmic bursts, we focused on the onsets of licking bouts, with the assumption that they indicate the attempts of the mice to obtain reward (Fig. 4a). We computed the proportion of lick burst onsets that fell within ± 100 ms of the virtual cursor entry in the rewardable position, which is approximately the duration of a tongue licking cycle. We found that this proportion increased significantly only in the Bar feedback condition (Fig. 4b,c; Mann-Whitney $p < 0.01$), and that again, a similar, non-significant trend was visible in the Barrel shuffle condition. We conclude from this data that the mice did learn to adjust their licking patterns to the virtual cursor dynamics.

Mice learn to bring the virtual cursor in the rewardable position dynamically

In parallel to this adaptation of the licking behavior, there could also be a change in the dynamics of the virtual cursor near and in the rewardable position, providing more opportunities for rewarded licks. To explore this hypothesis, we analyzed the virtual cursor dynamics at different time scales, focusing on how it changes from the first to the fifth training session. First, we measured the average time spent in the rewardable position across the whole duration of a session (Fig. 5a). We found that it increased significantly in the Bar feedback condition (Mann-Whitney $p < 0.05$), in contrast to all other tested feedback conditions. This confirms that mice learned to bring the cursor in the rewardable position more often. When we plotted the average virtual cursor position in time, first on a long timescale, we noticed that the curves for Sessions 1 and 5 started at the same level, followed by an upward shift 10 to 15 s after the start of the photostimulation in Session 5 (Fig. 5b; cursor position significantly higher in 15-100 s vs. 0-10 s, Wilcoxon test $p = 0.014$, only for the Bar feedback condition).

These delayed dynamics rule out the hypothesis that photostimulation could have non-specifically increased the overall activity, and consequently the virtual cursor position. We then investigated whether there was a dynamical control of the virtual cursor on a faster time scale leading to rewards. We observed that in the Bar feedback condition, and only in this condition, the mean cursor position was significantly larger after training than on session 1, up to 1.5 s around reward occurrence (Fig. 5c,d, Mann-Whitney, $p < 0.01$). In the same time windows, the virtual cursor spent a proportion of time in the rewardable position that was significantly larger after training compared to before (Fig. 5e, Mann-Whitney, $p < 0.01$). There were no changes in these measures in epochs further away from rewards (1.5-5 s and > 5 s from any reward, Mann-Whitney, $p > 0.05$), indicating that there was not a systematic additive shift in the virtual cursor position throughout the session, but rather numerous short explorations of higher cursor positions around rewards.

Overall, these results suggest that during training, the mice learned to manipulate the virtual cursor and bring it in the rewardable position more often, thus creating more opportunities for enhancing their performance by well-timed licks.

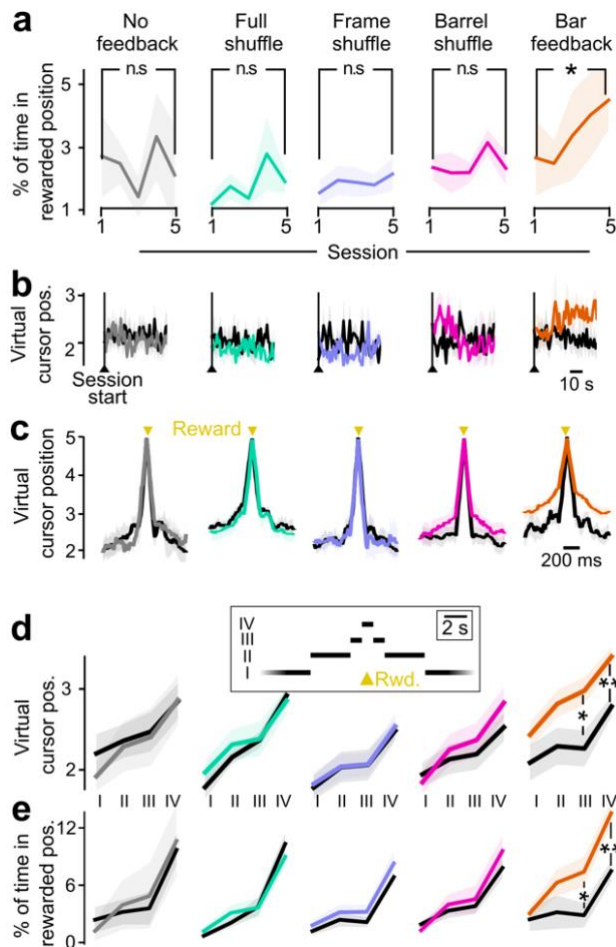


Fig. 5 Bar feedback enables the mice to actively control the virtual cursor position so that they spend more time in the rewardable position. **a** Proportion of time spent in the rewardable virtual cursor position (position 5) over the whole session duration. *: Mann-Whitney, $p < 0.05$. Shaded backgrounds: \pm SEM across mice. **b** Average virtual cursor position \pm SEM at the onset of the session, in the first versus last training session. Vertical line: start of the session, which is also the start of the photostimulation. **c** Average virtual cursor trajectory, aligned to the reward times, in the 5 feedback conditions. Black: first session. Colors: session 5. Shaded backgrounds: \pm SEM across mice. **d** Average virtual cursor position, in four time windows around reward: (I) More than 5 s away from any reward. (II) 1.5 to 5 s away. (III) 0.5 to 1.5 s away (IV) Within 0.5 s of a reward. *: Mann-Whitney, $p < 0.05$. **: $p < 0.01$. **e** Percentage of time spent in the rewardable position, in the four time windows around reward defined in d. Mean \pm SEM across mice.

One Master neuron dominates control of the virtual cursor

By design, changes in the dynamics of the virtual cursor are a direct consequence of changes in the underlying Master neurons activity, albeit in a non-linear way tailored to each mouse extracellular recording (see Methods and Supplementary Fig. 3). We verified the changes in firing rate underlying the observed changes in virtual cursor trajectory. In particular, since the activity of several Master neurons was summed to drive the cursor, we wondered whether all Master neurons contributed equally, or if instead motor control of the virtual cursor was dominated by a subset of the Master neurons. To investigate this question, we sorted the Master neurons as a function of their contribution to the virtual cursor position at reward time, and we looked at the evolution of their spiking activity over training. We termed “dominant” the Master neuron that on average fired the most at reward time, in a ± 100 ms window.

First, we checked the firing rate of Master neurons at the time scale of a whole session. Importantly, right at photostimulation onset, there was no detectable change of activity of Master neurons (Fig. 6a). This indicates the absence of an immediate photostimulation effect, in agreement with what we had observed on the virtual cursor position (Fig. 5b). Interestingly, the dominant Master neuron had a markedly increased firing rate in Session 5 compared to Session 1, including in the baseline period before photostimulation start (Fig. 6a). When averaged across the whole duration of each session, the firing rate of the dominant Master neuron was indeed significantly larger after training compared to before, and larger than any non-dominant Master neurons (Fig. 6b, Mann-Whitney, $p < 0.01$, see also Supplementary Fig. 6a). This increase was specific to the Bar feedback condition. Non-dominant neurons, on the contrary, showed little change in activity after training, in all feedback conditions (Fig. 6a,b).

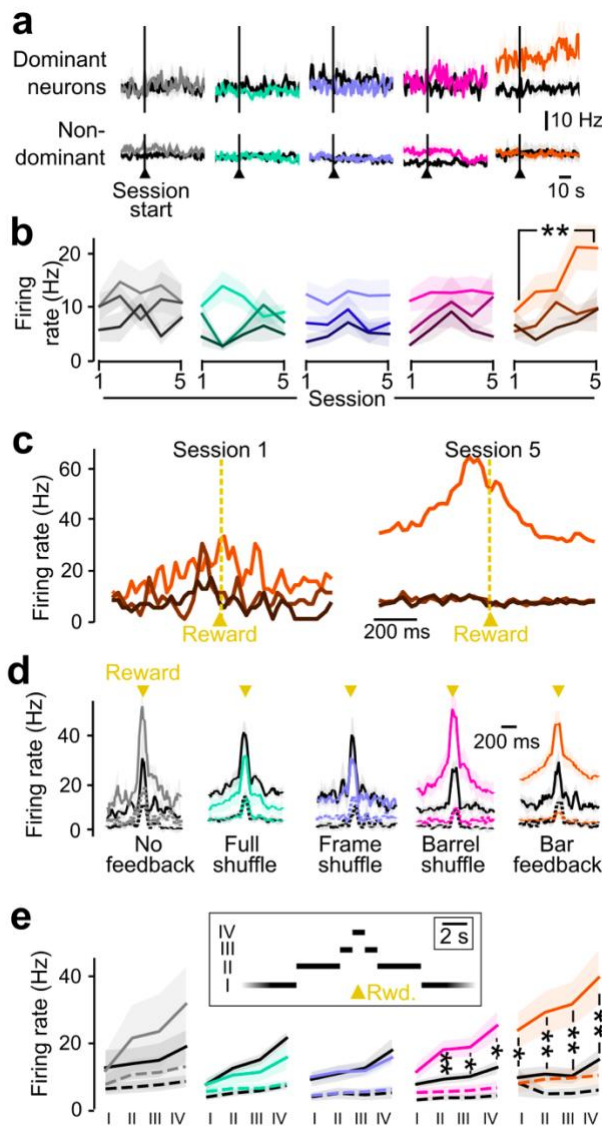


Fig. 6 Emergence of a dominant Master neuron in the Bar feedback condition. **a** Firing rate at the onset of the session, for dominant (top) and non-dominant (bottom) Master neurons in the first (black) versus last training session (colors). Shaded backgrounds: \pm SEM across mice. **b** Mean firing rate of the dominant (saturated colors) and non-dominant Master neurons, over training sessions. Shaded backgrounds: \pm SEM across mice. **: Mann-Whitney, $p < 0.01$. **c** Mouse case study of the time histogram of the activity of Master neurons around rewards, in the Bar feedback condition, sorted from the weakest (dark brown) to the dominant neuron (saturated orange) at the time of the reward, in the first (left) versus the fifth (right) training sessions. **d** Time histogram of the activity of Master neurons around rewards, in the 5 tested feedback conditions. Session 1 is shown in black, and session 5 in saturated colors. Continuous line: dominant Master neuron. Dashed line: average of non-dominant neurons. **e** Average firing rate of dominant (continuous line) and non-dominant (dashed line) Master neurons in the first (black) versus the last training session (colors), measured in the same time windows as in Fig. 5: (I) More than 5 s away from any reward. (II) 1.5 to 5 s away. (III) 0.5 to 1.5 s away (IV) Within 0.5 s of a reward. Shaded backgrounds: \pm SEM across mice. *: Comparison between the first and fifth training session. Mann-Whitney p value < 0.05 ; **: $p < 0.01$.

These observations on a long timescale could be due to persistent elevated firing after training, or to an accumulation of short bursts of high firing of the dominant Master neuron. We thus analyzed the fast dynamics around rewards, as done previously for the virtual cursor position (Fig. 5c). Figure 6c shows the firing rate of individual Master neurons around reward times, for Sessions 1 and 5 of one mouse trained in the Bar feedback condition. After training, one of the Master neurons showed a much higher firing rate with a prominent peak around the reward time. Population averages across mice confirms this tendency for the dominant neuron in the pool of Master neurons, whereas little changes were observed on non-dominant neurons (Fig. 6d). Again, the large increase after training compared to before was specific to the Bar feedback condition, although a more moderate trend was noted for the Barrel shuffle condition. We quantified the firing rate in several time windows around rewards (similar to Fig. 5d for the virtual cursor position). The firing rate of dominant Master neurons around reward times in the Bar feedback condition showed a strong and significant increase after training compared to before (Fig. 6e). This increase was specific to the dominant Master neurons, and was highest around reward times (Mann-Whitney $p < 0.01$). It was less pronounced but still significant more than 5 s away from any reward (Mann-Whitney $p = 0.04$), an observation that we relate to the elevated firing rate in the baseline period already before session start (Fig. 6a). We observed a similar, but more limited phenomenon in the Barrel shuffle condition (Fig. 6e).

Note that the tonic component of the increased firing rate of the dominant Master neuron was normalized by the motor control algorithm, and it could therefore not lead to a shift in virtual cursor position (see Methods). Thus, we conclude that in the Bar feedback, and to a lesser extent in the Barrel shuffle, the mice learned to control the virtual cursor position mostly by increasing the activity of one Master neuron in short bursts of elevated firing around lick times, enabling them to obtain rewards.

Playback experiments confirm the role of active motor control for task performance

Finally, to further explore the role of motor control on task performance, we performed playback experiments on three mice that had already learnt the full closed-loop task with the Bar feedback protocol. The mice received the same optogenetic stimulation sequence as in their last closed-loop session with Bar feedback, and they could still receive rewards by licking when the virtual cursor was in the rewardable position. However, the virtual cursor dynamics was now independent from the ongoing activity of motor cortex neurons. In other words, the animals were relieved of the motor control aspect of the full task (Fig. 7a,b). Interestingly, the frequency of rewards dropped significantly for each mouse in the playback condition (Fig. 7c) even though by design, the virtual cursor spent as much time in the rewardable position as during the Bar feedback last session. Analysis of the synchrony between licking onsets and the entries of the virtual cursor in the rewardable position revealed that these events were not coordinated anymore (Fig. 7d).

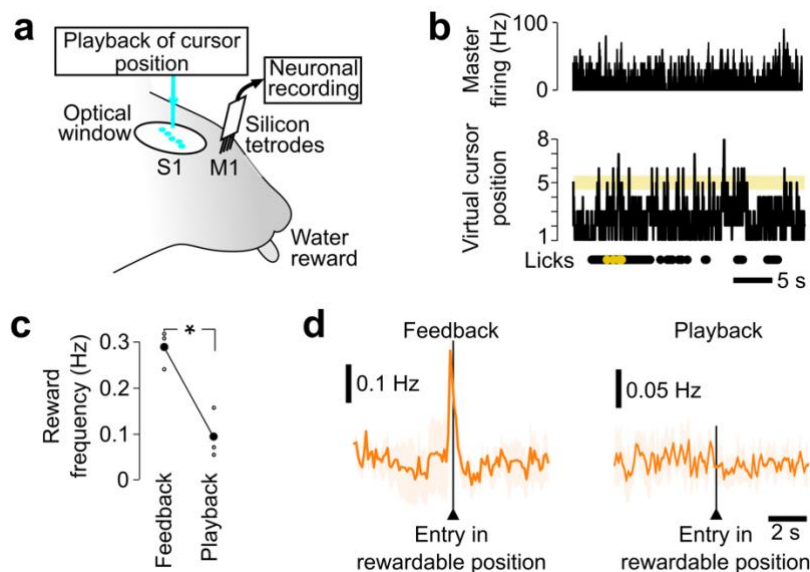


Fig. 7 Lick timing is not accurate in a playback condition. **a** Playback configuration with chronic extracellular recording in M1 and Bar feedback optogenetic stimulation on barrels in S1. Previously acquired sequences of cursor positions are played back, independent from M1 firing rates. As in closed-loop sessions, reward delivery is contingent on synchronous 1) licking and 2) presence of the virtual cursor in the rewardable position. **b** Top, histogram of Master neurons activity during a playback session (30 seconds shown). Bottom, time course of the virtual cursor position, disconnected from the Master firing. Below: licks, and rewarded licks during the same interval. Bin size 10 ms. **c** Frequency of rewards during the last session with closed-loop Bar feedback and the session with playback. *: Mann-Whitney, $p < 0.05$. Gray background: SEM. $n = 3$ mice. **d** Histogram of lick bursts onsets, with respect to the times of entry of the virtual cursor in the rewardable position, for the last session with Bar feedback (left) versus the session with Bar playback (right), averaged for the three tested mice.

To confirm that active motor control is necessary not only for task execution but also for learning, we trained three naive mice to perform the playback task during 5 sessions.

Consistent with the previous playback result, we found that the mice failed to increase significantly their performance during this playback training (Supplementary Fig. 7).

Overall, these playback experiments demonstrate that in the Bar feedback condition, the mice did not only respond to sensory cortex stimuli by licking, but instead actively coordinated their licking with timely modulations of the cursor position.

DISCUSSION

In this study, we demonstrate that in the context of improving motor control of a brain-machine interface, the integration of direct cortical feedback can be heavily impacted by its spatiotemporal organization. Specifically, we trained mice in a task for which the brain-machine interface could be used to move a virtual cursor into a rewardable position. We found that the performance after training was highest when feedback provided the position of the cursor in the form of a bar-like photostimulation across the cortical surface (Bar feedback condition). In contrast, we found that when we disrupted the spatial contiguity of simultaneously stimulated barrels (Barrel shuffle), learning was clearly reduced, and when we disrupted the continuity of the bar in time (Frame shuffle), it went down to levels observed without feedback.

This difference in performance was associated with a reorganization of the ongoing neuronal activity that was specific to the Bar feedback condition. More precisely, one of the M1 Master neurons driving the cursor became dominant in terms of activity levels and led the virtual cursor to spend more time in the rewardable position, thereby increasing the opportunity for rewards. In parallel, licks were more synchronized with entries in the rewardable position.

A fast bidirectional BMI setup for the mouse

Current research aimed at integrating somatosensory feedback in a cortical brain-machine interface relies on invasive techniques of recording and stimulation in awake behaving animals. Pioneering teams are developing prototypes in non-human primates as well as human participants (Flesher et al., 2019; O'Doherty et al., 2019). Here, we have developed a novel brain-machine interface tailored to the mouse whisker system, a sensorimotor loop that has been described in a comprehensive way, from the cellular to the network level (Diamond and Arabzadeh, 2013; Petersen, 2019). This approach has allowed us to take advantage of recent optogenetic tools available for these animals. We could activate excitatory neurons in the cortex according to spatial light patterns that were adapted, in each individual mouse, to the topographic map of the whiskers present in S1. Furthermore, we benefited from our low-latency (12 ± 5 ms) closed-loop design which enables the delivery of feedback in a dynamic way, so that the ongoing activity of the Master neurons controlled online the stimulation frames. Indeed, a low-latency somatosensory feedback could be an important parameter in the context of sensorimotor learning (Scott, 2016).

To provide distributed feedback to the mice, we chose to generate illumination patches above individual S1 barrels, rather than try to mimic the broad spread of activity that is generated by multiple whisker stimulation sequences (Vilarchao et al., 2018). The rationale has been to mimic activation patterns of multiple lemniscal thalamic inputs, which are known to project into barrel columns of corresponding whiskers, and which should then trigger broader activation of the cortex through intracortical connectivity, both within and across layers (Petersen, 2019). We hypothesize that this recruitment of intracortical mechanisms is key to the similarity between artificial and physiological stimulation. We certainly acknowledge that significant differences remain between the optogenetic activation and physiological activation of the barrel cortex. In particular, we did not attempt to reproduce non-lemniscal thalamic input patterns which don't follow a clear topographical mapping at the surface of the cortex, and which are thus difficult to activate specifically.

Impact of somatosensory feedback on neuroprosthetic learning

In our experiments, in the absence of optogenetic feedback, the mice failed to learn the task. In contrast, a few previous studies have suggested that BMI learning could take place without any feedback of the conditioned neuronal activity to the animal (Sakurai & Takahashi, 2013; Marzullo et al., 2016). Several differences could explain these seemingly opposite results. First, in those studies, the animals received the reward automatically once the neuronal activity reached the predefined threshold. In contrast, in our task, the mice have to learn also to lick in order to obtain the reward. This combination of firing rate modulation and required licking probably makes the task much more challenging. Second, in our study, movements of the virtual cursor occurred on average every 50 ms, so that temporal precision of licking was important. This must also have been challenging, particularly in the absence of any feedback. These reasons could explain the lack of learning that we report in the No feedback condition.

Our study shows that direct cortical feedback can enable the learning of a sensorimotor task in these conditions, pending that feedback with an adequate spatio-temporal structure is provided. This is consistent with recent work exploring cortical somatosensory closed-loop BMIs in humans with intracortical electrical stimulations (Flesher et al., 2021), as well as with previous work emphasizing the prevalent role of ongoing sensory feedback in motor learning (Johansson and Flanagan, 2009; Scott, 2016).

Importantly, our experimental design did not incorporate a physical implementation of a device to be moved by the animal towards a target. Instead, we computed the position of a virtual cursor and used it to select the next frame of the ongoing feedback. This choice ensured that the optogenetic feedback delivered to S1 was the sole source of sensory information about the virtual cursor position available to the animal during the task. This is in contrast to most previous closed-loop BMI studies, in which ongoing visual feedback of the neuroprosthesis was always available for adjusting motor control in addition to cortical stimulation (Flesher et al., 2019; O'Doherty et al., 2019).

Motor control of the virtual cursor

In this study, direct demonstration of voluntary motor control was challenging because virtual cursor movements were generated continuously rather than triggered. Still, we found several indications of active motor control of the virtual cursor, that were specific to the Bar feedback condition, and to a lesser extend to the Barrel shuffle condition. In particular, only in this feedback condition did the virtual cursor position shift towards the rewardable position, as the mouse prepared to collect rewards in the next seconds (Fig.5d,e). In addition, analysis of the neuronal activity of the Master neurons underlying the virtual cursor position revealed that throughout learning sessions, neuronal activity evolved towards the dominance of a single one of their Master neurons, in particular during the modulations of activity towards the rewardable position. This rearrangement took place only in the Bar feedback condition (Fig. 6). Finally, during additional playback sessions at the end of a sequence of training in the Bar feedback condition, the mice appeared unable to maintain the performance level they attained during previous closed-loop training sessions, indicating that active motor control was required for performance (Fig. 7).

Overall, we conclude from these analyses that in the Bar feedback condition, the mice did rely on the active modulation of their Master neurons to collect rewards. The lack of such motor control in other feedback conditions illustrates the impact of the spatiotemporal structure of our distributed feedback, not only for sensory information processing, but more generally for sensori-motor integration of the feedback.

Regarding the playback experiments, we should point out that in one study, after operant conditioning of motor cortex neurons based on a single barrel S1 optogenetic feedback, mice were able to efficiently gather rewards during playback training (Prsa et al., 2017). Similarly, we have previously shown that in our experimental setting, mice were able to detect a static,

single frame of the Bar feedback to obtain rewards (Abbasi et al., 2018, Fig. 5) or to track a continuous, slowly rotating bar (Lassagne et al., 2022). We hypothesize that what makes the playback condition here (Fig. 7) comparatively more challenging than these previous experiments is that it combined rapidly changing feedback with a distributed, more complex spatial pattern. In addition, a low-latency licking was necessary when the cursor entered the rewardable position. All these challenges meant that to be successful, the mice had to anticipate the entrance in the rewardable position, as the cursor could escape the rewardable position within milliseconds. In contrast to the playback condition, we hypothesize that in the closed-loop Bar feedback condition, the motor control of the virtual cursor provided the degree of rewardable position anticipation that allowed timely licks and an increase in the proportion of rewarded licks.

Pattern contiguity impacts learning and performance

We showed that direct cortical feedback should obey spatiotemporal rules of organization in order to be efficiently integrated into motor control. Specifically, we found that the mice were able to learn to control a virtual cursor using an S1 bar-like feedback that featured contiguity of the activated barrels both within a given frame, and across consecutive frames.

When across-frames contiguity was removed, in the Frame shuffle feedback condition and also the Full shuffle condition, we found no sign of learning, as in the absence of feedback altogether. We hypothesize that the lack of temporal continuity across consecutive feedback frames may have prevented the anticipation of upcoming cursor movements. Given our fast-paced cursor positioning task, this translated in an inability to learn the task. This hypothesis is consistent with the findings in our previous, open-loop work (Lassagne et al., 2022).

However, when only within-frame contiguity was removed (Barrel shuffle condition) learning was at intermediate levels. The mice were able to exploit the feedback to some degree, but lacked the accuracy that is required to really synchronize virtual cursor and licking efficiently. These results on the relevance of both the spatial and the temporal structure of intracortical feedback suggest that the sensorimotor task of driving the virtual cursor to the target draws upon pre-existing features of S1-M1 microcircuits, linked to their topographic organization (Ferezou et al., 2006). When the contiguity of the feedback was disrupted, the functional architecture of the cortex may not have been adapted anymore to the novel sensorimotor computations that were required to solve the task. Thus, learning to extract the relevant virtual cursor information from the different shuffled conditions may require multiple additional training sessions, if indeed the required functional connections can be recruited from the existing anatomical scaffold (Fu and Zuo, 2011). In fact, previous work does suggest that learning a spatially shuffled cortical stimulation is possible if training spans multiple training sessions, with the assistance of visual feedback (Dadarlat et al., 2015; Hartmann et al., 2016). This seems consistent with the signs of learning that we did observe in the Barrel shuffle condition (Fig. 3b,c).

Interestingly, in contrast to the limited capacity for processing sensory feedback with different feedback structures, we observed that the animals were able to readily adapt to the constraints that were set on the motor side. Indeed, consistent with previous studies (Arduin et al., 2013; Fetz, 1969; Moritz et al., 2008; Prsa et al., 2017), we found that an arbitrary set of a few M1 neurons could be conditioned in an operant way to learn to control a virtual cursor along one dimension. The sharp contrast between the necessity of spatially structured patterns on the sensory side, and the adaptability of the neuronal networks on the motor side, could have several explanations. One is that we used mesoscale patterns to encode sensory feedback, encompassing large numbers of neurons and connections. Plastic reorganization at this scale may be more demanding than when targeting only a few neurons. Indeed, there is evidence that as the number of neurons controlling motor brain-machine interfaces increases, it becomes necessary to take into account their initial functional connections in order to learn to

control the prosthesis rapidly (Athalye et al., 2017; Oby et al., 2019; Sadtler et al., 2014). Alternatively, another possibility is that primary sensory cortical circuits may be intrinsically less plastic than motor ones during motor skill learning (Papale and Hooks, 2018). Future experiments will need to address this question.

5

Functional role of the S1 somatotopic map

10 So far, the contribution of cortical maps to sensory information processing in general has remained unclear (Kaas, 1997) despite the thorough descriptions of the maps in primary sensory cortices. In the case of the barrel cortex, several of the functional properties encoded by its neurons are spatially organized inside the map beyond spatial topography (Andermann and Moore, 2006; Estebanez et al., 2016; Kremer et al., 2011; Simons, 1978), including some multi-whisker features (Estebanez et al., 2016; Vilarchao et al., 2018). The large-scale organization of feature encoding would be favored because of the dense lateral connectivity inside S1, enabling distributed cortical computations (Feldmeyer, 2012). Through this rich anatomical substrate, non-linear spatiotemporal integration in S1 results in enhanced responses to some input patterns, and suppression of responses to other patterns (Estebanez et al., 2012). However, so far, these feature extraction properties have not been causally linked to behavior, except the somatotopy itself recently (Lassagne et al., 2022).

20 Our results shed light on the functional role of topography of the somatosensory cortical map in the behaving animal, by testing causally the impact of different patterns of sensory input. In particular, our work reveals that feedback patterns that are contiguous within the frame of the barrel cortex topographical organization are best suited to sensorimotor integration. Such optimal patterning of dynamical distributed feedback could be combined with other means of transmitting feedback information to the brain, such as temporal and amplitude modulation of stimulation pulses (Prsa et al., 2017; Tabot et al., 2013; Valle et al., 2018).

25 Finally, current BMI prototypes require long training and lack precision and flexibility, probably because they lack the appropriate somatosensory feedback (Bensmaia and Miller, 2014). From our results, we propose that feedback strategies based on intracortical stimulation should favor spatial and temporal continuity within the known topography of the target areas. We hope that unveiling such fundamental constraints of neuronal circuits will enable the development of a new generation of BMIs, incorporating rich proprioceptive and tactile feedback essential to achieve dexterity and embodiment.

METHODS

35 Mouse preparation

All animal experiments were performed according to European and French law as well as CNRS guidelines and were approved by the French ministry for research (ethical committee 59, authorization 858-2015060516116339v5). The data were obtained from 16 adult (6-10 weeks old) Emx1-Cre;Ai27 mice (Madisen et al., 2012). The brain-machine interface methodology has been published previously (Abbasi et al., 2018). All surgeries were performed under isoflurane anesthesia in 100% air. Isoflurane concentration was adjusted in the range 1–4% depending on mouse state, assessed by breathing rate and response to tail pinch. Each mouse underwent two surgeries. During a first surgery, a 5 mm diameter glass optical window was implanted over the left primary somatosensory cortex (S1, P-1.5 mm and L-3.3 mm from bregma, (Holtmaat et al., 2009) and a head-fixation bar was implanted on the contralateral side of the skull (Guo et al., 2014). Eight days later, the clarity of the optical window was assessed, and if adequate, intrinsic imaging was performed to locate the S1 barrels (see below). If this first step was successful, a second surgery was performed to chronically implant (Okun et al., 2016) a 32 channel silicon probe in the shape of 8 tetrodes

(A1x32Poly35mm25s 177A32, NeuroNexus, USA, Fig. 1a-b, Supplementary Fig. 1,2). The electrode was implanted in the whisker zone of the motor cortex (M1, A1.5 mm L-0.6 mm from bregma, electrode recording sites 650 – 800 μ m deep in cortex).

Chronic neuronal recordings

Following the second surgery, mice were monitored for 5 days to allow the extracellular recordings to stabilize (bandpass 1Hz - 6000Hz). We then characterized the shape and amplitude of the units isolated by the online spike sorting (Blackrock microsystems, USA). Clusters corresponding to well-defined single units (consistent spike shape and an adequate autocorrelogram, with a clear refractory period, see Fig. 1b) were manually selected within the tetrode spike amplitude space. This manual selection was controlled before each session to ensure that we maintained unit separation while keeping track of the same units across sessions (Supplementary Fig. 1). Once the online spike sorting was ready, the training session began. At the start of the training sessions, we recorded a median of 25.5 neurons simultaneously, with an interquartile range (IQR) of 5.25 neurons ($n = 10$ mice). After 17 days (average last training session) we recorded a median of 25 neurons (IQR = 16 neurons, $n = 10$ mice).

Brain-machine interfacing

Among the recorded units of each mouse/session, a set of 3 putative pyramidal neurons – the Master neurons – were selected by the operator. In the first two mice, we initially enrolled 7 neurons. However, after a first round of experiments, we found that securing so many large and high-firing neurons was challenging in several of the mice, so we settled on a smaller count of 3 neurons. We did not find any major difference in the activity or behavior of these first two mice. We selected the Master neurons among all simultaneously recorded units because they displayed (1) a sufficient baseline frequency (target: 10 Hz), (2) spikes clearly separate from the multiunit baseline and with the largest possible amplitude, and (3) a spike shape that was visually different from any other spike shape across the 4 channels of the tetrode.

The activity of these Master neurons was transformed into a virtual cursor position (Fig. 1c) which determined the optogenetic frame to be displayed as well as possible reward delivery. The spiking activity of the Master neurons was summed, and the corresponding firing rate was measured over 10 ms time bins. To transform this Master firing rate into the position of the virtual cursor, it was convolved with a 100 ms box kernel, and then renormalized with respect to the distribution of Master activity observed during a baseline window of 3 minutes just preceding the start of the session. Specifically, we computed the 99th percentile of the baseline activity values, and the activity from 0 Hz up to this value was split in 7 equal positions, with an additional 8th position for activity values exceeding the 99th percentile threshold (Supplementary Fig. 3). The resulting movements of the virtual cursor were smooth. In the Bar feedback condition, on average 95% of the transitions were to a closest neighbor position, and less than 0.1% of the transitions were jumps larger than to a second neighbor position. This was similar in all other feedback conditions.

For most of the experiments, only the 5th position was rewarded, which means that whenever the virtual cursor was inside that position and the mouse simultaneously licked, it obtained a 5 μ L water drop. Note that rewards were not delivered automatically to the mouse whenever the virtual cursor entered the rewardable position. Instead, only if the mouse licked at the precise time when the virtual cursor was located in the rewardable position, the capacitive sensor detected the lick and triggered the delivery of a drop of water through the lick port, which was immediately swept away by the ongoing licking action.

However, in very first 3 experiments, only the 6th position was rewarded, and in 3 additional experiments, the rewardable position also included either the 6th or the 4th position. We did not

find any difference in activity or behavior that could be related to this difference in rewardable positions.

The logic of introducing a virtual cursor has been double. First, from a purely analytical point of view, it allows analysis of motor control in the non-linear discretized scale that is relevant for feedback stimulation and reward obtention, that is, regardless of the absolute values of firing rates which can be very different from one mouse and session to the next. Second, it emphasizes that the algorithm is the same in all feedback protocols. Only the final mapping between the eight different positions of the cursor and the effective photostimulation patterns changes with the protocol. This concept of a virtual cursor, in between the firing rate of the neurons and the photostimulation frames, is useful to describe unambiguously the protocols, the analyses and the results.

Optogenetic photostimulation of somatosensory cortex

Each virtual cursor position was associated with a specific feedback pattern that was projected onto the barrel cortex of the mice using a Digital Light Processing module (DLP, Vialux V-7001, Germany). The DLP contained a 1024 x 768 pixels Texas Instruments micro-mirror chip, which was illuminated by a high-power 462 nm blue LED. The frame stream generated by the device was focused onto the cortical optical window using a tandem-lens macroscope (Ceballo et al., 2019), and covered the entire barrel cortex. We displayed each frame for 5 ms, followed by 5 ms without photostimulation. We sent homogeneous light spots, 225 μ m in diameter, centered onto the barrel locations (see below). In a previous publication, we recorded activity in S1 in response to the exact same photostimulations, in the same mouse line, and verified that it triggered neuronal activation mostly limited to the targeted barrel area (Abbasi et al., 2018). In the same study we also compared the detection of five aligned spots flashed on the barrel cortex to the detection of five aligned spots flashed just outside the cranial window, in a GO/NOGO task. We found that mice detected the photostimulation only when it was targeted to the cortical window. This control ensured that the mice are unable to use any indirect clue, such as light reflection in the setup, to solve the task.

A set of at least 3 reference barrels, was localized on the mouse cortical surface via intrinsic signal imaging. These barrels were used to align a standard barrel map (Knutsen et al., 2016) that served later as the grid to align the photostimulation spots. Supplementary Fig. 8 shows an example of the intrinsic signals and of the strategy used to position the photostimulations onto the S1 surface.

We used five different sets of feedback frames: the Bar feedback (Fig. 1d,e); three shuffled versions of the Bar feedback that are described in Fig. 3 and Supplementary Fig. 4 ; and finally, a condition where no photostimulation was displayed (No feedback, all black frames). The Bar feedback design was based on the known selectivity of S1 neurons to features such as the global direction of bar-like stimulations (Drew and Feldman, 2007; Jacob et al., 2008; Vilarchao et al., 2018) and more broadly, tuning to progressive movement of objects across the whiskerpad (Laboy-Juárez et al., 2019). This choice of feedback structure was also supported by the observation, in awake behaving rodents, that structured sweeping sequences of rostrocaudal deflections of whiskers are significantly more prevalent than expected by chance (Hobbs et al., 2016). Note that all photostimulation frames used the same number of identically shaped photostimulation spots, and therefore generated the same amount of photoactivation (Abbasi et al., 2018). The total amount of light projected onto the cortex was thus constant throughout all sessions.

To verify that the selected photostimulation did not bias the M1 activity prior to training, we exposed 3 naive, BMI-ready mice, to one single session of Bar feedback playback, and one of the Full shuffle playback. The frame sequence originated from a previous mouse/training session. During playback, in each mouse we recorded three M1 neurons that would qualify as Master neurons. We found no firing rate modulation triggered by any of the displayed frames (data not shown), and in particular none in the Bar feedback. These experiments confirm that

prior to training, M1 neurons had no discriminative power or specific tuning to the photostimulation frames we designed.

Behavioral training

We started the behavioral training by removing free access to the water in the cage. At the same time, we started habituating the mice to head fixation. This lasted for 2 days, where the mice were head-fixed during 30 min sessions and were continuously presented with a spout that delivered a drop of water every time the mice licked, thanks to a capacitive sensor in the spout.

After these first habituation sessions, we transitioned to training the mice in the BMI task. The sessions took place once a day, and lasted 33 min. During these training sessions, the neuronal activity was continuously recorded, and one of the five photostimulation dynamical patterns was continuously applied to the mouse barrel cortex: Bar feedback, Barrel shuffle, Frame shuffle, Full shuffle, or No feedback, (Fig. 3a and Supplementary Fig. 4). The displayed frame was updated every 10 ms based on the measured neuronal activity (Fig. 1). At any time, the mice could move the virtual cursor to the rewardable zone by modulating the activity of Master neurons. If it licked at the precise time when the virtual cursor was located in the rewardable position, a small amount (~5 μ L) of water flowed immediately through the lick port, and the water droplet was swept away by the ongoing licking action.

The mice were trained with the same feedback protocol during 5 consecutive training sessions. There were no days off during these 5 days, except in the rare case of an unexpected technical problem. After the 5 training sessions, and if sufficient M1 activity was still present, we performed a new selection of Master neurons from scratch, and we restarted training the mouse with another feedback condition. There was generally a two days gap between different feedback protocols, except in three mice for which there was no pause in the training. We checked that previous learning did not bias the outcome of the following training (Supplementary Fig. 5b).

If the recording of one neuron was lost during the training, the active Neighbor neuron with the largest spike shape was enrolled to replace it. If no additional Neighbor neuron was available, the experiment kept going with a reduced count of Master neurons, down to a minimum of two Master neurons. We assessed the Master neuron population stability by counting cases where all Master units could not be reliably identified anymore at the start of one of the training sessions, and had to be replaced with new units. This situation occurred once for two mice for the Bar feedback condition, two mice for the Full shuffle condition and three mice for the No feedback condition. This amounts to 7 cases out of 152 transitions between sessions, thus about 5%. Note that in most of these cases, although we were unable to prove it, we suspected that a least one of the former Master neuron was picked as part of the new Master neuron pool.

Videography of the snout in three mice failed to reveal whisker movements that would be correlated to optogenetic stimulation or to the virtual cursor motor control, as previously reported in BMI studies (Chapin et al., 1999).

Through training, we monitored the weight loss that resulted from the water restriction schedule. We ensured that the weight never dropped below 80% of its initial value (Guo et al., 2014). To do so, mice were checked daily for weight and extra water/food intake was provided as needed to stabilize the weight.

Offline spike sorting

Offline extraction of neuronal activity was performed using SpyKING CIRCUS (Yger et al., 2018). We confirmed that each online-sorted Master unit was properly spike sorted by matching it with a specific offline-sorted unit through comparison of spike shapes and

amplitudes across tetrodes. All additional, non-Master offline-sorted units were labeled as Neighbor units.

Data Analysis

All statistical tests are non-parametric, either two-sided Mann-Whitney tests or Wilcoxon paired tests.

Intracortical microstimulation (ICMS) experiments

To confirm that the electrodes were located in the motor cortical area, we performed ICMS at the end of the behavior sessions ($n = 3$ mice, Supplementary Fig. 2). We injected bipolar current pulses (amplitude $21 \mu\text{A}/\text{channel}$, duration 1.4 s , frequency 60 Hz , 50% duty cycle) through the 32-channel NeuroNexus silicon probe implanted in M1, in awake head-fixed animals. The contralateral whiskers were imaged using a high-speed videography (camera – Baumer HXc-20, lens – 6 mm , $F/1.4$) at 300 frames per seconds for a duration of 9 s . A single trial consisted of 5 s pre-ICMS videography, followed by 1.4 s during ICMS stimulation and finally 2.6 s post-ICMS. This procedure was repeated 14 times during a single session of ICMS experiment, with a 1 s inter-trial delay. In the ICMS videos, a central whisker was identified amongst all the whiskers in the field of view, and tracked using the automated video tracking software DeepLabCut (Mathis et al., 2018). The amplitude of ICMS-evoked whisker movement was defined as the mean whisker angle during the first 1 s of stimulation versus the 1 s immediately before. Latency of whisker movement was measured at the first frame with significant whisker movement amplitude (2 standard deviations above the mean).

Histology

After the experiment, mice were deeply anaesthetized with isoflurane ($4\text{-}5\%$) and pentobarbital (150 mg/kg), then exsanguinated and perfused with 4% paraformaldehyde (PFA). The brains were extracted and stored overnight in 4% PFA. The brains were then transferred to a solution of phosphate-buffered saline for at least 24 hours. Fifty μm slices were cut in the coronal plane and stained for cytochrome C oxidase. The location and depth of the silicon probe in the brain were traced by Dil depositing on the electrodes prior to their implantation and by localizing afterwards the fluorescent dye present in the histological slices (Supplementary Fig. 2a).

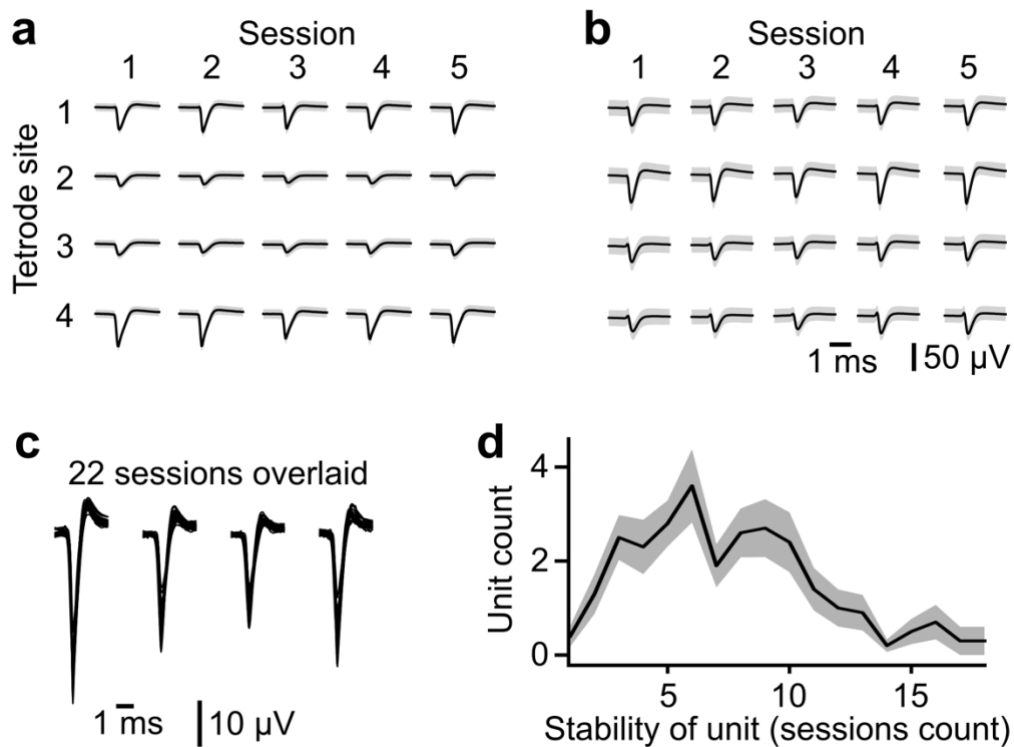
Acknowledgments

We thank Isabelle Férézou for advice on experimental design and analysis; Ehud Ahissar, Boris Barbour, Karim Benchenane, Suliann Ben Hamed, Sliman Bensmaia, Daniel Feldman, Evan Harrell and German Sumbre for comments on an earlier version of the manuscript. Aurélie Daret and Guillaume Hucher provided experimental support. FRM (Equipe FRM DEQ20170336761), CNRS (80|Prime), ANR Neurowhisk, ANR MesoBrain, ANR MotorSense Lidex NeuroSaclay, Idex Brainscopes and iCODE, and FRC (AAP 2018) provided funding.

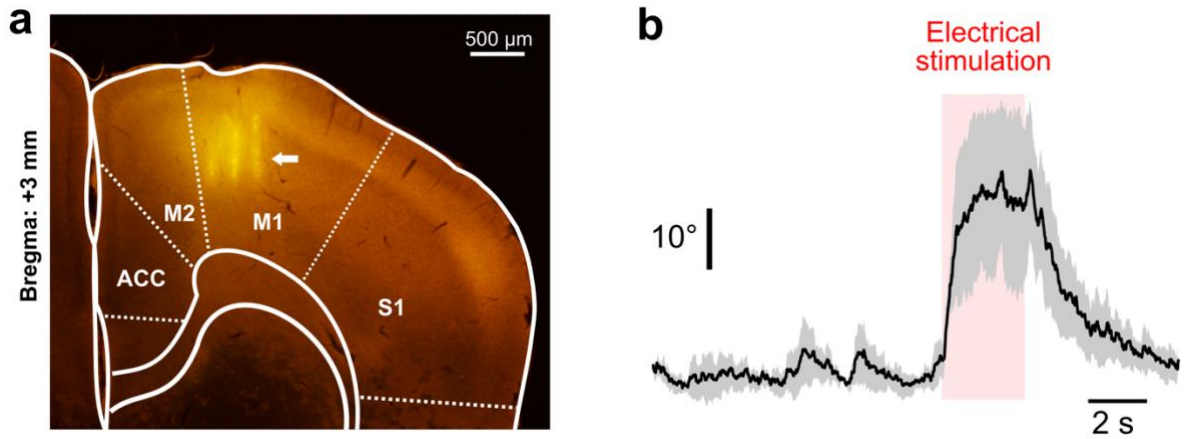
Author contributions

D.E.S. and V.E.S. obtained funding and administrated the project. D.E.S., L.E. and V.E.S. conceptualized and supervised the experiments and analysis; A.A. and H.L. carried the investigation with support from L.E. and D.G.; L.E. and A.A. analyzed the data with support from H.L.; L.E., V.E.S. and D.E.S. wrote the manuscript with input from all authors.

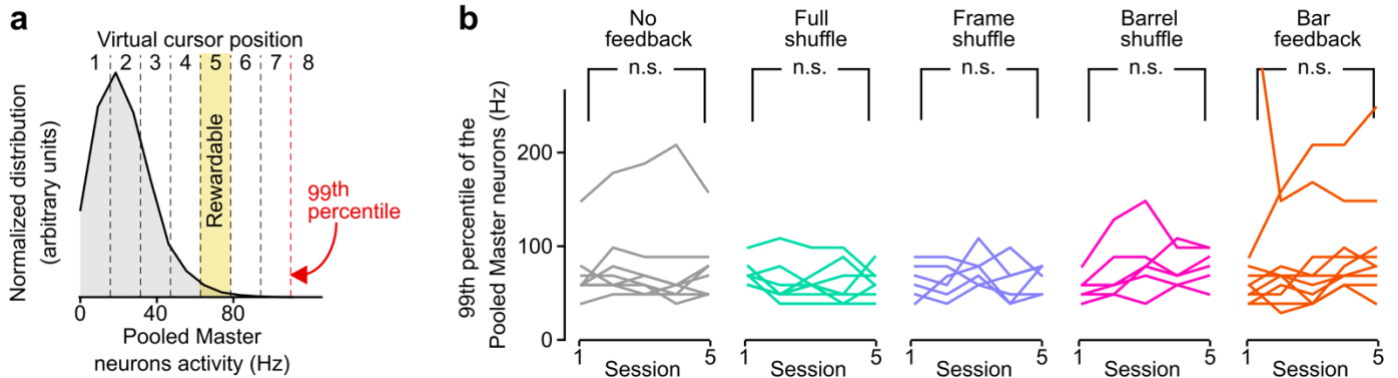
Declaration of interests: The authors declare no competing interests.



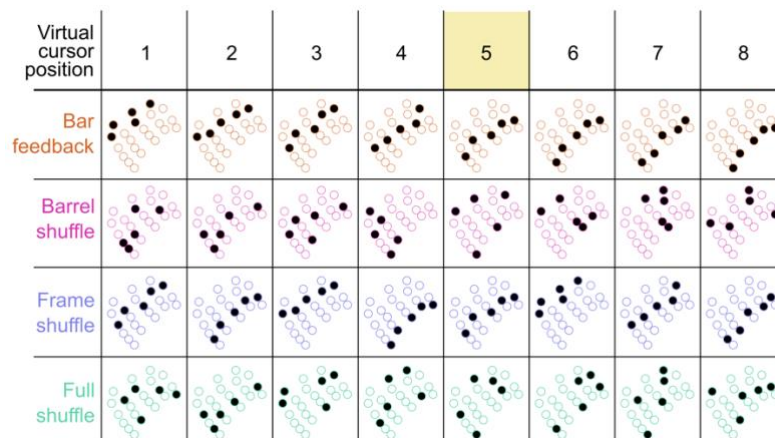
Supplementary Figure 1. Stability of the recorded neurons across sessions. **a** Stability of the spike shape of one Master neuron, shown for the 4 tetrode sites, across five training sessions, in the No feedback condition. **b** Same as a for a second Master neuron, this time in the Bar feedback condition. **c** Overlay of the spike shapes for one Master neuron across 22 successive sessions. **d** Average distribution across 10 mice of the count of sessions where the same Master unit could be identified. Shaded background: standard error of the mean of the histogram.



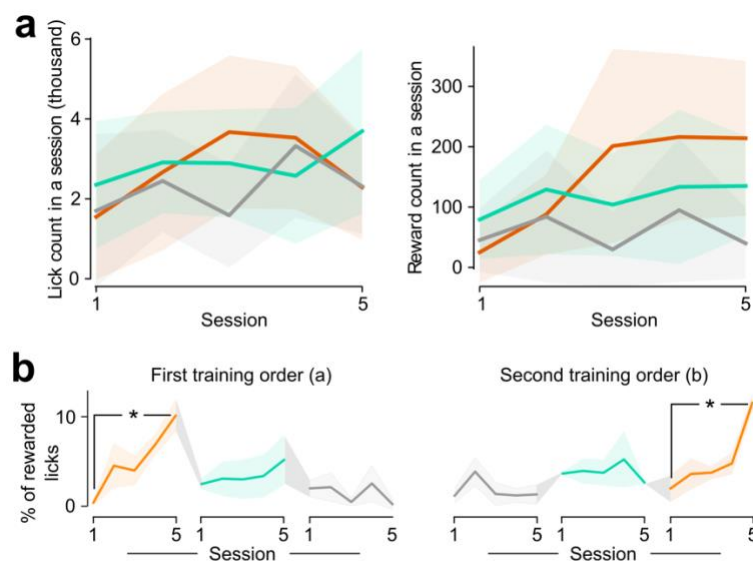
Supplementary Figure 2. Localization of the implanted silicon probes in whisker M1. **a** 50 μm coronal slice of a mouse brain, stained for Cytochrome oxidase. Dil coating of the shanks prior to insertion resulted in fluorescent lines indicative of the location of single shanks (yellow tracks) in M1 (white arrow). Dashed lines: area borders according to the Allen brain atlas. We identified the electrodes as being placed in the deeper layers of M1 based on: the location of the slice with respect to bregma; the lateral location of the electrode tracks with respect to the longitudinal fissure; and the depth of these tracks. **b** The amplitude of angular movements of a contralateral whisker evoked by ICMS stimulation through the silicon probe (60Hz, 21 microA, average of 3 mice) confirms that the electrode was located in M1 (see Methods). Shaded background: standard error of the mean.



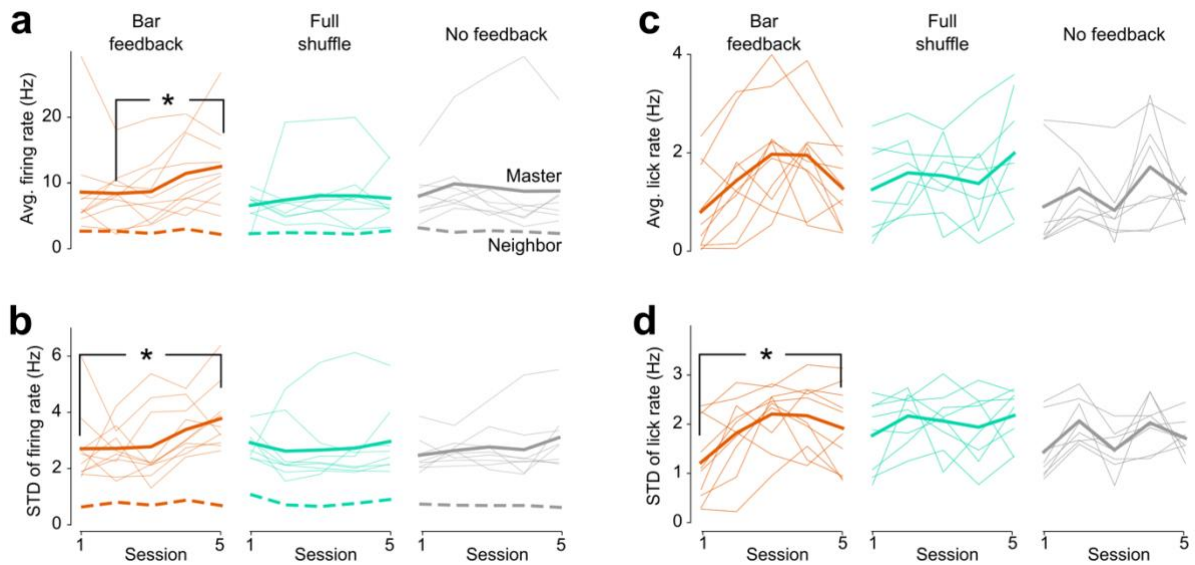
Supplementary Figure 3. Firing rate limits defining the eight possible positions of the virtual cursor. **a** Example distribution of the pooled firing rate of Master neurons during the 3 min baseline just before the start of one session. The transition between virtual cursor positions 7 and 8 is set at the 99th percentile of the firing rate distribution. The range from 0 Hz to the 99th percentile is divided into equal firing rate intervals. Each firing rate interval corresponds to one virtual cursor position from 1 to 7 as indicated. **b** The 99th percentile of the pooled Master neurons firing rate did not evolve significantly over training sessions, regardless of the protocol. Each line: 1 mouse. (n.s.: Mann-Whitney p value > 0.05).



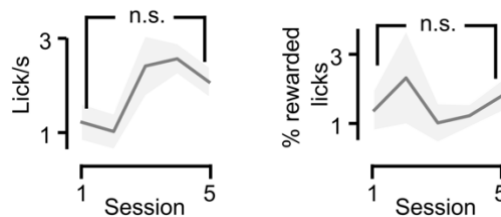
Supplementary Figure 4. Detail of the photostimulated barrels in the four feedback conditions, across the eight virtual cursor positions.



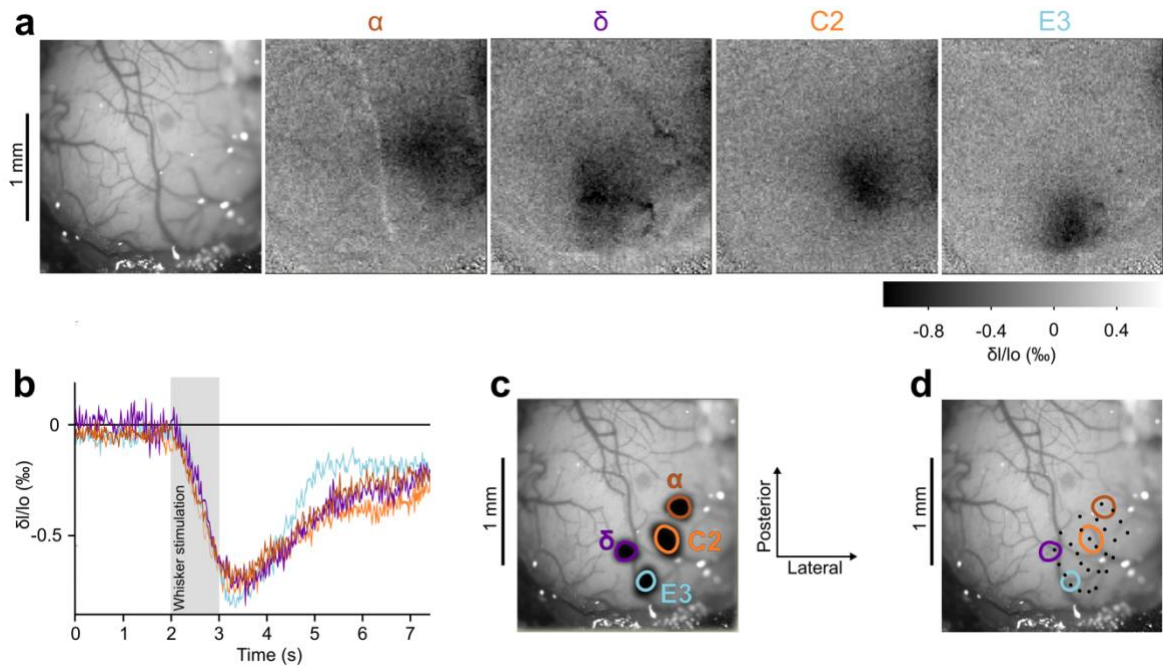
Supplementary Figure 5. Engagement and performance during training across feedback conditions. **a** Engagement of the mice during training sessions in the Bar feedback (orange), Full shuffle (green) and No feedback (gray) conditions. Left: total number of licks per session. Right: total number of rewards per session. Lines: average across mice. Shaded backgrounds: \pm SEM. **b** Learning curves for two groups of mice ($n = 3$ in each group) trained with two different orders of presentation of three protocols: Bar feedback (orange), Full shuffle (green) and No feedback (gray). *: $p < 0.05$. Mann-Whitney non-parametric tests. Lines: average across mice. Shaded backgrounds: \pm SEM.



Supplementary Figure 6. Firing statistics of Master and Neighbor neurons, and licking statistics, during closed-loop learning in 3 feedback conditions. **a** Thin lines: Firing rate averaged over the individual Master neurons of one mouse as a function of training sessions. Thick lines: Average of individual neuron firing rates across all mice, for Master (continuous line) and Neighbor (dashed line) neurons. Bar feedback (orange), Full shuffle (green) and No feedback (black) conditions. **b** Same as a, for the standard deviation of the firing rate (measured over 1 s windows). **c** Average lick rate over sessions. **d** Average standard deviation of the lick rate (measured over 1 s windows). All tests: Mann-Whitney. *: $p < 0.05$.



Supplementary Figure 7. Absence of learning during 5 sessions of bar playback training in five mice. Left: Mean (+/-SEM) frequency of licking per sessions. The increase was not significant. Right: Average (+/-SEM) proportion of rewarded licking over the 5 training sessions. The modulation is non-significant. n.s: Wilcoxon test $p > 0.05$.



Supplementary Figure 8. Identification of the barrels position within the chronic optical window using intrinsic imaging shown for one mouse. **a** Image of the barrel cortex showing the blood vessels and intrinsic imaging during stimulations of the Alpha, Delta, C2 and E3 whiskers. **b** Time course of the whisker stimulation and of the intrinsic signal. Each whisker was stimulated for 1 second (grey area) with 100 Hz rostro-caudal deflections. **c** Thresholded contours of the intrinsic signal peaks used to define the location of the barrels. Contours of barrels correspond to 85% of the maximum relative absorption, after applying a 20th order gaussian filter. **d** Alignment of the barrel map from Knutsen et al., 2016, with the 4 barrels localized by intrinsic imaging.

References

- 5 Abbasi, A., Goueytes, D., Shulz, D.E., Ego-Stengel, V., and Estebanez, L. (2018). A fast intracortical brain-machine interface with patterned optogenetic feedback. *J. Neural Eng.* 15, 046011. <https://doi.org/10.1088/1741-2552/aabb80>.
- Andermann, M.L., and Moore, C.I. (2006). A somatotopic map of vibrissa motion direction within a barrel column. *Nat. Neurosci.* 9, 543–551. <https://doi.org/10.1038/nn1671>.
- 10 Arduin, P.-J., Fregnac, Y., Shulz, D.E., and Ego-Stengel, V. (2013). “Master” Neurons Induced by Operant Conditioning in Rat Motor Cortex during a Brain-Machine Interface Task. *J. Neurosci.* 33, 8308–8320. <https://doi.org/10.1523/JNEUROSCI.2744-12.2013>.
- Armenta Salas, M., Bashford, L., Kellis, S., Jafari, M., Jo, H., Kramer, D., Shanfield, K., Pejsa, K., Lee, B., Liu, C.Y., et al. (2018). Proprioceptive and cutaneous sensations in humans elicited by intracortical microstimulation. *ELife* 7, e32904. <https://doi.org/10.7554/eLife.32904>.
- 15 Athalye, V.R., Ganguly, K., Costa, R.M., and Carmena, J.M. (2017). Emergence of Coordinated Neural Dynamics Underlies Neuroprosthetic Learning and Skillful Control. *Neuron* 93, 955-970.e5. <https://doi.org/10.1016/j.neuron.2017.01.016>.
- Badde, S., and Heed, T. (2016). Towards explaining spatial touch perception: Weighted integration of multiple location codes. *Cogn. Neuropsychol.* 33, 26–47. <https://doi.org/10.1080/02643294.2016.1168791>.
- 20 Bensmaia, S.J., and Miller, L.E. (2014). Restoring sensorimotor function through intracortical interfaces: progress and looming challenges. *Nat. Rev. Neurosci.* 15, 313–325. <https://doi.org/10.1038/nrn3724>.
- Brochier, T., Boudreau, M.-J., Paré, M., and Smith, A.M. (1999). The effects of muscimol inactivation of small regions of motor and somatosensory cortex on independent finger movements and force control in the precision grip. *Exp. Brain Res.* 128, 31–40. <https://doi.org/10.1007/s002210050814>.
- Chapin, J.K., Moxon, K.A., Markowitz, R.S., and Nicolelis, M.A.L. (1999). Real-time control of a robot arm using simultaneously recorded neurons in the motor cortex. *Nat. Neurosci.* 2, 664–670. <https://doi.org/10.1038/10223>.
- 30 Chesler, A.T., Szczot, M., Bharucha-Goebel, D., Čeko, M., Donkervoort, S., Laubacher, C., Hayes, L.H., Alter, K., Zampieri, C., Stanley, C., et al. (2016). The Role of *PIEZO2* in Human Mechanosensation. *N. Engl. J. Med.* 375, 1355–1364. <https://doi.org/10.1056/NEJMoa1602812>.
- Dadarlat, M.C., O’Doherty, J.E., and Sabes, P.N. (2015). A learning-based approach to artificial sensory feedback leads to optimal integration. *Nat. Neurosci.* 18, 138–144. <https://doi.org/10.1038/nn.3883>.
- 35 Deschenes, M. (2009). Vibrissal afferents from trigeminus to cortices. *Scholarpedia* 4, 7454. <https://doi.org/10.4249/scholarpedia.7454>.
- Diamond, M.E., and Arabzadeh, E. (2013). Whisker sensory system – From receptor to decision. *Prog. Neurobiol.* 103, 28–40. <https://doi.org/10.1016/j.pneurobio.2012.05.013>.
- 40 Drew, P.J., and Feldman, D.E. (2007). Intrinsic Signal Imaging of Deprivation-Induced Contraction of Whisker Representations in Rat Somatosensory Cortex. *Cereb. Cortex* 19, 331–348. <https://doi.org/10.1093/cercor/bhn085>.
- Estebanez, L., Boustani, S.E., Destexhe, A., and Shulz, D.E. (2012). Correlated input reveals coexisting coding schemes in a sensory cortex. *Nat. Neurosci.* 15, 1691–1699. <https://doi.org/10.1038/nn.3258>.
- 45 Estebanez, L., Bertherat, J., Shulz, D.E., Bourdieu, L., and Léger, J.-F. (2016). A radial map of multi-whisker correlation selectivity in the rat barrel cortex. *Nat. Commun.* 7. <https://doi.org/10.1038/ncomms13528>.
- 50 Estebanez, L., Férézou, I., Ego-Stengel, V., and Shulz, D.E. (2018). Representation of Tactile Scenes in the Rodent Barrel Cortex. *Neuroscience* 368, 81–94.

<https://doi.org/10.1016/j.neuroscience.2017.08.039>.

Feldmeyer, D. (2012). Excitatory neuronal connectivity in the barrel cortex. *Front. Neuroanat.* 6. <https://doi.org/10.3389/fnana.2012.00024>.

5 Ferezou, I., Bolea, S., and Petersen, C.C.H. (2006). Visualizing the Cortical Representation of Whisker Touch: Voltage-Sensitive Dye Imaging in Freely Moving Mice. *Neuron* 50, 617–629. <https://doi.org/10.1016/j.neuron.2006.03.043>.

Fetz, E.E. (1969). Operant Conditioning of Cortical Unit Activity. *Science* 163, 955–958. .

10 Flesher, S.N., Collinger, J.L., Foldes, S.T., Weiss, J.M., Downey, J.E., Tyler-Kabara, E.C., Bensmaia, S.J., Schwartz, A.B., Boninger, M.L., and Gaunt, R.A. (2016). Intracortical microstimulation of human somatosensory cortex. *Sci. Transl. Med.* 8, 361ra141–361ra141. <https://doi.org/10.1126/scitranslmed.aaf8083>.

Flesher, S.N., Downey, J.E., Weiss, J.M., Hughes, C.L., Herrera, A.J., Tyler-Kabara, E.C., Boninger, M.L., Collinger, J.L., and Gaunt, R.A. (2019). Restored tactile sensation improves neuroprosthetic arm control (Clinical Trials).

15 Flesher, S.N., Downey, J.E., Weiss, J.M., Hughes, C.L., Herrera, A.J., Tyler-Kabara, E.C., Boninger, M.L., Collinger, J.L., and Gaunt, R.A. (2021). A brain-computer interface that evokes tactile sensations improves robotic arm control. *Science* 372, 831–836. <https://doi.org/10.1126/science.abd0380>.

20 Fu, M., and Zuo, Y. (2011). Experience-dependent structural plasticity in the cortex. *Trends Neurosci.* 34, 177–187. <https://doi.org/10.1016/j.tins.2011.02.001>.

Guo, Z.V., Hires, S.A., Li, N., O'Connor, D.H., Komiyama, T., Ophir, E., Huber, D., Bonardi, C., Morandell, K., Gutnisky, D., et al. (2014). Procedures for Behavioral Experiments in Head-Fixed Mice. *PLoS ONE* 9, e88678. <https://doi.org/10.1371/journal.pone.0088678>.

25 Hartmann, K., Thomson, E.E., Zea, I., Yun, R., Mullen, P., Canarick, J., Huh, A., and Nicolelis, M.A.L. (2016). Embedding a Panoramic Representation of Infrared Light in the Adult Rat Somatosensory Cortex through a Sensory Neuroprosthesis. *J. Neurosci.* 36, 2406–2424. <https://doi.org/10.1523/JNEUROSCI.3285-15.2016>.

30 Hobbs, J.A., Towal, R.B., and Hartmann, M.J.Z. (2016). Spatiotemporal Patterns of Contact Across the Rat Vibrissal Array During Exploratory Behavior. *Front. Behav. Neurosci.* 9. <https://doi.org/10.3389/fnbeh.2015.00356>.

Holtmaat, A., Bonhoeffer, T., Chow, D.K., Chuckowree, J., De Paola, V., Hofer, S.B., Hübener, M., Keck, T., Knott, G., Lee, W.-C.A., et al. (2009). Long-term, high-resolution imaging in the mouse neocortex through a chronic cranial window. *Nat. Protoc.* 4, 1128–1144. <https://doi.org/10.1038/nprot.2009.89>.

35 Jacob, V., Le Cam, J., Ego-Stengel, V., and Shulz, D.E. (2008). Emergent Properties of Tactile Scenes Selectively Activate Barrel Cortex Neurons. *Neuron* 60, 1112–1125. <https://doi.org/10.1016/j.neuron.2008.10.017>.

Johansson, R.S., and Flanagan, J.R. (2009). Coding and use of tactile signals from the fingertips in object manipulation tasks. *Nat. Rev. Neurosci.* 10, 345–359. <https://doi.org/10.1038/nrn2621>.

40 Johansson, R.S., and Westling, G. (1984). Roles of glabrous skin receptors and sensorimotor memory in automatic control of precision grip when lifting rougher or more slippery objects. *Exp. Brain Res.* 56. <https://doi.org/10.1007/BF00237997>.

Johansson, R.S., Higer, C., and Bfickstr, L. (1992). Somatosensory control of precision grip during unpredictable pulling loads. *Exp. Brain Res.* 89, 192–203. .

45 Kaas, J.H. (1997). Topographic Maps are Fundamental to Sensory Processing. *Brain Res. Bull.* 44, 107–112. [https://doi.org/10.1016/S0361-9230\(97\)00094-4](https://doi.org/10.1016/S0361-9230(97)00094-4).

Knutsen, P.M., Mateo, C., and Kleinfeld, D. (2016). Precision mapping of the vibrissa representation within murine primary somatosensory cortex. *Philos. Trans. R. Soc. B Biol. Sci.* 371, 20150351. <https://doi.org/10.1098/rstb.2015.0351>.

50 Kremer, Y., Leger, J.-F., Goodman, D., Brette, R., and Bourdieu, L. (2011). Late Emergence of the

- Vibrissa Direction Selectivity Map in the Rat Barrel Cortex. *J. Neurosci.* 31, 10689–10700. <https://doi.org/10.1523/JNEUROSCI.6541-10.2011>.
- Laboy-Juárez, K.J., Langberg, T., Ahn, S., and Feldman, D.E. (2019). Elementary motion sequence detectors in whisker somatosensory cortex. *Nat. Neurosci.* 22, 1438–1449. <https://doi.org/10.1038/s41593-019-0448-6>.
- Lassagne, H., Goueytes, D., Shulz, D.E., Estebanez, L., and Ego-Stengel, V. (2022). Continuity within the somatosensory cortical map facilitates learning. *Cell Rep.* 39, 110617. <https://doi.org/10.1016/j.celrep.2022.110617>.
- Madisen, L., Mao, T., Koch, H., Zhuo, J., Berenyi, A., Fujisawa, S., Hsu, Y.-W.A., Garcia, A.J., Gu, X., Zanella, S., et al. (2012). A toolbox of Cre-dependent optogenetic transgenic mice for light-induced activation and silencing. *Nat. Neurosci.* 15, 793–802. <https://doi.org/10.1038/nn.3078>.
- Mathis, A., Mamidanna, P., Cury, K.M., Abe, T., Murthy, V.N., Mathis, M.W., and Bethge, M. (2018). DeepLabCut: markerless pose estimation of user-defined body parts with deep learning. *Nat. Neurosci.* 21, 1281–1289. <https://doi.org/10.1038/s41593-018-0209-y>.
- Mathis, M.W., Mathis, A., and Uchida, N. (2017). Somatosensory Cortex Plays an Essential Role in Forelimb Motor Adaptation in Mice. *Neuron* 93, 1493-1503.e6. <https://doi.org/10.1016/j.neuron.2017.02.049>.
- Miall, R.C., Kitchen, N.M., Nam, S.-H., Lefumat, H., Renault, A.G., Ørstavik, K., Cole, J.D., and Sarlegna, F.R. (2018). Proprioceptive loss and the perception, control and learning of arm movements in humans: evidence from sensory neuronopathy. *Exp. Brain Res.* 236, 2137–2155. <https://doi.org/10.1007/s00221-018-5289-0>.
- Monzée, J., Lamarre, Y., and Smith, A.M. (2003). The Effects of Digital Anesthesia on Force Control Using a Precision Grip. *J. Neurophysiol.* 89, 672–683. <https://doi.org/10.1152/jn.00434.2001>.
- Moritz, C.T., Perlmutter, S.I., and Fetzi, E.E. (2008). Direct control of paralysed muscles by cortical neurons. *Nature* 456, 639–642. <https://doi.org/10.1038/nature07418>.
- Oby, E.R., Golub, M.D., Hennig, J.A., Degenhart, A.D., Tyler-Kabara, E.C., Yu, B.M., Chase, S.M., and Batista, A.P. (2019). New neural activity patterns emerge with long-term learning. *Proc. Natl. Acad. Sci.* 116, 15210–15215. <https://doi.org/10.1073/pnas.1820296116>.
- O'Connor, D.H., Hires, S.A., Guo, Z.V., Li, N., Yu, J., Sun, Q.-Q., Huber, D., and Svoboda, K. (2013). Neural coding during active somatosensation revealed using illusory touch. *Nat. Neurosci.* 16, 958–965. <https://doi.org/10.1038/nn.3419>.
- O'Doherty, J.E., Lebedev, M.A., Ifft, P.J., Zhuang, K.Z., Shokur, S., Bleuler, H., and Nicolelis, M.A.L. (2011). Active tactile exploration using a brain–machine–brain interface. *Nature* 479, 228–231. <https://doi.org/10.1038/nature10489>.
- O'Doherty, J.E., Shokur, S., Medina, L.E., Lebedev, M.A., and Nicolelis, M.A.L. (2019). Creating a neuroprosthesis for active tactile exploration of textures. *Proc. Natl. Acad. Sci.* 116, 21821–21827. <https://doi.org/10.1073/pnas.1908008116>.
- Okun, M., Lak, A., Carandini, M., and Harris, K.D. (2016). Long Term Recordings with Immobile Silicon Probes in the Mouse Cortex. *PLOS ONE* 11, e0151180. <https://doi.org/10.1371/journal.pone.0151180>.
- Papale, A.E., and Hooks, B.M. (2018). Circuit Changes in Motor Cortex During Motor Skill Learning. *Neuroscience* 368, 283–297. <https://doi.org/10.1016/j.neuroscience.2017.09.010>.
- Penfield, W., and Boldrey, E. (1937). SOMATIC MOTOR AND SENSORY REPRESENTATION IN THE CEREBRAL CORTEX OF MAN AS STUDIED BY ELECTRICAL STIMULATION. *Brain* 60, 389–443. <https://doi.org/10.1093/brain/60.4.389>.
- Petersen, C.C.H. (2019). Sensorimotor processing in the rodent barrel cortex. *Nat. Rev. Neurosci.* 20, 533–546. <https://doi.org/10.1038/s41583-019-0200-y>.
- Prsa, M., Galiñanes, G.L., and Huber, D. (2017). Rapid Integration of Artificial Sensory Feedback during Operant Conditioning of Motor Cortex Neurons. *Neuron* 93, 929-939.e6. <https://doi.org/10.1016/j.neuron.2017.01.023>.

- Romo, R., Hernández, A., Zainos, A., and Salinas, E. (1998). Somatosensory discrimination based on cortical microstimulation. *Nature* 392, 387–390. <https://doi.org/10.1038/32891>.
- 5 Sadtler, P.T., Quick, K.M., Golub, M.D., Chase, S.M., Ryu, S.I., Tyler-Kabara, E.C., Yu, B.M., and Batista, A.P. (2014). Neural constraints on learning. *Nature* 512, 423–426. <https://doi.org/10.1038/nature13665>.
- Sainburg, R.L., Ghilardi, M.F., Poizner, H., and Ghez, C. (1995). Control of limb dynamics in normal subjects and patients without proprioception. *J. Neurophysiol.* 73, 820–835. <https://doi.org/10.1152/jn.1995.73.2.820>.
- 10 Scott, S.H. (2016). A Functional Taxonomy of Bottom-Up Sensory Feedback Processing for Motor Actions. *Trends Neurosci.* 39, 512–526. <https://doi.org/10.1016/j.tins.2016.06.001>.
- Simons, D.J. (1978). Response properties of vibrissa units in rat SI somatosensory neocortex. *J. Neurophysiol.* 41, 798–820. <https://doi.org/10.1152/jn.1978.41.3.798>.
- 15 Tabot, G.A., Dammann, J.F., Berg, J.A., Tenore, F.V., Boback, J.L., Vogelstein, R.J., and Bensmaia, S.J. (2013). Restoring the sense of touch with a prosthetic hand through a brain interface. *Proc. Natl. Acad. Sci.* 110, 18279–18284. <https://doi.org/10.1073/pnas.1221113110>.
- Vilarchao, M.E., Estebanez, L., Shulz, D.E., and Férézou, I. (2018). Supra-barrel Distribution of Directional Tuning for Global Motion in the Mouse Somatosensory Cortex. *Cell Rep.* 22, 3534–3547. <https://doi.org/10.1016/j.celrep.2018.03.006>.
- 20 Yger, P., Spampinato, G.L., Esposito, E., Lefebvre, B., Deny, S., Gardella, C., Stimberg, M., Jetter, F., Zeck, G., Picaud, S., et al. (2018). A spike sorting toolbox for up to thousands of electrodes validated with ground truth recordings in vitro and in vivo. *ELife* 7, e34518. <https://doi.org/10.7554/eLife.34518>.

4.3 Preliminary results: Matching natural closed loop latencies promotes sensorimotor learning

4.3.1 Summary

In this third study, we also aim to reveal spatio-temporal rules for BMI learning. In the lab, PhD student Dorian Goueytes has implemented a closed-loop BMI in a study to which I participated (see Supplementary Article 1), but due to several reasons, the control algorithm was running with very long latencies and jitters, and we wanted to improve this technical drawback with the hope of improving the performance of the animals. Specifically, our hypothesis is that sensorimotor learning for a prosthesis should follow the same temporal rules as for real limbs control. We know from the literature that whisker movements can be initiated at short latencies (around 40 ms) following electrical stimulation of M1 (Matyas et al., 2010), while it takes approximately 10-15 milliseconds for a sensory message from the whiskers to get to the brain (Ferezou et al., 2007), leading to a "natural" sensorimotor latency of approximately 50 ms. This range of "natural" closed-loop latencies that we want to test is below typical delays in bidirectional BMI, because of technological constraints. Thus, we had to design a new setup that would allow sensory stimulation within very short delays after an action potential (mean = 4.4ms, sd = 0.3 ms).

Once the setup was functional, we combined this ultra-fast reading of the neuronal activity with the rotating feedback described in study 4.1. We designed a point-process control algorithm for which each spike is treated in real time and can lead to a change of the photostimulation. We are able to inject artificially a delay in the loop, in order to either match the natural latency, or impose higher or lower delays. The study is still at its very beginning, but shows very promising results, with animals managing to reach fine control of a single degree of freedom.

4.3.2 Participation statement

For this study, I conceived the project and designed the protocol with inputs from my supervisors. I rebuilt a BMI setup combining the electrophysiological recordings methods of article 4.2 and the feedback pattern delivery of article 4.1. I changed the communication protocols to reduce the closed-loop latency, coded the new task and the control algorithm. I also did the first batch of surgeries, experiments and analyzed this preliminary data. Still, the preliminary results are promising and need to be completed, so I trained another PhD

student, Alexandre Tolboom, to the different methods and he is currently continuing the experiments.

4.3.3 Material and methods

Experimental Model and Subject Details

We used 6-week-old Ai-32 x EMX-Cre mice, expressing channelrhodopsin in excitatory neurons across the cortex (Madisen et al., 2012). Experimental procedures have been approved by the French Ministry of Research and Ethics Committee 59 as part of project 25932-2020060813556163. A total of 3 mice were successfully implanted, water regulated, and then trained in the task. During the training period, the mice only had access to water during the sessions as reward, and right after the session for supplementation whenever necessary.

Methods details

Most of the methods used in this study are very similar to the methods used in study 4.1. In particular, the implantation of the cranial window and the intrinsic imaging are the same. For clarity purpose in this thesis, these methods will not be detailed again exhaustively.

Mouse preparation

Two weeks after the window implantation over S1 and intrinsic imaging of at least 3 barrels (see Lassagne et al. (2022)), a second surgery was performed to implant an electrode in M1 to record the activity of single units. We followed an established protocol to implant a 32-channel electrode (8 tetrodes on 4 shanks, Neuronexus A4x2-tet- 5mm-150-200-121-CM32), 700 microns deep in M1. Grounding was achieved with a screw halfway inserted in the skull. After the dura over M1 was removed, the probe was slowly inserted into the cortex thanks to the stereotaxic frame. The craniotomy was then filled with Kwik-cast, and the probe was fixed to the skull using glue and dental cement. Using an extracellular recording system located next to the surgery setup, we were able to record single units even during the implantation of the electrode in the anesthetized mouse. This ensured good placement of the electrode (with several neurons recorded and high firing rates) before cementing it.

Brain-machine interfacing

Online spike sorting was done thanks to the central software of BlackRock Microsystems. The clusters defined were found to be sufficiently stable for

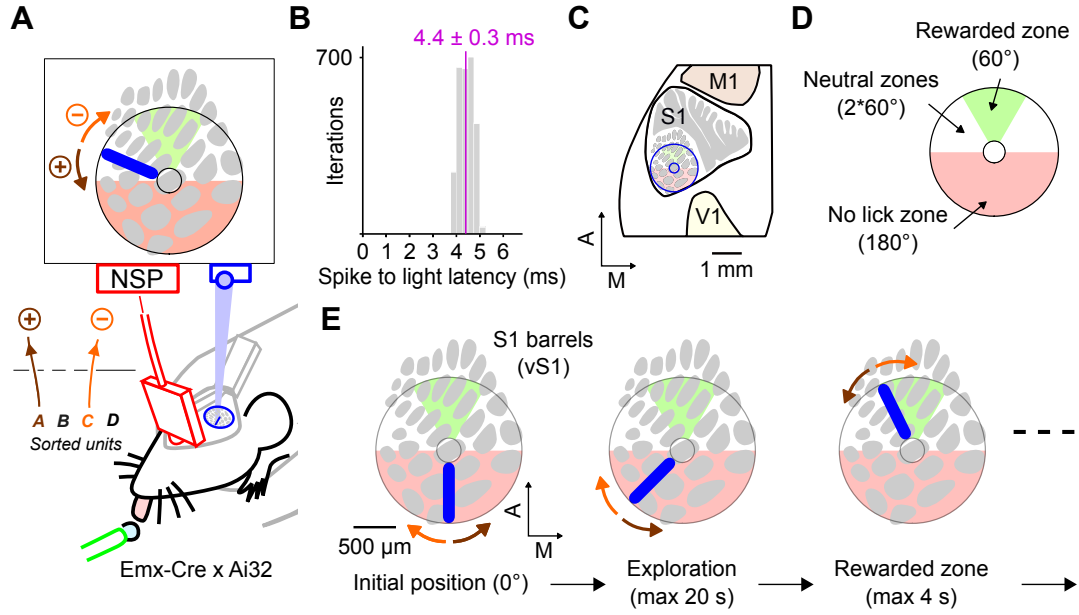


Figure 4.1: A closed-loop BMI with incremental control and optogenetic feedback.

(A) Schematic of the closed loop brain-machine interface: Out of the pool of neurons recorded in M1, two master neurons are arbitrarily chosen to drive the rotating cursor, which is then projected onto the cortex with our DLP projector.

(B) Latency of the closed-loop setup, measured from the occurrence of a spike until the arrival of the triggered light stimulation onto a photodiode.

(C) Location of the stimulation disk over vS1 (cortical map adapted from (Knutsen et al., 2016; Vanni et al., 2017)).

(D) When the bar was in the green zone, licks were rewarded. In the red zone, a lick ended the trial. In the white zones, licks were ignored.

(E) Snapshots from one trial.

our experiments, with the same clusters being visible across sessions. Our C++/Qt “master” program read the timestamps of the units recovered by the NSP through an UDP protocol, checked the occurrence of neural activity of different neurons every 1ms, ran the control algorithm (see below) and projected the correct frame onto the cortex in real time, either with the minimum latency (4.4 ms, Figure 4.1 A, B) or after a chosen delay. For the photostimulation part, we use a DLP projector (Vialux V-7001, 462 nm blue LED). Although the projected light bar stimulus is identical to the one used in study 4.1, targeting the whisker barrel cortex (Figure 4.1 C) with 360 frames, the illumination power and temporal patterns had to be changed due to the low latency paradigm and the change in mouse line. Each frame was projected for cycles of 500us ON/ 500us OFF, with a power of 0.5-0.75mW/mm². More importantly and in contrast to study 4.1, the photostimulation was driven by M1 spiking activity rather than following a predetermined trajectory.

Before starting the training and the water deprivation, we put the animal on the setup on 2-3 following days to record passively the neuronal activity. After this, out of the pool of units recorded by the tetrodes, we arbitrarily chose 2 stable neurons with similar and relatively high firing rates. We did not take into account fast spiking neurons, and only trained regular spiking ones. For the rest of the training sessions, these two neurons were the ones driving the rotating photostimulation. Each training session was preceded by a 3 minutes period with no photostimulation nor rewards during which we recorded the neurons passively for equilibration purposes. Basically the control algorithm transforming spiking activity was incremental, meaning that each spike contributes to a fixed change of bar position, and followed the following rules: - One neuron drives the photostimulation clockwise and the other neuron anti-clockwise. - Each spike contributes to at least 1 degree of movement so that it has an impact on the photostimulation - Weights are applied so that the sum of the bar movement is null if the mean spiking activity of each neuron is the same as the spiking activity during the equilibration period. - If one neuron fires alone for 5 seconds, the photostimulation should travel at least 150 degrees, so that the photostimulation enters the rewarded area. Based on these conditions, the formulas for one-spike movement contributions are the following:

$$Mvmt_{neuron1} = \max\left(\frac{fmean_{neuron2}}{\min(fmean_{neuron1}; fmean_{neuron2})}; \frac{150}{5 * fmean_{neuron1}}\right)$$

$$Mvmt_{neuron2} = -\max\left(\frac{fmean_{neuron1}}{\min(fmean_{neuron1}; fmean_{neuron2})}; \frac{150}{5 * fmean_{neuron2}}\right)$$

with $fmean_{neuron1}$ and $fmean_{neuron2}$ the mean firing rate of each neuron, in spike per second, measured during the 3 minutes equilibration period. Note that because our photostimulation consists of 360 different frames, the projected frame corresponds to the truncation of the computed new position.

Behavioral training

Each mouse started the training around one week after the electrode implantation. Mice started with one day of habituation during which they were getting familiar with being head-fixed on the setup and given water rewards for each lick on a lick-port. Training started the next day. Each day, mice were put on the setup and trained for a 30 minutes session. Each session was composed of a series of trials, separated by 5 seconds with no photostimulation. At the start of each trial, the light bar appeared at the most caudal position and rotated according to the mouse spiking activity (Figure 4.1 E). Licking when

the bar was in the No lick zone (red area) immediately ended the trial. Licking when the bar was in the Rewarded zone (green area) was rewarded with an immediate 10 uL water droplet. Note that if the mouse did not lick, the water droplet was not delivered on the spout. Licking in the Neutral zone (white area) was neither rewarded nor punished. In the first version, there was no maximum duration of a trial, but the trial ended after the bar spent 4 s in

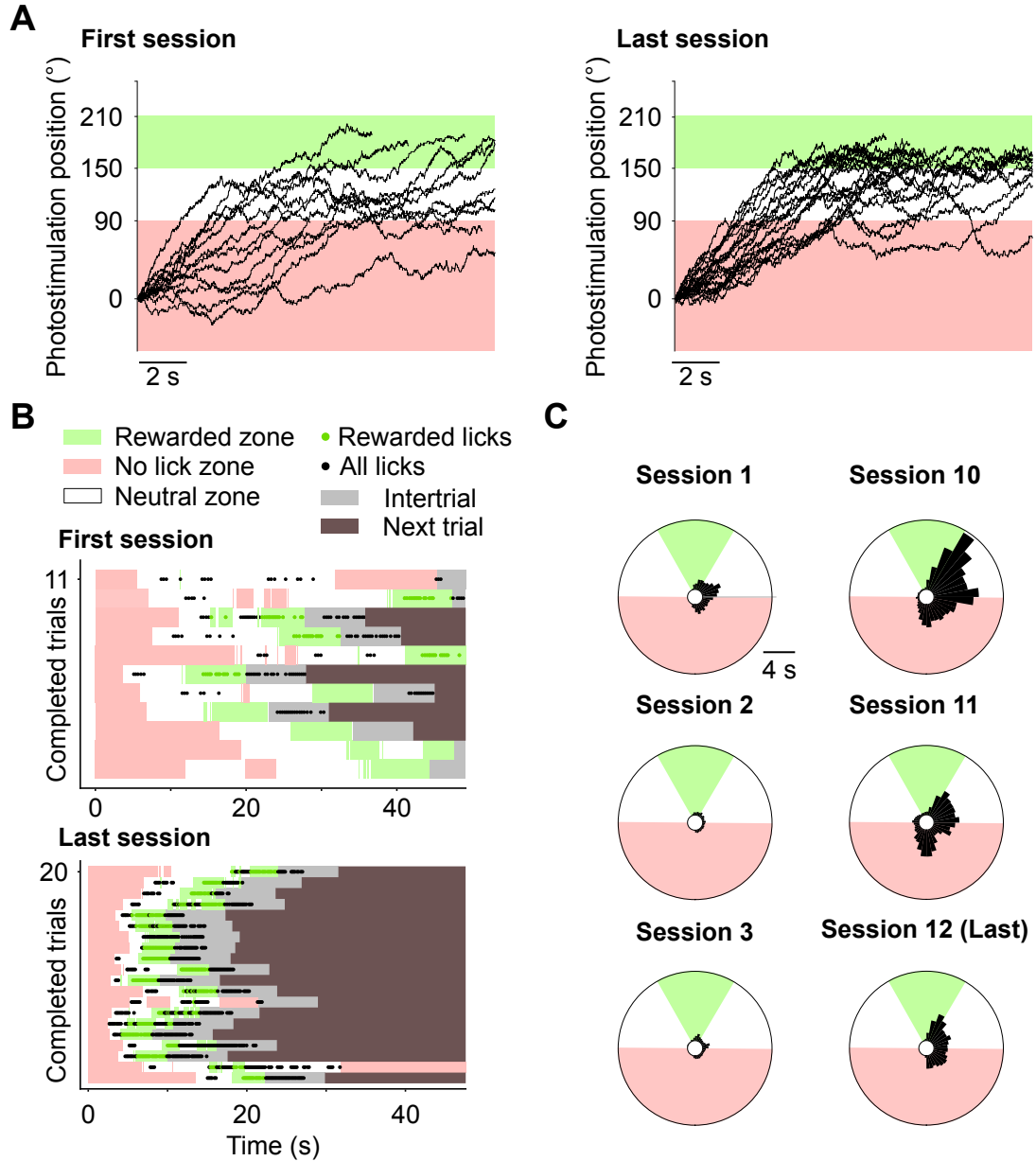


Figure 4.2: BMI learning example with physiological latency and incremental control.

(A) Example trajectories before and after learning the BMI task for one mouse. Each trial that entered the Neutral zone is shown for the first and the last session (session 12).

(B) Raster plots of licks (dots) for the same trials shown in A.

(C) Polar histograms of the time spent of the photostimulation in 10 degrees bins for the first 3 and last 3 sessions for one mouse.

he Rewarded zone. For new experiments, maximum duration of the trial will be set at 20 s (Figure 4.1 D, E). Mice were usually trained for about 15 days before the stability of the trained neurons and their signal-to-noise ratios were degraded.

4.3.4 Preliminary Results

Out of the three mice trained, only two showed signs of neural activity modulation, while all three of them were able to detect the optogenetic feedback. For the two following figures, only the best example is shown as a proof of concept that a mouse is capable of learning this complex task. Figure 4.2 A represents the trajectories of the photostimulation bar that crossed the Neutral zone for the first and last sessions for one mouse. Note that despite our efforts to equilibrate the kinematic weights for the two neurons, there remains a bias toward one direction. This bias could be different for another mouse, and could be due to some baseline change before and after beginning the session. During session 1, trajectories tended to explore a large part of the angular space. During the last session, trajectories were more stereotyped and converged towards the Rewarded zone, stabilizing at its border. The same trials are shown in Figure 4.2 B, as temporal rasters of licks, displayed with relation to the transitions between different zones. The trials arrive faster in the Rewarded area in the last session and the mouse starts licking as soon as it enters the Neutral zone, just as in study 4.1. The mouse increased the overall percentage of rewarded trials (from 2% in session 1 to 38% in session 12), as well as the percentage of rewarded trials among trials entering the Rewarded zone (from 36% to 100%). On Figure 4.2 C, we compare the distributions of the time spent by the photostimulation in 10 degrees bins, for the trials entering the neutral zone. We see a clear difference between the first three sessions and the last three sessions, providing evidence that the animal learned to adjust the firing rates of the conditioned neurons to slow down or stop the photostimulation movement.

By looking at the firing rates of the two neurons around specific events, the strategy used by the mouse can be revealed (Figure 4.3). While there is not much change across sessions between the firing rate (FR) profiles looking at the start of the trials, or when the photostimulation crossed the 30 degree line, by contrast, FR profiles triggered by the entry in the rewarded zone from the right side indicate a long increase of the clockwise neuron FR (orange). This change of activity, in turn, slows down the photostimulation or even reverses the kinematics, so that the photostimulation bar stays in or close to the Re-

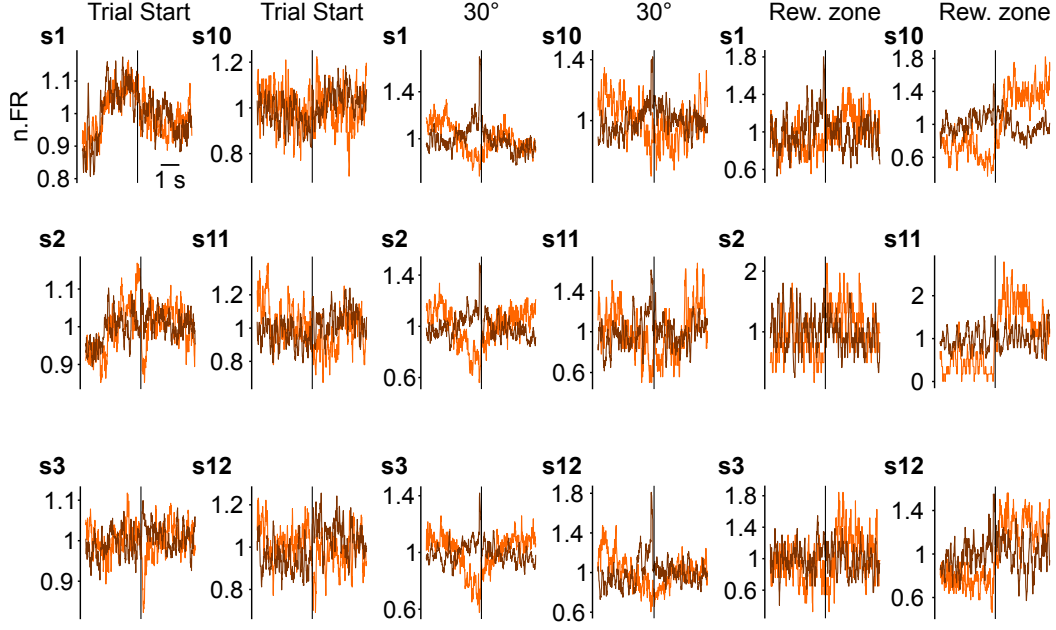


Figure 4.3: Neuronal strategy of solving the BMI task for one mouse.

Firing rate profiles of the two neurons used for controlling the photostimulation (brown: neuron driving the bar anti-clockwise; orange: neuron driving the bar clockwise), around certain events: The start of the trials, crossing the 30 degrees line inside the No lick zone, and entering the Rewarded zone from the right side. The activity is normalized by dividing the 100ms smoothed firing rate by its baseline activity. s: session.

warded zone longer. This change in activity and the resulting motor control is thus responsible for the performance of the animal in the task.

Note that when we trigger FR profiles with specific events like crossing a line, we bias the spiking activity of the conditioned neurons to a certain firing pattern. As such, the short peak of activity for the anti-clockwise neuron (brown) that is seen for all FR profiles for crossing the 30 degree line, corresponds to the selection of the event: A spike must be in this window for the bar to cross these lines. However, the transient inhibition of the clockwise neuron (orange) observed at the start of the trials start is probably due to the start of the photostimulation.

4.3.5 Perspectives

We plan to consolidate our results with new animals, training them with the same "natural" latency (50 ms) and then switching to either real-time (5 ms latency, faster than the physiology) or long latencies (200 ms or more, limit for a reciprocal tapping task in human). We hope to find an optimal latency value for which learning is facilitated, while comparing the task modulation of the conditioned neurons through learning for different latencies.

Part III

DISCUSSION

Biomimetism ? Horizontal connectivity and the function of cortical maps

Understanding how an animal may extract information from ongoing cortical patterns is an active area of research, with immediate relevance to the field of neuroprostheses. Recent studies question whether cortical stimulation should aim at biomimicry, by making the spatial and temporal aspects of the artificial stimulation as close as possible to the cortical response evoked by the targeted natural stimulus (Flesher et al., 2021; Tabot et al., 2015). In the somatosensory system, the main objective has been to restore the sense of touch and proprioception, either to reach a fine dexterity in a closed-loop context or to elicit sensory percepts and alleviate sensory deficits. In the visual system, the importance of biomimicry has also been investigated (Dobelle, 2000; Fernández et al., 2021).

One of the main results of this thesis concerns the spatial rules of artificial feedback delivery. We hypothesized that when artificial stimulation is delivered to sensory cortices to provide a percept, it may not be necessary to try to reproduce perfectly natural patterns of activity, but designing the stimulation according to the spatial organization of the targeted cortex should help learning. Basically, we wanted to know whether or not it is necessary to induce patterns of activity which would be spatially coherent with the natural functional mapping in sensory cortices. The results presented in this thesis in articles 4.1 and 4.2 tend to confirm this. The first study implemented a pure optogenetic discrimination task with rotating patterned continuous stimulation of the cortex. The second study consisted of a closed loop sensorimotor learning with discrete optogenetic patterns of feedback stimulation. In these two studies, mice were able to learn to lick when the optostimulation was at the right location, but only when the spatial organization of the stimulation made sense with the somatotopy of the targeted cortex. These results demonstrate that the geometry itself of mesoscale patterns is not critical, suggesting that the key to cortical integration lies in the spatio-temporal evolution of the patterns relative to the topography.

In study 4.1, the mice could learn the task when the stimulation was delivered to the whisker barrel cortex, thus in a modality for which there is a huge similarity between the peripheral and cortical organization, but not when it was delivered to the body representation of the primary somatosensory cortex or to the Posterior parietal cortex (PPC). While the organization of the body repre-

sentation in S1 contains more discontinuities than the whisker representation in S1, cortical maps of the PPC have been described (Wang and Burkhalter, 2007), but do not have any clear topography. Similarly, mice also had difficulties to learn when the organization of the stimulation was disrupted but still projected to the barrel cortex (shuffled stimulation). In study 4.2, discrete patterns are projected onto the barrel cortex in a closed-loop context. Beyond the nice demonstration that optogenetics can indeed be used in real-time in a closed loop neural operant conditioning BMI, the study also shows that the more spatio-temporally coherent the stimulation is, the better the learning: The bar-like feedback, composed of spatiotemporally continuous patterns, was the easiest to learn. A fixed shuffle of barrels (Barrel shuffle) kept some degree of continuity of the spatio-temporal properties and led to partial learning. In contrast, randomizing the barrels inside each frame (Full shuffle) or making the bar-like feedback lose its temporal continuity (Bar shuffle) prevented learning, or at least made it impossible to learn rapidly (see study 4.2, Figure 3).

What are the neuronal mechanisms behind these results? Why would spatio-temporally coherent artificial patterns of activity be more easily integrated by the network? There can be several anatomical and functional explanations for this. Supposing that perception of artificial activity relies at least partially on the activity of stellate cells of layer 4, which normally receive the sensory thalamic inputs, we could imagine that barrel-to-barrel horizontal connectivity explains the anticipation of the reward observed in Figure 2 and S4 of article 4.1. Even if layer 4 neurons do not project much to other barrels, lateral axonal and dendritic connections of pyramidal cells in layer 2/3 and layer 5 have been described in the literature, making the stellate cells of different barrels connect indirectly (Bureau et al., 2006; Lefort et al., 2009; Staiger and Petersen, 2021). When we stimulate through the layers with our photostimulation, we may activate these pathways even if it is sub-threshold, leading to a priming effect. This could make it easier to stimulate the nearby barrel columns right after, making the subsequent stimulation more salient and/or helping further anticipation of artificial activity. This could also work even without the hypothesis that stellate cells need to be activated for artificial perception by recruiting other intracortical connections. Another explanation would bring into play other brain structures, where there is substantial overlap between regions corresponding to neighboring whiskers. For example, in the secondary somatosensory cortex (S2), instead of single whisker representations, there are cortical "strips", each strip being the representation of a row of whiskers (Beni-

son et al., 2007). As for the thalamus, cortico-thalamic projections also include axons innervating several barreloids, while cells in the barreloids have dendritic trees also projecting to other close barreloids (Temereanca and Simons, 2004; Bourassa et al., 1995). This cross-talk between nearby barrels, be it inside the barrel cortex or via other brain areas, may explain why artificial stimulation needs to be spatio-temporally continuous with regards to the topographical organization of the targeted cortex.

Toward the use of optogenetics on humans

Either for recording or stimulation purposes, optogenetics have been a revolution in the field of neuroscience ever since the pioneering work of Karl Deisseroth and others, who freely distributed optogenetic tools all around the globe. By inserting a specific gene coding for a protein that can be activated with light of a specific wavelength, researchers managed to target and manipulate cell populations and develop causal approaches to uncover their functions (Huber et al., 2008; Cardin et al., 2010; Häusser, 2014).

This approach, compared to the traditional intracortical microstimulations performed with implanted electrodes, allows precise targeting of different cell types, by controlling the expression through cell-type specific promoters. Thanks to this versatility and cell-type specificity, optogenetics may also be the answer for the current difficulties faced in the field of sensory rehabilitation. In fact, the recent retinal implant Argus II with electrical stimulation of the retina was unfortunately not up to the challenge of restoring sight to the blind, but recent research on humans with optogenetic therapy of retinal foveal ganglion cells showed promising results with partial restoration of visual function (Sahel et al., 2021). In this study, a blind patient with late stage retinitis pigmentosa managed to locate and touch a large object placed on a white table with high success rate (96%). Meanwhile, Pieter Roelfsema's team is currently exploring the possibility of using optogenetics in the visual cortex of monkeys to restore sight. This is also explored in the auditory cortex of mice in Brice Bathellier's lab to restore audition.

Unfortunately, a lot of questions remain unanswered on the safety of using viral vectors to insert genes expressing non-humans opsins, and also on the effect of long term exposure of the human brain to the light and to the light-projecting devices. But if the safety and ethical questions are answered, then clinical trials will surely start. A lot of research on sensory rehabilitation will

be needed, and the benefits of stimulating the human brain with optogenetics rather than ICMS will be assessed in numerous pathologies, including patients suffering from epilepsy, Parkinson’s, as well as spinal cord lesions. In that case, there will be a strong need to understand how spatio-temporal patterns of artificial stimulation are integrated by the brain.

Perception of optostimulation and its precision

When artificially stimulating the cortex, either with ICMS or optogenetics, the first question asked is about how this stimulation is actually perceived: How is it localized? What is the sensation induced? What is the latency between the stimulation and the percept? If sensory rehabilitation through artificial stimulation is to reach the complexity of natural touch and proprioceptive inputs, these questions are critical. Some of these questions have been already answered through ICMS in the primary somatosensory cortex in human patients (Johnson et al., 2013; Hiremath et al., 2017; Caldwell et al., 2019). Patients implanted with electrocorticographic (eCoG) grids were stimulated with local trains of stimulation in S1. In these studies, subjects reported localized ”pins and needles”, ”buzz”, ”something brushing”, ”tingling”, ”pulse” and ”throb” like sensations. Beyond this and the perceptual thresholds for the current amplitude, they noted that response times to cortical stimulation were significantly slower than to haptic stimulations. Also interesting, they noted that for one subject for which they stimulated a language area, the percept was vague and non-localizable. Article 4.1 provide information on the spatial and temporal precision of the optogenetic integration by a mouse. The polar histograms of article 4.1 (Figure 2A,C and Figure S4E, G) are a clear demonstration that the angular spatial resolution of the integration is quite precise.

Very interestingly, we also noted that we could switch, for the same animals, from 5 ms ON/OFF projector cycles to 500us ON/OFF cycles, without affecting the animal performance. This suggests that at least in our task, the important parameter for behavioral integration would be the total amount of photons rather than the temporal patterns of light projections. Another interesting fact is that the spatial dynamics of the projection is very different between article 4.1 and 4.2: In article 4.1, the peak speed of the rotating bar is about 90 degrees per seconds, meaning a 0.7 mm sweep over the barrel cortex over one second. In article 4.2, the translating stimulation can sweep over the entire barrel cortex (1.5 mm) in less than 200 ms. While the two tasks are very different, it shows that mice are able to extract information from continuous

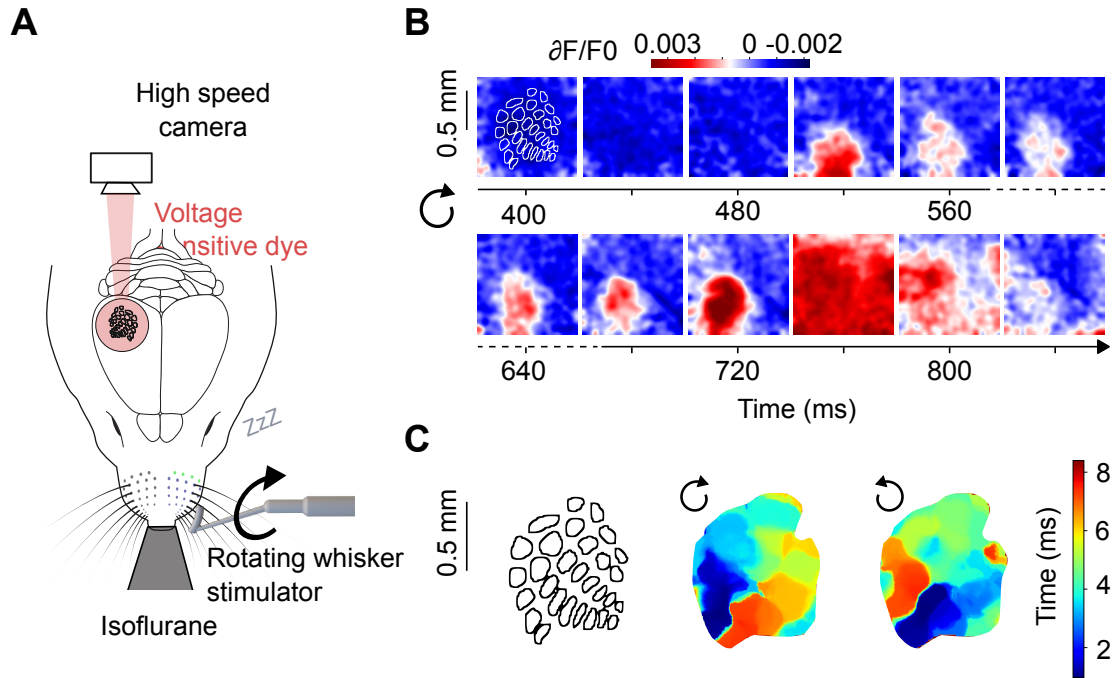


Figure 4.4: Cortical activity generated by rotation of an object in the whisker array.

(A) Schematic of the VSD experiment: A real bar, controlled by a stepper motor is rotating around the C2 whisker while we image the surface of the dyed cortex with a high speed camera.

(B) Series of snapshot of the VSD signal, starting from 400 ms after the bar starts moving and with an image every 40 ms for 440 ms, showing the appearance, expansion and disappearance of blobs of activity.

(C) Colormap of the spatially distributed blobs of activity shown in panel B, as a function of time. The discrete locations of the blobs in a time window was smoothed with a gaussian filter to obtain this map. Left: clockwise, right: anti-clockwise.

optogenetic stimulation with different dynamics. Finally, while we certainly can not ask the mouse how it feels, the reaction times of the mouse to the optogenetic stimulus (article 4.1, Figure 3D) were coherent with the literature (Ceballo et al., 2019; May et al., 2014), and similar to what is observed for a peripheral stimulation (around 300 ms).

Natural versus artificial stimulation

While the animals could reach high performance relying on optogenetic stimulation, it is not clear whether from the animal's point of view the optogenetic stimulus was experienced as a stimulus/deflection of the whiskers. Did the mouse experience the sensation of a rotating object in article 4.1 ? How was this stimulus translated by the internal body map? In order to obtain some an-

swers, with Alexandre Tolboom and Isabelle Ferezou, we performed mesoscale Voltage Sensitive Dye (VSD) recordings of the brain surface of anesthetized mice, while stimulating the whiskers with a plastic bar rotating physically next to the snout (Figure 4.4 A). Data shows that the cortex encoded the rotating bar with discrete "blobs" of activity on the barrel field (red structures in Figure 4.4 B). Throughout the recording these blobs could appear, move, disappear or expand to take the whole field of view, as seen in the 10th image. The positions and movements of these blobs of activity were consistent to the stimulation. Figure 4.4 C shows the spatial repartition of these events through time. When the real bar turned clockwise (resp. anti-clockwise) the blobs were indeed in locations turning clockwise around the center of the barrel field (resp. anti-clockwise). We hypothesize that individual blobs are the individual responses to stick-slip events on single whiskers or groups of whiskers.

Based on this data, it is very likely that the rotating continuous photostimulation of study 4.1 did not strictly recreate the activity corresponding to a peripheral bar rotation. Nonetheless, in our optogenetic experiments, the mouse was able to discriminate the rotating photostimulation with great success, even if the stimulation patterns were not necessarily 'physiological'.

Instantaneous incremental control following spiking activity

For scientific reasons related to real-time, the control algorithm for the last study for which I presented preliminary results 4.3 had to be different from what is presented in article 4.2 and Supplementary Article 1. In order to make sure that the animal is relying on the optogenetic stimulation in real time and at all training stages, firing rates could not be directly associated with a position of a stimulation. Otherwise, a specific activity pattern could be rewarded as the animal would perform a motor task, making the study of sensorimotor latencies pointless. For this reason, we had to use a derivative of the position for the command, for which succeeding the task requires different firing rate patterns depending on the photostimulation position. This constrained us to avoid border effects, so that at each time point of a trial, the photostimulation is controlled by the brain activity, meaning that the controlled space has to be circular. Finally, we needed to make sure that each spike had an instantaneous impact on the movement, so that there would not be any buffer adding delay on the latency. In order to satisfy all these constraints, and following our long-term interest in encoding the position of an articulation, we decided to implement the motor algorithm this rotating stimulation on the

barrel cortex with instantaneous incremental control. However, based on the first mouse tested, this type of instantaneous control surprisingly achieved better results than a more standard velocity algorithm for which we struggled to get stereotyped trajectories (see Supplementary Article 1). In that study, we also tested a motor control algorithm based on acceleration, which was even more difficult to learn. This is consistent with the idea that fast control and feedback rates may enable better results than standard prediction approaches like Kalman filters (Shanechi et al., 2017). To explain this, we speculated that the motor cortex has a limited capability to adapt to different timings between spiking activity and resulted movement, and tested this adaptation with the incremental control protocol. At the end of training sessions with physiological latency (50 ms spike-to-light), we switched the latency value to 200 ms for the next training session. We observed an initial drop in motor performance in term of trajectories (blue trajectories in Figure 4.5, which are not entering the Rewarded zone) and then a fast recovery over the course of the session. Due to the drop in motor control, this also led to a drop in raw number of rewards. Of course we would need more experiments to be able to conclude here, with additional mice starting to be trained with long or short latencies.

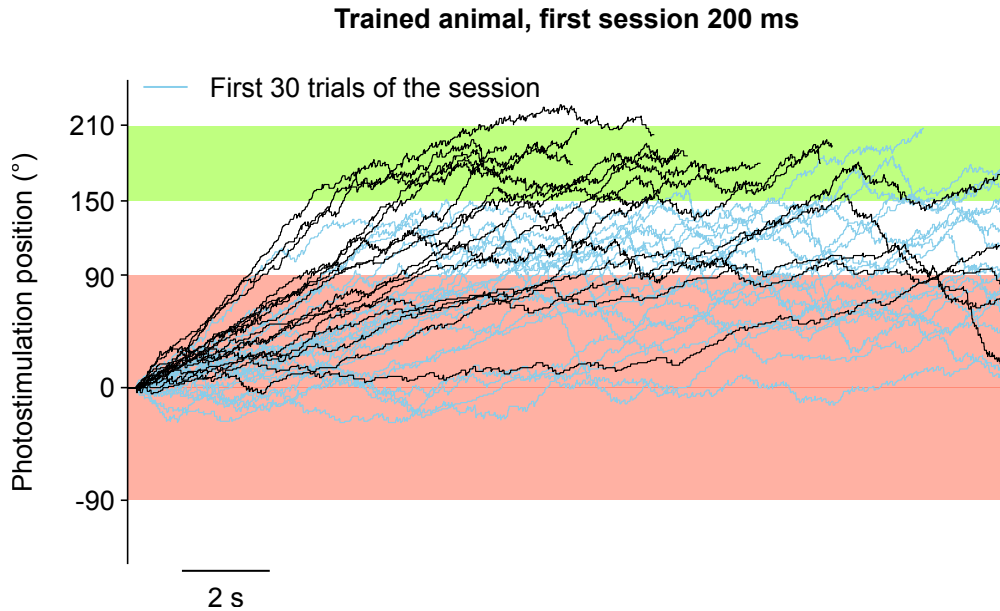


Figure 4.5: Switching to 200 ms latency for a trained animal

Example trajectories of a mouse having learning the BMI task with 50 ms latency and then switching to 200 ms for one session. Only trials crossing the 90 degree line are represented.

Operant conditioning of a few neurons in the motor cortex

Apart from study 4.1 for which the photostimulation is not driven by neuronal activity, all the other studies rely on neuronal operant conditioning, meaning that the mouse has access to rewards only if it modulates the activity of one or a few neurons. Just like a previous study of the lab (Arduin et al., 2013), what truly stood out when analysing the data is that after training, the modulation leading to the reward was relying only on the activity of a single dominant neuron. In the second paper, as the control command relies on a simple correspondence between spiking activity and cursor position, we observed that for each mouse, a single neuron drove behavior by increasing its average activity over training, specifically during a time window around rewards (study 4.2, Figure 6). In the incremental BMI presented in study 4.1, one neuron acts as the brake to stop the photostimulation from moving and the other neuron as the passive motor. It is hard to give an explanation for why only one neuron is actually conditioned in each of these scenarios. Interestingly, in the literature, it has already been described directly (Jeon et al., 2022) and indirectly (Patel et al., 2021). One explanation could be that the mice are opting for the simplest control, so if it can solve the task with only one neuron, why use two? Another explanation would involve the intrinsic connectivity of the recorded neurons. Patterns of activity involving two or more neurons may not be physiological or even possible if these patterns do not belong to the intrinsic manifold (Sadtlir et al., 2014) of neural firing. However, with the numerous experiments that have been performed here, it seems unlikely that we systematically chose neurons intrinsically not compatible.

Conclusion and perspectives

With this thesis, we hope to guide the sensory rehabilitation community with a few guidelines regarding the delivery of artificial feedback through optogenetic stimulation.

First, we have a clear demonstration that continuous, sweeping stimulation of the cortex can be interpreted by an animal with a high resolution. Unfortunately, due to the details of the design of the task we were not able to have a definite measure of this precision. We could certainly imagine a task with the same kind of optogenetic stimulation with constant feedback on performance sent to the animal through medial forebrain bundle stimulation. The mouse would then have to perform a task following in real-time the position of the stimulation, giving us a more accurate idea of the integration resolution.

Through a different type of optogenetic patterned stimulation paradigm, we also showed that cortical topography plays a role in the integration of inputs. However, our artificial input were limited and quite coarse: We use an Emx-Cre line for the promoter, meaning that all the excitatory neurons through the different layers of the cortex express the channelrhodopsin. If we want inputs that mimic the natural thalamic inputs, we would have to perform similar experiments with a Cre promoter focused solely on layer 4. In that scenario, would we still observe the anticipation like we did in the article 4.1, or would the animals train faster? Similarly, to investigate truly the mechanisms behind learning, we could try to block the horizontal connectivity of layer 2/3 while training the animals, with optogenetics or pharmacological methods.

Finally, we built a low-latency closed loop BMI with an incremental command to decipher the impact of motor-to-feedback latency on learning and dexterity. Timings have been shown to have great importance in motor execution, regardless of the anatomical structure involved. These natural sensorimotor loop work with specific timings, and we wondered here if these timings also have some relevance in an artificial BMI context. We could do this only because our BMI is fully virtualized with no movement from a real prosthesis, that could drastically increase the latencies and jitter of motor commands. Much is left to do if we want to improve the current robotic arms to achieve this kind of latency.

Part IV

APPENDIX

The two following articles are studies that I contributed to during my PhD, but they are not at the core of my project.

Article 1: Learning in a closed-loop brain-machine interface with distributed optogenetic cortical feedback

Summary: This article corresponds to our first try in connecting the optogenetic rotational feedback described in study 4.1 for neuronal motor control. In this article, mice were able to modulate neuronal activity in M1 to obtain more rewards, but we could not find any sign of fine dexterity. While it was interesting to implement a control on a realistic simulated prosthesis, a Jaco2 Kinova robotic arm, we found that its use was too heavy as it increased the delays and jitters of our closed-loop. This led to the development of the preliminary study in 4.3.

Contribution statement: In this work, I contributed to the experimental design and the building of the setup. I wrote some of the code for the hardware and for the analysis, participated in the analysis and provided figures and inputs to publish the article.

Article 2: Mechanical coupling through the skin affects whisker movements and tactile information encoding

Summary: This second article is a physiological study showing that multi-whisker integration also happens at the level of the follicle, through the mechanical coupling from the skin.

Contribution statement: This article was under review when I arrived in the lab, and participating to the revision allowed me to gain rapidly some critical knowledge on the sensorimotor system that I used in this entire PhD. I contributed by building the model of two whiskers and follicles described in figure 7 with the help of my supervisor, making the simulations and generating this figure. I also provided inputs for the answer to the reviewers and revised text relating to the model.

PAPER

Learning in a closed-loop brain-machine interface with distributed optogenetic cortical feedback

To cite this article: Dorian Goueytes *et al* 2022 *J. Neural Eng.* **19** 066045

View the [article online](#) for updates and enhancements.



You may also like

- [Recent advances in patterned photostimulation for optogenetics](#)
Emiliano Ronzitti, Cathie Ventalon, Marco Canepari et al.
- [Co-expressing fast channelrhodopsin with step-function opsin overcomes spike failure due to photocurrent desensitization in optogenetics: a theoretical study](#)
Himanshu Bansal, Gur Pyari and Sukhdev Roy
- [Optical cuff for optogenetic control of the peripheral nervous system](#)
Frédéric Michoud, Loïc Sottas, Liam E Browne et al.



PAPER

Learning in a closed-loop brain-machine interface with distributed optogenetic cortical feedback

Dorian Goueytes, Henri Lassagne, Daniel E Shulz, Valérie Ego-Stengel¹  and Luc Estebanez^{1,*} 

Université Paris-Saclay, CNRS, Institut de Neurosciences Paris-Saclay, 91400 Saclay, France

¹ These authors contributed equally.

* Author to whom any correspondence should be addressed.

E-mail: luc.estebanez@cnrs.fr**Keywords:** optogenetics, closed-loop, motor brain-machine interface, electrophysiology**Abstract**

Objective. Distributed microstimulations at the cortical surface can efficiently deliver feedback to a subject during the manipulation of a prosthesis through a brain-machine interface (BMI). Such feedback can convey vast amounts of information to the prosthesis user and may be key to obtain an accurate control and embodiment of the prosthesis. However, so far little is known of the physiological constraints on the decoding of such patterns. Here, we aimed to test a rotary optogenetic feedback that was designed to encode efficiently the 360° movements of the robotic actuators used in prosthetics. We sought to assess its use by mice that controlled a prosthesis joint through a closed-loop BMI. **Approach.** We tested the ability of mice to optimize the trajectory of a virtual prosthesis joint in order to solve a rewarded reaching task. They could control the speed of the joint by modulating the activity of individual neurons in the primary motor cortex. During the task, the patterned optogenetic stimulation projected on the primary somatosensory cortex continuously delivered information to the mouse about the position of the joint. **Main results.** We showed that mice are able to exploit the continuous, rotating cortical feedback in the active behaving context of the task. Mice achieved better control than in the absence of feedback by detecting reward opportunities more often, and also by moving the joint faster towards the reward angular zone, and by maintaining it longer in the reward zone. Mice controlling acceleration rather than speed of the joint failed to improve motor control. **Significance.** These findings suggest that in the context of a closed-loop BMI, distributed cortical feedback with optimized shapes and topology can be exploited to control movement. Our study has direct applications on the closed-loop control of rotary joints that are frequently encountered in robotic prostheses.

1. Introduction

Invasive motor brain-machine interfaces (BMIs) focus on establishing a stable translation from brain neuronal activity into motor commands (Chapin *et al* 1999, Carmena *et al* 2003, Collinger *et al* 2013, Wodlinger *et al* 2015). Most implementations rely on visual feedback to guide the prosthesis during the task. In particular, they lack somatosensory feedback like touch and proprioception. This feedback is however critical for movement accuracy, as shown by studies in humans in which local peripheral anesthesia blocking afferent tactile sensation reduced dexterity and impaired fine motor control of the hand

(Johansson and Westling 1984, Monzée *et al* 2003, Flesher *et al* 2021).

Implementing somatosensory-like feedback from a prosthesis back to the subject requires first to fit the prosthesis with touch and proprioceptive-like sensors (Roberts *et al* 2021), and then to relay this information to the central nervous system. In invasive closed-loop brain-machine interfaces, feedback stimulation generally targets the primary somatosensory cortex, where neuronal activation is integrated as touch inputs in the awake behaving rodent (O'Connor *et al* 2013, Sachidhanandam *et al* 2013, Prsa *et al* 2017) and primate (O'Doherty *et al* 2011) as well as in humans (Flesher *et al* 2021).

Strategies to provide behaviorally-relevant input using such cortical stimulation often rely on the intensity or frequency modulation of a stimulation targeting one spatially limited region of interest, which limits the amount of information that can be delivered (O'Doherty *et al* 2011, 2019, Prsa *et al* 2017). However, recent technical progress has made distributed neuronal activations possible, by using sophisticated multichannel electrical microstimulations (Dadarlat *et al* 2015, Weiss *et al* 2019, Fernández *et al* 2021, Flesher *et al* 2021) or by harnessing spatiotemporally patterned optogenetic stimulation of the cortex (Abbasi *et al* 2018, Ceballo *et al* 2019, Goueytes *et al* 2019, Lassagne *et al* 2022). Such distributed neuronal activation at the surface of the cortex can convey multiple information streams in parallel (Hartmann *et al* 2016), such as those arising from the multiple touch-like sensors (Roberts *et al* 2021) that are available in modern bidirectional prostheses (Johannes *et al* 2011, D'Anna *et al* 2019). Further, feedback spread across a large cortical area can be more robust and provides an opportunity to mimic physiological, distributed peripheral inputs by generating spatiotemporal patterns of activation that embrace the well-known topography of primary sensory areas, including the primary somatosensory cortex (Flesher *et al* 2016, 2021, Abbasi *et al* 2018), the primary visual cortex (Dobelle *et al* 1976, Dobelle 2000, Chen *et al* 2020) and the auditory cortex (Ceballo *et al* 2019).

This emerging capability to integrate distributed cortical feedback in a brain-machine interface (Pandarinath and Bensmaia 2022) raises multiple questions. One is that most robotic prostheses are fitted with rotary actuators that each drive one degree of freedom. The instantaneous angular position of these actuators is a critical information that should be channeled back to the subject. But such circular information cannot be conveyed unambiguously by modulating the activity in a single spot of the cortex. In earlier work (Lassagne *et al* 2022), we explored the use of a spatially distributed, continuous spatio-temporal pattern of photoactivation to convey this information in the form of a rotating bar projected on the surface of the somatosensory cortex of awake behaving mice. However, this previous study was a purely passive sensory task, while during physiological behavior, sensory integration cannot be dissociated from active motor control (Poulet and Petersen 2008).

Here, based on a recently developed closed-loop brain-machine interface (Abbasi *et al* 2018, Goueytes *et al* 2019) we asked if this feedback could be efficiently exploited by the mice beyond sensory processing, by helping to control the angular position of a simulated prosthesis. We found that the mice were able not only to detect the location of the Reward zone, but also to alter the dynamics of the rotary joint.

Notably, they learned to increase the speed of the movement towards the Reward zone while preserving the amount of time spent in it. This was not observed in trials where the feedback photostimulation was not activated.

2. Methods

We developed a neuroprosthetic bidirectional brain-machine interface in mice by combining electrophysiological recordings in M1 with patterned optogenetic stimulations in S1, using mice expressing channelrhodopsin in excitatory cortical neurons (see section 2, (Goueytes *et al* 2019)). Mice had to control a single rotary joint of an off-the-shelf prosthesis (Jaco 2, Kinova Robotics) that was simulated using the V-REP software (Rohmer *et al* 2013). The mice were trained to perform an exploratory sensorimotor task in this 360° angular space without boundaries, using as the sole feedback a dynamic patterned photostimulation projected on the surface of the barrel cortex (figure 1(a)).

2.1. Surgical preparation

We report data from 13 Emx1-Cre; Ai27 mice (both male and female) expressing channelrhodopsin in excitatory neurons across the cortex (Madisen *et al* 2012). All animals were implanted via two successive surgeries under Isoflurane anesthesia (1%–4% Isoflurane mixed in 100% air), combined with local Lidocaine analgesia (<7 mg kg⁻¹) and anti-inflammatory drug Meloxicam (1–8 mg kg⁻¹). During the first surgery, the cranial skin was resected, the skull was exposed, and after careful removal of residual soft tissue and complete air drying, a 5 mm diameter craniotomy was drilled over the 'barrel' whisker area of primary somatosensory cortex (S1, −1.5 mm P, −3.3 mm L relative to Bregma). At the same time, we labelled the position of the whisker area of the primary motor cortex (M1, +1.5 mm P, −0.6 mm L relative to Bregma).

A 5 mm diameter glass window was then positioned in direct contact with the dura mater, and sealed with cyanoacrylate glue (Loctite 'Super Glue Power Gel') to the skull, thereby resulting in a chronic, stable optical access to the barrel cortex. The remaining exposed skull was coated with a layer of liquid cyanoacrylate glue. A head-fixation bar was also glued on the skull, contralateral to the optical window side. Low reflection, black dental cement (Ortho Jet, Lang dental, USA) was applied on the skull to protect it and anchor the bar and the window. After a week of recovery, we mapped the barrel cortex through the optical window using intrinsic imaging (Lassagne *et al* 2022). In particular, we identified the location of the barrel corresponding to the C2 whisker. In a second surgery, using a similar preparation as the first one, we went back to the previously identified location of whisker

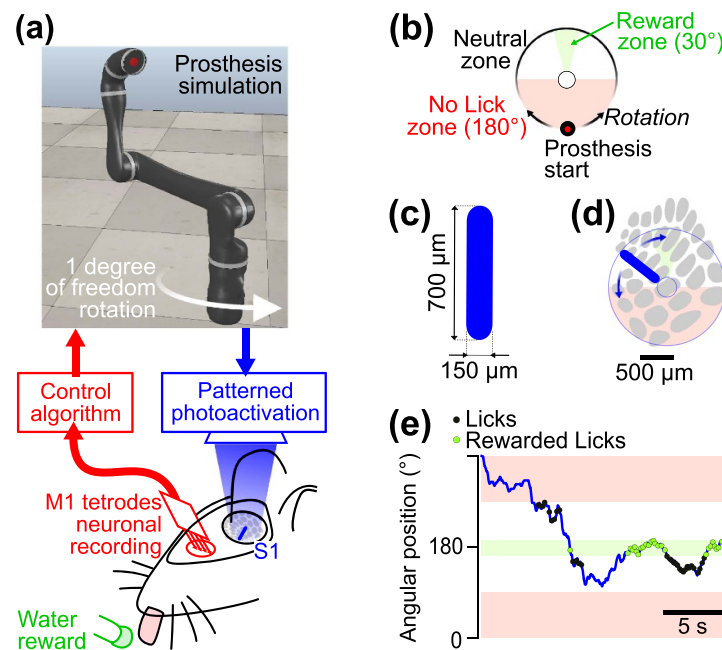


Figure 1. Closed-loop control of a virtual prosthesis with patterned optogenetic somatosensory feedback (a) Schematic representation of the closed-loop setup, including a snapshot of the prosthesis simulation in V-REP. The most proximal joint of the prosthesis is controlled by neuronal activity recorded in M1. The angular position of the joint is fed back to the mouse through spatio-temporally patterned photoactivation of S1. (b) The motor space explored by the prosthesis during the task was divided in distinct functional zones. Licks occurring when the prosthesis was in the Reward zone triggered water rewards. Licks occurring when the prosthesis was in the No lick zone aborted the trial. The start position of the prosthesis was always located at 0° . (c) Shape of the photostimulation pattern projected on the cortex. (d) Location of the targeted cortical surface with respect to the barrels of the whisker primary somatosensory cortex. The photostimulation bar rotates in synchrony with the proximal joint in prosthesis space in (b). The start position of the photostimulation corresponded to the most posterior position of the stimuli in brain coordinates. (e) Example trajectory of the rotating prosthesis, and associated licks (black dots) and rewarded licks (green dots), during the 20 s of one uninterrupted trial.

M1; we drilled and opened the skull, removed the dura mater locally, and implanted in a chronic fashion (Okun *et al* 2016) an extracellular recording electrode (32 channel silicon probe, A1x32Poly35mm25s 177A32, Neuronexus, USA). We descended the tip $800\ \mu\text{m}$ below the surface of the cortex, thereby targeting neurons from Layer five of M1.

2.2. Neuronal electrophysiological recordings

After electrode implantation, we monitored electrophysiological signals daily to control the stability of recording. After about one week, we started to acquire neuronal recordings. We manually isolated large amplitude units based on waveform shape and cluster separation (Blackrock microsystems, USA). All neuronal signals were sampled at 30 kHz and the records were stored. A detailed description of the quality of the signals and of their stability across sessions is available in (Abbasi *et al* 2019), where the very same methods were used. Given the duration of the experiments described here, we estimated that a single neuron picked arbitrarily at the start of the training may not be recorded stably across the whole training period. This was the motivation behind the choice of training a set of 6–8 master neurons during the experiment, so that the recording of a subset of

these neurons would always be stable while training continued.

2.3. Prosthetic simulation

A commercial Jaco2 (Kinova robotics) prosthesis was simulated using the robotic simulation software V-REP (Rohmer *et al* 2013). This simulation was based on a CAD model provided by the manufacturer, and cross-validated during the loan of a physical Jaco2 unit.

To connect the virtual robotic arm to our brain-machine interface (figure 1(a)), we developed a custom V-REP plugin. Thanks to this software bridge, the speed and direction commands for the proximal joint of the virtual prosthesis was updated approximately every 12 ms, based on the neuronal activity readout. In return, the current angular position of the joint was fed back to the brain-machine interface and was used to update the angular position of the optogenetic S1 stimulation (Goueytes *et al* 2019).

We measured an end-to-end latency of the combined BMI software and robotic arm system of 36 ms (standard deviation 4 ms).

2.4. Control algorithm

At the beginning of the first training session, among the neurons that were manually spike sorted, two

arbitrary groups of 3–4 Master neurons were selected using an automatic algorithm that minimized the difference in population firing rate between the two groups.

For 7 mice, speed control of the joint was implemented by linearly translating the population firing rate of each group into a speed command. To compute the speed command in one group, the activity of all neurons in that group was summed together and sampled every 10 ms, followed by convolution with a 100 ms box kernel. The speed command resulting from the first (resp. second) group was assigned to the clockwise (resp. counterclockwise) direction. The difference between the two speeds was directly relayed as a speed command to the proximal joint of the V-REP model of the prosthesis, leading it to rotate in its 360° circular space (figure 1(b)), without any limit to the extent of the circular rotations. Note that in speed control mode, the Kinova arm acceleration was set to a maximum of approximately 150° s^{-2} .

To calibrate the linear relationship between the smoothed group firing rate and the corresponding speed command, we computed the average activity of the two groups in a 5 min ‘baseline’ waiting period at the beginning of each training session, and the firing rate of each group was divided by this baseline value. This normalization ensured that the velocity distribution was centered around 0° s^{-1} for each session, despite day-to-day variability in individual firing rates. Finally, we scaled the resulting speed by a constant selected during the first session, defined so that the average absolute baseline joint speed would be $\sim 30^\circ \text{ s}^{-1}$. The resulting distributions of angular speeds in the first and last sessions are shown in figure 5(c).

In the last part of our study, we switched from speed to acceleration control on a separate group of 6 mice. We applied the exact same computation of neuronal activity, but the final conversion was into an acceleration command rather than a speed command. We adjusted the linear factor in the conversion so that the observed distributions of position and speed would be as close as possible to those observed in the speed control condition (figures 5(b) and (c)).

2.5. Optogenetic stimulation patterns

We designed optogenetic feedback patterns that took the form of a 700 μm long and 150 μm wide bar centered on the C2 barrel (figures 1(c) and (d)), based on the results of the intrinsic imaging session. The photostimulation was generated with a Digital Light Processing module (DLP, Vialux V-7001, Germany) containing a 1024×768 pixels Texas Instruments micro-mirror chip coupled with a high-power 462 nm blue LED. During training, the rotation of the bar over the somatosensory cortex followed at short latency the position of the arm. The C2 barrel was excluded from the stimulation in order to avoid its overstimulation. We have previously provided a full

description of the illumination optics and validation experiments (Abbasi *et al* 2018).

2.6. Task and behavioral training

Once the mice were implanted with the electrodes and the BMI appeared functional, they were water regulated in order to enable operant conditioning based on water reward (figure 1(a)). Their weight was monitored and maintained at 80% of their baseline (measured prior to the start of the water deprivation) by supplementing water if needed. Simultaneous to the start of the water regulation, the mice were habituated to head-fixation and trained to obtain rewards by licking a reward port placed in front of them (1–2 sessions). After habituation, training was performed on a daily basis without interruption for the whole duration of the training.

Each training session corresponded to approximately 10 min of online spike sorting, 5 min of baseline recording, 40 min of behavioral training and 5 min of post-training recording, for a total of one hour per day. The sessions were divided into trials lasting at most 20 s. At the beginning of each trial, the rotary joint position was initiated at 0° . The mice could freely displace the joint across a circular space in both directions by modulating the activity of the neurons in the two Master groups (figure 1(b)). The mice were rewarded only if they licked while the joint was located in a 30° zone centered on the 180° position.

In order to discourage strategies based on continuous licking independently from the joint position, we aborted any trial where licks occurred while the arm was in a 180° zone around the starting position (the ‘No lick zone’). This was followed by a 2 s timeout. The intertrial interval lasted for a minimum of 5 s and a maximum of 7 s in case of a timeout following a lick in the No lick zone. To maintain interest in the task over the full session, we averted long series of rewards by interrupting trials after more than 4 s continuously in the Reward zone. The optogenetic feedback was turned on at the onset of each trial, and switched off at its offset. An example trial is shown in figure 1(e).

In order to specifically test the contribution of the feedback to the mouse behavior, in four animals, at all phases of training, we included 20% of trials interleaved randomly where no optogenetic feedback was provided.

Training was interrupted when the number of neurons recorded in M1 became too low for the task requirement (less than 6), or when optical access to S1 through the glass window was degraded (opaque, blurry window).

3. Results

We trained 7 mice to obtain rewards by manipulating the speed of a virtual rotating joint through the

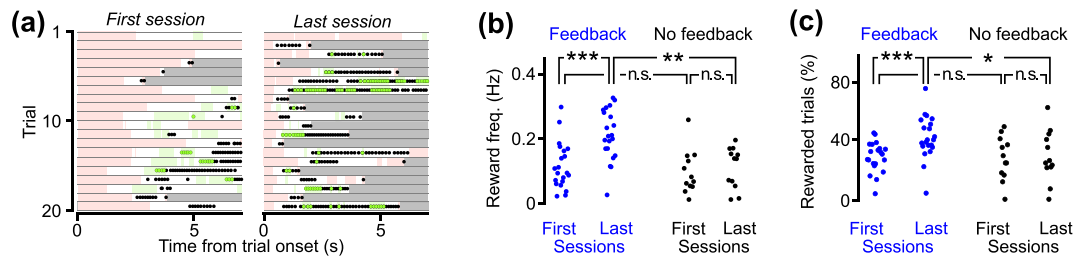


Figure 2. Feedback enables increased task performance after training. (a) Temporal sequence of spatial zones explored by the prosthesis during the first 20 trials of the first session (left) and of the last session (right) for which the joint reached at least once the Neutral zone. Each line represents the time course of a trial. Pink: No lick zone, in which licks interrupt the trial. Green: Reward zone. White: Neutral zone. Gray: the trial has already stopped. Black dots: licks. Green dots: rewarded licks. Note that licks take place in bursts, defined as lick sequences during which inter-lick interval is at most 300 ms. (b) Reward frequency averaged across each session, plotted for the first three and the last three training sessions of each mouse. Blue: Optogenetic feedback (7 mice, 21 sessions). Black: control, no feedback (subset of 4 mice, 12 sessions). (c) Same as b, for the proportion of rewarded trials, calculated as the percentage of trials where at least one lick was rewarded. Trials where the joint never went past the 'No lick' zone were excluded. All statistical comparisons are obtained from Mann-Whitney tests. *: $p < 0.05$; **: $p < 0.01$; ***: $p < 0.001$. Detailed statistics for each test, including number of samples and exact p value, are provided in the main text.

control of the neuronal activity of motor cortex neurons. Mice received feedback about the angular position of the joint by optogenetic stimulation in the somatosensory cortex (see section 2, figure 1). As a control, in 4 of the 7 mice no optogenetic feedback was available during 20% of trials. Mice were trained daily for at least 17 consecutive sessions (average 17.8 sessions). Training was interrupted when recording quality degraded or technical difficulties arose with the recordings. The last training session was systematically excluded from further analysis.

3.1. Mice learn to improve their performance in the feedback condition

Across training, the mice learned to increase the number of rewards they collected in the feedback condition. This can be observed on the example of figure 2(a) showing the motor exploration and licking behavior during the first 20 trials of the first and last session for one mouse. At the population level, the reward frequency was significantly larger in the last three training sessions compared to the first three sessions, when feedback was available (figure 2(b) left, Mann-Whitney $p = 0.00024$, $N = 21$ sessions from 7 mice, null hypothesis: 'there is no increase in reward frequency with learning'), but not in the no-feedback condition (figure 2(b) right, $p = 0.33$, $N = 12$ sessions from 4 mice). At the end of training, the mice performance in trials with feedback was also significantly higher than in trials when no feedback was provided (figure 2(b), $p = 0.0016$; feedback: $N = 21$; no-feedback: $N = 12$, null hypothesis: 'there is no difference in the reward frequency between the feedback and no-feedback condition'), in contrast to the start of the training ($p = 0.38$; feedback: $N = 21$; no-feedback: $N = 12$).

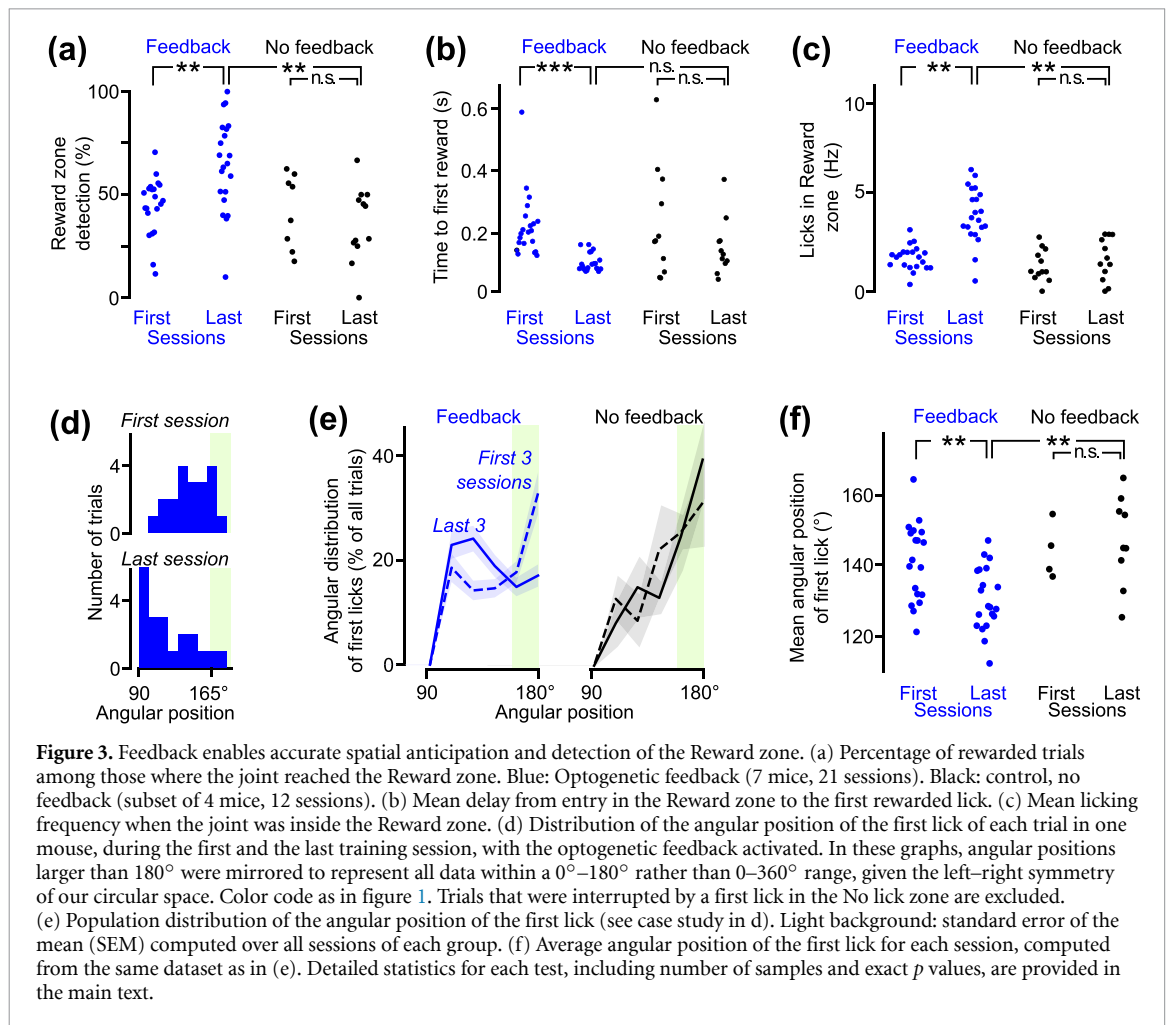
The role of optogenetic feedback in enabling learning was also clear when computing the

proportion of trials that were rewarded. Trials where optogenetic feedback was available resulted in more rewarded trials in the last three training sessions compared to the first three sessions (figure 2(c) left, Mann-Whitney $p = 0.00082$, $N = 21$ sessions), while this was not the case in the no-feedback condition (figure 2(c) right, $p = 0.93$, $N = 12$ sessions). Finally, after training, trials with optogenetic feedback were significantly more rewarded than no-feedback trials (figure 2(c), $p = 0.041$; feedback: $N = 21$; no feedback: $N = 12$). This was not the case at the start of the training ($p = 0.96$; feedback: $N = 21$; no feedback: $N = 12$). Note that in this analysis of percentages of rewarded trials, only trials reaching the No lick border were included.

3.2. Mice learn to detect and anticipate entry in the Reward zone

To better characterize the mice ability to track the joint position and lick appropriately, we first measured the proportion of rewarded trials among those where the joint entered the Reward zone. We found that in the optogenetic feedback condition, the proportion of detected entries in the Reward zone increased significantly between the first and last three training sessions (figure 3(a) left, Mann-Whitney $p = 0.0030$, $N = 21$ sessions), but not in the no-feedback condition (figure 3(a) right, $p = 0.52$, $N = 12$ sessions). As a result, at the end of training, the proportion of rewardable trials was significantly larger with optogenetic feedback than without (figure 3(a), $p = 0.0011$; feedback: $N = 21$; no feedback: $N = 12$).

We then looked at the delay from the entry of the joint in the Reward zone to the first rewarded lick. We found that with optogenetic feedback, the mice learned to lick faster following entry in the Reward zone (figure 3(b) left, Mann-Whitney $p = 6.3 \times 10^{-7}$,

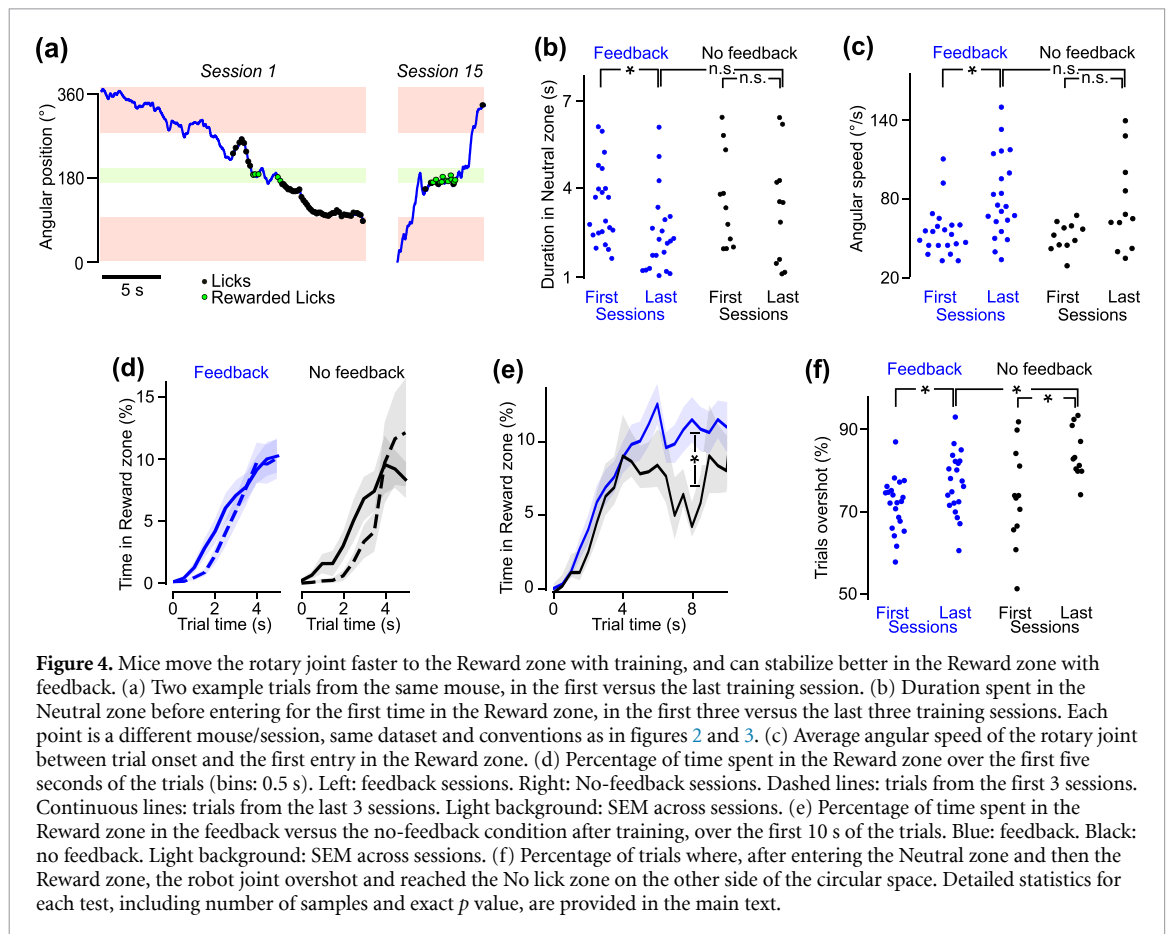


$N = 21$ sessions). This was not the case without optogenetic feedback (figure 3(b) right, $p = 0.32$, $N = 12$ sessions). Note that after training, the difference between the delay to first lick measured in the feedback versus no-feedback conditions was not quite significant (figure 3(b), $p = 0.056$; feedback: $N = 21$; no feedback: $N = 12$).

Finally, we found that the mice learned to collect rewards at a significantly higher frequency once inside the Reward zone (figure 3(c) left, Mann-Whitney $p = 3.3 \times 10^{-6}$, $N = 21$ sessions). This increase was not visible in the absence of feedback (figure 3(c) right, $p = 0.35$, $N = 12$ sessions), and after training, the frequency of licking in the reward zone was significantly higher with feedback compared to the no-feedback condition (figure 3(c), $p = 1.1 \times 10^{-4}$; feedback: $N = 21$; no feedback: $N = 12$). Overall, these results suggest that the mice did manage to exploit the optogenetic feedback to track the joint position and obtain rewards.

To better understand how the mice took advantage of the spatial organization of the optogenetic feedback, we focused on the licking patterns that occurred around the entry in the Reward zone, and analyzed the corresponding spatial position of the joint. In this analysis, we focused on trials that led to

rewards, because we aimed to characterize the behavioral sequences that are successful. Note that as a consequence, none of the trials that started (and ended) with a lick in the ‘No Lick zone’ were included in the analysis. We noticed that in the feedback condition, the onset of licking bursts took place for increasingly early angles after the transition between the No lick and the Neutral zones (example first and last sessions for one mouse in figure 3(d)). This shift was visible across the population on the histogram of the mean angular position of the first lick after trial onset (figure 3(e)). Consistently, the average angular position of the first lick significantly diminished between the first three and last three training sessions in the feedback condition (figure 3(f) left, Mann-Whitney $p = 0.0021$, $N = 21$ sessions), but not in the no-feedback condition (figure 3(f) right, $p = 0.71$, $N = 12$ sessions), and at the end of training, the average first lick angular position was significantly lower in the feedback condition than in the no-feedback condition (figure 3(f), $p = 0.004$, feedback: $N = 21$; no feedback: $N = 12$). This anticipation of licking towards the border of the No lick zone in the feedback condition did not result in an increase in premature licks in the No lick zone, that would have canceled the trial. Instead, there was a



significant reduction in aborted trials during learning with feedback (on average from 76% down to 64% of all initiated trials, Mann-Whitney $p = 0.42$, $N = 21$ sessions).

We hypothesized that this anticipation strategy may be driven by the mice tendency to perform long bouts of repeated licks ('bursts', where the interval between licks was of less than 300 ms) rather than individual licks. Indeed, generating a long lick burst before entering the Reward zone may be an efficient way to ensure that multiple licks land inside the Reward zone. Consistent with this hypothesis, we found that the mice generated increasingly long bursts of licks when they exited for the first time the No lick zone in a trial (from 6.8 to 16.3 licks per burst, first three vs. last three sessions, Mann-Whitney $p = 6.0 \times 10^{-6}$, $N = 21$ sessions). These first bursts in the trials were increasingly long enough to include licks that occurred while the robotic joint was located in the Reward zone, and therefore the proportion of trials where the first burst included rewarded licks increased on average from 6% to 15% during training (Mann-Whitney $p = 0.0013$, $N = 21$ sessions).

Overall, the mice learned that they could start licking as soon as the prosthesis joint entered the Neutral zone, and they took full advantage of this to initiate long bursts of licking that enabled them to collect multiple rewards.

3.3. Mice learn to accelerate movements of the prosthesis to the Reward zone, and stabilize it using feedback

So far, our analysis showed that during this task, the continuous, rotative bar-like optogenetic feedback provided sufficient information for the mice to increase their reward rate with training, by generating timely licking bursts. Beyond the contribution of feedback processing to performance, we next asked if the mice were able to actively modulate the rotation of the joint towards the Reward zone. To quantify motor control, we first focused on the beginning of the trial, before the first entry in the Reward zone. We found that the mice learned to spend less time in the Neutral zone as they moved the joint towards the Reward zone (case studies in figure 4(a)). This reduction was significant when feedback was available (figure 4(b) left, Mann-Whitney $p = 0.013$, $N = 21$ sessions) but non-significant without feedback (figure 4(b) right, $p = 0.65$, $N = 12$ sessions). Note that after training, we found no significant difference between the feedback and no-feedback conditions (figure 4(b), $p = 0.25$, feedback: $N = 21$; no feedback: $N = 12$).

This faster movement towards the Reward zone stemmed from an increased average angular speed of the joint before entry in the Reward zone. We observed this increased speed in the feedback condition (computed over 50 ms bins, figure 4(c) left, Mann-Whitney $p = 0.0015$, $N = 21$ sessions) but

not in the no-feedback condition (figure 4(c) right, $p = 0.088$, $N = 12$ sessions). Note that after training, the difference in speed measured in the feedback versus no-feedback conditions was not significant (figure 4(c), $p = 0.055$; feedback: $N = 21$; no feedback: $N = 12$).

These changes in joint movements after learning resulted in longer time spent in the Reward zone in the first seconds of the trials, regardless of the availability of feedback (figure 4(d)). However, the presence of feedback did impact the rotary joint motor control later in the trials. When we looked at the time course up to 10 s in the trial, we noticed that the percentage of time in the Reward zone increased and then, after 5 s, stabilized above 10% in the feedback condition, whereas it dropped back below 5% in the no-feedback condition (figure 4(e)). Note however that this difference was only significant in one 500 ms interval, 8 s after onset (Mann-Whitney $p = 0.0099$, feedback: $N = 21$ sessions; no feedback: $N = 12$ sessions). Given that we tested for significance the five intervals where the SEM of the two conditions did not overlap, the Bonferroni correction led to a significance threshold of 0.01 that was just met by the p -value of the test.

The difference in average time in the Reward zone led us to hypothesize that in the feedback trials, the mice were able to exploit the photostimulation to stabilize the joint in or close to the Reward zone, and thus increase the percentage of time spent there. By contrast, in the absence of feedback, the mice could not adjust the trajectory of the joint as well, possibly not decelerating early enough because of the lack of feedback. To test this hypothesis, we measured the proportion of trials where, after entering the Neutral zone from one side of the circular space, the rotary joint would go on, overshoot the Reward and Neutral zones, and exit the Neutral zone on the other side. We found that both with and without feedback, the proportion of overshoot trials increased significantly after training (figure 4(f); feedback: Mann-Whitney $p = 0.032$, $N = 21$ sessions; no-feedback: $p = 0.012$, $N = 12$ sessions). This was probably due to the faster joint movements, which led to many trajectories leaving the Reward zone fast. However, we found that this proportion was significantly smaller when the feedback photostimulation was available (figure 4(f), $p = 0.010$; feedback: $N = 21$; no feedback: $N = 12$), so that the mouse managed more often to stabilize the joint in the Reward zone or in the Neutral zone.

Overall, these observations suggest that mice learned to control the rotary joint movement. Better control was achieved with optogenetic feedback of the joint angular position, by allowing trajectory adjustments during the trial.

3.4. Motor control of the rotary joint depends on the controlled variable

The fact that the mice learned to move the rotary joint faster, and moreover that they could adjust

dynamically their motor control of the joint while the trials with feedback were ongoing, indicated that a motor control algorithm based on an angular speed command was successful. This prompted us to ask whether other motor control algorithms could be used. We hypothesized that controlling the angular acceleration of a rotary joint may be more straightforward, because it is directly related to muscle torque and thus possibly to neural activity. To test this, we trained 6 additional mice in the same closed-loop setting, but with an acceleration neural controller (example trajectory in figure 5(a)). Like in the speed condition, control of the rotary joint was achieved by the modulation of the firing rate of two antagonist groups of 3–4 neurons each (see Methods).

The average distributions of the position and speed of the rotary joint in the two control algorithm conditions were in the same ranges (figures 5(b) and (c)). Importantly, during the first training sessions, reward opportunities were as frequent in the two conditions. Mice spent 4.3% of the total time in the Reward zone in the speed control, versus 4.0% of the time in the acceleration control condition (not significantly different, Mann-Whitney $p = 1.0$; speed control: $N = 21$ sessions from 7 mice; acceleration control: $N = 18$ sessions from 6 mice). In addition, on average the joint moved with comparable speed through the circular space (47° s^{-1} vs 34° s^{-1} , not significantly different, Mann-Whitney $p = 0.44$). These results suggest that the photostimulation patterns conveying information about the joint angular position activated the cortex in similar ways.

The 6 mice that were trained with the acceleration controller received significantly more rewards in the last sessions of training compared to the first sessions, from a reward frequency of 0.066 rewards per second up to 0.17 (figure 5(d), Mann-Whitney $p = 0.0054$, $N = 18$ sessions). The mice also learned to lick for reward more often when the prosthesis trajectory reached the Reward zone (first vs. last sessions, figure 5(e), Mann-Whitney $p = 0.0012$, $N = 18$ sessions from 6 mice). In addition, like in the speed-controller condition, the mice anticipated the entry of the prosthesis into the Reward zone, and started licking before it happened (figure 5(f), Mann-Whitney $p = 0.007$, $N = 18$). These results suggest that these mice learned to exploit the feedback information to lick at appropriate times. However, we failed to find any sign of active motor control or of motor learning. In particular, none of the changes in joint dynamics that we observed in the speed control condition were present in the acceleration control condition. For example, the average speed of the controller (figure 5(g), Mann-Whitney $p = 0.42$, $N = 18$), the delay to enter the Reward zone, and the time spent in the Reward zone (figure 5(h)) were not modified through learning with the acceleration controller. We conclude from these data that the mice were unable to control the prosthesis movements

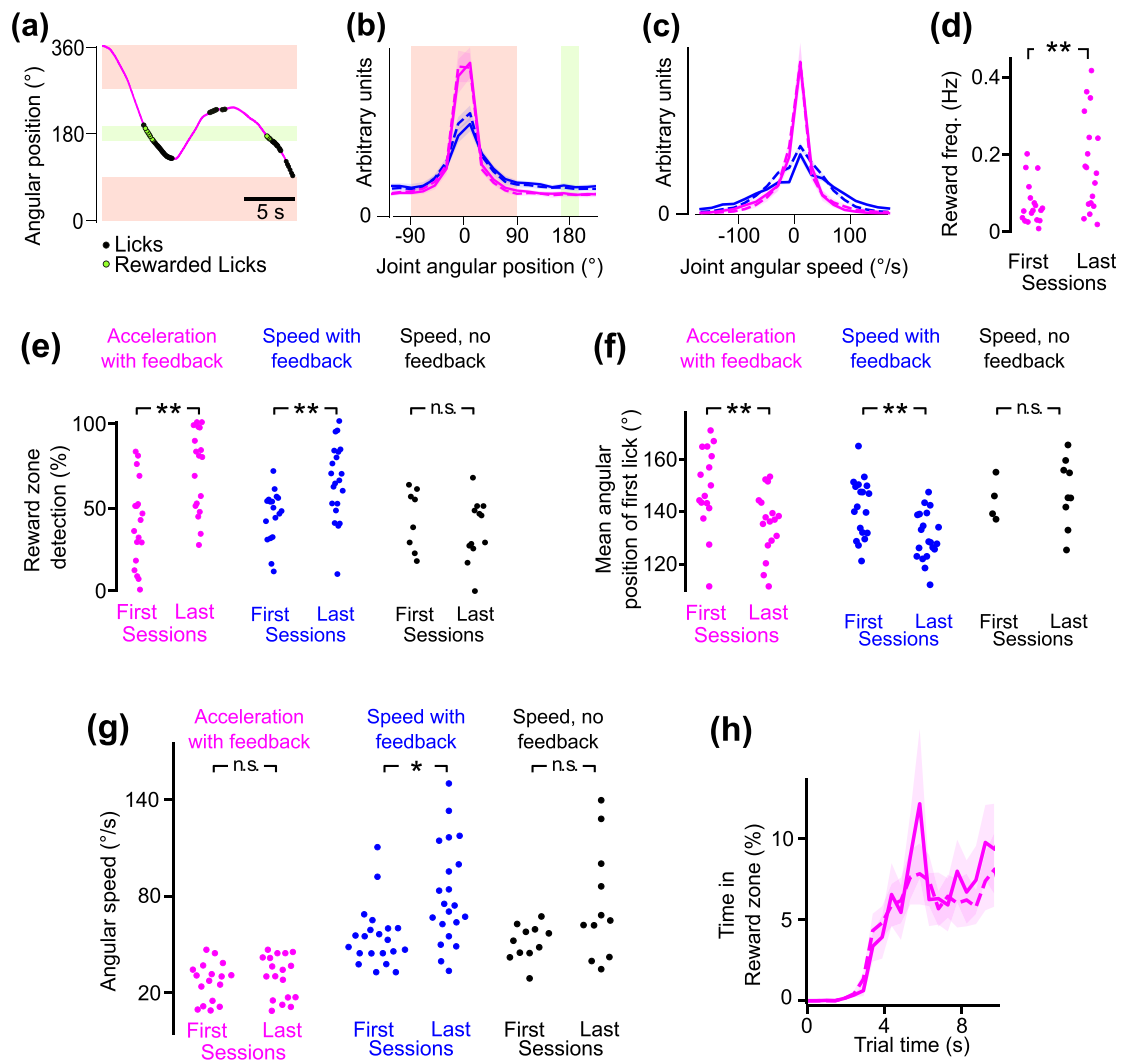


Figure 5. Mice fail to control the prosthesis movements using an acceleration-based joint controller. (a) Example trajectory of the prosthesis in the angular space, in a mouse trained with a controller that translated M1 firing rates into acceleration, instead of the speed of the rotary joint. (b) Distributions of the angular position of the rotary prosthesis joint in mice trained with the acceleration-based joint controller (purple, 6 mice) versus the speed-based controller (blue, 7 mice). Dashed lines: first 3 sessions. Continuous lines: last 3 sessions. The session start position is always 0° . Distributions are averaged across sessions/mice. Light background: standard error of the mean. (c) Distributions of the angular speed of the rotary joint for the same sessions as in (b). (d) Reward frequency averaged across each session, plotted for the first three and the last three training sessions of each mouse for the acceleration-based controller. (e) Percentage of trials where the joint entered the Reward zone for which the mouse obtained a reward, computed across each session/mouse, for the first three versus last three training sessions. The three tested conditions are shown: Acceleration control, always with optogenetic feedback; speed control, with feedback, and speed control, without feedback. The speed data is the same as figure 3(a). (f) Average angular position of the first lick of rewarded bursts for the same sessions as in (e). The speed data is the same as figure 3(f). (g) Average instantaneous angular speed of the rotary joint between trial onset and the first entry in the Reward zone for the same sessions as in (e). The speed data is the same as figure 4(c). (h) Percentage of time spent in the Reward zone over the first ten seconds of the acceleration trials (bins: 0.5 s). Dashed lines: trials from the first 3 sessions. Continuous lines: trials from the last 3 sessions. Detailed statistics, including number of samples and exact p values, are provided in the main text.

through the acceleration-based controller, while they could still benefit from the feedback about its angular position.

4. Discussion

Using a closed-loop brain-machine interface controlling a prosthesis simulation in the mouse model, we have shown that a mesoscopic scale feedback with a circular topography and rotating dynamics can be exploited to optimize the motor control of a robotic

joint. Specifically, the mice learned to improve both the rotation of the joint and the detection of the target location in order to obtain more rewards.

4.1. Integration of the optogenetic stimulation in open versus closed-loop experiments

Our experiments show that the guidance of licking based on the decoding of a mesoscopic cortical feedback can be as successful during an active, motor brain-machine interface task, as during a purely passive detection task (Lassagne *et al* 2022). We

therefore conclude that the sensory feedback part of a closed-loop brain-machine interface can be efficiently designed and tested independently from the motor part of the loop. This is consistent with the recent successful development of an invasive closed-loop neuroprosthesis (Flesher *et al* 2021), that was based on the independent validation of the microstimulations in the primary somatosensory cortex of humans (Flesher *et al* 2016) and primates (Kim *et al* 2015).

4.2. Anticipated licking

We found that throughout training, the mice learned to initiate their licking bursts increasingly early, and ultimately as soon as the photostimulation entered the Neutral zone, where licks were not rewarded but did not interrupt the trials (figure 3). It was also mainly in the Neutral zone that the mice increased the speed of the rotary joint as it headed towards the Reward zone. Together, these findings suggest that the mice motivation to obtain rewards was high enough to initiate licking as soon as possible without canceling the trial. At the same time, maintaining uninterrupted licking bursts was costly enough to lead the mice to increase the speed of the joint as it headed towards the Reward zone.

4.3. Limited motor learning

Overall, the two changes in motor strategy during learning with the speed-based motor control were an increased speed of the rotary joint at the beginning of the trials, followed by later adjustments to preserve the time spent in the Reward zone by limiting overshooting (figure 4(f)). We hypothesize that the limited scale of these changes was due to the design of the task, since in the naive state before training, the mice already spent approximately 6% of the trial time in the Reward zone (see Results section 3.4, and figures 4(d) and (e) for a time course comparison). In future experiments, it would be interesting to reduce the size of the Reward zone, in order to encourage more active stabilization of the joint in the Reward zone.

4.4. Comparison of speed versus acceleration-based controllers

The experiments based on controlling acceleration rather than speed highlighted the key impact of controller design on closed-loop performance and motor control (figures 5(g) and (h)). We are not aware of previous works describing BMIs based on acceleration. We hypothesize that the relative inefficiency of the acceleration-based controller may be due to the challenge of connecting the acceleration values to the position feedback, given that there are no less than two steps of temporal integration between acceleration and position, versus only one in the case of the speed controller. Nonetheless, these experiments confirmed that mice can take advantage of the sensory

feedback regardless of their ability to control the actuator (figures 5(e) and (f)).

4.5. Related works

To our knowledge, this is the first demonstration of a motor BMI that includes a distributed, dynamical cortical feedback that takes into account the mechanical constraints of a joint. Here, we aimed at optimizing the feedback based on a robotic implementation of a joint. We first tested the perception of cortical stimulation patterns in a passive detection task (Lassagne *et al* 2022). We specifically designed a 360° rotating pattern to encode the angle of the joint, similar to a proprioceptive signal, while still abiding to the continuity of the representations that can be found in the barrel cortex that we targeted. Our experimental results suggest that a similar approach may address the challenge of proprioceptive-like feedback in human neuroprosthetics (Delhaye *et al* 2018).

In our work, we chose to implement distributed optogenetics in order to write feedback information directly in the cortex. This approach has been used before in open-loop experiments in order to explore the functional properties of primary sensory cortices (Ceballo *et al* 2018, Lassagne *et al* 2022). In a BMI task, it was pioneered by (Prsa *et al* 2017) in the rodent. Translating it to the non-human primates and to humans, poses a specific set of challenges (Shen *et al* 2020). Therefore, so far, distributed stimulations of primary sensory cortex in primates and humans have been achieved through lower-resolution, invasive arrays of microelectrodes (Dadarlat *et al* 2015, Kim *et al* 2015, Flesher *et al* 2016, 2021).

Focusing more specifically on the control and behavioral paradigm, we can relate our study to a line of work initiated by Carmena and collaborators (Koralek *et al* 2012, Clancy *et al* 2014). These experiments are based on continuous feedback, in that case in auditory space, and on the assumption that neuronal plasticity enables BMI learning. In addition, similar to our work, continuous control of a cursor was achieved by rodents through the modulation of the difference between the firing rate of two ensembles of M1 neurons.

However, one key difference with our work is that the neuronal activity, motor control and feedback spaces were linearly related. The firing rate of neurons controlled directly the position of the cursor from a minimum to a maximum position, and feedback was provided in the form of a continuous sound with a pitch that varied also linearly with the cursor position.

In contrast, in our work the cursor space was circular, and the cursor could rotate without boundaries, as it was controlled by modulating its speed or its acceleration.

It appears that motor learning was stronger and faster in those studies (Koralek *et al* 2012, Clancy *et al* 2014) than in our work. As we hypothesized above, this may be mainly due to the fact that in these

studies, both the feedback and control were tied to the same variable (position). In contrast, in our study the feedback was tied to position in a more complex, circular space, while control was related to its first or second derivative (speed/acceleration). This distance between the control and feedback variables may have made learning and control more difficult in our setting.

5. Conclusion

Our findings suggest that using patterned cortical feedback with a spatio-temporal structure relevant to physical constraints is an efficient strategy to provide critical information about the position of a prosthesis, and support its active control. Here we have tested this strategy to encode the angular position of a single rotary joint. It could be extended to explore the simultaneous encoding of the angular position of multiple joints, as well as the addition of tactile-like feedback of strategic points on the prosthesis surface. Future experiments will be needed to probe the ability of mice to integrate such multiple-dimensional feedbacks to actively control a full prosthesis.

Data availability statement

The data that support the findings of this study are available upon request from the authors.

Acknowledgments

We thank Aurélie Daret for help with experiments and lab managing. We thank Dr Maria Makarov at CentraleSupélec for support regarding the robot modeling and control. We thank the robotic company Sysaxes (France) for the loan of a Kinova Jaco2 unit. We thank the following funding sources: ANR Neurowhisk ANR-14-CE24-0019; ANR Mesobrain ANR-20-CE37-0013; ANR Motorsense ANR-21-CE37-0012; FRM DEQ20170336761; iCODE and IDEX Paris-Saclay ANR-11-IDEX-0003-02; FRC AAP2018; CNRS 80 Prime 2020, and Fondation Dassault Systèmes.

Conflict of interest

The authors declare no competing interests.

Ethics approval and consent to participate

All animal experiments were performed according to European and French law as well as CNRS guidelines and were approved by the French ministry for research (ethical committee 59, authorization 858-2015060516116339v5).

Authorship contribution statement

D E S, V E and L E initiated and supervised the project. D G, D E S, V E and L E designed the experiments. D G performed the experiments. L E, D G and H L analyzed the data. L E wrote the paper with inputs from all authors.

ORCID iDs

Valérie Ego-Stengel  <https://orcid.org/0000-0002-9099-9051>

Luc Estebanez  <https://orcid.org/0000-0001-6253-7637>

References

- Abbasi A, Estebanez L, Goueytes D, Lassagne H, Shulz D E and Ego-Stengel V 2019 Cortical closed-loop brain-machine interface requires biomimetic sensory feedback *bioRxiv Preprint* (<https://doi.org/10.1101/2019.12.12.873794>) (posted online 14 July 2020, accessed September 2022)
- Abbasi A, Goueytes D, Shulz D E, Ego-Stengel V and Estebanez L 2018 A fast intracortical brain-machine interface with patterned optogenetic feedback *J. Neural Eng.* **15** 046011
- Carmena J M, Lebedev M A, Crist R E, O'Doherty J E, Santucci D M, Dimitrov D F, Patil P G, Henriquez C S and Nicolelis M A L 2003 Learning to control a brain-machine interface for reaching and grasping by primates *PLoS Biol.* **1** e42
- Ceballo S, Bourg J, Kempf A, Piwkowska Z, Daret A, Deneux T, Rumpel S and Bathellier B 2018 Cortical recruitment determines learning dynamics and strategy *bioRxiv Preprint* (available at: www.nature.com/articles/s41467-019-09450-0)
- Ceballo S, Piwkowska Z, Bourg J, Daret A and Bathellier B 2019 Targeted cortical manipulation of auditory perception *Neuron* **104** 1168–79.e5
- Chapin J K, Moxon K A, Markowitz R S and Nicolelis M A L 1999 Real-time control of a robot arm using simultaneously recorded neurons in the motor cortex *Nat. Neurosci.* **2** 664–70
- Chen X, Wang F, Fernandez E and Roelfsema P R 2020 Shape perception via a high-channel-count neuroprosthesis in monkey visual cortex *Science* **370** 1191–6
- Clancy K B, Koralek A C, Costa R M, Feldman D E and Carmena J M 2014 Volitional modulation of optically recorded calcium signals during neuroprosthetic learning *Nat. Neurosci.* **17** 807–9
- Collinger J L, Wodlinger B, Downey J E, Wang W, Tyler-Kabara E C, Weber D J, McMorland A J, Velliste M, Boninger M L and Schwartz A B 2013 High-performance neuroprosthetic control by an individual with tetraplegia *Lancet* **381** 557–64
- D'Anna E, Valle G, Mazzoni A, Strauss I, Iberite F, Patton J, Petrini F M, Raspopovic S, Granata G and Di Iorio R 2019 A closed-loop hand prosthesis with simultaneous intraneural tactile and position feedback *Sci. Robot.* **4** eaau8892
- Dadarlat M C, O'Doherty J E and Sabes P N 2015 A learning-based approach to artificial sensory feedback leads to optimal integration *Nat. Neurosci.* **18** 138–44
- Delhayre B P, Long K H and Bensmaia S J 2018 Neural basis of touch and proprioception in primate cortex *Compr. Physiol.* **15** 75–602
- Dobelle W H 2000 Artificial vision for the blind by connecting a television camera to the visual cortex *ASAIO J.* **46** 3–9

- Dobelle W H, Mladejovsky M G, Evans J R, Roberts T S and Girvin J P 1976 'Braille' reading by a blind volunteer by visual cortex stimulation *Nature* **259** 111–2
- Fernández E et al 2021 Visual percepts evoked with an intracortical 96-channel microelectrode array inserted in human occipital cortex *J. Clin. Invest.* **131** e151331
- Flesher S N, Collinger J L, Foldes S T, Weiss J M, Downey J E, Tyler-Kabara E C, Bensmaia S J, Schwartz A B, Boninger M L and Gaunt R A 2016 Intracortical microstimulation of human somatosensory cortex *Sci. Transl. Med.* **8** 361ra141
- Flesher S N, Downey J E, Weiss J M, Hughes C L, Herrera A J, Tyler-Kabara E C, Boninger M L, Collinger J L and Gaunt R A 2021 A brain-computer interface that evokes tactile sensations improves robotic arm control *Science* **372** 831–6
- Goueytes D, Abbasi A, Lassagne H, Shulz D E, Estebanez L and Ego-Stengel V 2019 Control of a robotic prosthesis simulation by a closed-loop intracortical brain-machine interface 2019 9th Int. IEEE/EMBS Conf. on Neural Engineering (NER) (San Francisco, CA, USA: IEEE) pp 183–6
- Hartmann K, Thomson E E, Zea I, Yun R, Mullen P, Canarick J, Huh A and Nicolelis M A L 2016 Embedding a panoramic representation of infrared light in the adult rat somatosensory cortex through a sensory neuroprosthesis *J. Neurosci.* **36** 2406–24
- Johannes M S, Bigelow J D, Burck J M, Harshbarger S D, Kozlowski M V and Doren T V 2011 An overview of the developmental process for the modular prosthetic limb *Johns Hopkins APL Tech. Dig.* **30** 10
- Johansson R S and Westling G 1984 Roles of glabrous skin receptors and sensorimotor memory in automatic control of precision grip when lifting rougher or more slippery objects *Exp. Brain Res.* **56** 550–64
- Kim S, Callier T, Tabot G A, Gaunt R A, Tenore F V and Bensmaia S J 2015 Behavioral assessment of sensitivity to intracortical microstimulation of primate somatosensory cortex *Proc. Natl Acad. Sci.* **112** 15202–7
- Koralek A C, Jin X, Long II J D, Costa R M and Carmena J M 2012 Corticostriatal plasticity is necessary for learning intentional neuroprosthetic skills *Nature* **483** 331–5
- Lassagne H, Goueytes D, Shulz D E, Estebanez L and Ego-Stengel V 2022 Continuity within the somatosensory cortical map facilitates learning *Cell Rep.* **39** 110617
- Madisen L et al 2012 A toolbox of Cre-dependent optogenetic transgenic mice for light-induced activation and silencing *Nat. Neurosci.* **15** 793–802
- Monzée J, Lamarre Y and Smith A M 2003 The effects of digital anesthesia on force control using a precision grip *J. Neurophysiol.* **89** 672–83
- O'Connor D H, Hires S A, Guo Z V, Li N, Yu J, Sun -Q-Q, Huber D and Svoboda K 2013 Neural coding during active somatosensation revealed using illusory touch *Nat. Neurosci.* **16** 958–65
- O'Doherty J E, Lebedev M A, Ifft P J, Zhuang K Z, Shokur S, Bleuler H and Nicolelis M A L 2011 Active tactile exploration using a brain-machine-brain interface *Nature* **479** 228–31
- O'Doherty J E, Shokur S, Medina L E, Lebedev M A and Nicolelis M A L 2019 Creating a neuroprosthesis for active tactile exploration of textures *Proc. Natl Acad. Sci.* **116** 21821–7
- Okun M, Lak A, Carandini M and Harris K D 2016 Long term recordings with immobile silicon probes in the mouse cortex *PLoS One* **11** e0151180
- Pandarinath C and Bensmaia S J 2022 The science and engineering behind sensitized brain-controlled bionic hands *Physiol. Rev.* **102** 551–604
- Poulet J F A and Petersen C C H 2008 Internal brain state regulates membrane potential synchrony in barrel cortex of behaving mice *Nature* **454** 881–5
- Prsa M, Galinanes G L and Huber D 2017 Rapid integration of artificial sensory feedback during operant conditioning of motor cortex neurons *Neuron* **93** 929–39.e6
- Roberts P, Zadan M and Majidi C 2021 Soft tactile sensing skins for robotics *Curr. Robot. Rep.* **2** 343–54
- Rohmer E, Singh S P N and Freese M 2013 V-REP: A versatile and scalable robot simulation framework 2013 IEEE/RSJ Int. Conf. on Intelligent Robots and Systems (IROS 2013) (Tokyo: IEEE) pp 1321–6
- Sachidhanandam S, Sreenivasan V, Kyriakatos A, Kremer Y and Petersen C C H 2013 Membrane potential correlates of sensory perception in mouse barrel cortex *Nat. Neurosci.* **16** 1671–7
- Shen Y, Campbell R E, Côté D C and Paquet M-E 2020 Challenges for therapeutic applications of opsin-based optogenetic tools in humans *Front. Neural Circuits* **14** 41
- Weiss J M, Flesher S N, Franklin R, Collinger J L and Gaunt R A 2019 Artifact-free recordings in human bidirectional brain-computer interfaces *J. Neural Eng.* **16** 016002
- Wodlinger B, Downey J E, Tyler-Kabara E C, Schwartz A B, Boninger M L and Collinger J L 2015 Ten-dimensional anthropomorphic arm control in a human brain-machine interface: difficulties, solutions, and limitations *J. Neural Eng.* **12** 016011

RESEARCH ARTICLE | *Sensory Processing*

Mechanical coupling through the skin affects whisker movements and tactile information encoding

 **Valerie Ego-Stengel, Aamir Abbasi, Margot Larroche, Henri Lassagne, Yves Boubenec, and Daniel E. Shulz**

Department of Integrative and Computational Neuroscience, Paris-Saclay Institute of Neuroscience (NeuroPSI), UMR9197 CNRS, University Paris-Sud, Gif-sur-Yvette, France

Submitted 21 December 2018; accepted in final form 6 August 2019

Ego-Stengel V, Abbasi A, Larroche M, Lassagne H, Boubenec Y, Shulz DE. Mechanical coupling through the skin affects whisker movements and tactile information encoding. *J Neurophysiol* 122: 1606–1622, 2019. First published August 14, 2019; doi:10.1152/jn.00863.2018.—Rats use their whiskers to extract sensory information from their environment. While exploring, they analyze peripheral stimuli distributed over several whiskers. Previous studies have reported cross-whisker integration of information at several levels of the neuronal pathways from whisker follicles to the somatosensory cortex. In the present study, we investigated the possible coupling between whiskers at a preneuronal level, transmitted by the skin and muscles between follicles. First, we quantified the movement induced on one whisker by deflecting another whisker. Our results show significant mechanical coupling, predominantly when a given whisker's caudal neighbor in the same row is deflected. The magnitude of the effect was correlated with the diameter of the deflected whisker. In addition to changes in whisker angle, we observed curvature changes when the whisker shaft was constrained distally from the base. Second, we found that trigeminal ganglion neurons innervating a given whisker follicle fire action potentials in response to high-magnitude deflections of an adjacent whisker. This functional coupling also shows a bias toward the caudal neighbor located in the same row. Finally, we designed a two-whisker biomechanical model to investigate transmission of forces across follicles. Analysis of the whisker-follicle contact forces suggests that activation of mechanoreceptors in the ring sinus region could account for our electrophysiological results. The model can fully explain the observed caudal bias by the gradient in whisker diameter, with possible contribution of the intrinsic muscles connecting follicles. Overall, our study demonstrates the functional relevance of mechanical coupling on early information processing in the whisker system.

NEW & NOTEWORTHY Rodents explore their environment actively by touching objects with their whiskers. A major challenge is to understand how sensory inputs from different whiskers are merged together to form a coherent tactile percept. We demonstrate that external sensory events on one whisker can influence the position of another whisker and, importantly, that they can trigger the activity of mechanoreceptors at its base. This cross-whisker interaction occurs pre-neuronally, through mechanical transmission of forces in the skin. biomechanics; electrophysiology; tactile processing; whisker system

INTRODUCTION

Rodents navigate and perform challenging tactile discriminations by touching surfaces and objects with their whiskers. The whisker system of the rat consists of ~30 whiskers on each side of the snout, which are arranged in a gridlike pattern. This striking discrete peripheral pattern is matched by the anatomical organization of upstream neuronal circuits in gridlike arrays of distinct substructures, called barrelettes, barreloids, and barrels in the brain stem, thalamus, and cortex, respectively (Ma and Woolsey 1984; Van Der Loos 1976; Woolsey and Van der Loos 1970). As a first-order description, sensory information travels in parallel pathways or “labelled lines” from each whisker to each cortical barrel (Deschênes and Urbain 2009).

However, in some of the first recordings in barrel cortex, neurons were already shown to exhibit responses to the individual deflection of several whiskers, demonstrating anatomical and functional convergence (Axelrad et al. 1976; Simons 1978). From a behavioral point of view, the analysis of information coming from several whiskers is indeed important for the animal to perform subtle discrimination tasks (Carvell and Simons 1995; Knutsen et al. 2006; Krupa et al. 2001). In fact, the complex patterns of whisker movements and contact characteristics are only beginning to be described in detail (Grant et al. 2009; Hobbs et al. 2016; Sherman et al. 2017). A major challenge will be to understand how multiple whisker inputs are merged together to form a coherent tactile percept. Despite an already large number of studies aimed at deciphering the mechanisms of multiwhisker integration, the anatomical and functional circuitry responsible for properties of cortical and thalamic receptive fields remains poorly understood.

At the most peripheral level, encoding of tactile stimuli is performed by several classes of mechanoreceptors located in the follicles at the base of the whiskers (Ebara et al. 2002, 2017). Approximately 150–200 first-order neurons from the trigeminal ganglion (TG) innervate each follicle (Vincent 1913) in an exclusive manner, that is, one TG neuron innervating only one follicle. This was originally inferred from functional studies, all of which reported that TG receptive fields contain a single whisker (Dykes 1975; Gibson and Welker 1983; Gottschaldt et al. 1973; Zucker and Welker 1969). It has been finally confirmed by anatomical means very recently (Tonomura et al. 2015).

Address for reprint requests and other correspondence: V. Ego-Stengel, ICN, Neuro-PSI, CNRS, Bldg. 32/33, 1 avenue de la Terrasse, 91190 Gif-sur-Yvette, France (e-mail: valerie.stengel@unic.cnrs-gif.fr).

Upstream, cross-whisker connections have been found among brain stem nuclei (Jacquin et al. 1990; Voisin et al. 2002) and in the thalamo-cortico-thalamic loop (Arnold et al. 2001; Lavallée and Deschênes 2004). They are especially numerous intracortically (Bernardo et al. 1990; Narayanan et al. 2015), where they constitute a potential substrate for multiple forms of multiwhisker sensory integration (reviewed in Estebanez et al. 2018).

Nonetheless, there remains another possibility for early generation of cross-whisker signals, namely, that external contact forces on one whisker could lead to activation of mechanoreceptors in a neighbor follicle. Indeed, in the whisker system, sensory contacts occur on the shaft of the whisker, up to several centimeters away from the receptors in the follicle. Preneuronal treatment by the whisker itself transforms the dynamics of contact into a time course of forces at the base of the whisker (Bagdasarian et al. 2013; Boubenec et al. 2012, 2014; Quist and Hartmann 2012). How these forces then translate into mechanoreceptor activation has just started to be studied (Whiteley et al. 2015). Interestingly, the possibility of cross-whisker mechanical coupling has been suggested more than 30 years ago following the report of one TG neuron activated by a second whisker beyond its principal whisker (see Fig. 4 in Simons 1985). This study suggested the existence of “mechanical spread of the stimulus energy through the mystacial pad.” Indeed, follicles are embedded in a complex mesh composed of skin, conjunctive tissue, and several muscles (Dörfl 1982; Haidarliu et al. 2010). Extrinsic muscles both for retraction (nasolabialis and maxillolabialis muscles) and protraction (nasalis muscle) run superficially, associated closely with the corium in the skin. Intrinsic muscles connect the top of each follicle with the deep part of its rostral neighbor. Interactions between follicles may be transmitted through the superficial layer of skin and/or via these different muscles.

We have developed two experimental approaches to study cross-whisker interactions. First, we have imaged individual whiskers using high-resolution videography of the snout of anesthetized rats while deflecting whiskers with high precision (Jacob et al. 2010). We quantified the deformation of a non-deflected whisker while another whisker was moved in terms of displacement, angle, and curvature. Second, we performed electrophysiological recordings of individual TG neurons. We investigated whether mechanical coupling can be sufficient to induce spikes in trigeminal neurons without stimulating their principal whisker. We integrate our results in a two-whisker biomechanical model bridging the gap between the external profile of the whisker on the one hand and the internal distribution of forces on the other hand, ultimately responsible for mechanoreceptor activation.

MATERIALS AND METHODS

Animal Preparation

All experiments were performed in conformity with French (Decree 2013-118, Ethics Committee project no. 3249-2015060516116339) and European (2010/63/EU) legislation on animal experimentation. Thirteen male Wistar rats (weight 250–300 g) were used in this study. Animals were housed in the NeuroPSI animal facility on a 12:12-h light-dark schedule, with two to four animals per cage. The animals were handled regularly and fed ad libitum. The experiment was always conducted during the light phase of the cycle. A group of seven rats was used for

videography experiments, and another group of six rats was used for electrophysiology experiments. Atropine methyl nitrate (0.3 mg/kg im) was injected to reduce secretions in the respiratory path. Rats were anesthetized with urethane (1.5 g/kg ip). The level of anesthesia was monitored by observing the absence of eye blink reflex, the lack of response to hind paw pinch, and the absence of spontaneous whisker movements. Supplementary doses of urethane (0.15 g/kg ip) were administered whenever necessary throughout the experiment to maintain an adequate level of anesthesia. Body temperature was maintained at 37°C by a regulated heating pad. The animal was placed in a stereotaxic frame. The snout was held by a modified head holder (Haidarliu 1996) allowing free access to the right whisker pad. A local anesthetic (lidocaine 1%) was injected subcutaneously, and the skin on top of the skull was resected. After the conjunctive tissues were cleaned, the skull was cemented to a metal bar fixed rigidly to the frame. This allowed us to remove the right ear bar and to position the multiwhisker stimulator near the right whisker pad.

Whisker Stimulation

We used a custom-made whisker stimulation matrix based on piezoelectric benders (Jacob et al. 2010) to deflect independently the 24 most caudal whiskers of the right whisker pad. Whiskers were trimmed to 10 mm in length to avoid unwanted deflections due to whisker tips accidentally touching neighboring stimulators. Whiskers were inserted 3 mm into small polypropylene tubes glued on each bender (Polytec-PI), thus stimulated at 7 mm from their base. Benders were driven with resistor-capacitor (RC)-filtered voltage pulses producing a trapezoidal deflection. Our standard parameters produced pulses of 10-ms ramp, 10-ms plateau, and 10-ms ramp back, with an amplitude of 1° applied at 7 mm from the follicle, in either a rostral or a caudal direction. We checked that the movement always stayed within $\pm 10\%$ of its expected value by laser measurement.

Videography Experiments

High-speed, high-resolution video recording. A high-speed camera (Photron Fastcam SA3/105mm f-2.8 DG Macro Sigma) was mounted vertically above the animal to record the whisker movements at a 1-kHz frame rate. The camera was triggered by a TTL sent by the whisker stimulator. Whiskers were illuminated from below using a backlight (SLLUB, Phlox; and PP520, Gardasoft). The camera was initially positioned to give a bird's-eye view of the C2 whisker and later translated above other whiskers. Given the geometrical constraints of the multiwhisker stimulator and the camera, we could only move the whiskers in a rostrocaudal direction and image them from the top. For calibration of the spatial scale of the camera field, we imaged a standard checkerboard sheet (1 mm \times 1 mm). Pixel resolution was checked for each series of movies and was in the range 16–20 μm .

Whisker stimulation protocols. To study the effects of mechanical coupling across the whisker pad, we first imaged whisker C2 while deflecting each of the other 23 whiskers individually. For each deflected whisker, we performed four trials in the caudal direction and four trials in the rostral direction. Nonstimulated whiskers were left free in air (not inside the stimulator tips). The whole protocol was first applied while the imaged whisker C2 itself was free in air (“free” condition). The protocol was then repeated (in 4 of 7 experiments) while whisker C2 was constrained in its corresponding stimulator tip without movement (“constrained” condition).

In 3 of 7 experiments, we tested mechanical coupling effects on other whiskers in addition to whisker C2. Given the camera angle and snout geometry, we were able to image whiskers located in rows B to D and arcs 1 to 3. Overall, we imaged 21 additional whiskers while deflecting either the immediately caudal or the immediately rostral adjacent whisker. Those tests were systematically done both in free and constrained conditions. For arc 1 whiskers, we chose to test their

coupling on the caudal side with the straddler resulting in the smoothest alignment of follicles (B1-beta, C1-gamma, D1-delta), which correlates with the presence of an intrinsic muscle (Haidarliu et al. 2010).

Measurement of whisker parameters. At the end of the experiment, after all movies were acquired, we estimated the point of the whisker shaft corresponding to follicle entry for each imaged whisker. First, a wide-field snapshot of all whiskers and of the snout fur was taken. We then spread depilatory cream on the fur between the whiskers, let it set for 3–5 min, carefully removed the cream, and rinsed the pad. We took a second wide-field snapshot of the whisker pad without the fur, adjusting the lighting so that the entry of the whiskers in their follicles was clearly visible. Finally, whiskers were cut at the follicle entry and mounted on histology slides for measurement of their diameter and length under an optical microscope. For the D row, which was located below the pad outline and/or below other whiskers, the follicle entry position could often not be directly visualized. In those instances, it was estimated on the wide-field snapshot using the visible tip and the known length of the whisker, and taking into account the angle of the whisker relative to the horizontal plane of focus.

Data analysis. Camera recordings were analyzed using custom scripts in Python. Each movie contained 150 or 200 frames at 1 kHz, corresponding to one trial. Frames were typically 384×512 pixels. Their exact dimension was adjusted from one imaged whisker to the next depending on the viewing conditions. A series of eight trials (4 rostral, 4 caudal deflections) was analyzed for each pair of imaged and moved whiskers, and for each of the free and constrained conditions tested.

In all movies, the imaged whisker was approximately vertical on each frame, with the fur visible at the bottom (Fig. 1A). We defined a range of pixel lines in which the imaged whisker appeared clearly as a dark bar on a lighter background. For each line, the center of the whisker shaft was defined as the center of mass of the pixels encompassing the whole section of the whisker on that line (usually ~15 pixels), where each pixel is weighed by its intensity value compared with a given threshold. The threshold was adjusted independently for each imaged whisker. This yielded a raw profile of the whisker corresponding to the current frame (such as one colored line in Fig. 1). The computation was applied independently to each frame. We systematically checked whisker tracking for each movie by plotting several calculated raw profiles on top of their corresponding images. This allowed us to correct tracking problems due to unexpected changes (background element, global shift), mainly by changing the threshold or modifying the range of lines tracked.

Raw profiles of whiskers were never smooth, displaying many irregularities. Subpixel high-frequency spatial oscillations, dependent on the initial angle of the whisker relative to the vertical axis of the frames, could be ascribed to pixelization artifacts by the camera and were ignored in our analysis. We also encountered enlarged portions of a shaft, particles sticking on it, or bends. To focus on the changes over time irrespective of these singularities, we subtracted the profile calculated on the frame just before the start of the stimulation from all other profiles of the movie. We characterized the resulting deformation profiles, as well as the reference raw profile, by fitting each of them with a second-degree polynomial. This allowed us to extract three parameters quantifying the deformation: the displacement along the rostrocaudal axis, the change in whisker angle, and the change in curvature. These three parameters could be estimated at any point along the whisker shaft.

The tracked portion of the whisker was limited by the imaging constraints, in particular on the follicle side for which the view was obstructed by other whiskers and fur. We extrapolated the fits of the whisker profiles down to the estimated follicle entry. For population analysis, we filtered out trials for which the displacement near the tip or the change in angle near the follicle was outside of the range of the mean ± 1.5 SD, either in the baseline window 20 to 10 ms before the start of stimulation or in a second baseline window 10 to 20 ms after

the end of stimulation. This eliminated 5–15% of trials on one given experiment, depending on the stability of the preparation.

To validate our method, in one animal we tracked the kinematic changes of whisker C1 while it was being deflected by its piezoelectric bender (Fig. 1, A–D). For each frame, a weighted average of pixel intensities across the whisker was performed line by line, in the region where the contrast of the whisker against the background was sufficiently good. The left side of Fig. 1B shows the expanded resulting profiles of whisker C1 for 20 frames, corresponding to 20 ms during its deflection by the stimulator. The whisker tip was indeed deflected by the expected amount (114 μm , i.e., ~7 pixels). Meanwhile, the whisker shaft showed a change in angle, which was largest toward the base of the whisker, as well as an increase in curvature that was best seen when looking at the deformation relative to rest (Fig. 1C, left). We fitted each profile independently by a second-order polynomial as described above. The fits (Fig. 1, B and C) were extrapolated down to the estimated follicle entry point. Overall, the C1 imposed deformation appears as a rotation of the whisker around the follicle entry point with a change in curvature. We quantified several kinematic parameters at each point along the shaft: displacement in the rostrocaudal direction, angle relative to rest, and curvature. Figure 1D displays the evolution of these parameters in time for the tip, middle, and follicle entry points. Note that residual ringing can be observed after ramp deflections, typical of piezoelectric stimulation (Jacob et al. 2010). Overall, these measures on the deflection of C1 confirm that our imaging method can measure subpixel deformations of a whisker at a 1-kHz resolution.

We report median and interquartile range values. We performed nonparametric statistical tests because of low sample sizes. Individual tests are referred to in the main text.

Electrophysiology Experiments

Signal acquisition and spike sorting. In addition to the surgical steps for head fixation, a craniotomy was made on the skull overlying the right TG (1.8 mm posterior and 2.1 mm lateral from bregma; Schneider et al. 1981). A dam of dental acrylic was constructed around the craniotomy and filled with saline to prevent the brain from drying. Extracellular neural activity was recorded from a tungsten electrode (FHC; 2–10 M Ω at 1 kHz) that was vertically lowered ~10 mm down in the TG using an electronically controlled manipulator (Luigs and Neumann). Custom-made software (Elphy; G. Sadoc, UNIC, France) was used for spike time acquisition, whisker stimulation, and data processing. In a first series of experiments (5 cells in 2 rats), signals were amplified and filtered (300–3,000 Hz) by an acquisition card (CyberAmp) connected to a template-matching hardware spike sorter (Alpha-Omega). In a second series (9 cells in 4 rats), signals were amplified and filtered (250–7,500 Hz) using a different acquisition system (Blackrock Microsystems). Single units were isolated using the integrated online spike sorter. In all experiments, baseline signals had a standard deviation of 10–15 μV . Single-unit spike waveforms had amplitudes of 100 μV or more. Because cell density and cell firing are sparse in the TG, we typically recorded at most one or a few action potentials per stimulus separated by long periods of silence. Thus action potential waveforms were clearly separated from the noise. The shape of action potentials was closely monitored online to ensure that only isolated single units were recorded throughout the protocols. The recording was terminated if the quality of spike classification was lost. At the end of recording at a given site, the electrode was advanced by at least 100 μm before the next recording site to avoid recording data from the same single units.

Whisker stimulation protocols. We first characterized the receptive field of each neuron by presenting pseudorandom sequences of 30–100 individual deflections of the 24 whiskers in the rostral and caudal directions. Initially, we applied pulses of 0.93° (2 experiments) or 1° (4 experiments), corresponding to angular speeds of 93–100°/s. Once the receptive field of the neuron was established, we tested mechanical

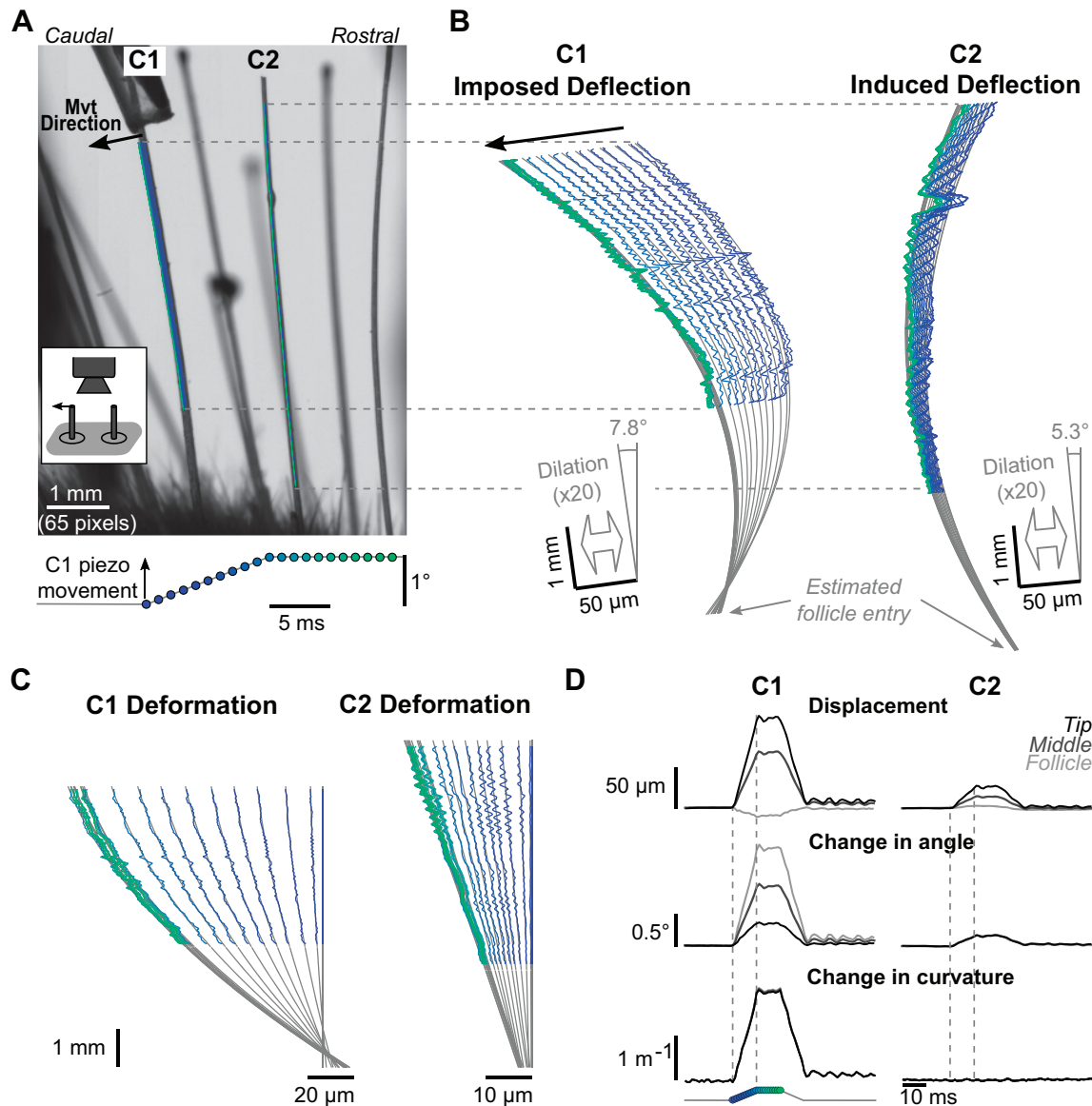


Fig. 1. An imposed 1° deflection of whisker C1 induces a rotation of whisker C2 around its follicle entry. **A**: raw image of the region of interest captured during study of the effect on whisker C2 of a ramp-plateau-ramp deflection of whisker C1. Time course of the C1 deflection is indicated below the image, along with the color code for 20 successive frames acquired at 1 kHz during the up-ramp and plateau of the pulse. The C1 and C2 whisker profiles calculated from these 20 frames are superimposed on the image. **B**: the same 20 raw profiles are displayed after a magnification factor (dilation) of gain 20 was applied in the direction orthogonal to the whisker. This anisotropic manipulation, solely used for display, was necessary to effectively observe the induced displacements. With these scales, the whisker profiles appear bumpy as a consequence of irregularities of the shaft and camera pixelization. Gray lines are second-order polynomial fits, extrapolated down to follicle entry estimates. **C**: deformation calculated by subtracting the profile right before the start of the deflection and after smoothing with a time window of 5 (C1) or 10 points (C2) solely for visual display. Note horizontal scales are different for the 2 whiskers. Curvature changes could be reliably visualized on these plots, whereas they were difficult to see before the subtraction. **D**: time course of displacement, change in angle, and change in curvature for the 2 whiskers at 3 different levels along the shaft (tip, middle, follicle). “Tip” indicates the point at which the stimulation contacts the whisker shaft. The induced deflection on C2 is a rigid rotation around the follicle entry, with no curvature change. Mvt, movement.

coupling across an increasing range of ramp speeds. We increased the deflection amplitude to 3° or 4°, resulting in an increase in ramp speed to 300 or 400°/s, respectively. We also reduced the ramp duration from 10 ms to 5 or 3 ms, to increase the deflection speed up to 1,200°/s. In a few cases, we approached further the stimulator tip along adjacent whiskers down to ~3 mm from the follicle, which resulted in an increased speed of the deflection to ~4,000°/s. These different parameter modifications were tested until a coupling effect was observed from one adjacent whisker, at which point we stopped increasing ramp speed. Interestingly, all neurons for which we were able to test this range of increasing ramp speeds displayed mechanical

coupling effects for at least one adjacent whisker. For other neurons, the quality of single-unit isolation was lost before high speeds could be tested.

Beyond a direct response of a primary afferent neuron to one of the adjacent whiskers, we tested whether a movement of an adjacent whisker could modify the response of the neuron to deflections of its principal whisker, through a subthreshold modulation. We first determined deflection parameters for the coupled adjacent whisker that elicited no response for either direction of movement. We then stimulated the principal whisker in its preferred direction with eight different pulses of increasing speed and fixed amplitude stimuli,

obtaining a response curve as a function of speed. Once all parameters were determined, we studied the modulation of this curve by adding subthreshold deflections to the adjacent whisker in either direction. Trials with only the principal whisker deflected, or with deflections of both the principal whisker and the adjacent whisker in either rostral or caudal direction, were pseudorandomly interleaved. We could only complete this final protocol satisfactorily in one case (see Fig. 6).

Data analysis. Peristimulus time histograms were constructed by summing the activity of the neuron relative to the stimulus trigger with a 1-ms time bin. Spontaneous activity was null for 13 of 14 neurons and below 1 Hz for the remaining neuron.

Biomechanical Model

A finite-element model of two whiskers and follicles was built in SolidWorks Simulation. Geometrical parameters such as whisker diameter, follicle dimensions, and inter-whisker spacing are known to vary across the whisker pad. We used values obtained from the literature (Haidarliu et al. 2010; Kim et al. 2011) and complemented from our own measurements taken in the center of the whisker pad on and around C2. Note that the chosen geometry needed to be compatible with a mesh model, thus avoiding very small features and very high curvature surfaces. This forced us in particular to use a larger whisker diameter than typical values for the rat. Hence, each whisker was modeled by a rod of diameter 300 μm , i.e., two times thicker than the C2 whisker of our animals (149 μm , $n = 4$ rats; see also Belli et al. 2017). To investigate the impact of whisker diameter on the forces inside the follicle, we also tested diameters of 250 and 350 μm (see RESULTS). The whisker rod was 10 mm long, modeling a cut whisker of which the tip would be manipulated. Each follicle was modeled by a cylinder of diameter 800 μm and length 2.5 mm in which a whisker was inserted. Follicle centers were 2 mm apart. Follicles and whiskers were attached at their base to a fixed plate. A layer of skin was added in which the top of the follicles was embedded. This rectangular skin component had a thickness of 80 μm and extended 750 μm in each direction from the follicle borders. We did not attempt to model the extrinsic muscles running along the corium separately, but considered the skin sheet as including those muscles. For one set of simulations, we modeled the intrinsic muscle as a single rod connecting two rings, one around the caudal follicle just below the skin and one around the rostral follicle centered at a depth of two-thirds the total follicle depth. The ring was 200 μm thick and 300 μm high. The connecting rod had a diameter of 100 μm .

Follicles and skin, as well as the intrinsic muscle when simulations included one, were modeled by a material with mechanical parameters close to rubber with Young's modulus = 0.12 GPa and Poisson's ratio = 0.49. Whiskers were modeled by a material close to polyvinyl chloride with Young's modulus = 7.2 GPa, in agreement with measures present in the literature (Carl et al. 2012; Hartmann et al. 2003; Neimark et al. 2003), and Poisson's ratio = 0.38.

The contact surfaces between components did not allow penetration. Follicles and skin, as well as the intrinsic muscle when present, were bonded, whereas follicles and whiskers could separate. The mesh size was 80 μm , which resulted in 51,567 elements and 83,978 nodes for our default geometrical parameters. Whisker deflection was modeled by a rotation of the whisker tip of 1° around the whisker base center at the bottom of the follicle. The neighboring whisker distal tip could be either free or constrained (fixed). These boundary conditions on the deflected whisker and its neighbor imposed the whisker angles at the distal end, which was not the case in the experimental conditions. The distal whisker profiles could thus sometimes differ from the observed ones. This did not affect deformations near and inside the follicles, which were the focus of our study.

Simulations were run for both rostral and caudal directions of movement. Because results were always found to be symmetric, we chose to report the effect of deflecting one whisker toward the other. Thus the rostral whisker was deflected caudally, and the caudal

whisker was deflected rostrally. The simulations all assumed a linear elastic behavior of the components and were restricted to small displacements.

RESULTS

High-Speed Videography Reveals Whisker Movements Induced by Mechanical Coupling

We investigated mechanical coupling between whiskers by imaging directly the whiskers on the snout of rats ($n = 7$ animals) using a high-frame rate, high-resolution camera and a custom-built multiwhisker stimulator (Jacob et al. 2010).

First, we validated our tracking method by verifying that the movement of a whisker deflected by a piezoelectric bender could be imaged at 1 kHz and quantified with adequate spatial resolution (Fig. 1, A–D, whisker C1; see MATERIALS AND METHODS). We then applied this tracking method to the neighboring whisker C2. As shown by the raw profiles and fits in Fig. 1B, whisker C2 also moved during the deflection of whisker C1, even though it was not directly deflected by the experimenter. Moving whisker C1 induced a displacement at the tip of C2 of 25 μm , representing 23% of the tip displacement imposed on C1. For both the deflected and the imaged whisker, there was little if any translation at the base of the whisker, as estimated by extrapolating the whisker profile down to the follicle entry point. The change in angle along whisker C2 reached 0.16°, that is, 11% of the imposed angle at the C1 follicle entry. There was no change in curvature of whisker C2 so that the overall deformation was well described by a change in angle (Fig. 1, C and D, right). These results demonstrate that even for small movements, there can be a measurable mechanical coupling between two neighboring whiskers. Deflection of one whisker induced a rigid transformation of its rostral neighbor, more precisely, a rotation around the follicle entry point.

Mechanical Coupling Is Strongest from a Caudal Whisker in the Same Row

We explored the effect of deflecting one by one each whisker, always measuring the movement of the nondeflected central whisker C2. The time course of the angular rotation of C2 for all trials of one experiment is shown on Fig. 2A, separately for deflections in the caudal (left) and rostral (right) directions. For each given deflected whisker, the observed profile was highly repeatable from one trial to the next. In this example, we observed mechanical coupling for deflections of whiskers beta, B1, gamma, C1, and C3. The effect was similar for deflections in the caudal and rostral directions, showing mirroring profiles. We thus pooled induced effects across the two conditions for all subsequent population analysis and figures. Analysis from seven experiments confirmed a consistent gradient of the amplitude of induced movement of C2 during movement of other whiskers around it (Fig. 2B). As observed in Fig. 1, induced movements were rigid rotations along the estimated follicle entry, with no curvature change or translation at the base of the whisker. For further analysis, we thus focused on changes in whisker angles (middle matrix of Fig. 2B). The effect tended to decrease as the distance between C2 and the deflected whisker increased. However, distance was clearly not the only factor determining the amplitude of the me-

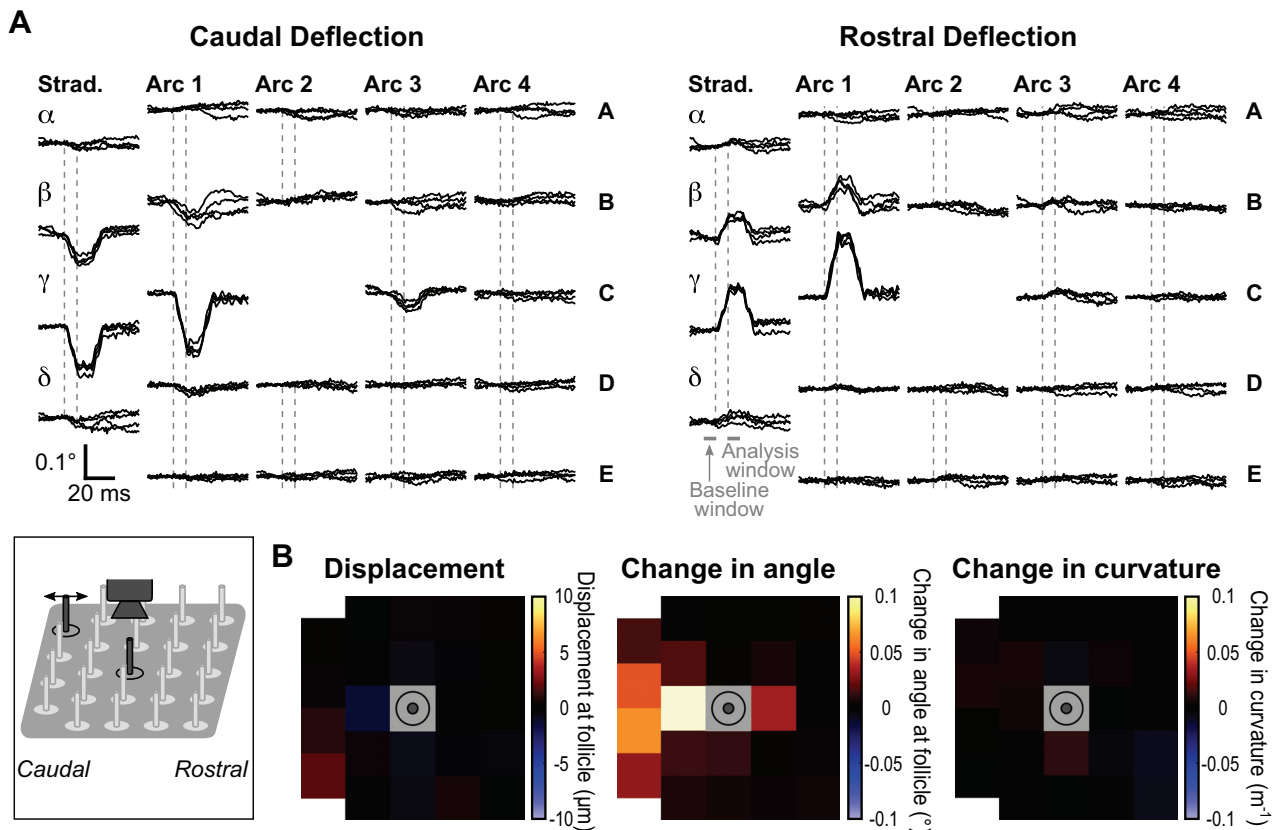


Fig. 2. Spatial map of mechanical coupling effects on whisker C2 from other whiskers on the pad. *A*: time course of whisker angle at the follicle level while every other whisker on the pad is deflected in either a caudal or rostral direction. Traces are aligned around their mean calculated in the 10-ms window before the stimulus. Strad., straddlers arc; *A–E* indicate rows; alpha, beta gamma, and delta indicate straddler whiskers between rows. *B*: displacement, change in angle, and change in curvature at the follicle level quantified in the time window 10–20 ms after stimulation (plateau of pulse) and pooled over rostral and caudal directions (median values over 7 rats).

chanical coupling. We observed a strong asymmetry among whiskers, with whiskers caudal to C2 generating much larger induced movements than those located rostrally. Also, whiskers in the same row as C2 were more effective, suggesting an effect more potent along rows than along arcs.

Strength of Mechanical Coupling Depends on Whisker Location

Given that not all whisker pairs exhibited detectable mechanical coupling, we wondered which parameters govern the amplitude of the coupling effect. Figure 2*B* suggests that distance between the whiskers is an important factor, as well as location in the same row. Also, it points to an asymmetry depending on whether the deflected whisker is located rostrally or caudally to the imaged whisker. However, these results were obtained by always imaging C2 so that the asymmetry could also be due to the identity of the whisker moved, and not to its rostral vs. caudal location relative to the imaged whisker.

We decided to investigate this question further by testing other combinations of whiskers distributed across the whisker pad. We focused on immediately neighboring pairs in one row, for which the effect was expected to be largest and for which the distance between the follicles was always around 2 mm. The results of this data set are summarized in Fig. 3. First, we checked whether the asymmetry observed for whisker C2 in Fig. 2 held when results were analyzed from all whiskers

imaged, located in rows B–D and arcs 1–3. Indeed, the coupling effect was consistently strongest when the whisker immediately caudal was deflected, compared with the rostral one (Fig. 3*A*; Wilcoxon signed-rank test, $P = 1.2 \times 10^{-5}$). In this same data set, we could also ask whether for a particular combination of whiskers, the effect was similar whichever whisker was the deflected one. We found again that induced movements were larger when the caudal whisker was deflected, compared with the rostral whisker (Fig. 3*B*; Wilcoxon signed-rank test, $P = 0.0023$). Moreover, when we compared the impact of deflecting a fixed whisker on its two immediate neighbors, we found that the effect was strongest on the rostral whisker compared with the caudal one in each of the five cases where we could image on both sides (Fig. 3*C*; Wilcoxon signed-rank test, $P = 0.043$). Together, these results point to a consistent underlying asymmetry such that mechanical coupling is strongest when the whisker inducing the movement of its neighbor is located caudally to it. Pooling results from all experiments, we looked at whether there was a systematic bias due to the location of the whiskers on the whisker pad (Fig. 3*D*). We observed strong variations in the coupling amplitude across the whisker pad, with larger effects in more caudal and ventral locations.

We reasoned that this spatial distribution must arise from a systematic gradient in one or several mechanical parameters across the whisker pad. Many such gradients have been re-

ported, and all of them follow a set of consistent rules. In particular, from rostrordorsal to caudoventral locations, the whisker diameter increases sharply (Belli et al. 2017; Ibrahim and Wright 1975; Voges et al. 2012), along with a moderate increase in follicle size and distance between follicles (Haidarliu et al. 2010; also observed in our sample). Because the thickness of the deflected whisker directly governs its mechanical rigidity, it could have a strong impact on the surrounding skin, including neighboring follicles and whiskers. We thus examined the relation between the diameter of the whiskers, measured in four animals, and the amplitude of the coupling effect. Median diameters are indicated in Fig. 3D and, as expected, covaried with the size of the coupling effect. Population

scatter plots confirmed a significant correlation between the observed coupling effect and the diameter of the moved whisker (Fig. 3E; Spearman's coefficient $\rho = 0.63$, $P = 1.27 \times 10^{-6}$) and less with the diameter of the imaged whisker (Fig. 3F; Spearman's coefficient $\rho = 0.14$, $P = 0.034$). We conclude from these data that mechanical coupling is dependent on properties local to the deflected whisker, such as its diameter. Nonetheless, we acknowledge that beyond the gradient of diameter of the deflected whisker, other gradients of mechanical properties of the whiskers, follicles, or skin may contribute to the observed asymmetries. Because all these gradients are correlated, it is difficult to disentangle their relative contribution. This is best addressed by manipulation of individual features in a biomechanical model, as we report in *Mechanical Model of Two Neighboring Whiskers and Follicles*.

Constraining the Whisker Tip Induces Curvature Changes

In all these observations, the imaged whisker was unrestrained while other whiskers were deflected. The induced movement consisted in a rotation around the follicle entry with no detectable change in curvature or displacement of the follicle entry point (Figs. 1 and 2B). In previous studies modeling the whisker as a rigid anchored beam, changes in curvature have been shown to be proportional to the moment of rotational forces along the whisker (Quist and Hartmann 2012; Solomon and Hartmann 2006). Our results reported above are consistent with the fact that since the whisker shaft was not touching any external object, there were no forces along it, and thus no curvature changes. Mechanical conditions are different when the shaft of the whisker is maintained in a given position or manipulated by a stimulator. The whisker is then constrained both at the follicle level and by the external contact. Forces are generated along the whisker shaft, and the whisker bends. In those conditions, the curvature changes give an estimate of the forces generated along the whisker shaft down to the follicle entry, where mechanoreceptors are located.

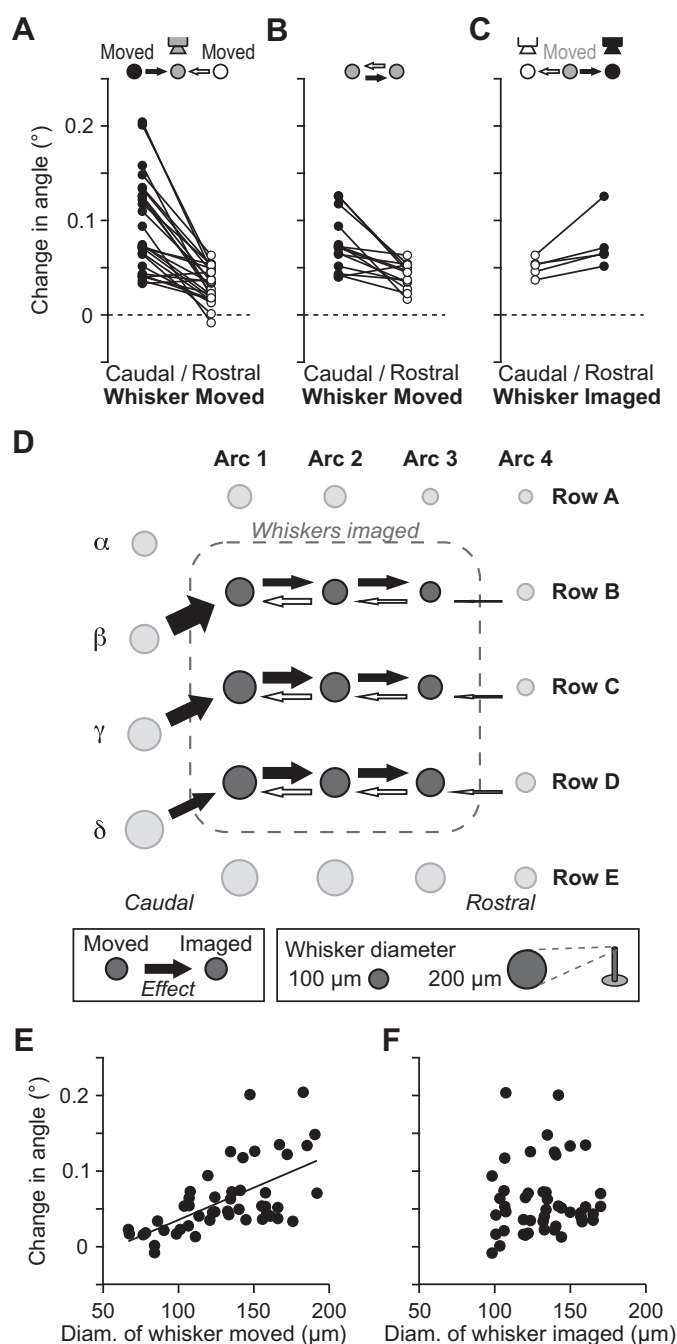


Fig. 3. Mechanical coupling between neighbors follows a systematic gradient on the whisker pad. A: median change in angle for a given imaged whisker when its caudal neighbor (closed circles) or rostral neighbor (open circles) was moved ($n = 26$ whisker pairs). The change in angle was significantly higher when the caudal whisker was moved (Wilcoxon signed-rank test, $P = 1.2 \times 10^{-5}$). In A–F, closed (or open) arrows indicate mechanical coupling due to deflection of a caudal (or rostral) whisker. B: median change in angle for a given whisker combination when the caudal whisker was moved and the rostral whisker was imaged (closed circles) vs. when the rostral whisker was moved and the caudal whisker was imaged (open circles) ($n = 14$ whisker pairs). The change in angle was significantly higher when the caudal whisker was moved (Wilcoxon signed-rank test, $P = 0.0023$). C: median change in angle for a given deflected whisker when its caudal neighbor (open circles) or rostral neighbor (closed circles) was imaged ($n = 5$ whisker pairs). The change in angle was significantly higher when the rostral whisker was imaged (Wilcoxon signed-rank test, $P = 0.043$). D: summary of the mechanical coupling effect pooled across experiments. The width of each arrow indicates the mean change in angle induced on one whisker (located at the end of the arrow) while a neighboring whisker (located at the start of the arrow) was deflected ($n = 52$ effects tested on 6 rats; 1–3 data points per arrow, except 6 data points for C2 imaged). Circles indicate the median diameter of each whisker ($n = 4$ rats). E: median change in angle as a function of the diameter of the whisker moved ($n = 48$ whisker pairs). There was a significant positive correlation between these variables (Spearman's coefficient $\rho = 0.63$, $P = 1.3 \times 10^{-6}$). F: median change in angle as a function of the diameter of the whisker imaged ($n = 48$ whisker pairs). These variables were not significantly correlated (Spearman's coefficient $\rho = 0.14$, $P = 0.034$).

To investigate these forces during mechanical coupling, we repeated the measures of whisker deformation after introducing the imaged whisker into the standard plastic cylinder attached to our multiwhisker stimulator, in the rest position. In this constrained configuration, deflecting a whisker could still induce a measurable movement in a neighboring whisker (Fig. 4A). As expected, the amplitude of the deformation and the change in angle were smaller than in the free condition (note the different horizontal scales for the profiles of Fig. 4A). However, we now observed a change in the whisker curvature. These results were confirmed in our population data set of videography recordings in which one whisker was imaged while its immediate neighbor in the same row was deflected, either free or constrained (Fig. 4, B and C, $n = 46$ whisker pairs). Specifically, changes in angle that were observed in the free condition were correlated with changes in angle of smaller amplitude in the constrained condition (Fig. 4B; Spearman's coefficient $\rho = -0.56$, $P = 5.4 \times 10^{-5}$), as in the example of Fig. 4A. Additionally, in the constrained condition, changes in curvature were significantly correlated with changes in angle (Fig. 4C; Spearman's coefficient $\rho = 0.47$, $P = 0.001$).

These results emphasize that in the constrained condition, because of the added external force at the tip counteracting the natural movement of the whisker, rotational forces are generated along the imaged whisker down to its base. As a consequence, below follicle entry, the distribution of forces at the whisker-follicle contact surface is likely to be different in the constrained vs. the free condition, leading to possible differences of mechanoreceptor activation.

Deflection of Adjacent Whiskers at High Amplitude Evoke Action Potentials in TG Neurons

The whisker imaging experiments demonstrated that neighboring whiskers and their follicles are indeed distorted when a

single whisker is deflected. Next, we wanted to assess whether mechanical coupling could directly elicit spiking activity in primary afferent axons. We recorded extracellularly from TG neurons while stimulating the ipsilateral whiskers in six anesthetized rats. All 24 whiskers were constrained in their respective stimulators throughout the experiment to minimize manipulation of the animal snout during the electrophysiological recordings. Because TG neurons each have a different threshold for evoked activity, we routinely tested several speeds and amplitudes of stimulation to determine both the whisker follicle innervated by each neuron and the stimulation threshold. In each case, we determined a relatively low level of stimulation at which we observed evoked spikes for the deflection of only 1 whisker out of 24. This is in line with previous studies of TG receptive fields, reported to be monovibrissal (Gibson and Welker 1983; Zucker and Welker 1969). For example, the first neuron displayed in Fig. 5A responded only to the deflection of whisker E1, and only in the caudal direction (*top* row of rasters and histograms). There was no spiking for the rostral direction of movement, or for either direction when the stimulation was applied on any of the other 23 whiskers (shown as an example for whisker delta). We conclude that E1 is the principal whisker of this neuron.

To estimate the impact of mechanical coupling on the firing of this neuron, we then stimulated all whiskers individually at a higher speed ($1,330^\circ/\text{s}$ vs. $800^\circ/\text{s}$ previously). Spikes were now reliably evoked following the deflection of the adjacent whisker delta in the rostral direction (Fig. 5A, second row of rasters and histograms). This additional response indicates sufficient mechanical coupling between follicles delta and E1 to induce spikes in the E1-innervating neuron when deflecting delta. The response disappeared entirely if we removed the E1 whisker from its stimulator, indicating that the constrained state of the principal whisker contributed to the mechanical

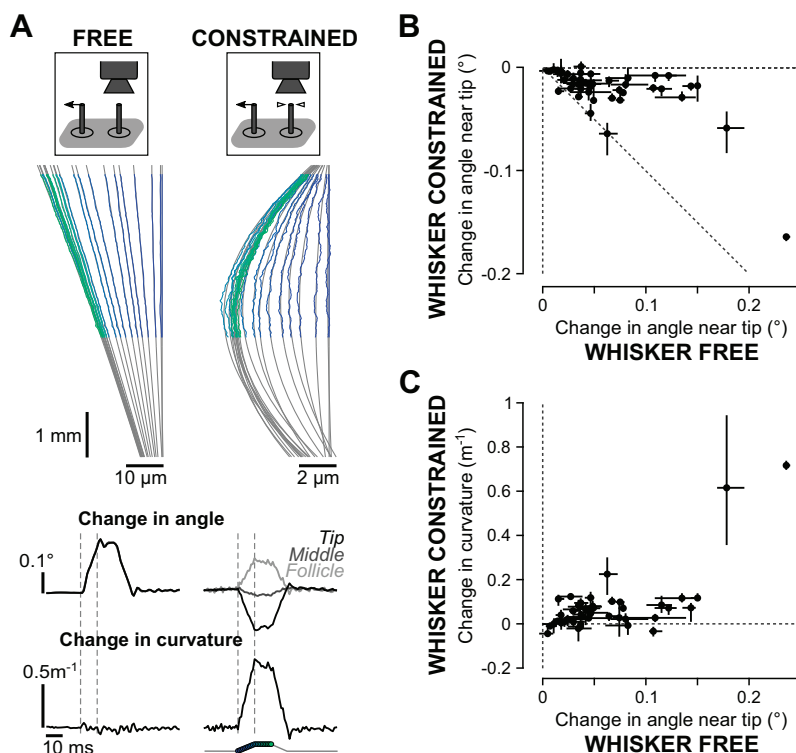
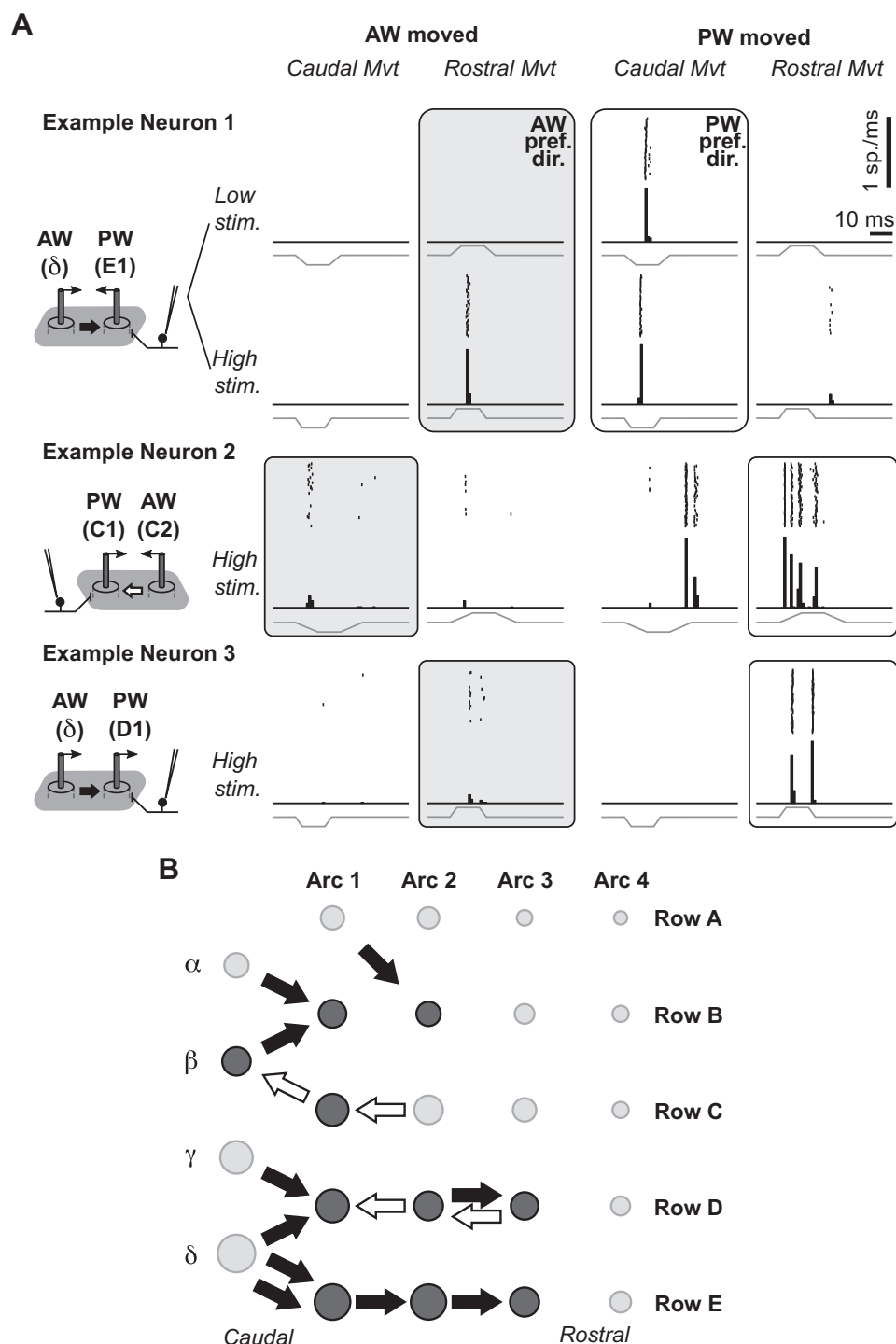


Fig. 4. Constraining the whisker tip results in a curvature change. *A, top*: deformation profiles (colored lines) and fits (gray lines) for a whisker either free (*left*) or constrained at its tip (*right*) while its neighbor is being deflected. A 10-point smoothing procedure was applied solely for visual display. Note that the horizontal scales are different in the 2 conditions. *Bottom*: time course of change in angle and change in curvature at 3 different levels along the shaft (tip, middle, and follicle, where "tip" indicates the point at which the stimulation contacts the whisker shaft) for the 2 conditions. The induced movement was a rigid rotation in the free condition and a bend of the whisker in the constrained condition. *B*: change in angle near the tip of the whisker in the constrained condition vs. the free condition ($n = 46$ whisker pairs; Spearman's coefficient $\rho = -0.56$, $P = 5.4 \times 10^{-5}$). In *B* and *C*, each point represents one combination of whiskers. Data points are the median value calculated over the 8 trials (4 rostral and 4 caudal, mirrored), and error bars indicate the 25th and 75th percentiles. *C*: change in curvature in the constrained condition vs. change in angle in the free condition ($n = 46$ whisker pairs; Spearman's coefficient $\rho = 0.47$, $P = 0.001$). The very large error bar for one point comes from one case of different absolute values between rostral and caudal evoked movements.

Fig. 5. Primary afferent neurons fire in response to their principal whisker (PW) and to a coupled neighbor whisker. **A**: action potential raster plots and peristimulus time histograms (1-ms bins) of the spiking activity of 3 example neurons, evoked by stimulation of their PW and an adjacent whisker (AW) for which mechanical coupling was revealed. Plots in two *left* and two *right* columns display responses to deflections of the AW and PW, respectively, whether it is the rostral or caudal whisker of the pair, for caudal and rostral deflections as indicated above the columns. The stimulation time course is shown below each histogram. For example *neuron 1*, spiking activity is shown for 2 different stimulation levels. For each neuron, the response to the PW in the PW preferred direction is indicated with an open background. The response to the AW in the AW preferred direction is indicated with a shaded background, highlighting the mechanical coupling effect at high stimulation levels. Parameters are *neuron 1*, low stimulation: 4°, 800°/s, $n = 53$ trials, and high stimulation: 4°, 1,330°/s, $n = 42$ trials; *neuron 2*: 3°, 300°/s, $n = 60$ trials; *neuron 3*, PW (D1): 4°, 1,330°/s; AW (delta): ~11°, ~3,800°/s, $n = 68$ trials. In this last case, the piezo tip for delta was advanced to ~3 mm from follicle entry. **B**: summary of mechanical coupling effects resulting in spiking activity. Each arrow indicates that spiking activity could be elicited in a neuron with its PW located at the end of the arrow while a neighboring AW, located at the start of the arrow, was deflected ($n = 14$ neurons on 6 rats). Closed (or open) arrows indicate cases where the AW was a caudal (or rostral) neighbor. Darker whisker symbols indicate whiskers for which we obtained at least one primary afferent recording on which we were able to thoroughly test responses. Mvt, movement; pref. dir., preferred direction; sp., spike; stim., stimulation.



coupling effect. Interestingly, the direction of movement that had to be applied to the adjacent whisker to evoke spikes was opposite to the preferred direction for the principal whisker.

We report 14 cases of mechanical coupling leading to evoked spikes in TG neurons, of 14 TG recordings for which we were able to test responses to caudal and rostral neighboring whiskers at high deflection speeds (up to 4,000°/s; see MATERIALS AND METHODS). On the summary map of Fig. 5B, each arrow indicates coupling from an adjacent whisker whose deflection evoked spikes in a TG neuron innervating a neigh-

boring follicle. The functional response resulting from mechanical coupling was almost always observed for the stimulation of an immediately adjacent whisker in the same row, although it was always tested for all other 23 whiskers. We observed only one case of coupling across two different rows, from whisker A1 to whisker B2. Interestingly, most coupling effects (10/14; closed arrows in Fig. 5B) originated from the caudal adjacent whisker, in agreement with the larger mechanical coupling revealed in the videography experiments from immediately caudal whiskers (Figs. 2B and 3A). The example

neuron 2 of Fig. 5A displays one of the four rostral interactions that we observed (open arrows in Fig. 5B). In this example, whisker C2 deflections elicited spikes in a C1-innervating neuron. Finally, preferred directions for the principal whisker and adjacent whiskers were usually opposite, except in two cases, one of which is shown in the *bottom* row of Fig. 5A (example neuron 3).

Adjacent Whisker Deflections Can Modify Responses of TG Neurons to Principal Whisker Deflections

These recordings confirmed that deflecting an adjacent whisker could induce spiking activity in a TG neuron. However, it should be emphasized that this usually required strong stimulation pulses, from 330 to ~4,000°/s, thus above the stimulation thresholds observed for principal whisker stimulation in our sample (usually 100°/s or less). Nonetheless, we reasoned that even subthreshold stimulation of an adjacent whisker could induce deformation of a follicle and modulate the firing properties of mechanoreceptors. We present one example cell suggesting that this subthreshold modulation can indeed occur. The *middle* row of Fig. 6A displays the action potentials and average activity in time of a TG neuron for 36 rostral deflections of its principal whisker, D1, for two different speeds (left, 12.5°/s; right, 20°/s). During the same protocol, we also tested responses obtained when a deflection of whisker D2 was added, either in the caudal (Fig. 6A, *top* row) or in the rostral (*bottom* row) direction. In these randomly interleaved trials, D2 was deflected at a subthreshold stimulation level. We observed that the joint stimulation of D2 and D1 led to either more activity (Fig. 6A, *top* row, D2 caudally deflected) or less activity (*bottom* row, D2 rostrally deflected) than the single stimulation of D1. These effects were present for a range of stimulation speeds of the principal whisker and disappeared at very small speeds, when the principal whisker response itself occurred at a very long latency (Fig. 6B). Although we could not test this modulatory effect systematically, it suggests that neighboring whiskers have an ongoing influence on responses to the principal whisker through mechanical coupling.

Mechanical Model of Two Neighboring Whiskers and Follicles

Videography and electrophysiology experiments give us important but indirect clues about the mechanical interactions between follicles inside the skin. To estimate the transfer of mechanical forces from one follicle to a neighboring one and gain better understanding of its functional implications, we built a finite-element model of two whiskers and their follicles, linked by a layer of skin that takes into account superficial muscles (Fig. 7A). We used geometrical and mechanical parameter values in the ranges reported in the literature (see MATERIALS AND METHODS). The static deformations and forces resulting from the deflection of one whisker were calculated using SolidWorks Simulation. The model reproduced the expected induced movement of an adjacent whisker when one whisker is deflected at the tip (Fig. 7B, *left*, deflected whisker; *middle*, adjacent whisker). The change in angle, when the whisker was free in air, reached 0.2° (20% of the imposed deflection), in the same range as the experimental measurement shown in Fig. 1, and the external whisker shaft was straight (no curvature). When the whisker was constrained at the tip, it

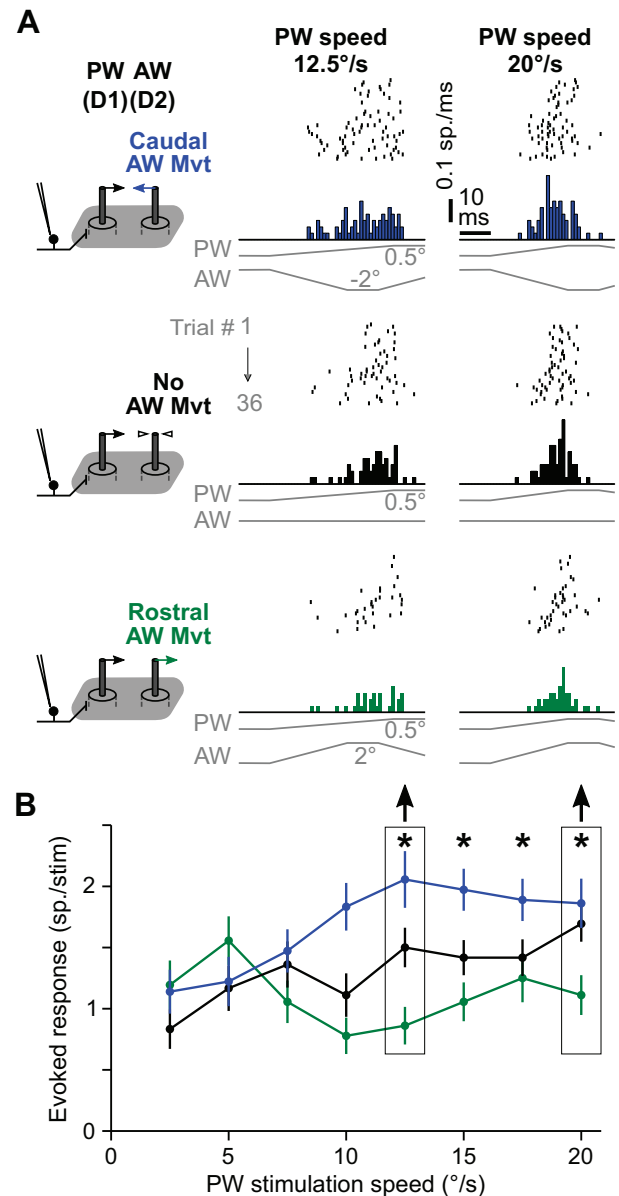


Fig. 6. Mechanical coupling between whiskers can modulate the response of a primary afferent neuron to its principal whisker (PW). A: raster plots and peristimulus time histograms of response of a neuron to rostral deflections of its PW at 2 different speed levels (*left*, 12.5°/s; *right*, 20°/s) while its adjacent whisker (AW) is either deflected caudally (*top* row), not deflected (*middle* row), or deflected rostrally (*bottom* row). B: evoked response (mean \pm SE in time window from start of stimulation to 10 ms after the end of the PW ramp) for 8 speed levels ($n = 36$ trials each). * $P \leq 0.01$, significant effect of AW direction (Welch's unpaired t test).

showed changes in curvature along the whisker shaft (Fig. 7B, *right*), as was observed in the experimental data. The curvature reversed inside the follicle so that the whisker had an inverted S shape inside the follicle and protruded rostrally. When the whisker was free in air, there was only a C-shaped bend inside the follicle.

We were particularly interested in the forces generated inside the follicles, which are the source of the input signals for downstream neural sensory processing. We extracted the contact pressure of the deflected and adjacent whiskers on their follicles, thus obtaining two-dimensional profiles of forces

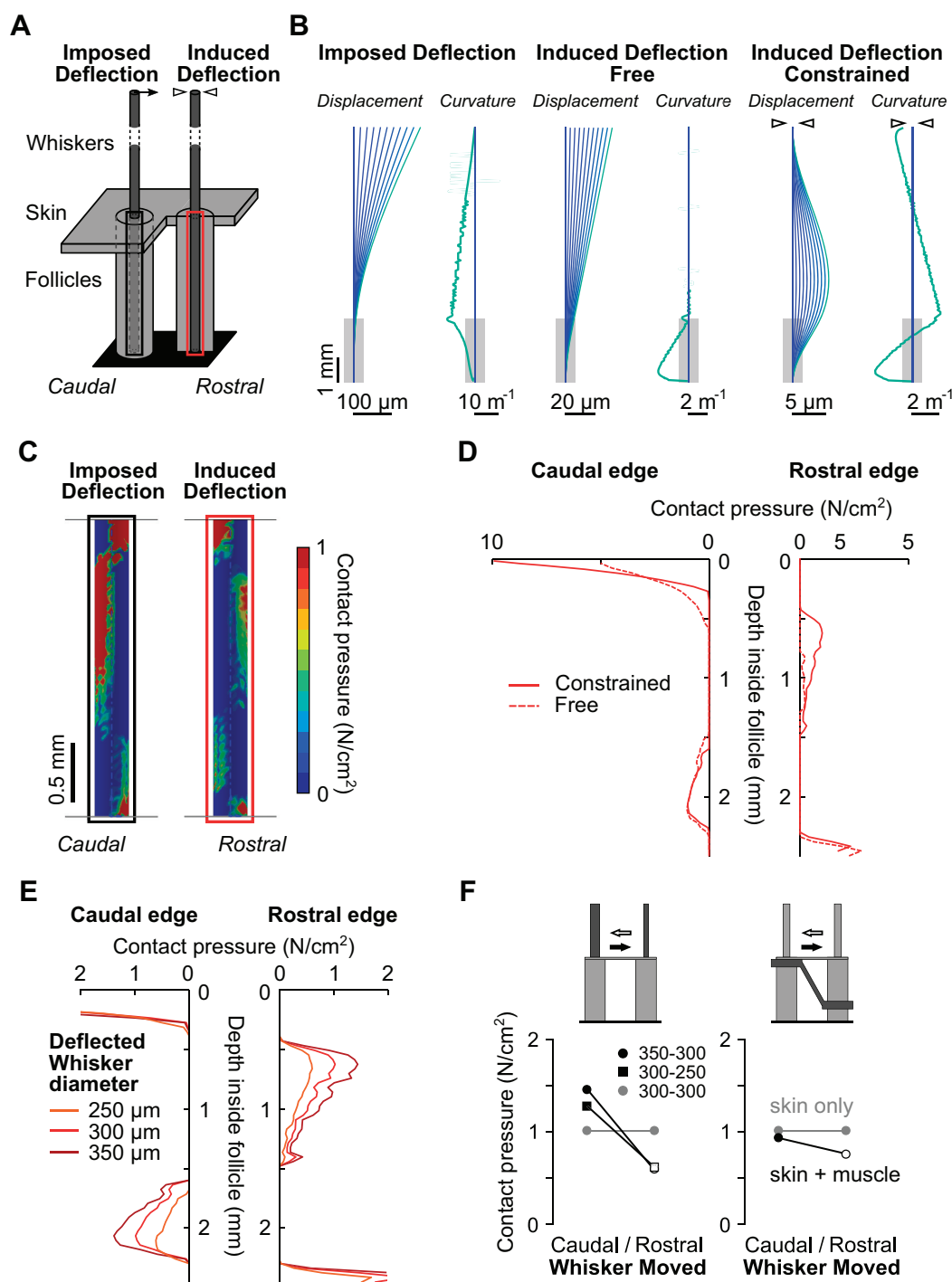


Fig. 7. A simple finite-element model predicts the location of mechanoreceptor activation due to mechanical coupling and the impact of whisker diameter. **A**: schematics of the model. Whiskers are represented as slender cylinders inside the follicles. The base of the whiskers and cylinders is fixed. The skin is modeled by a sheet embedding the top of the follicles. On this schematic, the front right quarter of the model has been removed to show the whisker-follicle arrangement. The *left* whisker is deflected by moving its tip while the *right* whisker is either left free or constrained. Caudal is arbitrarily set to the left. Note that some dimensions have been altered to better show the overall structure. **B**: displacement and curvature along the 2 whiskers. The profiles are shown for 10 deflections of 0.1 to 1°, thus corresponding to experimental profiles of Figs. 1 and 4. Negative curvature corresponds to a C-shaped bend and positive curvature to its mirror image. **C**: snapshot from SolidWorks Simulation of the contact pressure at the whisker-follicle interface, for the deflected whisker (*left*) and the neighbor whisker (*right*). The color scale was adjusted to best show the distribution of pressure; the overall maximum value was 30 N/cm^2 . **D**: contact pressure on the caudal and rostral edges of the whisker-follicle interface for the induced deflection. Solid lines represent the constrained condition, and dashed lines represent the free condition. A 2-point running average was performed to attenuate mesh size artifacts. **E**: same curves as in **D** for the induced deflection in the constrained case, but with the diameter of the deflected whisker varying from 250 to 350 μ m. Note that the contact pressure scale is different than in **D**. **F**, *left*: peak induced contact pressure in the upper middle zone for 3 different combinations of whisker diameters (in μ m). The thicker whisker was always caudal. *Right*: peak induced contact pressure in the upper middle zone for identical 300- μ m whiskers with or without the intrinsic muscle element added to the model.

represented on two cylinders (Fig. 7C). For the whisker that was deflected at its tip in a rostral direction, these forces were distributed in several areas: mainly a rostral zone in the very top part and a large caudal zone in the upper middle (Fig. 7C). This distribution of forces matches the deformation of the whisker toward the front, i.e., the negative curvature in Fig. 7B, left. Functionally, the upper middle zone of the follicle is thought to contain the highest density of mechanoreceptors (Ebara et al. 2017). Our simulation results suggest that they would be activated because of the deflected whisker bending inside the follicle and pushing internally on that zone.

For the neighboring whisker, we further extracted the one-dimensional profiles on the caudal and rostral lines along the cylinder modeling its follicle (Fig. 7D). The distribution of contact forces depended on whether the whisker shaft was let free in air or constrained at the tip. Specifically, when it was in the constrained condition, we obtained contact pressure areas mirroring those of the deflected whisker in the upper part of the follicle, with a reduced amplitude (Fig. 7, C and D). Thus forces were present in a caudal zone at the top and a rostral zone in the upper middle part of the follicle. This distribution matches the S-shaped whisker bending revealed by the displacement and curvature profiles (Fig. 7B).

By contrast, when the nonmanipulated whisker was let free in air, the middle rostral zone of positive contact pressure largely disappeared (Fig. 7D). This corresponds to the whisker bending smoothly toward the front (Fig. 7B). The top caudal zone was still present, but contact forces were smaller. Overall, this result confirms that the free and constrained conditions indeed lead to different distributions of forces inside the follicle, and thus potentially to different ensembles of activated mechanoreceptors. In the following, we focus on the constrained condition and on contact pressure values in the upper middle zone of the follicle, given its importance in coding whisker deflections.

Note that if the imposed deflection is applied in the opposite direction, i.e., caudally, the displacement, curvature, and distribution of forces of the deflected and induced whisker-follicle ensembles are essentially symmetric to the rostral case. The mechanical coupling strength between the two whiskers is thus independent of the direction of stimulation, as in the videography experiments (Fig. 2A).

Using this simple model, we tested the causal link between whisker diameter and the amplitude of mechanical coupling. We increased or decreased the whisker diameter by $\sim 17\%$ ($50\ \mu\text{m}$), which is in the range of whisker diameter differences between neighbors in a row of the whisker pad. When we modified the diameter of the deflected whisker while keeping the neighboring whisker diameter at $300\ \mu\text{m}$, the peak contact pressure inside the follicle varied by 40–45% (Fig. 7E). The curvature along the whisker changed little ($350\ \mu\text{m}$: 7% decrease; $250\ \mu\text{m}$: 15% increase). However, the whisker stiffness was almost doubled for the $350\text{-}\mu\text{m}$ whisker, and conversely halved for the $250\text{-}\mu\text{m}$ whisker. The bending moment and whisker-follicle forces were thus largely governed by the whisker diameter via the change in stiffness. This result confirms from a biomechanical point of view that the whisker diameter could indeed be a major factor in mechanical coupling effects.

We quantified the asymmetry created by these differences in diameter by the peak contact pressure in the upper middle zone

(Fig. 7F, left). We found that when the thicker whisker of an asymmetric pair was deflected, it induced a peak contact pressure in the neighboring follicle two times larger than when the thinner whisker was deflected. This ratio is in the range of what has been measured experimentally on induced deflections (Fig. 3B, mean change in angle 0.077° vs. 0.042° , $n = 14$ whisker pairs). Additionally, we observed in the model that the deflection of a whisker of $300\text{-}\mu\text{m}$ diameter had a stronger effect on a $250\text{-}\mu\text{m}$ neighbor than on a $350\text{-}\mu\text{m}$ neighbor (contact pressure 1.26 vs. $0.60\ \text{N/cm}^2$; Fig. 7F, left, closed square vs. open circle), thus reproducing the asymmetric results of Fig. 3C for a given deflected whisker. We conclude from these simulations that the distribution of mechanical coupling strength observed in the experiments, as well as the rostrocaudal asymmetry, can be fully explained by the gradient of whisker diameter.

Certainly, other elements of the model could be modified to study their impact on the mechanical coupling and its anisotropy. Increasing the follicle diameter tended to reduce coupling, probably because of increased mechanical absorption by the follicle. Increasing whisker spacing from 2 to 5 mm had very little effect (6% decrease in peak contact pressure).

Given that these geometrical parameters could not explain the mechanical coupling anisotropies, we then sought to test the impact of the different muscles of the whisker pad. Extrinsic muscles in the model were part of the skin volume. We found that modifying the skin thickness had little effect ($<3\%$ for twice the thickness), even when a 2:1 thickness gradient was created along the rostrocaudal axis. On the other hand, doubling Young's modulus of the skin material increased the peak contact pressure by 60%. Interestingly, it did not change the distribution of the contact forces inside the follicle. Indeed, this distribution is essentially governed by the boundary conditions at both ends of the whisker and can be changed by modifying those boundaries, as in the free vs. constrained conditions (Fig. 7, B and D). Overall, these results from investigation of skin parameters suggest that a gradient of skin stiffness might contribute to the caudo-rostral gradient of mechanical coupling observed in the experiments.

Finally, we modeled the intrinsic muscle by a stiff oblique rod connecting two rings placed around the follicles (Fig. 7F, right). The presence of this asymmetric element created an asymmetry of coupling between the two whiskers while decreasing both values. Although the real intrinsic muscle is likely to be weaker than modeled here, this result suggests it could participate to the mechanical coupling asymmetry between whiskers.

From this simple model, we conclude that the gradient of mechanical coupling observed in the videography and electrophysiology experiments could be explained largely by the gradient in whisker diameter, with a possible contribution of the intrinsic muscles connecting the follicles.

DISCUSSION

In this study, we show that deflection of a single whisker on the rat snout is accompanied by measurable movements of neighboring whiskers. Moreover, if the deflection is sufficiently strong, it evokes spiking activity in primary afferent neurons innervating the follicles of neighboring whiskers. We use a simple mechanical model to show how transmission of

mechanical forces through the skin is responsible for this cross-whisker interaction.

Characteristics of Mechanical Coupling and Possible Underlying Mechanisms

Both our videography and electrophysiology results emphasized intra-row interactions relative to intra-arc ones (Figs. 2*B* and 5*B*). This could be due to the particular direction of our stimuli, along the rostrocaudal axis (see *Methodological Considerations*). This bias could also arise from the presence of intrinsic muscles between adjacent follicles in a row (Dörfl 1982; Haidarliu et al. 2010), responsible for pivoting the whisker around the follicle entry during whisking protraction. Recently, several laboratories reported the presence of additional oblique intrinsic muscles further connecting follicles along rows (Grant et al. 2013, 2017; Haidarliu et al. 2017). Together, these intrinsic muscles likely increase the stiffness of the skin particularly along the rostrocaudal direction, thus favoring the transmission of movements and forces along rows compared with arcs. Interestingly, intrinsic muscles can connect a straddler to both anterior follicles (Dörfl 1982), a pattern corresponding to the interaction of straddlers with both neighbors in our electrophysiological data (Fig. 5*B*).

A second striking result concerns the spatial distribution of mechanical coupling across the whisker pad. We found that effects were largely biased to the caudal half of the whisker pad, with an additional ventral emphasis especially in the electrophysiological data (Figs. 3*D* and 5*B*). These results have led us to hypothesize that the size of the whisker, known to exhibit a strong caudoventral bias (Belli et al. 2017), could be an important factor governing the amplitude of mechanical coupling. In fact, many biomechanical studies assume the whisker diameter to be the only parameter distinguishing one whisker from another when describing the preneuronal transformation of contact events into forces at the follicle entry (Boubenec et al. 2012; Carvell and Simons 2017; Oladazimi et al. 2018; Quist and Hartmann 2012). Indeed, the hypothesis that mechanical coupling varies due to the gradient of the deflected whisker diameter seems the most parsimonious interpretation of our data. Interestingly, the dependence on the deflected whisker diameter was very strong in the biomechanical simulations, whereas the model was constructed and calibrated without this test in mind. Increasing the diameter of the whisker by ~17%, as is found between neighbors in a row, increases its stiffness by 85%, according to the power law with exponent 4 applying to a cantilevered beam. An identical displacement at the tip thus requires a much larger bending moment and induces larger contact forces between the whisker and the follicle (Fig. 7*E*). The whisker diameter gradient could thus account for the overall spatial distribution of the cross-whisker coupling effect on the snout.

To definitively establish whisker diameter as a main factor in shaping the gradient of mechanical coupling on the whisker pad, several concerns will need to be addressed. First, the expected ventral bias was not clear in our videography data. Unfortunately, we could not test all combinations of deflected and imaged whiskers (see *Methodological Considerations*).

Second, the distribution of coupling effects revealed in the electrophysiology experiments necessarily includes a recording bias. In the TG, the number of neurons innervating large

whisker follicles is higher than for small whiskers (Welker and Van der Loos 1986; Zucker and Welker 1969). There could also be a systematic bias in our electrode location in the ganglion, which is known to be loosely topographically organized (Leiser and Moxon 2006). Nonetheless, the strong caudoventral gradient suggests predominant mechanical coupling effects in that part of the pad. Note that we do not rule out the possibility that mechanical coupling could potentially influence the firing of any whisker-sensitive TG neuron, provided a neighbor whisker is deflected with sufficiently high magnitude.

In addition to the spatial gradient, for a given whisker combination, we found an asymmetry favoring mechanical coupling from the caudal to its immediately rostral neighbor, compared with the opposite sequence (Fig. 3*B*). We will consider several possible sources of this asymmetry. First, the systematic gradient in whisker diameter across the pad can suffice to explain a strong asymmetry in coupling inside a given whisker pair, as confirmed by the model simulations (Fig. 7, *E* and *F*). This gradient can also explain that deflecting a fixed whisker affects differently its two neighbors (Fig. 3*C*), because the mechanical coupling strength is clearly dependent on the whisker diameter of the neighbor (Fig. 7*F*, *left*). Thus the rostral vs. caudal asymmetry observed in the experimental data can be fully explained by the gradient in whisker diameter across the pad.

Another factor that could play a role in the asymmetry of the mechanical coupling is the intrinsic muscle between follicles. As mentioned already, this muscle is attached to the superficial part of the caudal follicle and skin, and to the deep part of the rostral follicle. We have investigated the potential asymmetric mechanical effects resulting from this diagonal muscle by adding it to the biomechanical model as a rod connecting the follicles. We found that it could create an asymmetry favoring stronger coupling from the caudal whisker while at the same time reducing the overall values (Fig. 7*F*, *right*). Note that in the simulations, we chose to use the same material for the intrinsic muscle as for the skin and follicles, even though the real muscle is likely to be much less stiff than the tough, protective skin layer on the snout. The effect of the intrinsic muscle is thus probably largely overestimated in the model. Overall, we conclude that the intrinsic muscle could contribute to the asymmetry in cross-whisker effects but that it has probably much less influence than whisker diameter.

Other factors beyond whisker diameters and intrinsic muscles could contribute to the amplitude of mechanical coupling and to its asymmetry. For example, the size of follicle elements and surrounding muscles vary in a systematic way, correlated with the average whisker diameter (Haidarliu et al. 2010), and are likely to influence the transmission of forces from one whisker-follicle to another. The superficial extrinsic muscles maxillolabialis and nasolabialis probably stiffen the pad and could thus increase mechanical coupling and its asymmetry, in particular when the muscle tone is high, such as in the active exploring state. Moreover, because there are more fibers in the caudal section of the pad, the extrinsic muscles could contribute to the gradient that we observed. The nasolabialis fibers extending from the dorsocaudal region could particularly enhance mechanical coupling in that region compared with the ventrocaudal gradient expected from the gradient in whisker diameter.

Our simulations suggested that the size of the follicles and the skin thickness were unlikely to explain the mechanical coupling distribution but that the stiffness of the skin layer could be important. This opens the possibility that the tone of the extrinsic muscles could have a significant impact. A more detailed model could be built to study specifically the effect of the different whisker pad elements. It could include variations in whisker taper and whisker low-density core (medulla), which recently were shown to vary across the pad, beyond the expected variations of length and diameter (Belli et al. 2017). Finally, in addition to these established gradients, an important source of variability could arise from the current phase of the whisker in the growth cycle, affecting directly its size (Ibrahim and Wright 1975).

Distribution of Forces Activating Mechanoreceptors

The biomechanical model was constructed to qualitatively bridge the gap between external whisker deformations and spiking activity in primary afferent neurons. We included only one element per whisker and follicle, embedded in a skin sheet. Minimal calibration was necessary to produce induced deformations compatible with experimental measures. With this simple model, the whisker shaft, when deflected, compresses the leading edge of the top of the follicle, as well as the trailing edge at a deeper location because of internal bending. This agrees with a recent *ex vivo* study (Whiteley et al. 2015) describing a distribution of strain along the depth of the follicle in which compression and dilation zones alternate. When the neighboring whisker is constrained at its tip, induced contact forces on its follicle adopt a mirror configuration with a smaller amplitude (Fig. 7C). As a consequence, a mechanoreceptor located in a zone of compression for an imposed deflection of its principal whisker will be best stimulated if the adjacent whisker is deflected in the opposite direction. Indeed, in most (12/14) TG neurons, we observed that the preferred direction of deflection for the adjacent whisker was opposite to the preferred direction for the principal whisker (Fig. 5).

The density of mechanoreceptors is highest in the top half of the follicle, and more specifically in the ring sinus region (Ebara et al. 2017). In a recent study combining anatomical and functional characterization, the most numerous and most responsive TG neurons were found to be those terminating with clublike endings in the ring sinus region. These terminals are particularly suited to encode a specific direction of movement (Tonomura et al. 2015). This class of mechanoreceptors has previously been underestimated because of their tiny axonal endings, easily mistaken as cut axons. Interestingly, our model does predict contact forces in this region induced by deflection of an adjacent whisker, particularly when the principal whisker is constrained (Fig. 7).

In this respect, we have systematically explored two different conditions in the experiments and the model: the free and constrained conditions. It is interesting to note that constraining the neighboring whisker led to increased curvature changes along the shaft and, at the same time, to increased responses in the putative mechanoreceptors of the associated follicle. This is in line with the idea that the rotational moment at the base of the whisker, known to be proportional to the curvature, is indeed what is encoded by mechanoreceptors, in both the passive and active states (Campagner et al. 2016; Quist and

Hartmann 2012). The model simulations, by illustrating the distribution of forces inside the follicle, offer a mechanistic explanation. When the whisker is constrained, a large contact pressure zone is present in the ring sinus region, compared with the free condition (Fig. 7C). Thus the model confirms that the external forces on the whisker produce a bending moment along the shaft that causes pressure forces in a specific localized zone of the follicle. Mechanoreceptors terminating in this zone are activated, encoding directional and amplitude information about the deflection event.

Functional Relevance

Our results imply that the skin tissue and muscles making up the whisker pad transmit forces between follicles and that this additional force field can, depending on its direction, either counteract or augment the ongoing forces due to external events on the whisker shaft. It brings forward a theory that has already been proposed, namely, that the whisker system, despite its discreteness, could function as a continuous sensory organ just as the skin does (Simons 1995).

From a practical point of view, our results imply that there can be no pure single-whisker movement, because the biomechanical forces move all elements of the pad (muscles, follicles, whiskers) in an automatic fashion. These induced deformations could reach up to 10–20% in our experimental conditions. Their impact on sensory processing should be considered. It has been shown that the most sensitive primary afferents respond to extremely small deflections of amplitude less than 0.01° , and one-third of all afferents have a velocity threshold below $3^\circ/\text{s}$ (Gibson and Welker 1983). For very small single-whisker deflections, only a handful of TG neurons spike action potentials, and all these neurons are likely to innervate the deflected whisker, conforming to the labeled line hypothesis. When deflection parameters increase, more and more mechanoreceptors are activated, including some with low thresholds located in surrounding follicles. Upstream, we thus expect some amount of divergence of the sensory signal from a single whisker to TG neurons innervating other whiskers, and further, to surrounding barrelettes. This divergence will of course depend on the particular whisker considered, and we propose that the whisker diameter is an important parameter of the extent of this spatial spread.

During stimulation of several whiskers overlapping in time, our results suggest that modulation of responses to the principal whisker by the simultaneous deflection of surrounding whiskers is also already present at the TG level. The example neuron of Fig. 6 shows that even for very low deflection values, mechanical coupling can modify responses to external events occurring on the principal whisker. As confirmed by the model, even low deflections modulate the distribution of forces present in neighboring follicles. When two deflections occur at the same time, forces inside the follicles will be enhanced for opposite directions of movement or, on the contrary, attenuated. Functionally, these ongoing mechanical effects could for example emphasize detection of surfaces tending to bring whiskers together, such as corners.

In our view, this peripheral cross-whisker interaction can be thought of as a first nonlinearity in the information processing pathway, before the other known nonlinearities at the trigeminal nuclei, thalamic, and cortical levels. Several laboratories,

including our own, have reported that cortical neurons are able to extract multiwhisker features of tactile scenes (review in Estebanez et al. 2018), suggesting that cortical neuronal tuning could underlie the ability of animals to identify relevant perceptual features. The existence of multiwhisker interactions within the whisker pad does not contradict these findings. Rather, it confirms that multiwhisker integration starts already before the cortex. In other words, we need to be careful about claiming that nonlinearities observed in the cortex are not already present at a subcortical or even peripheral level. Such mechanisms have been known to exist for a long time in the trigeminal nuclei (Minnery and Simons 2003; Timofeeva et al. 2004) and also have been described in the thalamus, including the extraction of high-order features such as global apparent motion (Ego-Stengel et al. 2012). In this last study, multiwhisker selectivity was shown to be present in the thalamus, but to a lesser extent than in the cortex, and to be amplified at the cortical level. Our current view on tactile processing mechanisms is that intracortical circuitry builds an additional layer of computation that uses the results of nonlinearities in the previous stages of the system to transform the tactile signals further. Future experiments should help to understand the precise role of each of these stages.

Methodological Considerations

Following the description of a single case of cross-whisker spiking response in a TG neuron (Simons 1985), this is the first study directly investigating mechanical coupling between whiskers and its consequences on neuronal encoding of tactile information. In most laboratories, including our own, only relatively low-amplitude, low-speed stimuli are routinely implemented. Indeed, a known limitation of piezoelectric stimulators, widely used in the field, is that high-velocity stimuli quickly produce ringing (Jacob et al. 2010), thereby constraining their useful range. In the summary drawn by Ritt and collaborators (2008), they concluded that the highest speed explored in electrophysiological studies across laboratories was 2,500°/s, and the highest amplitude of deflection was 3°. In the present study, we raised the deflection amplitude to 3° or more, and the speed up to 4,000°/s, to reveal direct mechanical cross-whisker effects on neurons. These parameters could only be achieved by placing the stimulator close to the whisker base, a procedure performed very carefully under the microscope to touch neither the fur nor a neighboring whisker or stimulator.

The use of high-resolution videography allowed us to track the profile of whiskers with extreme precision, below 1 μm and at 1 kHz, using minimal image processing. We quantified mechanical coupling effects in a systematic way by measuring the deformation profile of whiskers. We only imaged whiskers for which the shaft was relatively horizontal, thus in focus along its length, and unobstructed by bulging of the pad or by excessive fur. Future experiments could take advantage of new cameras that are more compact and easier to position with different angles around the animal, potentially allowing tracking of all macrovibrissae.

The experiments were performed on an anesthetized preparation to ensure stable conditions and full control of the stimulus. Assessing the magnitude of cross-whisker coupling in awake behaving animals will be particularly challenging. Animals will have to be trained, for example, by head fixation,

to enable high-resolution imaging of their whiskers. Importantly, the awake preparation will introduce multiple factors that can influence the state of the follicles and that will require monitoring. The baseline tonus of skin muscles involved in the whisker array positioning is likely to be larger in the awake animal, possibly transmitting mechanical energy more efficiently across follicles. By using anesthesia, we may in fact have underestimated the coupling effect. Electromyographic recordings have further shown that the pad muscles are tightly regulated by a feedback loop triggered by whisker contact (Bellavance et al. 2017; Nguyen and Kleinfeld 2005). Accompanying changes in the pressure inside the follicle blood sinus could affect the receptors dynamic range of encoding. The magnitude of cross-whisker coupling is thus likely to vary continuously during the awake state, even in a passive condition.

When animals explore their environment, they actively move their whiskers in a coordinated way, including whisking but also asymmetric behaviors (Grant et al. 2009; Sofroniew and Svoboda 2015). The activation of the pad musculature controls rostrocaudal translation of follicles, along with the protraction of individual whiskers and more subtle deformations (pad bulging, whisker torsion, etc.). In our study, we have purposefully avoided these internally generated movements and focused on mechanical coupling effects at rest, extracting whisker profile deviations from a stable baseline. In an active animal, evaluating the impact of cross-whisker effects will require an analysis that can disentangle the movements due to active behavior from the movements due to skin coupling. We hypothesize that the passive mechanical coupling effects that we have described add to the underlying global movements of the different structures of the whisker pad. Thus an external touch on one whisker will modify the trajectory of that whisker but also that of neighboring whiskers relative to what it would have been without that touch. How this superposition of internally and externally generated deformations of follicles and whiskers translates into patterns of mechanoreceptor activation will have to be investigated in future studies.

ACKNOWLEDGMENTS

We thank Camila Pulido and David Davila for contributions to early whisker tracking and electrophysiology experiments. We are grateful to the whole Shulz laboratory for advice throughout the project, to Evan Harrell for comments on the manuscript, and to Yannick Passarelli for help finalizing the submission. We thank Guillaume Hucher for measuring whisker parameters and for trigeminal ganglion histology, and Aurélie Daret for help with animal experiments and general laboratory managing.

Present address of Y. Boubenec: Laboratoire des Systèmes Perceptifs, Département d'Etudes Cognitives, École Normale Supérieure, 29 rue d'Ulm, 75005 Paris, France.

GRANTS

This work was supported by International Human Frontier Science Program Organization Grant CDA 00044-2010, Agence Nationale de la Recherche (ANR) Grant NeuroWhisk ANR-14-CE24-0019-01, Equipe Fondation de la Recherche Médicale Grant DEQ20170336761, Paris-Saclay University (Lidex iCODE), and IDEX NeuroSaclay Grant ANR-11-IDEX-0003-02.

DISCLOSURES

No conflicts of interest, financial or otherwise, are declared by the authors.

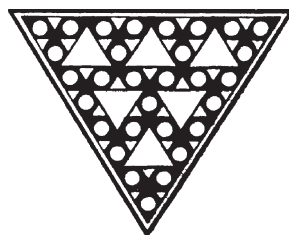
AUTHOR CONTRIBUTIONS

V.E.-S. and D.E.S. conceived and designed research; V.E.-S., A.A., M.L., and Y.B. performed experiments; V.E.-S., A.A., M.L., H.L., and Y.B. analyzed data; V.E.-S. interpreted results of experiments; V.E.-S. and H.L. prepared figures; V.E.-S. drafted manuscript; A.A., M.L., Y.B., and D.E.S. approved final version of manuscript; H.L. and D.E.S. edited and revised manuscript.

REFERENCES

- Arnold PB, Li CX, Waters RS. Thalamocortical arbors extend beyond single cortical barrels: an in vivo intracellular tracing study in rat. *Exp Brain Res* 136: 152–168, 2001. doi:10.1007/s002210000570.
- Axelrad H, Verley R, Farkas E. Responses evoked in mouse and rat SI cortex by vibrissa stimulation. *Neurosci Lett* 3: 265–274, 1976. doi:10.1016/0304-3940(76)90053-7.
- Bagdasarian K, Szwed M, Knutsen PM, Deutsch D, Derdikman D, Pietr M, Simony E, Ahissar E. Pre-neuronal morphological processing of object location by individual whiskers. *Nat Neurosci* 16: 622–631, 2013. doi:10.1038/nn.3378.
- Bellavance MA, Takatoh J, Lu J, Demers M, Kleinfeld D, Wang F, Deschênes M. Parallel inhibitory and excitatory trigemino-facial feedback circuitry for reflexive vibrissa movement. *Neuron* 95: 673–682.e4, 2017. [Erratum in *Neuron* 95: 722–723, 2017.] doi:10.1016/j.neuron.2017.06.045.
- Belli HM, Yang AE, Breese CS, Hartmann MJ. Variations in vibrissal geometry across the rat mystacial pad: base diameter, medulla, and taper. *J Neurophysiol* 117: 1807–1820, 2017. doi:10.1152/jn.00054.2016.
- Bernardo KL, McCasland JS, Woolsey TA. Local axonal trajectories in mouse barrel cortex. *Exp Brain Res* 82: 247–253, 1990. doi:10.1007/BF00231244.
- Boubenec Y, Clavier LN, Shulz DE, Debréas G. An amplitude modulation/demodulation scheme for whisker-based texture perception. *J Neurosci* 34: 10832–10843, 2014. doi:10.1523/JNEUROSCI.0534-14.2014.
- Boubenec Y, Shulz DE, Debréas G. Whisker encoding of mechanical events during active tactile exploration. *Front Behav Neurosci* 6: 74, 2012. doi:10.3389/fnbeh.2012.00074.
- Campagner D, Evans MH, Bale MR, Erskine A, Petersen RS. Prediction of primary somatosensory neuron activity during active tactile exploration. *eLife* 5: e10696, 2016. doi:10.7554/eLife.10696.
- Carl K, Hild W, Mämpel J, Schilling C, Uhlig R, Witte H. Characterization of static properties of rat's whisker system. *IEEE Sens J* 12: 340–349, 2012. doi:10.1109/ISEN.2011.2114341.
- Carvell GE, Simons DJ. Task- and subject-related differences in sensorimotor behavior during active touch. *Somatosens Mot Res* 12: 1–9, 1995. doi:10.3109/08990229509063138.
- Carvell GE, Simons DJ. Effect of whisker geometry on contact force produced by vibrissae moving at different velocities. *J Neurophysiol* 118: 1637–1649, 2017. doi:10.1152/jn.00046.2017.
- Deschênes M, Urbain N. Vibrissal afferents from trigeminal to cortices. *Scholarpedia* 4: 7454, 2009. doi:10.4249/scholarpedia.7454.
- Dörfel J. The musculature of the mystacial vibrissae of the white mouse. *J Anat* 135: 147–154, 1982.
- Dykes RW. Afferent fibers from mystacial vibrissae of cats and seals. *J Neurophysiol* 38: 650–662, 1975. doi:10.1152/jn.1975.38.3.650.
- Ebara S, Furuta T, Kumamoto K. Vibrissal mechanoreceptors. *Scholarpedia* 12: 32372, 2017. doi:10.4249/scholarpedia.32372.
- Ebara S, Kumamoto K, Matsuura T, Mazurkiewicz JE, Rice FL. Similarities and differences in the innervation of mystacial vibrissal follicle-sinus complexes in the rat and cat: a confocal microscopic study. *J Comp Neurol* 449: 103–119, 2002. doi:10.1002/cne.10277.
- Ego-Stengel V, Le Cam J, Shulz DE. Coding of apparent motion in the thalamic nucleus of the rat vibrissal somatosensory system. *J Neurosci* 32: 3339–3351, 2012. doi:10.1523/JNEUROSCI.3890-11.2012.
- Estebanez L, Férézou I, Ego-Stengel V, Shulz DE. Representation of tactile scenes in the rodent barrel cortex. *Neuroscience* 368: 81–94, 2018. doi:10.1016/j.neuroscience.2017.08.039.
- Gibson JM, Welker WL. Quantitative studies of stimulus coding in first-order vibrissa afferents of rats. 1. Receptive field properties and threshold distributions. *Somatosens Res* 1: 51–67, 1983. doi:10.3109/07367228309144540.
- Gottschaldt KM, Iggo A, Young DW. Functional characteristics of mechanoreceptors in sinus hair follicles of the cat. *J Physiol* 235: 287–315, 1973. doi:10.1113/jphysiol.1973.sp010388.
- Grant RA, Delaunay MG, Haidarliu S. Mystacial whisker layout and musculature in the guinea pig (*Cavia porcellus*): a social, diurnal mammal. *Anat Rec (Hoboken)* 300: 527–536, 2017. doi:10.1002/ar.23504.
- Grant RA, Haidarliu S, Kennerley NJ, Prescott TJ. The evolution of active vibrissal sensing in mammals: evidence from vibrissal musculature and function in the marsupial opossum *Monodelphis domestica*. *J Exp Biol* 216: 3483–3494, 2013. doi:10.1242/jeb.087452.
- Grant RA, Mitchinson B, Fox CW, Prescott TJ. Active touch sensing in the rat: anticipatory and regulatory control of whisker movements during surface exploration. *J Neurophysiol* 101: 862–874, 2009. doi:10.1152/jn.90783.2008.
- Haidarliu S. An anatomically adapted, injury-free headholder for guinea pigs. *Physiol Behav* 60: 111–114, 1996. doi:10.1016/0031-9384(95)02257-0.
- Haidarliu S, Bagdasarian K, Shinde N, Ahissar E. Muscular basis of whisker torsion in mice and rats. *Anat Rec (Hoboken)* 300: 1643–1653, 2017. doi:10.1002/ar.23623.
- Haidarliu S, Simony E, Golomb D, Ahissar E. Muscle architecture in the mystacial pad of the rat. *Anat Rec (Hoboken)* 293: 1192–1206, 2010. doi:10.1002/ar.21156.
- Hartmann MJ, Johnson NJ, Towal RB, Assad C. Mechanical characteristics of rat vibrissae: resonant frequencies and damping in isolated whiskers and in the awake behaving animal. *J Neurosci* 23: 6510–6519, 2003. doi:10.1523/JNEUROSCI.23-16-06510.2003.
- Hobbs JA, Towal RB, Hartmann MJ. Spatiotemporal patterns of contact across the rat vibrissal array during exploratory behavior. *Front Behav Neurosci* 9: 356, 2016. doi:10.3389/fnbeh.2015.00356.
- Ibrahim L, Wright EA. The growth of rats and mice vibrissae under normal and some abnormal conditions. *J Embryol Exp Morphol* 33: 831–844, 1975.
- Jacob V, Estebanez L, Le Cam J, Tiercelin JY, Parra P, Parésys G, Shulz DE. The Matrix: a new tool for probing the whisker-to-barrel system with natural stimuli. *J Neurosci Methods* 189: 65–74, 2010. doi:10.1016/j.jneumeth.2010.03.020.
- Jacquin MF, Chiaia NL, Haring JH, Rhoades RW. Intersubnuclear connections within the rat trigeminal brainstem complex. *Somatosens Mot Res* 7: 399–420, 1990. doi:10.3109/08990229009144716.
- Kim JN, Koh KS, Lee E, Park SC, Song WC. The morphology of the rat vibrissal follicle-sinus complex revealed by three-dimensional computer-aided reconstruction. *Cells Tissues Organs* 193: 207–214, 2011. doi:10.1159/000319394.
- Knutsen PM, Pietr M, Ahissar E. Haptic object localization in the vibrissal system: behavior and performance. *J Neurosci* 26: 8451–8464, 2006. doi:10.1523/JNEUROSCI.1516-06.2006.
- Krupa DJ, Matell MS, Brisben AJ, Oliveira LM, Nicolelis MA. Behavioral properties of the trigeminal somatosensory system in rats performing whisker-dependent tactile discriminations. *J Neurosci* 21: 5752–5763, 2001. doi:10.1523/JNEUROSCI.21-15-05752.2001.
- Lavallée P, Deschênes M. Dendroarchitecture and lateral inhibition in thalamic barrelloids. *J Neurosci* 24: 6098–6105, 2004. doi:10.1523/JNEUROSCI.0973-04.2004.
- Leiser SC, Moxon KA. Relationship between physiological response type (RA and SA) and vibrissal receptive field of neurons within the rat trigeminal ganglion. *J Neurophysiol* 95: 3129–3145, 2006. doi:10.1152/jn.00157.2005.
- Ma PM, Woolsey TA. Cytoarchitectonic correlates of the vibrissae in the medullary trigeminal complex of the mouse. *Brain Res* 306: 374–379, 1984. doi:10.1016/0006-8993(84)90390-1.
- Minnery BS, Simons DJ. Response properties of whisker-associated trigeminothalamic neurons in rat nucleus principalis. *J Neurophysiol* 89: 40–56, 2003. doi:10.1152/jn.00272.2002.
- Narayanan RT, Egger R, Johnson AS, Mansvelder HD, Sakmann B, de Kock CP, Oberlaender M. Beyond columnar organization: cell type- and target layer-specific principles of horizontal axon projection patterns in rat vibrissal cortex. *Cereb Cortex* 25: 4450–4468, 2015. doi:10.1093/cercor/bhv053.
- Neimark MA, Andermann ML, Hopfield JJ, Moore CI. Vibrissa resonance as a transduction mechanism for tactile encoding. *J Neurosci* 23: 6499–6509, 2003. doi:10.1523/JNEUROSCI.23-16-06499.2003.
- Nguyen QT, Kleinfeld D. Positive feedback in a brainstem tactile sensorimotor loop. *Neuron* 45: 447–457, 2005. doi:10.1016/j.neuron.2004.12.042.
- Oladazimi M, Brendel W, Schwarz C. Biomechanical texture coding in rat whiskers. *Sci Rep* 8: 11139, 2018. doi:10.1038/s41598-018-29225-9.
- Quist BW, Hartmann MJ. Mechanical signals at the base of a rat vibrissa: the effect of intrinsic vibrissa curvature and implications for tactile exploration. *J Neurophysiol* 107: 2298–2312, 2012. doi:10.1152/jn.00372.2011.
- Ritt JT, Andermann ML, Moore CI. Embodied information processing: vibrissa mechanics and texture features shape micromotions in actively sensing rats. *Neuron* 57: 599–613, 2018. doi:10.1016/j.neuron.2007.12.024.

- Schneider JS, Denaro FJ, Olazabal UE, Leard HO.** Stereotaxic atlas of the trigeminal ganglion in rat, cat, and monkey. *Brain Res Bull* 7: 93–95, 1981. doi:[10.1016/0361-9230\(81\)90103-9](https://doi.org/10.1016/0361-9230(81)90103-9).
- Sherman D, Oram T, Harel D, Ahissar E.** Attention robustly gates a closed-loop touch reflex. *Curr Biol* 27: 1836–1843.e7, 2017. doi:[10.1016/j.cub.2017.05.058](https://doi.org/10.1016/j.cub.2017.05.058).
- Simons DJ.** Response properties of vibrissa units in rat SI somatosensory neocortex. *J Neurophysiol* 41: 798–820, 1978. doi:[10.1152/jn.1978.41.3.798](https://doi.org/10.1152/jn.1978.41.3.798).
- Simons DJ.** Temporal and spatial integration in the rat SI vibrissa cortex. *J Neurophysiol* 54: 615–635, 1985. doi:[10.1152/jn.1985.54.3.615](https://doi.org/10.1152/jn.1985.54.3.615).
- Simons DJ.** Neuronal integration in the somatosensory whisker/barrel cortex. In: *The Barrel Cortex of Rodents*. Cerebral Cortex, edited by Jones EG, Diamond IT. Boston, MA: Springer, 1995, vol. 11, p. 263–297. doi:[10.1007/978-1-4757-9616-2_6](https://doi.org/10.1007/978-1-4757-9616-2_6).
- Sofroniew NJ, Svoboda K.** Whisking. *Curr Biol* 25: R137–R140, 2015. doi:[10.1016/j.cub.2015.01.008](https://doi.org/10.1016/j.cub.2015.01.008).
- Solomon JH, Hartmann MJ.** Biomechanics: robotic whiskers used to sense features. *Nature* 443: 525, 2006. doi:[10.1038/443525a](https://doi.org/10.1038/443525a).
- Timofeeva E, Lavallée P, Arsenault D, Deschênes M.** Synthesis of multi-whisker-receptive fields in subcortical stations of the vibrissa system. *J Neurophysiol* 91: 1510–1515, 2004. doi:[10.1152/jn.01109.2003](https://doi.org/10.1152/jn.01109.2003).
- Tonomura S, Ebara S, Bagdasarian K, Uta D, Ahissar E, Meir I, Lampl I, Kuroda D, Furuta T, Furue H, Kumamoto K.** Structure-function correlations of rat trigeminal primary neurons: Emphasis on club-like endings, a vibrissal mechanoreceptor. *Proc Jpn Acad Ser B Phys Biol Sci* 91: 560–576, 2015. doi:[10.2183/pjab.91.560](https://doi.org/10.2183/pjab.91.560).
- Van Der Loos H.** Barreloids in mouse somatosensory thalamus. *Neurosci Lett* 2: 1–6, 1976. doi:[10.1016/0304-3940\(76\)90036-7](https://doi.org/10.1016/0304-3940(76)90036-7).
- Vincent S.** The tactile hair of the white rat. *J Comp Neurol* 23: 1–36, 1913. doi:[10.1002/cne.900230101](https://doi.org/10.1002/cne.900230101).
- Voges D, Carl K, Klauer GJ, Uhlig R, Schilling C, Behn C, Witte H.** Structural characterization of the whisker system of the rat. *IEEE Sens J* 12: 332–339, 2012. doi:[10.1109/JSEN.2011.2161464](https://doi.org/10.1109/JSEN.2011.2161464).
- Voisin DL, Doméjean-Orliaguet S, Chalus M, Dallel R, Woda A.** Ascending connections from the caudal part to the oral part of the spinal trigeminal nucleus in the rat. *Neuroscience* 109: 183–193, 2002. doi:[10.1016/S0306-4522\(01\)00456-0](https://doi.org/10.1016/S0306-4522(01)00456-0).
- Welker E, Van der Loos H.** Quantitative correlation between barrel-field size and the sensory innervation of the whiskerpad: a comparative study in six strains of mice bred for different patterns of mystacial vibrissae. *J Neurosci* 6: 3355–3373, 1986. doi:[10.1523/JNEUROSCI.06-11-03355.1986](https://doi.org/10.1523/JNEUROSCI.06-11-03355.1986).
- Whiteley SJ, Knutsen PM, Matthews DW, Kleinfeld D.** Deflection of a vibrissa leads to a gradient of strain across mechanoreceptors in a mystacial follicle. *J Neurophysiol* 114: 138–145, 2015. doi:[10.1152/jn.00179.2015](https://doi.org/10.1152/jn.00179.2015).
- Woolsey TA, Van der Loos H.** The structural organization of layer IV in the somatosensory region (SI) of mouse cerebral cortex. The description of a cortical field composed of discrete cytoarchitectonic units. *Brain Res* 17: 205–242, 1970. doi:[10.1016/0006-8993\(70\)90079-X](https://doi.org/10.1016/0006-8993(70)90079-X).
- Zucker E, Welker WI.** Coding of somatic sensory input by vibrissae neurons in the rat's trigeminal ganglion. *Brain Res* 12: 138–156, 1969. doi:[10.1016/0006-8993\(69\)90061-4](https://doi.org/10.1016/0006-8993(69)90061-4).



Bibliography

- Abbasi, A., Goueytes, D., Shulz, D. E., Ego-Stengel, V. and Estebanez, L. (2018). A fast intracortical brain-machine interface with patterned optogenetic feedback. *Journal of Neural Engineering* *15*, 046011.
- Ahissar, E. and Assa, E. (2016). Perception as a closed-loop convergence process. *eLife* *5*, e12830.
- Akram, F., Han, H.-S. and Kim, T.-S. (2014). A P300-based brain computer interface system for words typing. *Computers in Biology and Medicine* *45*, 118–125.
- Allard, T., Clark, S. A., Jenkins, W. M. and Merzenich, M. M. (1991). Reorganization of somatosensory area 3b representations in adult owl monkeys after digital syndactyly. *Journal of Neurophysiology* *66*, 1048–1058.
- Alloway, K. D., Zhang, M. and Chakrabarti, S. (2004). Septal columns in rodent barrel cortex: Functional circuits for modulating whisking behavior. *The Journal of Comparative Neurology* *480*, 299–309.
- Andermann, M. L. and Moore, C. I. (2006). A somatotopic map of vibrissa motion direction within a barrel column. *Nature Neuroscience* *9*, 543–551.
- Andersen, R. A. and Aflalo, T. (2022). Preserved cortical somatotopic and motor representations in tetraplegic humans. *Current Opinion in Neurobiology* *74*, 102547.
- Arduin, P.-J., Fregnac, Y., Shulz, D. E. and Ego-Stengel, V. (2013). "Master" Neurons Induced by Operant Conditioning in Rat Motor Cortex during a Brain-Machine Interface Task. *Journal of Neuroscience* *33*, 8308–8320.
- Arduin, P.-J., Fregnac, Y., Shulz, D. E. and Ego-Stengel, V. (2014). Bidirectional control of a one-dimensional robotic actuator by operant conditioning of a single unit in rat motor cortex. *Frontiers in Neuroscience* *8*, 206.
- Armenta Salas, M., Bashford, L., Kellis, S., Jafari, M., Jo, H., Kramer, D., Shanfield, K., Pejsa, K., Lee, B., Liu, C. Y. and Andersen, R. A. (2018). Proprioceptive and cutaneous sensations in humans elicited by intracortical microstimulation. *eLife* *7*, e32904.
- Asboth, L., Friedli, L., Beauparlant, J., Martinez-Gonzalez, C., Anil, S., Rey, E., Baud, L., Pidpruzhnykova, G., Anderson, M. A., Shkorbatova, P., Batti, L., Pagès, S., Kreider, J., Schneider, B. L., Barraud, Q. and Courtine, G. (2018). Cortico-reticulo-spinal circuit reorganization enables functional recovery after severe spinal cord contusion. *Nature Neuroscience* *21*, 576–588.
- Athalye, V. R., Santos, F. J., Carmena, J. M. and Costa, R. M. (2018). Evidence for a neural law of effect. *Science* *359*, 1024–1029.
- Basmajian, J. V. (1963). Control and Training of Individual Motor Units. *Science* *141*, 440–441.
- Bender, K. J. (2006). Synaptic Basis for Whisker Deprivation-Induced Synaptic Depression in Rat Somatosensory Cortex. *Journal of Neuroscience* *26*, 4155–4165.
- Benison, A. M., Rector, D. M. and Barth, D. S. (2007). Hemispheric Mapping of Secondary Somatosensory Cortex in the Rat. *Journal of Neurophysiology* *97*, 200–207.
- Bensmaia, S. J. and Miller, L. E. (2014). Restoring sensorimotor function through intracortical interfaces: progress and looming challenges. *Nature Reviews Neuroscience* *15*, 313–325.

- Birbaumer, N. (2006). Breaking the silence: Brain–computer interfaces (BCI) for communication and motor control. *Psychophysiology* *43*, 517–532.
- Botvinick, M. and Cohen, J. (1998). Rubber hands ‘feel’ touch that eyes see. *Nature* *391*, 756–756.
- Bourassa, J., Pinault, D. and Deschênes, M. (1995). Corticothalamic Projections from the Cortical Barrel Field to the Somatosensory Thalamus in Rats: A Single-fibre Study Using Biocytin as an Anterograde Tracer. *European Journal of Neuroscience* *7*, 19–30.
- Brecht, M. (2017). The Body Model Theory of Somatosensory Cortex. *Neuron* *94*, 985–992.
- Brochier, T., Boudreau, M.-J., Paré, M. and Smith, A. M. (1999). The effects of muscimol inactivation of small regions of motor and somatosensory cortex on independent finger movements and force control in the precision grip. *Experimental Brain Research* *128*, 31–40.
- Bureau, I., von Saint Paul, F. and Svoboda, K. (2006). Interdigitated Paralemniscal and Lemniscal Pathways in the Mouse Barrel Cortex. *PLoS Biology* *4*, e382.
- Caldwell, D. J., Cronin, J. A., Wu, J., Weaver, K. E., Ko, A. L., Rao, R. P. N. and Ojemann, J. G. (2019). Direct stimulation of somatosensory cortex results in slower reaction times compared to peripheral touch in humans. *Scientific Reports* *9*, 3292.
- Cardin, J. A., Carlén, M., Meletis, K., Knoblich, U., Zhang, F., Deisseroth, K., Tsai, L.-H. and Moore, C. I. (2010). Targeted optogenetic stimulation and recording of neurons in vivo using cell-type-specific expression of Channelrhodopsin-2. *Nature Protocols* *5*, 247–254.
- Carmena, J. M., Lebedev, M. A., Crist, R. E., O’Doherty, J. E., Santucci, D. M., Dimitrov, D. F., Patil, P. G., Henriquez, C. S. and Nicolelis, M. A. L. (2003). Learning to Control a Brain–Machine Interface for Reaching and Grasping by Primates. *PLoS Biology* *1*, e42.
- Catani, M., Dell’Acqua, F., Vergani, F., Malik, F., Hodge, H., Roy, P., Valabregue, R. and Thiebaut de Schotten, M. (2012). Short frontal lobe connections of the human brain. *Cortex* *48*, 273–291.
- Ceballo, S., Piwowska, Z., Bourg, J., Daret, A. and Bathellier, B. (2019). Targeted Cortical Manipulation of Auditory Perception. *Neuron* *104*, 1168–1179.e5.
- Cerf, M., Thiruvengadam, N., Mormann, F., Kraskov, A., Quiroga, R. Q., Koch, C. and Fried, I. (2010). On-line, voluntary control of human temporal lobe neurons. *Nature* *467*, 1104–1108.
- Chen, J. L., Margolis, D. J., Stankov, A., Sumanovski, L. T., Schneider, B. L. and Helmchen, F. (2015a). Pathway-specific reorganization of projection neurons in somatosensory cortex during learning. *Nature Neuroscience* *18*, 1101–1108.
- Chen, S. X., Kim, A. N., Peters, A. J. and Komiyama, T. (2015b). Subtype-specific plasticity of inhibitory circuits in motor cortex during motor learning. *Nature Neuroscience* *18*, 1109–1115.
- Chen, X., Wang, F., Fernandez, E. and Roelfsema, P. R. (2020). Shape perception via a high-channel-count neuroprosthesis in monkey visual cortex. *Science* *370*, 1191–1196.
- Chesler, A., Szczot, M., Bharucha-Goebel, D., Čeko, M., Donkervoort, S., Laubacher, C., Hayes, L., Alter, K., Zampieri, C., Stanley, C., Innes, A., Mah, J., Grosmann, C., Bradley, N., Nguyen, D., Foley, A., Pichon, C. and Bönnemann, C. (2016). The role of PIEZO2 in human mechanosensation. *New England Journal of Medicine* *375*, 1355–1364.
- Chestek, C. A., Batista, A. P., Santhanam, G., Yu, B. M., Afshar, A., Cunningham, J. P., Gilja, V., Ryu, S. I., Churchland, M. M. and Shenoy, K. V. (2007). Single-Neuron Stability during Repeated Reaching in Macaque Premotor Cortex. *Journal of Neuroscience* *27*, 10742–10750.
- Churchland, M. M., Cunningham, J. P., Kaufman, M. T., Foster, J. D., Nuyujukian, P., Ryu, S. I. and Shenoy, K. V. (2012). Neural population dynamics during reaching. *Neural population dynamics during reaching* *487*, 51–56.
- Cole, J. (2016). *Losing Touch, a man without his body*. USA Oxford University Press.

- Collinger, J. L., Wodlinger, B., Downey, J. E., Wang, W., Tyler-Kabara, E. C., Weber, D. J., McMorland, A. J. C., Velliste, M., Boninger, M. L. and Schwartz, A. B. (2013). High-performance neuroprosthetic control by an individual with tetraplegia. *Lancet (London, England)* *381*, 557–564.
- Collins, K. L., Guterstam, A., Cronin, J., Olson, J. D., Ehrsson, H. H. and Ojemann, J. G. (2017). Ownership of an artificial limb induced by electrical brain stimulation. *Proceedings of the National Academy of Sciences* *114*, 166–171.
- de Celis Alonso, B., Lowe, A. S., Dear, J. P., Lee, K. C., Williams, S. C. R. and Finnerty, G. T. (2008). Sensory Inputs from Whisking Movements Modify Cortical Whisker Maps Visualized with Functional Magnetic Resonance Imaging. *Cerebral Cortex* *18*, 1314–1325.
- Diamond, M. E., Armstrong-James, M. and Ebner, F. F. (1993). Experience-dependent plasticity in adult rat barrel cortex. *Proceedings of the National Academy of Sciences* *90*, 2082–2086.
- DiGiovanna, J., Dominici, N., Friedli, L., Rigosa, J., Duis, S., Kreider, J., Beuparlant, J., Brand, R. v. d., Schieppati, M., Micera, S. and Courtine, G. (2016). Engagement of the Rat Hindlimb Motor Cortex across Natural Locomotor Behaviors. *Journal of Neuroscience* *36*, 10440–10455.
- Dobelle, W. H. (2000). Artificial Vision for the Blind by Connecting a Television Camera to the Visual Cortex. *ASAIO Journal* *46*, 3–9.
- Ebara, S., Furuta, T. and Kumamoto, K. (2017). Vibrissal mechanoreceptors. *Scholarpedia* *12*, 32372.
- Ebara, S., Kumamoto, K., Matsuura, T., Mazurkiewicz, J. E. and Rice, F. L. (2002). Similarities and differences in the innervation of mystacial vibrissal follicle-sinus complexes in the rat and cat: A confocal microscopic study. *The Journal of Comparative Neurology* *449*, 103–119.
- Ego-Stengel, V., Abbasi, A., Larroche, M., Lassagne, H., Boubenec, Y. and Shulz, D. E. (2019). Mechanical coupling through the skin affects whisker movements and tactile information encoding. *Journal of Neurophysiology* *122*, 1606–1622.
- Estebanez, L., Bertherat, J., Shulz, D. E., Bourdieu, L. and Léger, J.-F. (2016). A radial map of multi-whisker correlation selectivity in the rat barrel cortex. *Nature Communications* *7*, 13528.
- Estebanez, L., Boustani, S. E., Destexhe, A. and Shulz, D. E. (2012). Correlated input reveals coexisting coding schemes in a sensory cortex. *Nature Neuroscience* *15*, 1691–1699.
- Estebanez, L., Férézou, I., Ego-Stengel, V. and Shulz, D. E. (2018). Representation of Tactile Scenes in the Rodent Barrel Cortex. *Neuroscience* *368*, 81–94.
- Ferezou, I., Haiss, F., Gentet, L. J., Aronoff, R., Weber, B. and Petersen, C. C. (2007). Spatiotemporal Dynamics of Cortical Sensorimotor Integration in Behaving Mice. *Neuron* *56*, 907–923.
- Fernández, E., Alfaro, A., Soto-Sánchez, C., Gonzalez-Lopez, P., Lozano, A. M., Peña, S., Grima, M. D., Rodil, A., Gómez, B., Chen, X., Roelfsema, P. R., Rolston, J. D., Davis, T. S. and Normann, R. A. (2021). Visual percepts evoked with an intracortical 96-channel microelectrode array inserted in human occipital cortex. *The Journal of Clinical Investigation* *131*, e151331.
- Fetz, E. E. (1969). Operant Conditioning of Cortical Unit Activity. *Science, New Series* *163*, 955–958.
- Fishman, R. S. (1997). Gordon Holmes, the cortical retina, and the wounds of war. *Documenta Ophthalmologica* *93*, 9–28.
- Fletcher, S. N., Downey, J. E., Weiss, J. M., Hughes, C. L., Herrera, A. J., Tyler-Kabara, E. C., Boninger, M. L., Collinger, J. L. and Gaunt, R. A. (2021). A brain-computer interface that evokes tactile sensations improves robotic arm control. *Science* *372*, 831–836.
- Fountas, K. N. and Smith, J. R. (2007). A novel closed-loop stimulation system in the control of focal, medically refractory epilepsy. In *Operative Neuromodulation: Volume 2: Neural Networks Surgery Acta Neurochirurgica Supplements* pp. 357–362. Springer.
- Fregnac, Y., Shulz, D., Thorpe, S. and Bienenstock, E. (1988). A cellular analogue of visual cortical plasticity. *Nature* *333*, 367–370.

- Frey, U., Krug, M., Reymann, K. G. and Matthies, H. (1988). Anisomycin, an inhibitor of protein synthesis, blocks late phases of LTP phenomena in the hippocampal CA1 region in vitro. *Brain Research* 452, 57–65.
- Fu, M. and Zuo, Y. (2011). Experience-dependent Structural Plasticity in the Cortex. *Trends in neurosciences* 34, 177–187.
- Ganguly, K. and Carmena, J. M. (2009). Emergence of a Stable Cortical Map for Neuroprosthetic Control. *PLoS Biology* 7, e1000153.
- Georgopoulos, A. P., Schwartz, A. B. and Kettner, R. E. (1986). Neuronal population coding of movement direction. *Science (New York, N.Y.)* 233, 1416–1419.
- Ghosh, A., Sydekum, E., Haiss, F., Peduzzi, S., Zörner, B., Schneider, R., Baltes, C., Rudin, M., Weber, B. and Schwab, M. E. (2009). Functional and Anatomical Reorganization of the Sensory-Motor Cortex after Incomplete Spinal Cord Injury in Adult Rats. *The Journal of Neuroscience* 29, 12210–12219.
- Gilbert, C. D. (1977). Laminar differences in receptive field properties of cells in cat primary visual cortex. *The Journal of Physiology* 268, 391–421.
- Gilbert, C. D. and Wiesel, T. N. (1979). Morphology and intracortical projections of functionally characterised neurones in the cat visual cortex. *Nature* 280, 120–125.
- Glazewski, S. and Fox, K. (1996). Time course of experience-dependent synaptic potentiation and depression in barrel cortex of adolescent rats. *Journal of Neurophysiology* 75, 1714–1729.
- Golub, M. D., Sadtler, P. T., Oby, E. R., Quick, K. M., Ryu, S. I., Tyler-Kabara, E. C., Batista, A. P., Chase, S. M. and Yu, B. M. (2018). Learning by neural reassociation. *Nature Neuroscience* 21, 607–616.
- Graziano, M. S. A. and Aflalo, T. N. (2007). Mapping Behavioral Repertoire onto the Cortex. *Neuron* 56, 239–251.
- Graziano, M. S. A., Aflalo, T. N. S. and Cooke, D. F. (2005). Arm Movements Evoked by Electrical Stimulation in the Motor Cortex of Monkeys. *Journal of Neurophysiology* 94, 4209–4223.
- Graziano, M. S. A., Taylor, C. S. R. and Moore, T. (2002). Complex Movements Evoked by Microstimulation of Precentral Cortex. *Neuron* 34, 841–851.
- Guo, J.-Z., Graves, A. R., Guo, W. W., Zheng, J., Lee, A., Rodríguez-González, J., Li, N., Macklin, J. J., Phillips, J. W., Mensh, B. D., Branson, K. and Hantman, A. W. (2015). Cortex commands the performance of skilled movement. *eLife* 4, e10774.
- Haiss, F. and Schwarz, C. (2005). Spatial Segregation of Different Modes of Movement Control in the Whisker Representation of Rat Primary Motor Cortex. *The Journal of neuroscience : the official journal of the Society for Neuroscience* 25, 1579–87.
- Harrison, V. F. and Mortensen, O. A. (1962). Identification and voluntary control of single motor unit activity in the tibialis anterior muscle. *The Anatomical Record* 144, 109–116.
- Hartmann, K., Thomson, E. E., Zea, I., Yun, R., Mullen, P., Canarick, J., Huh, A. and Nicolelis, M. A. L. (2016). Embedding a Panoramic Representation of Infrared Light in the Adult Rat Somatosensory Cortex through a Sensory Neuroprosthesis. *The Journal of Neuroscience: The Official Journal of the Society for Neuroscience* 36, 2406–2424.
- Häusser, M. (2014). Optogenetics: the age of light. *Nature Methods* 11, 1012–1014.
- Hayashi-Takagi, A., Yagishita, S., Nakamura, M., Shirai, F., Wu, Y. I., Loshbaugh, A. L., Kuhlman, B., Hahn, K. M. and Kasai, H. (2015). Labelling and optical erasure of synaptic memory traces in the motor cortex. *Nature* 525, 333–338.
- Hebb, D. O. (1949). *The organization of behavior; a neuropsychological theory*. The organization of behavior; a neuropsychological theory, Wiley, Oxford, England.

- Hiremath, S. V., Tyler-Kabara, E. C., Wheeler, J. J., Moran, D. W., Gaunt, R. A., Collinger, J. L., Foldes, S. T., Weber, D. J., Chen, W., Boninger, M. L. and Wang, W. (2017). Human perception of electrical stimulation on the surface of somatosensory cortex. *PloS One* *12*, e0176020.
- Hochberg, L. R., Bacher, D., Jarosiewicz, B., Masse, N. Y., Simeral, J. D., Vogel, J., Haddadin, S., Liu, J., Cash, S. S., van der Smagt, P. and Donoghue, J. P. (2012). Reach and grasp by people with tetraplegia using a neurally controlled robotic arm. *Nature* *485*, 372–375.
- Hubel, D. H. and Wiesel, T. N. (1959). Receptive fields of single neurones in the cat’s striate cortex. *The Journal of Physiology* *148*, 574–591.
- Hubel, D. H. and Wiesel, T. N. (1962). Receptive fields, binocular interaction and functional architecture in the cat’s visual cortex. *The Journal of Physiology* *160*, 106–154.
- Hubener, M., Shoham, D., Grinvald, A. and Bonhoeffer, T. (1998). Spatial Relationships among Three Columnar Systems in Cat Area 17. *The Journal of neuroscience : the official journal of the Society for Neuroscience* *17*, 9270–84.
- Huber, D., Petreanu, L., Ghitani, N., Ranade, S., Hromádka, T., Mainen, Z. and Svoboda, K. (2008). Sparse optical microstimulation in barrel cortex drives learned behaviour in freely moving mice. *Nature* *451*, 61–64.
- Jacob, V., Cam, J. L., Ego-Stengel, V. and Shulz, D. E. (2008). Emergent Properties of Tactile Scenes Selectively Activate Barrel Cortex Neurons. *Neuron* *60*, 1112–1125.
- Jay, C., Glencross, M. and Hubbard, R. (2007). Modeling the effects of delayed haptic and visual feedback in a collaborative virtual environment. *ACM Trans. Comput.-Hum. Interact.* *14*.
- Jay, C. and Hubbard, R. (2005). Delayed Visual and Haptic Feedback in a Reciprocal Tapping Task. In *First Joint Eurohaptics Conference and Symposium on Haptic Interfaces for Virtual Environment and Teleoperator Systems* pp. 655–656, IEEE.
- Jeannerod, M. (1995). Mental imagery in the motor context. *Neuropsychologia* *33*, 1419–1432.
- Jenkins, W. M., Merzenich, M. M., Ochs, M. T., Allard, T. and Guic-Robles, E. (1990). Functional reorganization of primary somatosensory cortex in adult owl monkeys after behaviorally controlled tactile stimulation. *Journal of Neurophysiology* *63*, 82–104.
- Jensen, K. T., Kadmon Harpaz, N., Dhawale, A. K., Wolff, S. B. E. and Ölveczky, B. P. (2022). Long-term stability of single neuron activity in the motor system. *Nature Neuroscience* *25*, 1664–1674.
- Jeon, B. B., Fuchs, T., Chase, S. M. and Kuhlman, S. J. (2022). Existing function in primary visual cortex is not perturbed by new skill acquisition of a non-matched sensory task. *Nature Communications* *13*, 3638.
- Johansson, R. and Westling, G. (1984). Roles of glabrous skin receptors and sensorimotor memory in automatic control of precision grip when lifting rougher or more slippery objects. *Experimental Brain Research* *56*.
- Johansson, R. S. and Flanagan, J. R. (2009). Coding and use of tactile signals from the fingertips in object manipulation tasks. *Coding and use of tactile signals from the fingertips in object manipulation tasks* *10*, 345–359.
- Johnson, L. A., Wander, J. D., Sarma, D., Su, D. K., Fetz, E. E. and Ojemann, J. G. (2013). Direct electrical stimulation of the somatosensory cortex in humans using electrocorticography electrodes: a qualitative and quantitative report. *Journal of Neural Engineering* *10*, 036021.
- Kaas, J. H. (1997). Topographic Maps are Fundamental to Sensory Processing. *Brain Research Bulletin* *44*, 107–112.
- Kao, J. C., Nuyujukian, P., Ryu, S. I., Churchland, M. M., Cunningham, J. P. and Shenoy, K. V. (2015). Single-trial dynamics of motor cortex and their applications to brain-machine interfaces. *Nature Communications* *6*, 7759.
- Kaufman, M. T., Churchland, M. M., Ryu, S. I. and Shenoy, K. V. (2015). Vacillation, indecision and hesitation in moment-by-moment decoding of monkey motor cortex. *eLife* *4*, e04677.

- Kawai, R., Markman, T., Poddar, R., Ko, R., Fantana, A. L., Dhawale, A. K., Kampff, A. R. and Öveczky, B. P. (2015). Motor Cortex Is Required for Learning but Not for Executing a Motor Skill. *Neuron* *86*, 800–812.
- Kerr, J. N. D., Kock, C. P. J. d., Greenberg, D. S., Bruno, R. M., Sakmann, B. and Helmchen, F. (2007). Spatial Organization of Neuronal Population Responses in Layer 2/3 of Rat Barrel Cortex. *Journal of Neuroscience* *27*, 13316–13328.
- Knutsen, P. M., Mateo, C. and Kleinfeld, D. (2016). Precision mapping of the vibrissa representation within murine primary somatosensory cortex. *Philosophical Transactions of the Royal Society B: Biological Sciences* *371*, 20150351.
- Kremer, Y., Léger, J.-F., Goodman, D., Brette, R. and Bourdieu, L. (2011). Late Emergence of the Vibrissa Direction Selectivity Map in the Rat Barrel Cortex. *Journal of Neuroscience* *31*, 10689–10700.
- Kumar, S., Zomorodi, R., Ghazala, Z., Goodman, M. S., Blumberger, D. M., Cheam, A., Fischer, C., Daskalakis, Z. J., Mulsant, B. H., Pollock, B. G. and Rajji, T. K. (2017). Extent of Dorsolateral Prefrontal Cortex Plasticity and Its Association With Working Memory in Patients With Alzheimer Disease. *JAMA Psychiatry* *74*, 1266–1274.
- Lassagne, H., Goueytes, D., Shulz, D. E., Estebanez, L. and Ego-Stengel, V. (2022). Continuity within the somatosensory cortical map facilitates learning. *Cell Reports* *39*, 110617.
- Lawrence, D. G. and Kuypers, H. G. J. M. (1968). The functional organization of the motor system in the monkey. *Brain* *91*, 15–36.
- Le Cam, J., Estebanez, L., Jacob, V. and Shulz, D. E. (2011). Spatial structure of multiwhisker receptive fields in the barrel cortex is stimulus dependent. *Journal of Neurophysiology* *106*, 986–998.
- Leal-Campanario, R., Delgado-Garcia, J. M. and Gruart, A. (2006). Microstimulation of the somatosensory cortex can substitute for vibrissa stimulation during Pavlovian conditioning. *Proceedings of the National Academy of Sciences* *103*, 10052–10057.
- Lebedev, M. A. and Nicolelis, M. A. L. (2017). Brain-Machine Interfaces: From Basic Science to Neuroprostheses and Neurorehabilitation. *Physiological Reviews* *97*, 767–837.
- Lefort, S., Tómm, C., Floyd Sarria, J.-C. and Petersen, C. C. (2009). The Excitatory Neuronal Network of the C2 Barrel Column in Mouse Primary Somatosensory Cortex. *Neuron* *61*, 301–316.
- Lenarz, T. (2018). Cochlear implant – state of the art. *GMS Current Topics in Otorhinolaryngology, Head and Neck Surgery* *16*, Doc04.
- Luo, Y., Bresee, C. S., Rudnicki, J. W. and Hartmann, M. J. Z. (2021). Constraints on the deformation of the vibrissa within the follicle. *PLOS Computational Biology* *17*, e1007887.
- Madisen, L., Mao, T., Koch, H., Zhuo, J.-m., Berenyi, A., Fujisawa, S., Hsu, Y.-W. A., Garcia, A. J., Gu, X., Zanella, S., Kidney, J., Gu, H., Mao, Y., Hooks, B. M., Boyden, E. S., Buzsáki, G., Ramirez, J. M., Jones, A. R., Svoboda, K., Han, X., Turner, E. E. and Zeng, H. (2012). A toolbox of Cre-dependent optogenetic transgenic mice for light-induced activation and silencing. *Nature Neuroscience* *15*, 793–802.
- Mao, T., Kusefoglul, D., Hooks, B. M., Huber, D., Petreanu, L. and Svoboda, K. (2011). Long-Range Neuronal Circuits Underlying the Interaction between Sensory and Motor Cortex. *Neuron* *72*, 111–123.
- Marasco, P. D., Kim, K., Colgate, J. E., Peshkin, M. A. and Kuiken, T. A. (2011). Robotic touch shifts perception of embodiment to a prosthesis in targeted reinnervation amputees. *Brain* *134*, 747–758.
- Mathis, M. W., Mathis, A. and Uchida, N. (2017). Somatosensory Cortex Plays an Essential Role in Forelimb Motor Adaptation in Mice. *Neuron* *93*, 1493–1503.e6.
- Matyas, F., Sreenivasan, V., Marbach, F., Wacongne, C., Barsy, B., Mateo, C., Aronoff, R. and Petersen, C. C. H. (2010). Motor Control by Sensory Cortex. *Science* *330*, 1240–1243.

- May, T., Ozden, I., Brush, B., Borton, D., Wagner, F., Agha, N., Sheinberg, D. L. and Nurmikko, A. V. (2014). Detection of Optogenetic Stimulation in Somatosensory Cortex by Non-Human Primates - Towards Artificial Tactile Sensation. *PLoS ONE* *9*, e114529.
- Merzenich, M. M., Nelson, R. J., Stryker, M. P., Cynader, M. S., Schoppmann, A. and Zook, J. M. (1984). Somatosensory cortical map changes following digit amputation in adult monkeys. *The Journal of Comparative Neurology* *224*, 591–605.
- Monzée, J., Lamarre, Y. and Smith, A. M. (2003). The Effects of Digital Anesthesia on Force Control Using a Precision Grip. *Journal of Neurophysiology* *89*, 672–683.
- Mountcastle, V. B. (1957). Modality and topographic properties of single neurons of cat’s somatic sensory cortex. *Journal of Neurophysiology* *20*, 408–434.
- Muller, L., Chavane, F., Reynolds, J. and Sejnowski, T. J. (2018). Cortical travelling waves: mechanisms and computational principles. *Nature Reviews Neuroscience* *19*, 255–268.
- Nadel, L. and Land, C. (2000). Memory traces revisited. *Nature Reviews Neuroscience* *1*, 209–212.
- Neely, R. M., Koralek, A. C., Athalye, V. R., Costa, R. M. and Carmena, J. M. (2018). Volitional Modulation of Primary Visual Cortex Activity Requires the Basal Ganglia. *Neuron* *97*, 1356–1368.e4.
- Nitsche, M. A., Müller-Dahlhaus, F., Paulus, W. and Ziemann, U. (2012). The pharmacology of neuroplasticity induced by non-invasive brain stimulation: building models for the clinical use of CNS active drugs. *The Journal of Physiology* *590*, 4641–4662.
- O’Connor, D. H., Hires, S. A., Guo, Z. V., Li, N., Yu, J., Sun, Q.-Q., Huber, D. and Svoboda, K. (2013). Neural coding during active somatosensation revealed using illusory touch. *Nature Neuroscience* *16*, 958–965.
- O’Doherty, J. E., Lebedev, M. A., Ifft, P. J., Zhuang, K. Z., Shokur, S., Bleuler, H. and Nicolelis, M. A. L. (2011). Active tactile exploration using a brain–machine–brain interface. *Nature* *479*, 228–231.
- Omrani, M., Kaufman, M. T., Hatsopoulos, N. G. and Cheney, P. D. (2017). Perspectives on classical controversies about the motor cortex. *Journal of Neurophysiology* *118*, 1828–1848.
- Orsborn, A. L., Moorman, H. G., Overduin, S. A., Shanechi, M. M., Dimitrov, D. F. and Carmena, J. M. (2014). Closed-loop decoder adaptation shapes neural plasticity for skillful neuroprosthetic control. *Neuron* *82*, 1380–1393.
- Papale, A. E. and Hooks, B. M. (2018). Circuit Changes in Motor Cortex During Motor Skill Learning. *Neuroscience* *368*, 283–297.
- Patel, K., Katz, C. N., Kalia, S. K., Popovic, M. R. and Valiante, T. A. (2021). Volitional control of individual neurons in the human brain. *Brain: A Journal of Neurology* *144*, 3651–3663.
- Penfield, W. and Boldrey, E. (1937). Somatic motor and sensory representation in the cerebral cortex of man as studied by electrical stimulation. *Brain* *60*, 389–443.
- Peng, Y., Gillis-Smith, S., Jin, H., Tränkner, D., Ryba, N. J. P. and Zuker, C. S. (2015). Sweet and bitter taste in the brain of awake behaving animals. *Nature* *527*, 512–515.
- Perronnet, L., Vilarchao, M. E., Hucher, G., Shulz, D. E., Peyré, G. and Ferezou, I. (2016). An automated workflow for the anatomo-functional mapping of the barrel cortex. *Journal of Neuroscience Methods* *263*, 145–154.
- Petersen, C. C. H. (2014). Cortical control of whisker movement. *Annual Review of Neuroscience* *37*, 183–203.
- Petersen, C. C. H. and Crochet, S. (2013). Synaptic Computation and Sensory Processing in Neocortical Layer 2/3. *Neuron* *78*, 28–48.
- Petreanu, L., Mao, T., Sternson, S. M. and Svoboda, K. (2009). The subcellular organization of neocortical excitatory connections. *Nature* *457*, 1142–1145.

- Polley, D. B., Kvasnák, E. and Frostig, R. D. (2004). Naturalistic experience transforms sensory maps in the adult cortex of caged animals. *Nature* 429, 67–71.
- Prsa, M., Galiñanes, G. L. and Huber, D. (2017). Rapid Integration of Artificial Sensory Feedback during Operant Conditioning of Motor Cortex Neurons. *Neuron* 93, 929–939.e6.
- Ramachandran, V. S. (1998). Consciousness and body image: lessons from phantom limbs, Capgras syndrome and pain asymbolia. *Philosophical Transactions of the Royal Society of London. Series B: Biological Sciences* 353, 1851–1859.
- Rice, F. L., Kinnman, E., Aldskogius, H., Johansson, O. and Arvidsson, J. (1993). The innervation of the mystacial pad of the rat as revealed by PGP 9.5 immunofluorescence. *The Journal of Comparative Neurology* 337, 366–385.
- Robinson, N. T., Descamps, L. A., Russell, L. E., Buchholz, M. O., Bicknell, B. A., Antonov, G. K., Lau, J. Y., Nutbrown, R., Schmidt-Hieber, C. and Häusser, M. (2020). Targeted Activation of Hippocampal Place Cells Drives Memory-Guided Spatial Behavior. *Cell* 183, 1586–1599.e10.
- Rokni, U., Richardson, A. G., Bizzi, E. and Seung, H. S. (2007). Motor Learning with Unstable Neural Representations. *Neuron* 54, 653–666.
- Romo, R., Hernández, A., Zainos, A. and Salinas, E. (1998). Somatosensory discrimination based on cortical microstimulation. *Nature* 392, 387–390.
- Rosselet, C., Zennou-Azogui, Y., Escoffier, G., Kirmaci, F. and Xerri, C. (2008). Experience-dependent changes in spatiotemporal properties of cutaneous inputs remodel somatosensory cortical maps following skin flap rotation. *European Journal of Neuroscience* 27, 1245–1260.
- Sachidhanandam, S., Sreenivasan, V., Kyriakatos, A., Kremer, Y. and Petersen, C. C. H. (2013). Membrane potential correlates of sensory perception in mouse barrel cortex. *Nature Neuroscience* 16, 1671–1677.
- Sacks, O. (1985). The man who mistook his wife for a hat. Summit Books.
- Sadtler, P. T., Quick, K. M., Golub, M. D., Chase, S. M., Ryu, S. I., Tyler-Kabara, E. C., Yu, B. M. and Batista, A. P. (2014). Neural constraints on learning. *Nature* 512, 423–426.
- Sahel, J.-A., Boulanger-Scemama, E., Pagot, C., Arleo, A., Galluppi, F., Martel, J. N., Esposti, S. D., Delaux, A., de Saint Aubert, J.-B., de Montleau, C., Gutman, E., Audo, I., Duebel, J., Picaud, S., Dalkara, D., Blouin, L., Taiel, M. and Roska, B. (2021). Partial recovery of visual function in a blind patient after optogenetic therapy. *Nature Medicine* 27, 1223–1229.
- Sauerbrei, B. A., Guo, J.-Z., Cohen, J. D., Mischiati, M., Guo, W., Kabra, M., Verma, N., Mensh, B., Branson, K. and Hantman, A. W. (2020). Cortical pattern generation during dexterous movement is input-driven. *Nature* 577, 386–391.
- Schmidt, E. M., McIntosh, J. S., Durelli, L. and Bak, M. J. (1978). Fine control of operantly conditioned firing patterns of cortical neurons. *Experimental Neurology* 61, 349–369.
- Scott, S. H. (2016). A Functional Taxonomy of Bottom-Up Sensory Feedback Processing for Motor Actions. *Trends in Neurosciences* 39, 512–526.
- Sergio, L. E. and Kalaska, J. F. (2003). Systematic Changes in Motor Cortex Cell Activity With Arm Posture During Directional Isometric Force Generation. *Journal of Neurophysiology* 89, 212–228.
- Shanechi, M. M., Orsborn, A. L., Moorman, H. G., Gowda, S., Dangi, S. and Carmena, J. M. (2017). Rapid control and feedback rates enhance neuroprosthetic control. *Nature Communications* 8, 13825.
- Shulz, D. and Fregnac, Y. (1992). Cellular analogs of visual cortical epigenesis. II. Plasticity of binocular integration. *The Journal of Neuroscience* 12, 1301–1318.
- Shulz, D. E. and Ego-Stengel, V. (2012). S1 long-term plasticity. *Scholarpedia* 7, 7615.
- Sofroniew, N. J. and Svoboda, K. (2015). Whisking. *Current Biology* 25, R137–R140.

- Staiger, J. F. and Petersen, C. C. H. (2021). Neuronal Circuits in Barrel Cortex for Whisker Sensory Perception. *Physiological Reviews* 101, 353–415.
- Staudt, M. (2010). Reorganization after pre- and perinatal brain lesions. *Journal of Anatomy* 217, 469–474.
- Stronks, H. C. and Dagnelie, G. (2014). The functional performance of the Argus II retinal prosthesis. *Expert review of medical devices* 11, 23–30.
- Tabot, G. A., Dammann, J. F., Berg, J. A., Tenore, F. V., Boback, J. L., Vogelstein, R. J. and Bensmaia, S. J. (2013). Restoring the sense of touch with a prosthetic hand through a brain interface. *Proceedings of the National Academy of Sciences* 110, 18279–18284.
- Tabot, G. A., Kim, S. S., Winberry, J. E. and Bensmaia, S. J. (2015). Restoring tactile and proprioceptive sensation through a brain interface. *Neurobiology of Disease* 83, 191–198.
- Temereanca, S. and Simons, D. J. (2004). Functional Topography of Corticothalamic Feedback Enhances Thalamic Spatial Response Tuning in the Somatosensory Whisker/Barrel System. *Neuron* 41, 639–651.
- Thompson, A., Murphy, D., Dell’Acqua, F., Ecker, C., McAlonan, G., Howells, H., Baron-Cohen, S., Lai, M.-C. and Lombardo, M. V. (2017). Impaired Communication Between the Motor and Somatosensory Homunculus Is Associated With Poor Manual Dexterity in Autism Spectrum Disorder. *Biological Psychiatry* 81, 211–219.
- Thomson, E. E., Carra, R. and Nicoletis, M. A. L. (2013). Perceiving invisible light through a somatosensory cortical prosthesis. *Nature Communications* 4, 1482.
- Thukral, A., Ershad, F., Enan, N., Rao, Z. and Yu, C. (2018). Soft Neural Interfaces for Ultrathin Electronics. *IEEE Nanotechnology Magazine* PP, 1–1.
- Tonomura, S., Ebara, S., Bagdasarian, K., Uta, D., Ahissar, E., Meir, I., Lampl, I., Kuroda, D., Furuta, T., Furue, H. and Kumamoto, K. (2015). Structure-function correlations of rat trigeminal primary neurons: Emphasis on club-like endings, a vibrissal mechanoreceptor. *Proceedings of the Japan Academy, Series B* 91, 560–576.
- Tsukano, H., Horie, M., Bo, T., Uchimura, A., Hishida, R., Kudoh, M., Takahashi, K., Takebayashi, H. and Shibuki, K. (2015). Delineation of a frequency-organized region isolated from the mouse primary auditory cortex. *Journal of neurophysiology* 113, jn.00932.2014.
- van Beest, E. H., Mukherjee, S., Kirchberger, L., Schnabel, U. H., van der Togt, C., Teeuwen, R. R. M., Barsegyan, A., Meyer, A. F., Poort, J., Roelfsema, P. R. and Self, M. W. (2021). Mouse visual cortex contains a region of enhanced spatial resolution. *Nature Communications* 12, 4029.
- Van der Loos, H. and Woolsey, T. A. (1973). Somatosensory cortex: structural alterations following early injury to sense organs. *Science (New York, N.Y.)* 179, 395–398.
- Van Horn, J. D., Irimia, A., Torgerson, C. M., Chambers, M. C., Kikinis, R. and Toga, A. W. (2012). Mapping Connectivity Damage in the Case of Phineas Gage. *PLoS ONE* 7, e37454.
- Vanni, M. P., Chan, A. W., Balbi, M., Silasi, G. and Murphy, T. H. (2017). Mesoscale Mapping of Mouse Cortex Reveals Frequency-Dependent Cycling between Distinct Macroscale Functional Modules. *Journal of Neuroscience* 37, 7513–7533.
- Velliste, M., Perel, S., Spalding, M. C., Whitford, A. S. and Schwartz, A. B. (2008). Cortical control of a prosthetic arm for self-feeding. *Nature* 453, 1098–1101.
- Vetere, G., Tran, L. M., Moberg, S., Steadman, P. E., Restivo, L., Morrison, F. G., Ressler, K. J., Josselyn, S. A. and Frankland, P. W. (2019). Memory formation in the absence of experience. *Nature Neuroscience* 22, 933–940.
- Wada, M., Takano, K., Ora, H., Ide, M. and Kansaku, K. (2016). The Rubber Tail Illusion as Evidence of Body Ownership in Mice. *Journal of Neuroscience* 36, 11133–11137.

- Wagner, F. B., Mignardot, J.-B., Le Goff-Mignardot, C. G., Demesmaeker, R., Komi, S., Capogrosso, M., Rowald, A., Seáñez, I., Caban, M., Pirondini, E., Vat, M., McCracken, L. A., Heimgartner, R., Fodor, I., Watrin, A., Seguin, P., Paoles, E., Van Den Keybus, K., Eberle, G., Schurch, B., Pralong, E., Becce, F., Prior, J., Buse, N., Buschman, R., Neufeld, E., Kuster, N., Carda, S., von Zitzewitz, J., Delattre, V., Denison, T., Lambert, H., Minassian, K., Bloch, J. and Courtine, G. (2018). Targeted neurotechnology restores walking in humans with spinal cord injury. *Nature* 563, 65–71.
- Wang, Q. and Burkhalter, A. (2007). Area map of mouse visual cortex. *The Journal of Comparative Neurology* 502, 339–357.
- Wise, S. P. (1985). The primate promoter cortex fifty years after Fulton. *Behavioural Brain Research* 18, 79–88.
- Wolpert, D. M., Miall, R. C. and Kawato, M. (1998). Internal models in the cerebellum. *Trends in Cognitive Sciences* 2, 338–347.
- Woolsey, T. A. and Van der Loos, H. (1970). The structural organization of layer IV in the somatosensory region (S I) of mouse cerebral cortex: The description of a cortical field composed of discrete cytoarchitectonic units. *Brain Research* 17, 205–242.
- Wyller, A. R. and Burchiel, K. J. (1978). Factors influencing accuracy of operant control of pyramidal tract neurons in monkey. *Brain Research* 152, 418–421.
- Xu, T., Yu, X., Perlik, A. J., Tobin, W. F., Zweig, J. A., Tennant, K., Jones, T. and Zuo, Y. (2009). Rapid formation and selective stabilization of synapses for enduring motor memories. *Nature* 462, 915–919.
- Yu, C., Derdikman, D., Haidarliu, S. and Ahissar, E. (2006). Parallel Thalamic Pathways for Whisking and Touch Signals in the Rat. *PLoS Biology* 4, e124.
- Zagha, E., Ge, X. and McCormick, D. A. (2015). Competing Neural Ensembles in Motor Cortex Gate Goal-Directed Motor Output. *Neuron* 88, 565–577.
- Zhang, H., Zhang, C., Vincent, J., Zala, D., Benstaali, C., Sainlos, M., Grillo-Bosch, D., Daburon, S., Coussen, F., Cho, Y., David, D. J., Saudou, F., Humeau, Y. and Choquet, D. (2018). Modulation of AMPA receptor surface diffusion restores hippocampal plasticity and memory in Huntington’s disease models. *Nature Communications* 9, 4272.